

# **The Design and Assembly of Tailored Oligosaccharides as Polymer Therapeutics for Improved Treatment of Chronic Respiratory Disease**

A thesis submitted to Cardiff University in partial fulfilment  
of the requirements for the degree of  
Doctor of Philosophy

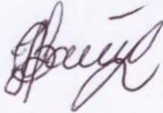


February 2019

**Joana Stokniene**  
Advanced Therapies Group  
School of Dentistry  
Cardiff University  
United Kingdom

## DECLARATION

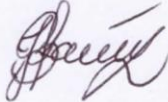
This work has not previously been accepted in substance for any degree and is not concurrently submitted in candidature for any degree.

Signed 

Date 10/05/2019

## STATEMENT 1

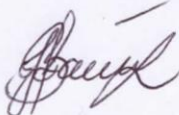
This thesis is being submitted in partial fulfilment of the requirements for the degree of PhD.

Signed 

Date 10/05/2019

## STATEMENT 2

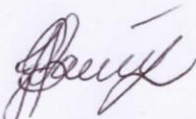
This thesis is the result of my own independent work/investigation, except where otherwise stated. Other sources are acknowledged by explicit references.

Signed 

Date 10/05/2019

## STATEMENT 3

I hereby give consent for my thesis, if accepted, to be available for photocopying and for inter-library loan, and for the title and summary to be made available to outside organisations.

Signed 

Date 10/05/2019

## **Acknowledgements**

I would like to express my sincere gratitude to my supervisors Professor David Thomas, Dr Elaine Ferguson and Dr Katja Hill for the patient guidance, endless encouragement and valuable advice throughout my PhD. I would also like to acknowledge the Research Council of Norway and the biopharmaceutical company AlgiPharma AS for funding my PhD studentship (Grant number: 228542/O30).

I am grateful to all my friends and colleagues with whom I have had the pleasure of working throughout this research project. Special thanks to Dr Mathieu Varache, Dr Lydia Powell and Dr Manon Pritchard for your wonderful support, guidance and invaluable help.

I would like to express my very great appreciation to Dr Olav Aarstad (Norwegian University of Science and Technology), Dr Diego Andrey and Dr Owen Spiller (Cardiff University) for your kind help in the laboratory.

Finally, I wish to thank my family for their unconditional support and enthusiastic encouragement throughout my PhD study.

## Abstract

Healthcare-associated infections affect 4 million patients annually in the EU and result in an estimated 37,000 deaths per year. Of particular concern are the rapidly increasing resistance rates of Gram-negative bacterial pathogens to many, or even all, commonly used antibiotics, with a corresponding decrease in the design/development of new antibiotic compounds. Thus, there remains an urgent need for novel therapies for these 'hard to treat' infections. Fortunately, polypeptide antibiotics, such as colistin and polymyxin B, still retain potent antimicrobial activity against multidrug resistant (MDR) Gram-negative pathogens. In addition, polymer therapeutics are finding increasing utility as antimicrobial agents. The aim of this thesis was to generate and characterise an alginate oligosaccharide ("OligoG")-polymyxin conjugate library to optimise the antimicrobial functions of these last resort drugs.

Reproducible conjugation of polymyxin to OligoG was achieved using amide or ester cross-linkers, producing conjugates with 6.1-12.9% (w/w) antibiotic loading and molecular weights of 14,500-27,000 g/mol (relative to pullulan MW standards). TNF $\alpha$  ELISA and MTT assays revealed that OligoG conjugation significantly decreased inflammatory cytokine production and cytotoxicity of colistin (2.2-9.3-fold) and polymyxin B (2.9-27.2-fold) from a human kidney cell line. Minimum inhibitory concentration (MIC) assays and bacterial growth curves demonstrated that antimicrobial activity of the OligoG-polymyxin conjugates was similar to that of the parent antibiotic, but with more sustained bacterial growth inhibition. Importantly, ester-linked conjugates showed full retention of the antibiotic's antimicrobial activity, while the MIC of the amide-linked conjugates increased by more than 2 log-fold. Confocal laser scanning microscopy revealed that both amide- and ester-linked colistin conjugates significantly disrupted the formation of *P. aeruginosa* biofilms and induced bacterial death. An *in vitro* 'time-to-kill' experiment using *A. baumannii* indicated that colistin and OligoG-ester-colistin conjugates reduced viable bacterial counts (~2 fold) after 4 h, with no significant activity observed with OligoG-amide-colistin conjugates. OligoG-induced disruption of the 3-dimensional architecture and clumping of *P. aeruginosa* and *E. coli* biofilms was demonstrated using a Transwell diffusion model and biofilm disruption assays, while fluorescent labelling of OligoG confirmed its rapid diffusion and distribution within the whole biofilm structure.

These studies confirm that bi-functional polymer therapeutics such as OligoG-polymyxin conjugates have potential benefits in the treatment of MDR Gram-negative bacterial infections.

## Contents

Thesis title.....	i
Declaration.....	ii
Acknowledgements.....	iii
Abstract.....	iv
Contents .....	v
List of Figures .....	x
List of Tables.....	xiv
Abbreviations .....	xvi

## Chapter 1: General Introduction

1.1 Introduction .....	2
1.2 Antibiotics in clinical development.....	5
1.3 Bacterial cell wall structure.....	7
1.4 Mechanisms of antibiotic resistance .....	10
1.4.1 Biofilms .....	14
1.5 Modification of polymyxin .....	16
1.6 Nanomedicines as novel antibiotic therapies .....	17
1.6.1 Polymer therapeutics .....	20
1.6.2 Enhanced permeability and retention effect.....	23
1.7 Polymeric carrier .....	24
1.7.1 Alginates.....	26
1.7.2 OligoG CF-5/20.....	28
1.8 Examples of polysaccharide-antibiotic conjugates.....	30
1.9 Aims of the project .....	31

## Chapter 2: General Materials and Methods

2.1 Chemicals .....	33
2.1.1 General chemicals .....	33
2.1.2 Alginates .....	33
2.1.3 Antibiotics .....	33
2.1.4 Fluorescent probes .....	33
2.1.5 Chemicals for bacterial culture.....	34
2.1.6 Chemicals for cell culture.....	34

2.2 Cell line .....	34
2.3 Bacterial isolates.....	34
2.4. Equipment.....	36
2.4.1 General equipment for bacterial and cell culture.....	36
2.4.2 Analytical equipment.....	36
2.4.2.1 Gel permeation chromatography (GPC).....	36
2.4.2.2 Fast protein liquid chromatography (FPLC).....	37
2.4.2.3 Spectrophotometry: Ultraviolet/visible (UV/vis) .....	37
2.4.2.4 Confocal laser scanning microscopy (CLSM).....	37
2.4.2.5 Miscellaneous equipment.....	37
2.5 Sterilisation .....	38
2.6 General methods .....	38
2.6.1 Purification of OligoG-antibiotic conjugates .....	38
2.6.2 Characterisation of OligoG-antibiotic conjugates.....	39
2.6.2.1 Characterisation by GPC.....	39
2.6.2.2 Characterisation by FPLC .....	39
2.6.2.3 Characterisation by BCA .....	42
2.6.2.4 Characterisation by ninhydrin assay.....	42
2.6.3 Biological characterisation of OligoG-antibiotic conjugates .....	45
2.6.3.1 Cell maintenance .....	45
2.6.3.2 Defrosting cells.....	45
2.6.3.3 Cell passaging.....	45
2.6.3.4 Cell counting .....	47
2.6.3.5 Characterisation by MTT .....	47
2.6.3.6 Characterisation by TNF $\alpha$ ELISA .....	48
2.6.4 Microbiological characterisation of OligoG-antibiotic conjugates ....	48
2.6.4.1 Preparation of microbiological growth media and agar.....	48
2.6.4.2 Bacterial cultures maintenance .....	48
2.6.4.3 Preparation of overnight bacterial culture.....	50
2.6.4.4 Minimum inhibitory concentration (MIC) assay.....	50
2.6.4.5 Colistin quantification .....	50
2.7 Statistical analysis.....	52
<b>Chapter 3: Synthesis and Characterisation of OligoG-Polymyxin Conjugates</b>	
3.1 Introduction .....	55

3.1.1 Choice of polymer .....	55
3.1.2 Selection of bioactive compound .....	58
3.1.3 Selection of appropriate linker .....	62
3.2 Experimental aims and objectives.....	65
3.3 Methods .....	68
3.3.1 Synthesis of OligoG-antibiotic conjugates .....	68
3.3.2 Purification and characterisation of OligoG-polymyxin conjugates .	69
3.3.3 Cytotoxicity of OligoG-antibiotic conjugates.....	69
3.3.4 TNF $\alpha$ ELISA assay .....	69
3.4 Results .....	70
3.4.1 Synthesis and purification of OligoG-polymyxin conjugates.....	70
3.4.2 Characterisation of OligoG-polymyxin conjugates .....	70
3.4.3 Biological characterisation of OligoG-antibiotic conjugates .....	73
3.5 Discussion.....	78
3.6 Conclusions .....	85
<b>Chapter 4: Antimicrobial Activity of OligoG-Polymyxin Conjugates</b>	
4.1 Introduction .....	87
4.1.1 Mechanism of action of polymyxin antibiotics .....	87
4.1.2 Antimicrobial susceptibility testing .....	89
4.1.3 Combination therapy for Gram-negative infections.....	93
4.1.4 Environmental factors affecting Minimum Inhibitory Concentration	94
4.2 Experimental aims and objectives.....	95
4.3 Methods .....	96
4.3.1 Bacterial strains .....	96
4.3.2 Susceptibility testing using MIC assays .....	96
4.3.3 Susceptibility testing using MIC assays modified with mucin.....	96
4.3.4 Susceptibility testing using MIC assays modified with artificial sputum medium .....	99
4.3.5 Bacterial growth curves .....	101
4.3.6 Checkerboard assay.....	101
4.3.7 Biofilm formation assay.....	103
4.4 Results .....	104
4.4.1 Microbiological characterisation of OligoG-polymyxin conjugates	104
4.4.2 Characterisation of bacterial growth curves .....	110
4.4.3 Checkerboard assays with azithromycin.....	110

4.4.4 The effect of OligoG-colistin conjugates on biofilm formation .....	115
4.5 Discussion.....	115
4.6 Conclusions .....	126
<b>Chapter 5: <i>In vitro</i> Pharmacokinetic-Pharmacodynamic Model</b>	
5.1 Introduction .....	128
5.1.1 PK-PD models described in the literature .....	128
5.2 Experimental aims and objectives.....	131
5.3 Methods .....	132
5.3.1 Development of the two-compartment PK-PD model using the Slide-a-lyzer dialysis cassettes.....	132
5.3.1.1 Phase 1: Method validation using the dialysis cassettes.....	132
5.3.1.2 Phase 2: Method validation using the dialysis cassettes.....	135
5.3.1.3 Phase 3: TTK model using the dialysis cassettes .....	135
5.3.2 Development of a two-compartment PK-PD model using a dialysis bag.....	136
5.3.2.1 Phase 1: Method validation using the dialysis bag model .....	136
5.3.2.2 Phase 2: TTK model using the dialysis bag .....	136
5.4 Results.....	139
5.4.1 Characterisation of the two-compartment PK-PD model using Slide-a-lyzer dialysis cassettes.....	139
5.4.2 Characterisation of the two-compartment PK-PD model using dialysis tubing .....	146
5.5 Discussion.....	146
5.6 Conclusions .....	155
<b>Chapter 6: Diffusion Modelling and Antimicrobial Activity of OligoG in Bacterial Biofilms</b>	
6.1 Introduction .....	157
6.1.1 Extracellular polymeric substance (EPS).....	157
6.1.2 Selection of fluorescent probes.....	158
6.2 Experimental aims and objectives.....	161
6.3 Methods .....	162
6.3.1. Development of a Transwell diffusion model .....	162
6.3.1.1 Validation of the Transwell diffusion model .....	162
6.3.1.2 Transwell biofilm diffusion model using rhodamine .....	164
6.3.2 Biofilm disruption assay .....	165
6.3.4 Fluorescent labelling of OligoG.....	165

6.3.5 Characterisation of the fluorescently labelled OligoG .....	167
6.3.6 The effect of fluorescently labelled OligoG on biofilm disruption...	168
6.4 Results .....	169
6.4.1 Transwell biofilm diffusion assay .....	169
6.4.2 Confocal Laser Scanning Microscopy of <i>E. coli</i> IR57 biofilm disruption studies.....	169
6.4.3 Characterisation of TxRd- or OrGr-labelled OligoG .....	176
6.4.4 <i>E. coli</i> IR57 biofilm disruption studies using fluorescently labelled OligoG .....	176
6.5 Discussion.....	184
6.6 Conclusions .....	191
<b>Chapter 7: General Discussion</b>	
7.1 Evaluation of the present study.....	194
7.2 Suggestions for future development of OligoG-polymyxin conjugates .	197
7.3 Contribution of this thesis to antibiotic development .....	200
<b>Bibliography</b> .....	201
<b>Appendices</b>	
Appendix 1: Publications.....	232
Appendix 2: Bacterial growth curves in the presence of colistin sulfate and OligoG-colistin conjugates .....	234
Appendix 3: Bacterial growth curves in the presence of OligoG or NaCl ...	244
Appendix 4: MIC assays in the presence of Gram-positive antibiotics and OligoG against Gram-negative bacteria.....	248
Appendix 5: OligoG-bacitracin optimisation .....	250

## List of Figures

<b>Figure 1.1</b> A timeline of antimicrobial discovery and emergence of resistance. ....	3
<b>Figure 1.2</b> Schematic diagrams of the cell envelope in (a) Gram-negative and (b) Gram-positive bacteria.....	9
<b>Figure 1.3</b> Schematic representation of different mechanisms of antibiotic resistance. ....	11
<b>Figure 1.4</b> Schematic representation of biofilm formation stages.....	15
<b>Figure 1.5</b> Schematic representation of polymer therapeutics including polymeric drugs, polymer-protein conjugates, polymer-drug conjugates, polyplexes and polymeric micelles.....	21
<b>Figure 1.6</b> Schematic representation of localisation of the polymer-antibiotic conjugates. ....	25
<b>Figure 1.7</b> Chemical structure of OligoG, including $\alpha$ -L-gulonate (G) and $\beta$ -D-manuronate (M) blocks. ....	29
<b>Figure 2.1</b> Morphology of the HK-2 cells. ....	35
<b>Figure 2.2</b> Typical FPLC calibration using Superdex 75 (16/600) column..	40
<b>Figure 2.3</b> Typical GPC calibration using pullulan molecular weight standards. ....	41
<b>Figure 2.4</b> Typical FPLC calibration using Superdex 75 column (10/300 GL) column. ....	43
<b>Figure 2.5</b> Typical BCA assay calibration curves using colistin sulfate, polymyxin B and bacitracin as protein standards. ....	44
<b>Figure 2.6</b> Typical ninhydrin assay calibration curve using ethanolamine standards. ....	46
<b>Figure 2.7</b> Typical ELISA assay calibration curve using TNF $\alpha$ standards ..	49
<b>Figure 2.8</b> Typical plate layout for susceptibility testing of OligoG-antibiotic conjugates using the MIC assay. ....	51
<b>Figure 2.9</b> Typical ELISA assay calibration curve using colistin standards....	53
<b>Figure 3.1</b> (a) Graphic and (b) chemical structure of colistin. ....	59
<b>Figure 3.2</b> (a) Graphic and (b) chemical structure of polymyxin B.....	60
<b>Figure 3.3</b> Schematic diagram showing synthesis of the OligoG-amide-polymyxin conjugate. ....	64
<b>Figure 3.4</b> Schematic diagram showing synthesis of the OligoG-ester-polymyxin conjugate. ....	66
<b>Figure 3.5</b> Schematic diagram showing alginate antibiotic conjugation and drug release from the polymer of (a) the OligoG-AMIDE-colistin conjugate and (b) the OligoG-ESTER-colistin conjugate. ....	67

<b>Figure 3.6</b> Typical elution profile of conjugate reaction mixture before purification using a Superdex 75 (16/600) size exclusion column.....	71
<b>Figure 3.7</b> Typical elution profile of OligoG-polymyxin conjugates using GPC analysis.....	72
<b>Figure 3.8</b> Characterisation of OligoG-polymyxin conjugates using FPLC..	74
<b>Figure 3.9</b> <i>In vitro</i> cytotoxicity of OligoG-polymyxin conjugates in HK-2 cells.....	76
<b>Figure 3.10</b> TNF $\alpha$ release in HK-2 cells after incubation with OligoG-polymyxin conjugates for 72 h.....	79
<b>Figure 4.1</b> Antibacterial mechanisms mediated by polymyxins. ....	90
<b>Figure 4.2</b> Typical MIC plate set up.....	100
<b>Figure 4.3</b> Typical plate layout for checkerboard MIC assay using OligoG-A-colistin and azithromycin in combination against <i>P. aeruginosa</i> MDR 301 (MIC = 1 and 8 $\mu$ g/ml, respectively). ....	102
<b>Figure 4.4</b> Bacterial growth curves for <i>P. aeruginosa</i> MDR 301 (48 h) in the presence of (a) colistin sulfate, (b and f) OligoG-colistin conjugates (amide and ester linked). ....	111
<b>Figure 4.5</b> Biofilm formation assay showing LIVE (green)/DEAD (red) stained CLSM (aerial and cross-sectional views) of <i>P. aeruginosa</i> R22 biofilms grown for 24 h in the presence of free- and OligoG-conjugated colistin.....	116
<b>Figure 4.6</b> Comstat image analysis of <i>P. aeruginosa</i> R22 biofilms grown for 24 h in the presence of free- and OligoG-conjugated colistin. ....	117
<b>Figure 5.1</b> Representative picture of the two-compartment PK-PD model using a Slide-a-lyzer dialysis cassette. ....	133
<b>Figure 5.2</b> Representative picture of the two-compartment PK-PD model using a dialysis bag.....	137
<b>Figure 5.3</b> Phase 1 method validation: Colistin concentration, measured by BCA assay, in the (a) IC and (b) OC following diffusion through 2,000 g/mol MWCO dialysis cassettes over 48 h.....	140
<b>Figure 5.4</b> Phase 1 method validation: Colistin concentration, measured by BCA assay, in the (a) IC and (b) OC following diffusion through 10,000 g/mol MWCO dialysis cassettes over 48 h.....	141
<b>Figure 5.5</b> Phase 2 method validation: Quantification of colistin concentration, measured by ELISA, in the IC after 24 h using (a) 2,000 and (b) 10,000 g/mol MWCO dialysis cassettes. ....	143
<b>Figure 5.6</b> Phase 3: Effect of antibiotic treatments (at 1 x MIC) on the cell viability of <i>A. baumannii</i> 7789 in a TTK model using (a) 2,000 g/mol and (b) 10,000 g/mol MWCO dialysis cassettes. ....	144
<b>Figure 5.7</b> Phase 3: Effect of antibiotic treatments (at 2 x MIC) on the cell	

viability of <i>A. baumannii</i> 7789 in a TTK model using (a) 2,000 g/mol and (b) 10,000 g/mol MWCO dialysis cassettes. ....	145
<b>Figure 5.8</b> Phase 3: Effect of colistin sulfate on the viability of <i>A. baumannii</i> 7789 in a TTK model using 2,000-20,000 g/mol MWCO dialysis cassettes.....	147
<b>Figure 5.9</b> Phase 1 method validation: Colistin concentration, measured by BCA assay, in the (a) IC and (b) OC following diffusion through dialysis tubing over 48 h. ....	148
<b>Figure 5.10</b> Phase 2: Effect of antibiotic treatments on the viability of <i>A. baumannii</i> 7789 in a TTK model using dialysis tubing. ....	149
<b>Figure 6.1</b> Schematic diagram of the Transwell biofilm diffusion model, indicating (a) start (with the fluorescent probe added to the donor compartment) and (b) end (with the fluorescent probe diffused throughout the acceptor well) of the experiment. ....	163
<b>Figure 6.2</b> Schematic diagram showing synthesis of the TxRd- or OrGr-OligoG conjugates. ....	166
<b>Figure 6.3</b> Typical Transwell assay calibration curve for rhodamine. ....	170
<b>Figure 6.4</b> Rhodamine diffusion through <i>P. aeruginosa</i> NH57388A biofilms grown at different seeding densities ( $1 \times 10^2$ to $1 \times 10^8$ CFU/ml)...	171
<b>Figure 6.5</b> Rhodamine diffusion through a microporous membrane in the presence of (a) OligoG (0%, 0.5% or 1%) or (b) EDTA (0 mM, 1 mM, 50 mM or 100 mM).....	172
<b>Figure 6.6</b> Rhodamine diffusion through the <i>P. aeruginosa</i> NH57388A biofilms after (a) OligoG treatment with and without a washing step or (b) cell permeabiliser EDTA. ....	173
<b>Figure 6.7</b> Biofilm disruption assay showing LIVE (green)/DEAD (red) stained CLSM (aerial and cross-sectional views) of <i>E. coli</i> IR57 biofilms grown for 24 h, followed by (a) 4 h and (b) 24 h treatment with OligoG. ....	174
<b>Figure 6.8</b> Median fluorescence intensity and interquartile ranges obtained from CLSM imaging of the <i>E. coli</i> IR57 biofilms stained with SYTO 9 ( <b>Figure 6.7</b> ).....	175
<b>Figure 6.9</b> Biofilm disruption assay showing SYTO 9 and ConA stained (nucleic acid [green] and EPS polysaccharides [red], respectively) CLSM imaging (aerial and cross-sectional views) of <i>E. coli</i> IR57 biofilms grown for 24 h, followed by (a) 4 h and (b) 24 h treatment with OligoG (zoom factor 2).....	177
<b>Figure 6.10</b> Median fluorescence intensity and interquartile ranges obtained from CLSM imaging of the <i>E. coli</i> IR57 biofilms stained with ConA ( <b>Figure 6.9</b> ).....	178
<b>Figure 6.11</b> Analysis of the reaction time on the reaction yield of (a) TxRd-OligoG and (b) OrGr-OligoG conjugates using a PD-10 column.....	179

<b>Figure 6.12</b> Characterisation of the elution profile of crude and purified mixtures of (a) TxRd-OligoG and (b) OrGr-OligoG conjugates using a PD-10 column. ....	180
<b>Figure 6.13</b> Calibration curve for (a) TxRd cadaverine absorbance at a wavelength of 587 nm and (b) OrGr cadaverine absorbance at a wavelength of 493 nm. ....	181
<b>Figure 6.14</b> Biofilm disruption assay showing SYTO 9 (green) stained CLSM of <i>E. coli</i> IR57 biofilms grown for 24 h, followed by 24 h treatment with TxRd-OligoG. ....	183
<b>Figure 6.15</b> CLSM image analysis (aerial and cross-sectional views) of <i>E. coli</i> IR57 biofilms grown for 24 h , followed by 24 h treatment with 4.8%OrGr-OligoG (green). ....	185
<b>Figure 6.16</b> Characterisation of supernatant from <i>E. coli</i> IR57 biofilms grown for 24 h, followed by 24 h treatment with (a) TxRd-OligoG and (b) OrGr-OligoG using a PD-10 column. ....	186
<b>Appendix 2.1</b> Bacterial growth curves for <i>K. pneumoniae</i> KP05 506 (48 h) in the presence of (a) colistin sulfate, (b and f) OligoG-colistin conjugates (amide and ester linked). ....	235
<b>Appendix 2.2</b> Bacterial growth curves for <i>E. coli</i> IR57 (48 h) in the presence of (a) colistin sulfate, (b and f) OligoG-colistin conjugates (amide and ester linked). ....	238
<b>Appendix 2.3</b> Bacterial growth curves for <i>A. baumannii</i> 7789 (48 h) in the presence of (a) colistin sulfate, (b and f) OligoG-colistin conjugates (amide and ester linked). ....	241
<b>Appendix 3.1</b> Bacterial growth curves (48 h) for (a) <i>P. aeruginosa</i> NH57388A, (b) <i>K. pneumoniae</i> KP05 506, (c) <i>E. coli</i> IR57 and (d) <i>A. baumannii</i> 7789 in the presence of OligoG or NaCl, at equivalent concentration to the Na <sup>+</sup> content of OligoG (n = 3). ....	246
<b>Appendix 5.4</b> <i>In vitro</i> cytotoxicity of OligoG-A-bacitracin conjugates in HK-2 cells. ....	255

## List of Tables

<b>Table 1.1</b> Novel antibiotics against priority pathogens currently in the clinical development pipeline. ....	8
<b>Table 1.2</b> Examples of polymyxin derivatives currently in clinical development. ....	18
<b>Table 3.1</b> Examples of alginate conjugates in clinical development.....	56
<b>Table 3.2</b> Characterisation summary of OligoG-polymyxin conjugates. ....	75
<b>Table 3.3</b> IC <sub>50</sub> values ( $\pm$ SEM) and fold-change of OligoG-polymyxin conjugates derived from MTT assay in HK-2 cells. ....	77
<b>Table 4.1</b> Bacterial isolates used for characterisation of OligoG-antibiotic conjugates. ....	97
<b>Table 4.2</b> MIC breakpoints ( $\mu\text{g/ml}$ ) for colistin sulfate and polymyxin B recommended by the Clinical and Laboratory Standards Institute (CLSI) and the European Committee on Antimicrobial Susceptibility Testing (EUCAST) in 2018. ....	98
<b>Table 4.3</b> MIC determinations of OligoG-polymyxin conjugates against a range of Gram-negative bacterial pathogens.....	105
<b>Table 4.4</b> Comparison of the antimicrobial activity MIC ( $\mu\text{g/ml}$ ) of OligoG-A-colistin and dextrin-A-colistin conjugates.....	106
<b>Table 4.5</b> Batch-to-batch reproducibility of MIC determinations of OligoG-colistin conjugates against a range of Gram-negative bacterial pathogens	107
<b>Table 4.6</b> Microbiological efficacy (MICs) of antibiotics in the absence and presence of mucin against Gram-negative bacterial pathogens. ....	108
<b>Table 4.7</b> Comparison of the effect of growth medium (AS medium and MH broth) on antimicrobial activity (MIC determinations) of antibiotics.....	109
<b>Table 4.8</b> MIC and FICI values of OligoG-colistin conjugates, colistin and azithromycin, alone and in combination. ....	114
<b>Table 5.1</b> Examples of bacterial quantification methods used in time-to-kill assays.....	130
<b>Table 5.2</b> Developmental phases of the PK-PD model using the Slide-a-lyzer dialysis cassettes. ....	134
<b>Table 5.3</b> Developmental phases of the PK-PD model using the dialysis bag.....	138
<b>Table 5.4</b> Summary of the percentage of the original colistin dose detected in the IC after 24 h.....	142
<b>Table 6.1</b> Characteristics of Texas Red (TxRd) and Oregon Green (OrGr) fluorescent probes and their use in previous polymer-labelling studies. ....	160
<b>Table 6.2</b> Quantities (mg) of reactants used for TxRd-OligoG and OrGr-	

OligoG conjugation. ....	167
<b>Table 6.3</b> Characterisation of TxRd- or OrGr-labelled OligoG. ....	182
<b>Appendix 4.1</b> Microbiological efficacy of so called ‘Gram-positive antibiotics’ (i.e. those commonly prescribed for Gram-positive bacteria) in the absence and presence of OligoG against Gram-negative bacteria.....	249
<b>Appendix 5.1</b> Optimisation of OligoG-A-bacitracin conjugate synthesis..	252
<b>Appendix 5.2</b> Characterisation summary of OligoG-A-bacitracin conjugates. ....	253
<b>Appendix 5.3</b> MIC determinations of OligoG-A-bacitracin conjugates against a range of Gram-negative and Gram-positive bacterial pathogens	254
<b>Appendix 5.5</b> IC <sub>50</sub> values (± SEM) of OligoG-A-bacitracin conjugates derived from MTT assay in HK-2 cells. ....	255

## Abbreviations

A.U.	Arbitrary units
ABC	ATP-binding cassette
ANOVA	Analysis of variance
AS	Artificial sputum
ASTM	American Society for Testing and Materials
ATCC	American Type Culture Collection
BA	Blood agar
BCA	Bicinchoninic acid
BPE	Bovine pituitary extract
CC <sub>50</sub>	Concentration of the 50% cytotoxic effect
CF	Cystic fibrosis
CFU	Colony forming units
CLSI	Clinical and Laboratory Standards Institute
CLSM	Confocal laser scanning microscopy
CMS	Colistimethate sodium
ConA	Concanavalin A
DCC	N,N'-dicyclohexyl carbodiimide
dH <sub>2</sub> O	Distilled water
DMAP	4-dimethylaminopyridine
DMF	N,N-dimethylformamide
DMSO	Dimethyl sulfoxide
DNA	Deoxyribonucleic acid
DTPA	Diethylenetriaminepentaacetic acid
EC <sub>50</sub>	50% effective concentration
EDC	1-ethyl-3-[3-dimethylaminopropyl] carbodiimide hydrochloride
EDTA	Ethylenediaminetetraacetic acid
EGF	Human recombinant epidermal growth factor
ELISA	Enzyme-linked immunosorbent assay`
EPR	Enhanced permeability and retention
EPS	Extracellular polymeric substance
Equiv.	Equivalent
ESF	European Science Foundation

EUCAST	European Committee on Antimicrobial Susceptibility Testing
FDA	Food and Drug Administration
FICI	Fractional inhibitory concentration index
FPLC	Fast protein liquid chromatography
GPC	Gel permeation chromatography
HK-2	Human kidney proximal tubule cell line
HPLC	High-performance liquid chromatography
HPMA	N-(2-hydroxypropyl) methacrylamide
IC	Inner compartment
IC <sub>50</sub>	Half maximal inhibitory concentration
IDSA	Infectious Diseases Society of America
IL-1	Interleukin-1
IM	Inner membrane
IV	Intravenous
K-SFM	Keratinocyte serum-free medium
LC-MS	Liquid chromatography-mass spectrometry
LPS	Lipopolysaccharide
MALLS	Multi-angle laser light scattering
MATE	Multidrug and toxic compound extrusion
MDR	Multidrug-resistant
MFS	Major facilitator superfamily
MH	Mueller-Hinton
MIC	Minimum inhibitory concentration
MTT	3-(4,5-dimethylthiazol-2-yl)-2,5-diphenyltetrazolium bromide
Mw	Molecular weight average of the weight
MWCO	Molecular weight cut-off
NaOH	Sodium hydroxide
NCTC	National Collection of Type Culture
ND	Not determined
OC	Outer compartment
OrGr	Oregon Green
PAMAM	Polyamidoamine
PBS	Phosphate buffered saline

PD	Pharmacodynamic
PD-10	Prepacked Sephadex G25 column
PDI	Polydispersity index
PEG	Poly(ethyl glycol)
PEI	Polyethylenimine
PGA	Polyglutamic acid
PK	Pharmacokinetic
pKa	Acid dissociation constant
PUMPT	Polymer-masked unmasked protein therapy
R <sup>2</sup>	Coefficient of determination
RI	Refractive index
RND	Resistance-nodulation-cell division
ROUT	Robust regression and Outlier removal
SANS	Small-angle neutron scattering
SD	Standard deviation
SEC	Size exclusion chromatography
SEM	Standard error of the mean
SMR	Small multidrug resistance
Sulfo-NHS`	N-hydroxysulfosuccinimide
TC <sub>50</sub>	50% of toxic concentration
TNF $\alpha$	Tumour necrosis factor alpha
TS	Tryptone soy
TSA	Tryptone soy agar
TTK	Time-to-kill
TxRd	Texas Red
UV	Ultraviolet
UV/vis	Ultraviolet/visible
V <sub>b</sub>	Bed volume
V <sub>o</sub>	Void volume
WHO	World Health Organisation

# **Chapter 1**

## **General Introduction**

## 1.1 Introduction

Infections with multidrug-resistant (MDR) bacteria represent a significant cause of morbidity and mortality worldwide, accounting for more than 700,000 deaths annually (O'Neill, 2014, O'Neill, 2016, Zaman et al., 2017). The economic burden of antibiotic resistance and its associated productivity losses in Europe and the USA have been estimated to be 1.5€ billion and \$55 billion per annum, respectively (Gandra et al., 2014, Smith and Coast, 2013). Excessive use and misuse of antibiotics in human medicine, as well as in agriculture, animal husbandry and veterinary fields has contributed to a dramatic increase in antimicrobial resistance (**Figure 1.1**), the treatment of which, in turn, requires high doses of multiple antibiotics that can cause serious toxicity and death (Zaman et al., 2017). The lack of development of new therapeutics to treat MDR bacterial infections, especially those caused by Gram-negative bacteria, is a major clinical challenge. As highlighted by the World Health Organisation (WHO), carbapenem-resistant *Acinetobacter baumannii* (*A. baumannii*) and *Pseudomonas aeruginosa* (*P. aeruginosa*), as well as extended spectrum  $\beta$ -lactamase-producing and carbapenem-resistant *Klebsiella pneumoniae* (*K. pneumoniae*) and *Escherichia coli* (*E. coli*) are the biggest threats to public health (WHO, 2017). Infections caused by MDR pathogens are not only associated with poor patient prognosis, high healthcare costs, elevated morbidity and mortality rates, but also increased persistence and chronicity of infection due to bacterial tolerance and limited therapeutic options (Tanwar et al., 2014). The discovery of new antimicrobial agents, or chemical modification of existing antibiotics, is urgently required to potentiate treatment against these increasingly life-threatening infectious diseases.

Every year in the United States, more than 40 million people are prescribed antibiotics for respiratory tract infections, however, over 65% of these are inappropriately prescribed (Shapiro et al., 2014). As a result, the number of life-threatening MDR, as well as extensively- or pan-drug resistant infections is increasing, while development of novel antimicrobial agents is decreasing (Schäberle and Hack, 2014). More than 20 classes of novel antibiotics were marketed between 1940 and 1962 and this is therefore considered the

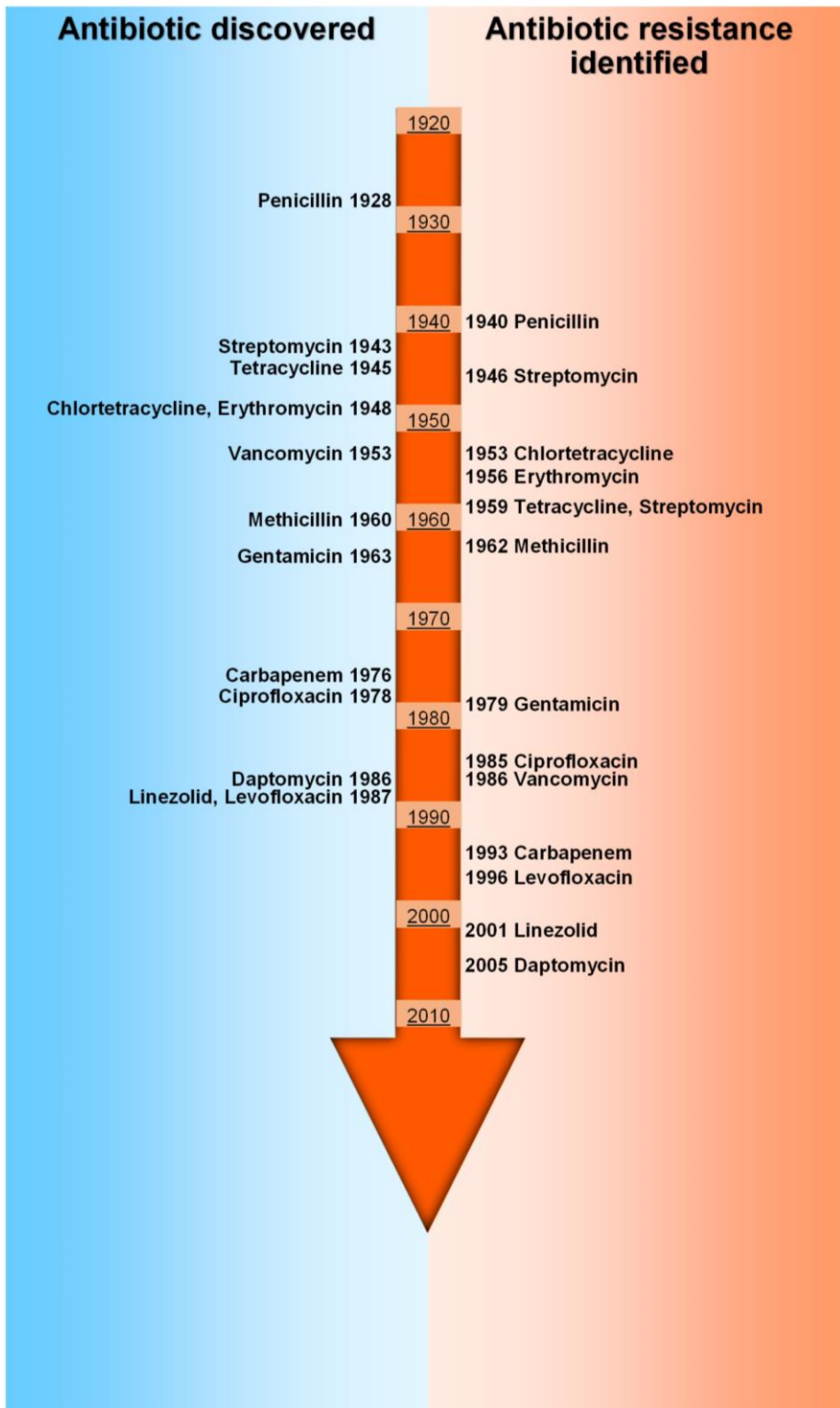


**Figure 1.1** A timeline of antimicrobial discovery and emergence of resistance. (Adapted from Ventola, 2015).

'golden era' of antibiotic discovery (Zaman et al., 2017). Since then, many derivatives and analogues have been marketed, with only a few new classes of antibiotics approved for clinical use (Niranjana et al., 2018). To address the lack of innovative antimicrobial agents in the clinical development pipeline, Infectious Diseases Society of America (IDSA) launched the "10 × '20" initiative in 2010 to support the development of 10 new, safe and effective classes of systemic antibiotics by 2020 (IDSA, 2010). Unfortunately, the lack of diverse novel metabolic or structural targets, limited duration of therapy, inevitable emergence of resistance and escalation of the approval requirements during clinical trials have, not only substantially stifled advances in novel antimicrobial development, but also make antibiotic discovery financially unattractive (Coates et al., 2011, Fair and Tor, 2014). Less than 5% of total venture capital investment by the pharmaceutical companies was attributed to the research and development of novel antimicrobials between 2003 and 2013 (O'Neill, 2016). If the issue is not rapidly addressed, it is estimated that, by 2050, antimicrobial resistance could cause 10 million extra deaths each year, (more than currently caused by cancer), with costs to the world economy of \$100 trillion dollars (O'Neill, 2014). This further highlights the urgent need for alternative and efficient approaches to deliver antibiotics to the site of infection.

According to the Infectious Diseases Society of America, *Enterococcus faecium* (*E. faecium*), *Staphylococcus aureus* (*S. aureus*), *K. pneumoniae*, *A. baumannii*, *P. aeruginosa* and *Enterobacter* spp., referred to as the 'ESKAPE bacteria', are the main bacterial pathogens responsible for life-threatening hospital-acquired infections, especially amongst chronically ill or immunosuppressed patients (Boucher et al., 2009, Pendleton et al., 2013, Rice, 2008). Bacterial infections and airway inflammation are the main factors causing premature death in patients with chronic respiratory diseases such as cystic fibrosis or chronic obstructive pulmonary disease. Here, an altered ability to clear the thick accumulated mucus from the respiratory tract, along with chronic bacterial infections by Gram-negative MDR pathogens such as *P. aeruginosa*, *K. pneumoniae* and *E. coli*, lead to a decline in pulmonary function, and eventually, lung damage and death (Pritchard et al., 2016).

Cationic polypeptide antibiotics, such as colistin (polymyxin E) and polymyxin B, were isolated from *Paenibacillus polymyxa* in the 1940s. They exhibit a potent, detergent-like antimicrobial activity against Gram-negative bacteria, resulting in neutralisation of lipopolysaccharide (LPS), destabilisation of the outer membrane and leakage of the intracellular contents (Kádár et al., 2013). Despite initial widespread use of colistin after its discovery in 1947, serious adverse effects, such as nephrotoxicity and neurotoxicity, led to its use being discontinued in the 1970s (Gurjar, 2015, Stansly et al., 1947, Taneja and Kaur, 2016).

To overcome antibiotic resistance, this study aimed to develop new strategies to exploit the ability of alginate oligomers to potentiate (enhance) antibiotic treatment and impede bacterial adherence/biofilm development, by acting as stimuli-responsive carriers of polymyxins.

## **1.2 Antibiotics in clinical development**

Antibiotics can be classified based on their mode of action, bacterial spectrum, chemical structure or target site (Ullah and Ali, 2017). Typically, antibiotics listed in the same structural class share common characteristics of toxicity and efficacy and exhibit similar allergic patterns. The major structural classes of antibiotics are beta-lactams, aminoglycosides, tetracyclines, macrolides, fluoroquinolones, sulphonamides, glycopeptides and polypeptides (Etebu and Ariekpar, 2016). Antimicrobials can be classified as 'broad spectrum' if they are active towards both Gram-positive and Gram-negative bacteria, such as tetracyclines, or 'narrow spectrum' if they are only active against a specific type of bacteria, such as glycopeptides. The latter are preferable clinically, since they contribute less to the development of resistance. The polymyxin antibiotics target the cell envelope and are bactericidal, while other antimicrobials, such as azithromycin, inhibit protein synthesis and thus, bacterial growth and are bacteriostatic (Etebu and Ariekpar, 2016, Ullah and Ali, 2017). Antibiotics are generally designed to target fundamental metabolic and/or physiological functions in the bacteria. For example, penicillins, cephalosporins, carbapenems and bacitracin inhibit the biosynthesis of cell

wall peptidoglycan; tetracyclines and macrolides interfere with protein synthesis by binding to ribosomal subunit 30S or 50S, respectively; fluoroquinolones target DNA gyrase and inhibit DNA replication; sulphonamides act as competitive inhibitors of dihydropteroate synthase enzyme and thus, disrupt the folic acid synthesis; rifampicin interferes with bacterial RNA synthesis by inhibiting DNA-dependent RNA polymerase; and polymyxins disrupt the integrity of bacterial membrane (Etebu and Ariekpar, 2016, Ullah and Ali, 2017).

According to the WHO's latest report (May 2017), there are currently 51 antibiotics or combinations in clinical development trials. However, only 33 of them target the ESKAPE pathogens, and only 8 of them are defined as new therapeutic entities, assigned to a new class of antibiotics, or exhibit a novel mode of action. Although many antibiotics currently in clinical phase I trials are designed to target Gram-negative infections, most of them are chemical modifications of existing antibiotics, and target only a few bacterial pathogens with specific resistance mechanisms. Currently, murepavadin is one of the most innovative antibiotics in the clinical development pipeline since it exhibits a novel mechanism of action by binding to the LPS transport protein D in the outer membrane of Gram-negative bacteria and interfering with LPS translocation to the cell surface from the periplasm, which ultimately leads to bacterial death (Werneburg et al., 2012). It has been demonstrated that murepavadin has 8-fold more potent antimicrobial activity than colistin against a range of extensively drug resistant *P. aeruginosa* pathogens (Sader et al., 2018). Recently, the United States Food and Drug Administration (FDA) approved two new antibiotics for systemic use (WHO, 2017). In June 2017, delafloxacin, a fluoroquinolone antibiotic, which acts by inhibiting bacterial DNA gyrase and topoisomerase IV activity, was approved for the treatment of acute bacterial skin and skin structure infections caused by methicillin-resistant *Staphylococcus aureus* (MRSA), streptococci or staphylococcal species, *P. aeruginosa* and *Enterobacteriaceae* (Pfaller et al., 2018). In August 2017, vabomere, a combination of meropenem (a carbapenem) and vaborbactam (a novel  $\beta$ -lactamase inhibitor), was approved for severe urinary tract infections caused by carbapenem and third generation

cephalosporin resistant *Enterobacteriaceae* (Castanheira et al., 2016, Cho et al., 2018). Other examples of novel antibiotics in clinical development are summarised in **Table 1.1**. However, it is important to bear in mind that only ~14% of antibiotic candidates in Phase I clinical trials will ultimately be approved for clinical use (WHO, 2017).

### **1.3 Bacterial cell wall structure**

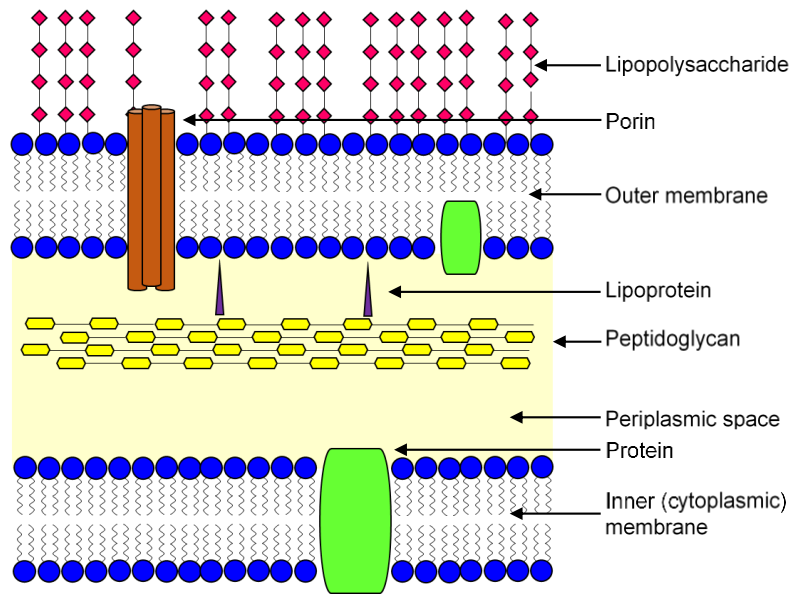
The complex and specialised structure of the bacterial cell envelope provides a first line defence mechanism against hostile environments (**Figure 1.2**), allowing the cell to regulate and limit entry of small toxic molecules, including many antibiotics (Silhavy et al., 2010). The bacterial cytoplasm is surrounded by a ~7.5 nm thick, semi-permeable inner (or cytoplasmic) membrane that is mainly comprised of phospholipids and proteins. Its role is to protect the intracellular contents from leakage and control the passage of secreted proteins or small molecules between the cytoplasm, periplasm and external space (Strahl and Errington, 2017). Importantly, many enzymes required for lipid biosynthesis, electron transport and oxidative phosphorylation are embedded in the inner (or cytoplasmic) membrane (Silhavy et al., 2010). The outer layer of cytoplasmic membrane is surrounded by a cell wall composed of peptidoglycan, which provides rigidity, shape and structure. Peptidoglycan is composed of crosslinked repeating units of N-acetylmuramic acid and N-acetylglucosamine residues, which protects the bacteria from osmotic lysis by its elasticity (Huang et al., 2008, Vollmer, 2008). Gram-positive bacteria are surrounded by many 30-100 nm thick peptidoglycan envelopes, which act as the main physiological defense mechanism due to lack of an outer membrane, while Gram-negative bacteria contain only a few relatively thin peptidoglycan layers (Silhavy et al., 2010). Gram-positive bacteria also contain polymers, such as teichoic acids or lipoteichoic acids, covalently linked to peptidoglycan or the outer layer of the cytoplasmic membrane, respectively, which, contribute to its negative surface charge and play a significant role in bacterial adherence to mucosal surfaces and pathogenesis (Malanovic and Lohner, 2016). In contrast, Gram-negative bacteria have an outer membrane which is non-covalently bound to lipoproteins, which, in turn, are covalently attached to the

**Table 1.1** Novel antibiotics against priority pathogens currently in the clinical development

<b>Antibiotic</b>	<b>Class</b>	<b>Phase</b>	<b>Mode of action</b>	<b>Reference</b>
Lefamulin	Pleuromutilin	III	Specifically binds to peptidyl transferase center of the 50S ribosome subunit and interferes with protein synthesis.	(Veve and Wagner, 2018)
Gepotidacin	Triazaacenaphthylene	II	Selectively binds to GyrA and ParC subunits of bacterial DNA gyrase or topoisomerase IV, respectively and therefore, inhibits the replication of bacterial DNA.	(Taylor et al., 2018b)
∞ Zoliflodacin	Spiropyrimidenetrione	II	Inhibits DNA biosynthesis through accumulation of double-stranded DNA cleavages and prevention of DNA re-ligation.	(Taylor et al., 2018a)
Brilacidin	Novel membrane targeting	II	Depolarises the bacterial cell wall and upregulates various regulons, chaperones and proteases, causing misfolding of the cytoplasmic proteins.	(Mensa et al., 2014)
Afabicin	FabI inhibitors	II	Selectively targets the FabI enzyme in the <i>Staphylococcus</i> genus and therefore, inhibits the fatty acid biosynthesis.	(Menetrey et al., 2017)

(a)

**Gram-negative bacteria**



(b)

**Gram-positive bacteria**

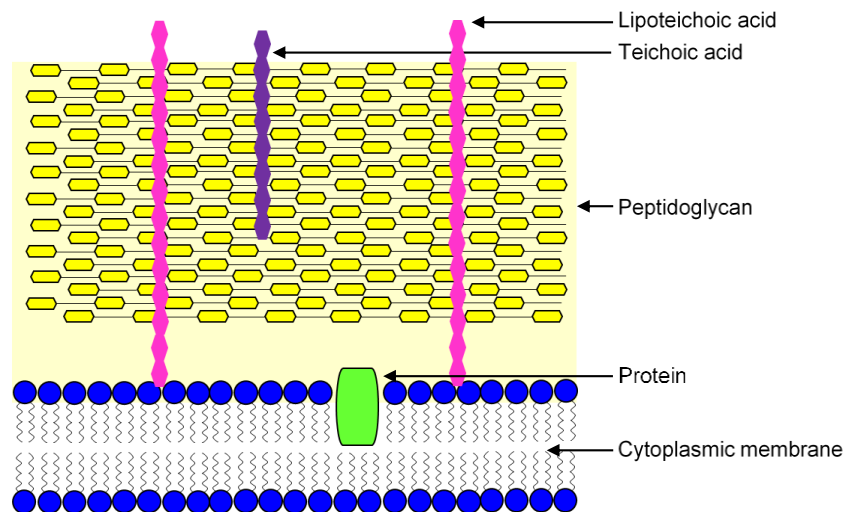


**Figure 1.2** Schematic diagrams of the cell envelope in (a) Gram-negative and (b) Gram-positive bacteria.

peptidoglycan layer. Since the peptidoglycan layer is permeable to most antimicrobial agents with molecular weights below ~50,000 Da, Gram-positive bacteria are more susceptible to antibiotic-mediated toxicity than Gram-negative pathogens (Lambert, 2002). The main constituent of the outer membrane of Gram-negative bacteria is a complex lipopolysaccharide (LPS) composed of lipid A (a disaccharide of glucosamine with 6-7 acyl chains), a polysaccharide core and a specific O-antigen polysaccharide (Erridge et al., 2002). LPS plays a critical role in endotoxic shock and permeability of the outer membrane, impeding the diffusion of hydrophobic molecules, while the presence of outer membrane transport proteins such as porins, restrict the diffusion of hydrophilic molecules with molecular weights larger than ~700 Da (Silhavy et al., 2010). Thus, the heterogeneity of LPS due to the structural diversity of O-antigen, and the effective permeability barrier of the outer membrane further complicate and limit the efficacy of currently available antibiotic options against the Gram-negative bacteria.

#### **1.4 Mechanisms of antibiotic resistance**

Many different mechanisms of resistance against antimicrobial drugs have been identified (**Figure 1.3**), including biofilm formation, expression of resistance genes that cause reduced uptake and increased efflux of antibiotics, production of enzymes that cause covalent modification of the drug or an altered version of the substrate, and several bacterial phenotypic states such as persistence and swarming, all of which result in reduced antibiotic activity (Brauner et al., 2016, Corona and Martinez, 2013, Levin and Rozen, 2006, Munita and Arias, 2016). The rate of antimicrobial resistance depends on many factors including mechanism of action and efficacy of the drug, duration of antibiotic exposure and patient compliance. The latter is particularly important for antibiotics with a short plasma half-life as they require more frequent administration, and inadequate doses will be unable to eradicate the bacterial pathogen (Li et al., 2017).

Acquisition of antibiotic resistance arises from spontaneous gene mutation or by horizontal gene transfer among bacterial pathogens or other species using

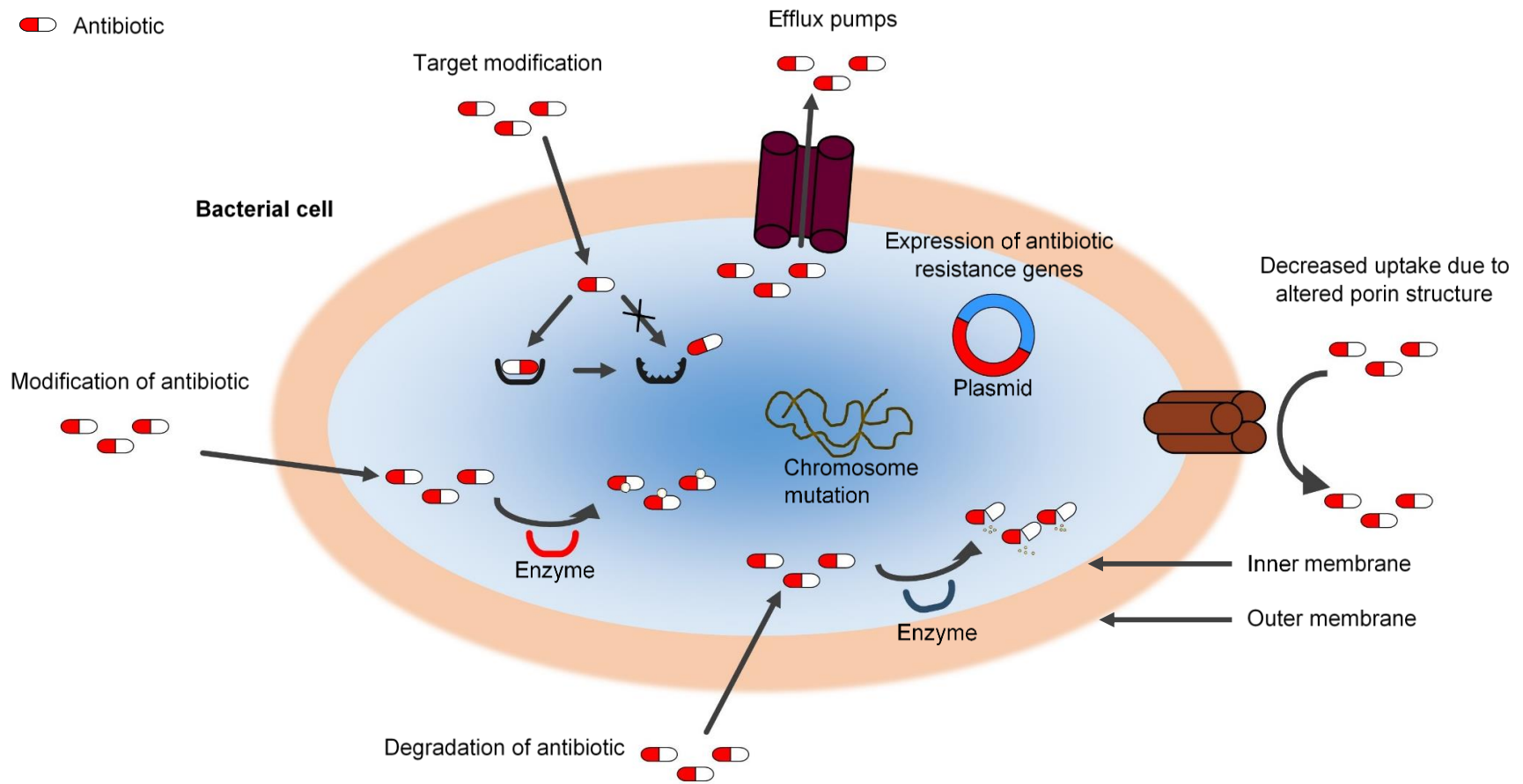


**Figure 1.3** Schematic representation of different mechanisms of antibiotic resistance.

mobile genetic elements such as plasmids, transposons, integrons and bacteriophages (Giedraitienė et al., 2011). Antimicrobial resistance caused by spontaneous chromosomal mutations due to errors in DNA replication or faulty repair of damaged DNA is quite rare, usually occurring only once in a population of  $10^6$ - $10^8$  microorganisms, yet it contributes to cross-resistance of structurally similar antibiotics (Hooper, 2001). Dissemination of antimicrobial resistance genes between bacteria occurs via main three pathways: i) conjugation, via hair-like structures called pili, ii) transformation, by incorporation of free DNA from “dead” or degraded bacteria into the cytoplasm and the recipient’s own DNA, and iii) transduction, using bacteriophage carriers to infect a recipient bacterial cell with antimicrobial-resistant viral DNA, causing the bacteria to produce more copies of infecting bacteriophages or incorporate the viral DNA into its genome (Harbottle et al., 2006).

Although polymyxin resistance rates are still relatively low due to their limited utilisation over the past 50 years, an increasing number of colistin or polymyxin B resistant bacterial isolates are being identified (Ko et al., 2017). One of the most common strategies of polymyxin resistance in Gram-negative bacteria is the overexpression of efflux pumps. There are five main families of bacterial antibiotic efflux pumps: i) the ATP-binding cassette (ABC) superfamily, which utilises energy produced from ATP hydrolysis. The other efflux pumps use proton or sodium gradients as an energy source and include: ii) the major facilitator superfamily (MFS), iii) the small multidrug resistance (SMR) family, iv) the resistance-nodulation-cell division (RND) family and v) the multidrug and toxic compound extrusion (MATE) family (Kumar and Schweizer, 2005). Multidrug resistant *E. coli* express more than nine proton-dependent efflux pumps which confer resistance to at least two different classes of antibiotics (Viveiros et al., 2007). Highly specific efflux systems belonging to the MFS family, such as Tet efflux pumps, extrude only tetracyclines in several bacterial species, while other efflux pumps such as AcrAB-TolC and MexAB-OprM, belonging to the RND family, contribute to multidrug resistance in *Enterobacteriaceae* and *P. aeruginosa*, respectively (Li et al., 2015). Tolerance to colistin has been identified in *P. aeruginosa* biofilms as being due to increased expression of *pmr*-mediated lipopolysaccharide modification and

*mexAB-OprM*-mediated efflux (Pamp et al., 2008) whilst resistance to polymyxin B in *Yersinia* species has been shown to be mediated by the efflux pump/potassium antiporter system (RosAB) (Bengoechea and Skurnik, 2000). Furthermore, the AcrAB efflux system was shown to contribute to polymyxin B resistance in *K. pneumoniae* and *E. coli* (Padilla et al., 2010, Warner and Levy, 2010).

Degradation of antibiotics results in elimination of reactive functional groups or structural rearrangement of the molecule. More recently, identification of New Delhi metallo- $\beta$ -lactamase-1 (NDM-1) in Gram-negative *Enterobacteriaceae* has been shown to be associated with high resistance to  $\beta$ -lactams, aminoglycosides and fluoroquinolones, but not colistin or tigecycline (Kumarasamy et al., 2010). Previously, a colistin-inactivating enzyme, colistinase, was reported in *Bacillus polymyxa* that caused selective hydrolysis of the peptide bond between the two diaminobutyric acid residues at positions 3 and 4 (Ito-Kagawa and Koyama, 1980). However, no recent reports have been published regarding colistinase activity.

Another widespread mechanism of resistance that affects a range of different classes of antibiotics is alteration of the target site, which weakens antibiotic-substrate binding. The loss of negative surface charge due to covalent attachment of aminoarabinose residues to the phosphate group of the LPS lipid A moiety in Gram-negative bacteria, causes a lower affinity between positively charged polymyxins and the bacterial outer membrane and therefore, contributes to resistance to polypeptide antimicrobials (Gunn et al., 1998, Kline et al., 2008). Similarly, the incorporation of a D-alanine residue into teichoic acids embedded in the Gram-positive bacterial cell wall causes resistance to cationic antimicrobial peptides (Peschel et al., 1999). Resistance of MDR *A. baumannii* to polymyxins was associated with modification of the lipid A component with phosphoethanolamine or galactosamine residues, causing the complete loss of LPS from the outer membrane (Cheah et al., 2016). In addition, overproduction of capsular polysaccharide in *K. pneumoniae* limited the interaction of polymyxin B with the bacterial cell surface thereby promoting emergence of resistance (Campos et al., 2004).

Until recently, polymyxin resistance was conferred by chromosomal mutations, but the discovery and dissemination of plasmid-mediated resistance genes (*mcr*) which encode phosphoethanolamine transferases (Chapter 4), has caused worrying concerns (Xu et al., 2018). Since the first report of the colistin resistance gene *mcr-1* from *E. coli* isolates in China (Liu et al., 2016), seven other *mcr* homologs have so far been characterised (Wang et al., 2018). Many different plasmids have been identified, including IncI2 or IncFII plasmids harbouring colistin resistance genes *mcr-7.1* and *mcr-8* in *K. pneumoniae*, respectively (Wang et al., 2018, Zhang et al., 2018), IncX4 plasmids facilitating the dissemination of *mcr-1* and *mcr-2* in *E. coli* (Bai et al., 2018, Xavier et al., 2016) or IncP and IncHI2 plasmids carrying *mcr-1* in *K. pneumoniae*, and *E. coli* bacteria (Zhao et al., 2017a, Zurfluh et al., 2016). The *mcr-2* gene was identified with 77.3% nucleotide sequence homology to *mcr-1*, while *mcr-3*, with 45% and 47% nucleotide identity to *mcr-1* and *mcr-2* colistin resistance genes, respectively (Xavier et al., 2016, Yin et al., 2017). Recently, *mcr-7.1* and *mcr-8* genes were identified in *K. pneumoniae* of animal origin and in patients with respiratory tract infections, respectively (Wang et al., 2018, Yang et al., 2018). This further highlights the importance of exploring the alternative and complementary approaches of targeted antimicrobial delivery to combat the potential risk of antimicrobial resistance crisis.

#### 1.4.1 Biofilms

Biofilms are complex bacterial communities that exhibit up to 1,000 times higher resistance/tolerance to antimicrobial agents compared to planktonically growing isogenic forms and therefore, can significantly contribute to the severity and persistence of infections (Potera, 2010). Bacteria within the biofilm are protected from accumulation and penetration of inflammatory cells, antibodies, disinfectants, antimicrobial drugs and environmental factors such as changes in pH or temperature (Vatansever and Turetgen, 2018).

Typically, bacterial biofilms form in several distinct reversible and irreversible stages (**Figure 1.4**). First, a conditioning layer, composed of various organic and organic particles, forms on solid surfaces, such as host tissue or medical

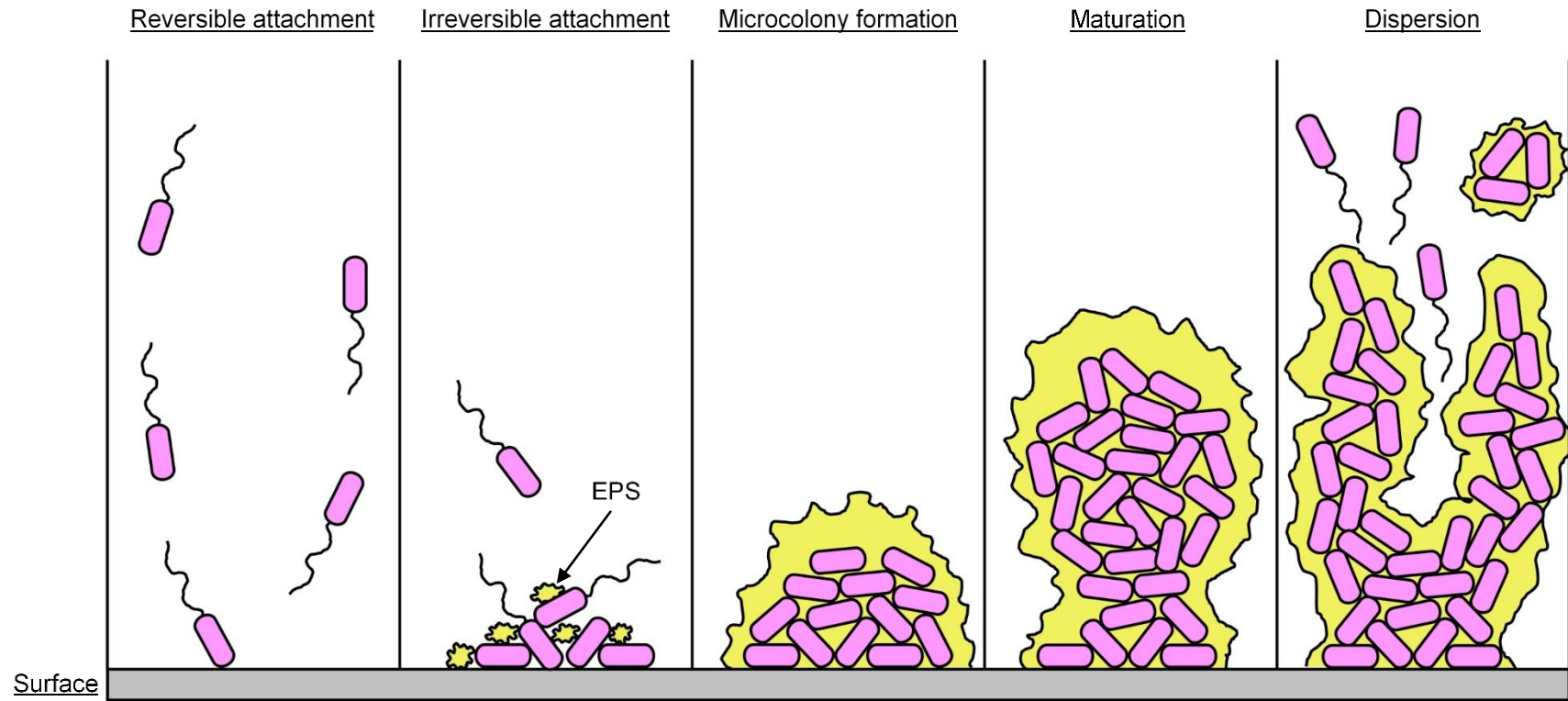


**Figure 1.4** Schematic representation of biofilm formation stages. (EPS, extracellular polymeric substance).

appliance including catheters, implants or contact lenses (Donlan, 2002, Garrett et al., 2008, Lorite et al., 2011). This layer (film) is believed to influence modifications to the surface charge as well as surface tension and surface potential, inducing attachment and providing the nutrient source for the bacteria (Donlan, 2002). The initial reversible adhesion of planktonic bacterial cells to the conditioning layer involves only a fraction of cells and therefore, is driven by gravitational and hydrodynamic forces (Kostakioti et al., 2013). The availability of nutrients, ionic strength, temperature and pH are main factors influencing bacterial attraction or repulsion behaviour (Garrett et al., 2008).

Flagella-mediated motility of *P. aeruginosa* and *E. coli* has been associated with improved adhesion to the conditioning layer as well as the ability to overcome repulsive and hydrodynamic forces (Pratt and Kolter, 1998, Toutain et al., 2007). The physical forces that mediate bacterial attachment include van der Waals forces, electrostatic and steric interactions (Marshall, 1986). A fraction of attached planktonic bacteria become irreversibly immobilised, suggesting the involvement of hydrophobic/hydrophilic interactions between the bacteria and the surface (Liu et al., 2004). As the bacterial cells multiply and divide by binary division, cell signalling, (defined as quorum sensing), between the bacteria triggers changes in gene expression that initiates the formation of microcolonies and secretion of a protective matrix consisting of extracellular polymeric substance (EPS) (Chapter 6), which eventually covers the bacterial community (Jamal et al., 2018). The expression of cell surface proteins allows for the transportation and excretion of various polysaccharides and therefore, along with divalent cations, induces strong cross-linking between the cells, conferring to mechanical stability of the biofilm (Garrett et al., 2008). Eventually, the dispersal of small parts of the biofilm or the release of individual or groups of planktonic bacteria into host environment allows for bacteria to travel and re-colonise a new surface, thereby starting a whole new cycle of biofilm formation. It has been suggested that bacteria dispersed from biofilms have a unique, transitional phenotype and therefore might retain levels of virulence that can be significantly more pathogenic than their planktonic counterparts (Uppuluri and Lopez-Ribot, 2016).

## 1.5 Modification of polymyxin

The lack of novel therapeutics to combat MDR bacterial infections has forced researchers to consider alternative strategies, such as modification of the chemical structure of existing antibiotics (Cotter et al., 2012, Fernandes, 2006). More recently, in an attempt to tackle MDR bacteria, polymyxins have been used as 'drugs of last resort' for the primary treatment of life-threatening conditions, such as lung and burn wound infections caused by *A. baumannii*, *P. aeruginosa* and *Enterobacteriaceae* (Azzopardi et al., 2013a, Falagas et al., 2005, Hashemi et al., 2017, Nikola et al., 2015). Nevertheless, issues of severe dose-limiting toxicity remain. Thus, a number of strategies have been explored to reduce the nephrotoxicity and optimise the activity of polymyxins, mainly by focusing on structural modifications of the N-terminal fatty acyl moiety and Dab side chains, as summarised in **Table 1.2**. However, none of these polymyxin derivatives, has as yet, progressed further in clinical development trials due to either a too narrow spectrum of antimicrobial activity or inconsistent cytotoxicity results and poor tolerability observed in animal studies (Velkov et al., 2016).

Systemic administration of conventional low molecular weight antibiotics is commonly associated with an inadequate volume of distribution, short plasma half-life, systemic toxicity, lack of target specificity, emergence of bacterial resistance and therefore, requires high daily doses to reach effective therapeutic activity *in vivo* (Miao et al., 2018). Thus, modification of the antibiotic to improve drug delivery may offer many potential therapeutic benefits over conventional small molecule antibacterial agents, including improved solubility, bioavailability and decreased toxicity due to controlled release of the antibiotic at the sites of infection or inflammation (Larson and Ghandehari, 2012).

## 1.6 Nanomedicines as novel antibiotic therapies

In recent years, nanomedicines have gained a great deal of attention in the field of drug delivery, mainly due to the unmet clinical need for new drugs to treat life-threatening conditions, such as infectious diseases. The field of

**Table 1.2** Examples of polymyxin derivatives currently in clinical development.

Polymyxin derivative	Modification of polymyxin molecule	Observations	Reference
CB-182,804	Substitution of N-terminal fatty acyl moiety by an aromatic urea	Toxicity of the polymyxin B derivative ( $EC_{50} > 1000 \mu\text{g/ml}$ ) was substantially lower compared to the parent compound ( $EC_{50} = 318 \mu\text{g/ml}$ ) in rat kidney proximal tubular cells but exhibited similar or slightly less potent antimicrobial activity.	(Leese, 2010)
5x	Substitution of (Dab) amino acid residue by diaminopropanoic acid (Dap) at position 3	The compound demonstrated an improved antimicrobial activity against polymyxin resistant clinical isolates and reduced cytotoxicity ( $TC_{50} > 100 \mu\text{M}$ ) compared to polymyxin B ( $TC_{50} = 22 \mu\text{M}$ ) in HK-2 cells. However, it lacked an improved therapeutic index <i>in vivo</i> .	(Magee et al., 2013)
Compounds 12 and 18	Incorporation of an ester bond to link fatty acyl tail with the peptide	Both compounds demonstrated desired antimicrobial efficacy and a significant reduction in cytotoxicity ( $IC_{50} > 200 \mu\text{M}$ ) compared to polymyxin B ( $IC_{50} = 82 \mu\text{M}$ ) in HK-2 cells. A decrease in <i>in vivo</i> nephrotoxicity of both analogues was also confirmed by low levels of urine biomarker such as neutrophil gelatinase-associated lipocalin in a rat model.	(Gordeev et al., 2016)
CA824, CA900, CA1049	Modification of N-terminal fragments	All analogues exhibited potent antimicrobial activity against Gram-negative bacteria and were significantly less cytotoxic ( $IC_{50} = 148, 167$ and $64 \mu\text{g/ml}$ for CA824, CA900 and CA1049, respectively) compared to polymyxin B ( $IC_{50} = 15 \mu\text{g/ml}$ ) in HK-2 cells.	(Wiederhold et al., 2015)

$EC_{50}$ , 50% effective concentration;  $TC_{50}$ , 50% of toxic concentration,  $CC_{50}$ , concentration of the 50% cytotoxic effect;  $IC_{50}$ , half maximal inhibitory concentration. HK-2, human kidney proximal tubule cells.

Table 1.2 (continued).

Polymyxin derivative	Modification of polymyxin molecule	Observations	Reference
NAB739	Removal of 2 Dab amino acid residues	The polymyxin B derivative containing only three cationic amine groups retained antimicrobial activity against <i>E. coli</i> but not against <i>P. aeruginosa</i> and <i>A. baumannii</i> . The derivative was significantly less nephrotoxic than the parent drug, leading to an up to 7-fold decrease in binding to brush border membrane isolated from rat kidney. Cytotoxicity of the compound was 26-fold lower (IC <sub>50</sub> = 337 µg/ml) compared to polymyxin B (IC <sub>50</sub> = 13 µg/ml) and 7.5-fold lower compared to colistin (IC <sub>50</sub> = 45 µg/ml) in HK-2 cells.	(Vaara and Vaara, 2013, Vaara et al., 2008)
19 Compounds 10, 14, 15 and 38	Replacement of fatty acyl tail with biphenyl or biphenyl ether (compounds 10, 14 and 15) or Dab residue substitution with glycine at position 3 (compound 38)	All demonstrated promising antimicrobial potency. Compounds 10 (CC <sub>50</sub> = 298 µM and 297 µM), 14 (CC <sub>50</sub> = 287 µM and 296 µM), 15 (CC <sub>50</sub> = 316 µM and > 300 µM) and 38 (CC <sub>50</sub> = > 300 µM) exhibited similar or greater cytotoxicity in human hepatocyte carcinoma cells (HepG2) and human embryonic kidney cells (HEK293; respectively) compared to polymyxin B (CC <sub>50</sub> = >300 µM). <i>In vitro</i> nephrotoxicity assays measuring lactate dehydrogenase and γ-glutamyl transferase release in HK-2 cells demonstrated that compounds 10, 14, 15 (CC <sub>50</sub> = > 128 µM/ml) and 38 (CC <sub>50</sub> = 122 µM/ml and > 128 µM/ml) were less or similarly nephrotoxic compared to polymyxin B (CC <sub>50</sub> = 23 µM/ml and 177 µM/ml), respectively.	(Gallardo-Godoy et al., 2016)
PEG-colistin	PEG-modified colistin	The PEG-colistin conjugate demonstrated good antimicrobial activity <i>in vitro</i> and reduced toxicity of colistin in mice. The latter caused degeneration and necrosis of renal tubular cells.	(Zhu et al., 2017)

'nanomedicine' is defined by the European Science Foundation (ESF) as 'the science and technology of diagnosing, treating and preventing disease and traumatic injury, of relieving pain, and of preserving and improving human health, using molecular tools and molecular knowledge of the human body (ESF, 2005). Nanomedicines have also been defined as nanometre-sized, complex systems composed of at least two components, one being the active ingredient. They are divided into different groups based on their physico-chemical features and size range, and include liposomes, micelles, dendrimers, nanoparticles, nanocrystals and polymer therapeutics (Choi and Han, 2018). By 2016, fifty-one nanomedicines had been approved by the FDA (Choi and Han, 2018).

### **1.6.1 Polymer therapeutics**

Duncan coined the term 'polymer therapeutics' to describe a class of nanosized therapeutic agents comprising a water-soluble polymer, which may be bioactive in its own right or covalently attached to an active constituent, such as a drug, protein, peptide or gene (Duncan, 2003). Polymer therapeutics encompasses many structures, including polymeric drugs, polymer-protein conjugates, polymer-drug conjugates, polymeric micelles and polyplexes (**Figure 1.5**). Polymeric drugs are natural or synthetic polymers with inherent biological activity. Polymeric micelles are self-assembling polymeric structures with drug attached at the core via a covalent bond, while polyplexes are multicomponent polyelectrolyte complexes that are used for DNA transfer (Duncan, 2003). Polymer-protein conjugates have protein attached to one or more water-soluble polymeric chains through a spacer group, and lastly, polymer-drug conjugates contain a water-soluble polymer and bioactive drug attached through a covalent bond via a spacer group. Thus, polymer therapeutics are often defined as new chemical entities rather than the traditional drug delivery systems, which makes them very attractive to the pharmaceutical industry (Vicent et al., 2009).

Polymer therapeutics are the most successful class of nanomedicines, with fifteen products currently in clinical use (Duncan, 2014, Duro-Castano et al.,

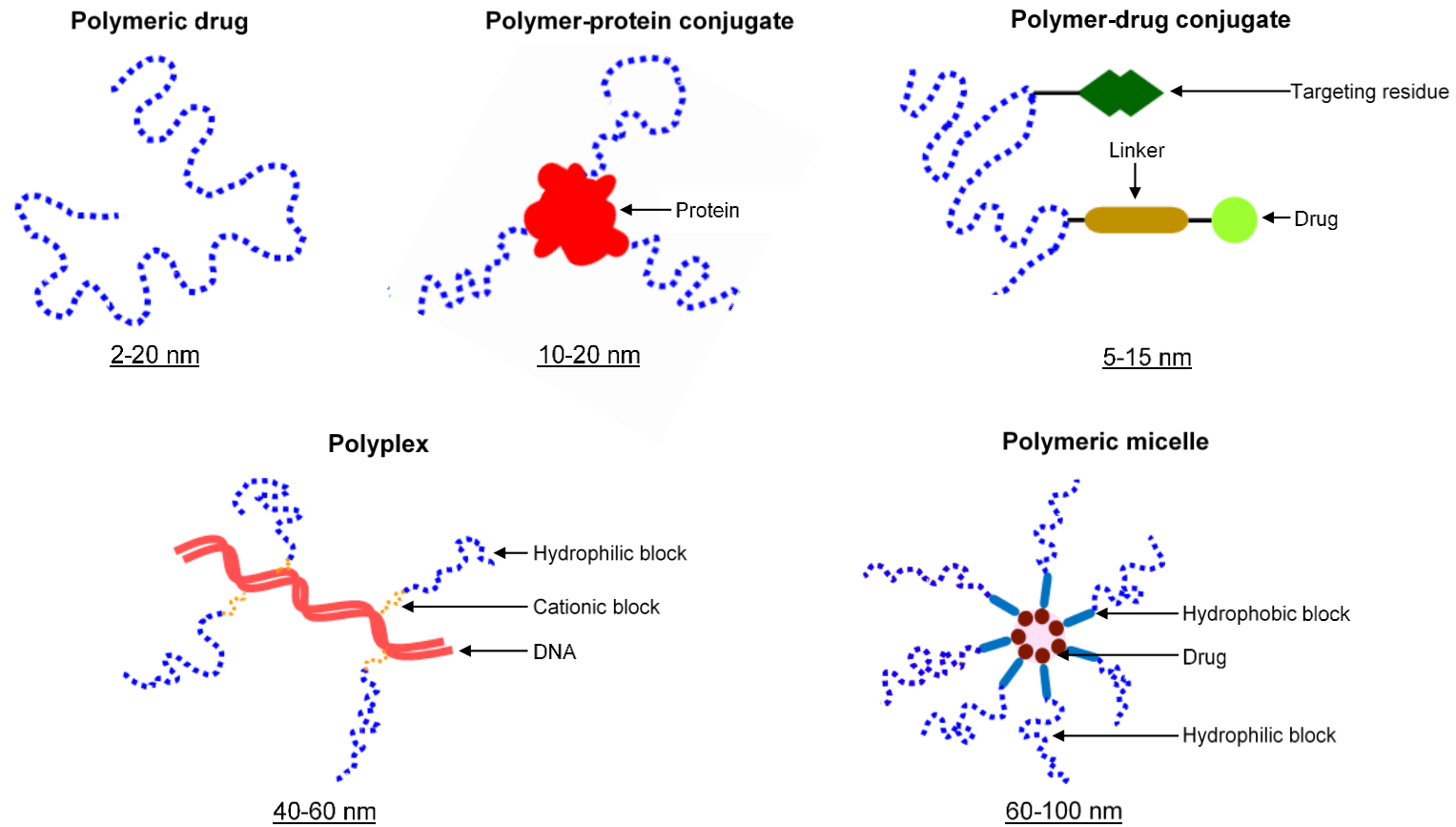


**Figure 1.5** Schematic representation of polymer therapeutics including polymeric drugs, polymer-protein conjugates, polymer-drug conjugates, polyplexes and polymeric micelles. (Adapted from Duncan, 2003).

2015). The first polymer therapeutic approved by the FDA for clinical use was a polyethylene glycol (PEG)-adenosine deaminase (Adagen<sup>®</sup>) conjugate for the treatment of severe combined immunodeficiency (Levy et al., 1988). PEG-filgrastim (an analogue of recombinant granulocyte colony-stimulating factor) conjugate (Neulasta<sup>®</sup>), for the treatment of neutropenia in chemotherapy patients, and glatiramer acetate (Copaxone<sup>®</sup>), a random copolymer composed of glutamate, lysine, alanine and tyrosine residues, for patients with relapsing-remitting multiple sclerosis, are already two of the ten most profitable drugs in the United States (Duncan, 2014, Lambertini et al., 2015, Scott, 2013). Currently, PEG-naloxegol (Movantik<sup>®</sup>) is the only polymer-drug conjugate approved by FDA (Duncan, 2017, Ekladius et al., 2018, Floettmann et al., 2017). Despite the success of polymer therapeutics, especially PEGylated protein conjugates, progression of polymer-drug conjugates to the market has been very slow, mainly due to poor rational design and lack of suitable polymeric carriers (Canal et al., 2011, Duro-Castano et al., 2015, Vicent et al., 2008).

The idea of using natural or synthetic macromolecules as drug carriers was first proposed by Jatzkewitz in the 1950s. Using a dipeptide spacer to attach polyvinylpyrrolidone to mescaline, Ushakov and his team synthesised the first water-soluble polymer-drug conjugates in the following years (Givental et al., 1965, Jatzkewitz, 1955). The first polymer-drug conjugate designed to reduce toxicity and improve drug efficacy and target specificity was proposed by Ringsdorf in 1975 (Ringsdorf, 1975). It contained a biocompatible polymer backbone, a covalently bound drug attached by a linker group, a targeting moiety and a solubilising agent to ensure water solubility. The proposed model offered many advantageous features to the field of drug delivery compared to low molecular weight drugs, mainly by improving drug pharmacokinetic properties. Drug plasma half-life and bioavailability can also be drastically improved, which is particularly important since more than 40% of drugs in clinical development have poor bioavailability due to low aqueous solubility (Lipinski, 2002). For instance, the hydrophobicity and high systemic toxicity of paclitaxel was reduced by covalent conjugation to polyglutamic acid (Chipman et al., 2006). What is more, drug conjugation to a water-soluble polymer can

significantly improve bio-distribution and targeting due to the enhanced permeability and retention (EPR) effect, mask immunogenicity, enhance cellular uptake, reduce systemic toxicity and prevent enzymatic degradation, especially of proteins or peptides (Xiong et al., 2014).

### **1.6.2 Enhanced permeability and retention effect**

The EPR effect was first reported in cancer patients by Matsumura and Maeda in 1986 as a promising mechanism for targeted delivery of chemotherapeutic agents. Accumulation of the anti-tumour protein neocarzinostatin conjugated to a styrene and maleic acid copolymer (SMANCS) was found to be significantly higher in tumours than in healthy tissues (Matsumura and Maeda, 1986). In the following years, evidence of the EPR phenomenon in infectious diseases was also proposed, although it was still not fully exploited for passive targeting of antibiotics (Maeda et al., 1999). Conventional low molecular weight drugs distribute indiscriminately throughout the body, diffuse through vasculature and internalise inside both, healthy and diseased tissues, leading to an inadequate volume of distribution, lack of target specificity and toxicity. Importantly, the endothelium of healthy blood vessels is almost impermeable to larger macromolecules, thus restricting their entry to tissues almost exclusively via gaps in “leaky” veins/arteries (Markovsky et al., 2012). The characteristic features of tumour tissues, which allow preferential accumulation of macromolecules, include a disorganised vasculature, discontinuous endothelium, high vascular density, angiogenesis and elevated levels of vascular permeability mediators, while defective lymphatic drainage enables conjugate retention at the target site (Maeda et al., 2000, Maeda, 2013). A variety of other pathological conditions such as diabetes, thrombosis, atherosclerosis, asthma and infections have also been characterised by excessive angiogenesis since they share a similar microenvironment and inflammatory features with tumours (Fiedler and Augustin, 2006). More recently, Azzopardi et al. (2013) described the presence of an EPR effect in infection, permitting passive accumulation of macromolecular conjugates at sites of infection due to increased vascular permeability. Ongoing inflammation, remodelling and angiogenesis, along with increased interstitial

tissue pressure and destruction, further enhance macromolecule retention at the infected site (Azzopardi et al., 2013b). The principle of the EPR effect is shown in **Figure 1.6**.

The feasibility of the EPR effect for targeted antimicrobial delivery has been proven in several studies. Following intravenous injection in rats, PEGylated liposomes containing gold were preferentially localised in tissues infected with *S. aureus* (Laverman et al., 2001). Additionally, 2 hours after intravenous administration of technetium<sup>99</sup>-labelled ubiquicidin conjugated to poly(ethylene glycol)-N-(N-(3-diphenylphosphinopropionyl) glyceryl)-S-trityl-cysteine (PEG-PN<sub>2</sub>S) in mice, accumulation of the conjugate was observed at the site of *S. aureus* infection (Meléndez-Alafort et al., 2009).

### **1.7 Polymeric carrier**

The ideal polymeric carrier for antibiotic conjugation should be water-soluble, non-toxic, non-immunogenic, biodegradable and contain suitable functional groups for drug attachment. The backbone of the polymeric carrier determines the pharmacodynamic and pharmacokinetic properties of the drug, while the structure, molecular weight, polydispersity, charge and hydrophilicity are the main features of the polymer which contribute to the drug loading, solubility, elimination, distribution and toxicity (Markovsky et al., 2012). Many different polymers have been used in drug conjugation including PEG, N-(2-hydroxypropyl) methacrylamide (HPMA) copolymer, polyglutamic acid (PGA) and natural polysaccharides, such as dextrin and chitosan (Gaspar and Duncan, 2009). Although the most successful polymeric carriers that entered trials in clinical development were non-biodegradable, such as PEG and HPMA copolymer, increased awareness of the potential safety implications of chronic administration and high doses is required (Duncan, 2009, Schütz et al., 2013, Swierczewska et al., 2015). Toxic accumulation of non-biodegradable polymers may occur if their molecular weight exceeds the renal threshold, which may result in lysosomal storage disease or intracellular vacuolation (Duncan, 2017, Markovsky et al., 2012). Consequently, researchers are increasingly turning to biodegradable polymers for conjugation

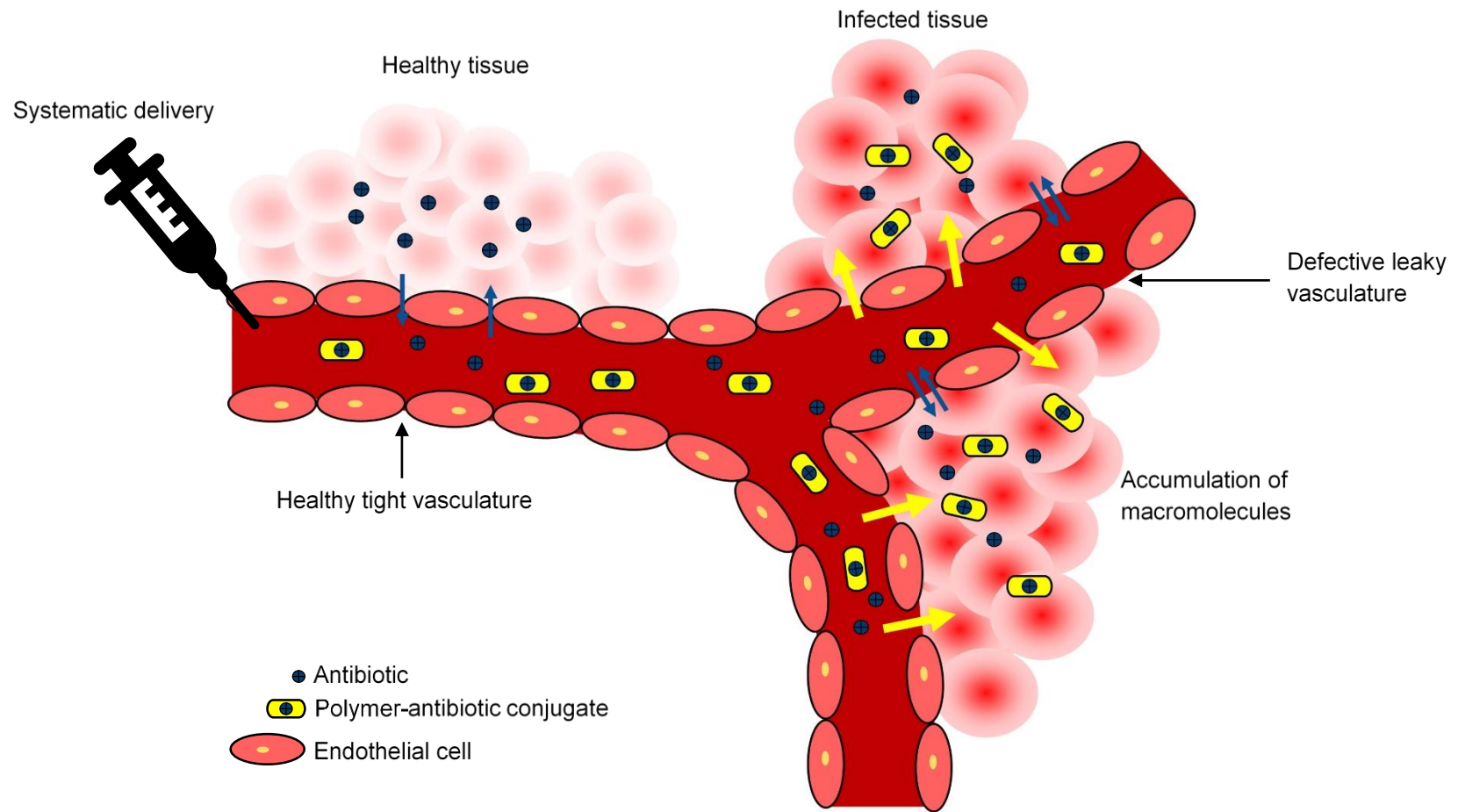


**Figure 1.6** Schematic representation of localisation of the polymer-antibiotic conjugates.

of bioactive molecules. Due to its biodegradability and high primary amine content, low molecular weight chitosan has been used to enhance the delivery of orally administered insulin, leading to increased bioavailability and intestinal absorption of the peptide (Lee et al., 2010). In addition, thanks to the presence of  $\alpha$ -amylase in plasma and in extracellular fluids, dextrin is also commonly exploited for controlled release of protein and peptide drugs due to its biocompatibility and biodegradability (Gaspar and Duncan, 2009). Since dextrin lacks a convenient amino or carboxyl groups, functionalisation is required to couple it with bioactive substances. However, increasing the degree of chemical modification of dextran was found to decrease the rate of biodegradability of the polymer, so this must be carefully controlled (Vercauteren et al., 1990).

### **1.7.1 Alginates**

This study proposed that alginates may also be successfully and safely exploited for drug delivery, as they possess many favourable features. Alginates are naturally-occurring polysaccharides, non-toxic and non-immunogenic, whose physical and biological properties can be controlled by tailoring their size and composition. Alginates are linear copolymers composed of  $\beta$ -D-mannuronic acid (M) and  $\alpha$ -L-guluronic acid (G) residues that are linked by 1-4 glycosidic bonds and exhibit a stereochemical difference at the C-5 position (Draget and Taylor, 2011). The monomers are arranged into various lengths and distributions of polymeric blocks of repeating M, G or mixed MG residues which define the physicochemical characteristics of the polysaccharide. In this way,  $\beta$ -(1-4) linkages formed by mannuronic acid residues lead to a more flexible, linear conformation of M-blocks, whereas guluronic acid forms an  $\alpha$ -(1-4) bond, which results in the folded, more rigid and stiff G-block structure (Yang et al., 2011). The distribution and quantity of M and G residues in the resulting alginate can vary significantly between the species of brown algae used, which part of the plant is used (leaves or stems) and is highly dependent on the growth conditions of the seaweed.

Most commercially produced alginates are extracted from brown seaweed

such as *Macrocystis*, *Laminaria* and *Ascophyllum* species (Qin, 2008). Naturally, alginate exists as calcium, sodium, magnesium or even potassium salts which can be converted into water-soluble sodium alginate when treated with alkali solutions such as sodium hydroxide followed by further filtration and precipitation by calcium chloride (Qin, 2008). Bacterial sources also exist, with *Pseudomonas* and *Azotobacter* spp. able to produce the exopolysaccharide alginates during their normal growth cycles. Typically, the molecular weight of alginate is between  $10^5$ - $10^6$  Da, equivalent to 500-5000 residues per chain. However, alginates isolated from bacteria are often larger (Andersen et al., 2012). The physical properties of alginates, such as viscosity, are highly dependent on molecular size. Since alginates are polydisperse and their chains vary in size and composition, low molecular weight alginates are typically prepared by hydrolysis using a weak acid, such as hydrochloric acid (Andersen et al., 2012).

While polysaccharides are generally considered to be biodegradable, not all of them are broken down by mammalian enzymes. For example, alginate is readily degraded by alginate lyases, which are secreted by many species including marine algae, marine molluscs, and a wide range of microorganisms. However, alginate is inherently non-degradable in mammals since they do not produce the enzyme to digest the polymer chains (Wong et al., 2000). Since commercially available alginates have a molecular weight above the renal threshold, they may not be completely removed from the body following systemic administration (Al-Shamkhani and Duncan, 1995), which could be problematic for alginate-protein conjugates designed to treat chronic conditions. Studies have shown that mouse and human phagocytic cells were unable to degrade bacterial alginate due to inadequate enzymatic and free radical capacities (Simpson et al., 1993). These findings suggest that, after endocytosis of alginate conjugates, lysosomal glucosidases, esterases and proteases may not be capable of degrading the polymer. Therefore, Yang et al. (2011) developed sulfation, oxidation, amidation and esterification methods to modify the free hydroxyl and carboxyl groups of alginates, thereby rendering the polymer degradable. For example, oxidation of the hydroxyl groups of alginate with sodium periodate led to complete polymer degradation at

physiological conditions after 100 h (He et al., 2005). The optimal stability of alginate chains is around pH 6. Thus, depolymerisation of alginate biomaterials occurs *in vivo* under physiological conditions at pH 7.4 by spontaneous  $\beta$ -elimination (Andersen et al., 2012). At sites of infection, alginates can be degraded by reactive oxygen species, especially hydroxyl radicals, or by bacterial alginate lyase that catalyses the  $\beta$ -elimination reaction. The ability of alginate lyase, produced by *K. pneumoniae*, to cleave linkages of GM and GG blocks has already been shown (Sutherland, 1995).

Alginates are recognised as a safe material by the FDA (Sosnik, 2014) and are widely used in medicine and biotechnology due to their stabilising, viscosifying and gelling properties (Andersen et al., 2012, Laurienzo, 2010). Not only are alginates extensively used in the food industry, but they have also been widely used for various medical applications including drug delivery, wound dressings, dental impression materials and in tablet formulations for gastric reflux, such as Gaviscon (Chatfield, 1999, Draget and Taylor, 2011). One of the most important features of alginate is its ability to selectively bind to divalent cations such as  $\text{Ca}^{2+}$ , leading to gel formation (Draget and Taylor, 2011). Increasing the G-block content of the alginate actually augments its ability to bind to divalent cations.

### 1.7.2 OligoG CF-5/20

Although alginates are known to be biodegradable, hydrophilic and non-toxic, until recently, few investigations had used alginates for protein and peptide conjugation, due to the lack of alginate-degrading mammalian enzymes and their relatively large size. OligoG CF-5/20 is a G-block oligosaccharide with > 85% G residues and a narrow molecular weight distribution (mean molecular weight ~3,200 g/mol; equivalent to ~16 monomer units) that is produced from the stem of brown seaweed (*Laminaria hyperbora*) (Hengzhuang et al., 2016). OligoG is an anionic, highly water-soluble oligomer, although in practice, its high viscosity at concentrations > 15% limits its solubility (Khan et al., 2012). The chemical structure of OligoG is presented in **Figure 1.7**. OligoG powder is prepared by purification using charcoal filters, followed by “spray-drying”.

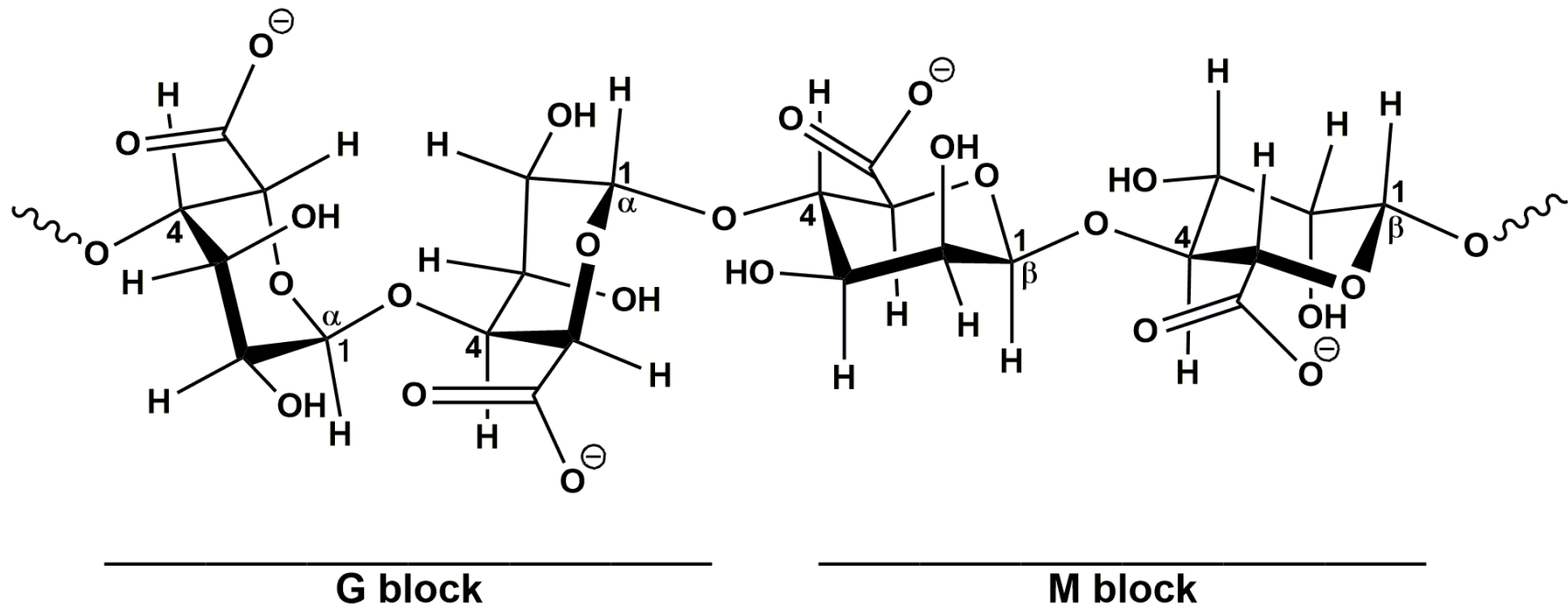


**Figure 1.7** Chemical structure of OligoG, including  $\alpha$ -L-gulonate (G) and  $\beta$ -D-manuronate (M) blocks.

Quality control of the final product is carried out using  $H^1$ -nuclear magnetic resonance and high-performance anion-exchange chromatography with pulsed amperometric detection (Khan et al., 2012). The intrinsic antimicrobial activity of the prototypical OligoG CF-5/20 product is discussed in Chapter 3.

### **1.8 Examples of polysaccharide-antibiotic conjugates**

Polysaccharides, such as alginates, possess many favourable features for targeted delivery of antimicrobial drugs including biodegradability, hydrophilicity and a lack of toxicity. Various studies have demonstrated the potential value of polysaccharides as antibiotic carriers for targeted drug delivery. For example, colistin has been conjugated to dextrin (Mw 7500 g/mol with 1 mol % succinylation) using EDC and sulfo-NHS carbodiimide linking agents (~10% colistin loading). The resulting dextrin-colistin conjugates maintained potent antimicrobial activity against a panel of MDR Gram-negative bacteria whilst exhibiting markedly decreased *in vitro* cytotoxicity compared to the unmodified antibiotic in HK-2 cells, leading to a 4-5-fold improved  $IC_{50}$  concentration (Azzopardi et al., 2015, Ferguson et al., 2014). In addition, *in vivo* studies also demonstrated improved pharmacokinetics of the dextrin-colistin conjugates, leading to a considerably prolonged plasma half-life of the drug (Ferguson et al., 2014).

In another example, the antibiotic norfloxacin has also been coupled to dextran (Mw 64000 g/mol) bearing mannose (2.3 mol %) through a tetrapeptide Gly-Phe-Gly-Gly linker (8.2% w/w norfloxacin loading) to facilitate targeted drug delivery to macrophages (Balazuc et al., 2005, Roseeuw et al., 2003). While unconjugated norfloxacin lacked antimicrobial activity against intracellular *Mycobacteria in vivo* due to rapid renal clearance, antibiotic efficacy was restored following conjugation to dextran.

Additionally, the conjugation of chitosan (Mw 13000 g/mol) to streptomycin (22% w/w streptomycin loading) has also been shown and was linked by reduction of the resulting Schiff base, which significantly improved the internalisation of antibiotic into macrophages and improved its antimicrobial activity 100-fold more in comparison to a mixture of the individual components

(Mu et al., 2016). The chitosan-streptomycin conjugate showed significant bactericidal activity against multiple intracellular bacterial pathogens, including *Listeria monocytogenes*, *S. aureus* and *Salmonella typhimurium* in infected human umbilical vein endothelial cells (HUVEC), epithelial cells (HaCaT) and macrophages, however, cytotoxicity was observed when RAW264.7 cells were treated at concentrations > 300 µg/ml.

### **1.9 Aims of the project**

The aim of this project was to develop a bi-functional antibiotic delivery system using the alginate oligosaccharide, OligoG CF-5/20, to reduce the toxicity and optimise the antimicrobial efficacy of antibiotics of last resort against MDR Gram-negative bacterial pathogens. This project hypothesised that passive targeting of OligoG-polymyxin conjugates to sites of infection by the EPR effect, followed by separation of the parent molecules via intrinsic, complementary antimicrobial enzyme activities at the target site, would significantly enhance the efficacy of the antibiotics and reduce their toxicity.

#### **The specific aims of the study were:**

- To generate a library of OligoG-polymyxin conjugates and characterise their physicochemical and toxicological properties.
- To evaluate the antimicrobial efficacy of OligoG-polymyxin conjugates against a panel of MDR Gram-negative bacteria.
- To investigate the *in vitro* pharmacokinetic/pharmacodynamic profile of OligoG-colistin conjugates, in respect to antibiotic release and effectiveness.
- To assess the activity of OligoG to disrupt the physical structure and architecture of biofilms of MDR Gram-negative bacteria and to study its localisation within the biofilm polymeric network.

# **Chapter 2**

## **General Materials and Methods**

## **2.1 Chemicals**

### **2.1.1 General chemicals**

Aprotinin from bovine lung, cytochrome c from equine heart, carbonic anhydrase from bovine erythrocytes, albumin from bovine serum, blue dextran, bicinchoninic acid (BCA) solution, copper (II) sulfate pentahydrate (4% w/v), 1-ethyl-3-(3-dimethylaminopropyl) carbodiimide hydrochloride (EDC), sodium hydroxide, sodium chloride, potassium chloride, disodium hydrogen phosphate, potassium dihydrogen phosphate and Tween<sup>®</sup> 20 were from Thermo Fisher Scientific (Loughborough, UK). Ninhydrin, hydrindantin, lithium acetate dihydrate, ethanolamine, acetic acid (glacial), acetonitrile, anhydrous dimethyl sulfoxide (DMSO), ethanol, chloroform, 4-dimethylaminopyridine (DMAP), N,N'-dicyclohexyl carbodiimide (DCC), N-hydroxysulfosuccinimide (sulfo-NHS) and sucrose were from Sigma Aldrich (Poole, UK). Pullulan gel filtration standards were obtained from Polymer Laboratories (Church Stretton, UK). All chemicals were of analytical grade, except for DMSO used in cell culture.

### **2.1.2 Alginates**

OligoG CF-5/20 (Lot: BU-1211-35;  $\geq$  85% guluronic acid and Mn of 3,200 g/mol) and high molecular weight alginate PRONOVA UP MVG (Batch: FP-505-01) medium viscosity,  $>$  60% guluronic acid and Mw of 200,000 g/mol) were provided by Algipharma AS (Sandvika, Norway).

### **2.1.3 Antibiotics**

Colistin sulfate, polymyxin B, bacitracin, azithromycin, vancomycin hydrochloride, spiramycin, spectinomycin and rifampicin were from Sigma Aldrich (Poole, UK).

### **2.1.4 Fluorescent probes**

Oregon Green 488 cadaverine 5-isomer (OrGr), LIVE/DEAD<sup>®</sup> Baclight<sup>™</sup> Bacterial Viability kit, SYTO 9<sup>™</sup> and Concanavalin A Alexa Fluor<sup>™</sup> 633

conjugate (ConA) were from Invitrogen Molecular Probes (Paisley, UK). Sulforhodamine 101 (Texas Red) cadaverine (TxRd) was from Chemometec (Allerød, Denmark). Rhodamine 6G was from Sigma Aldrich (Poole, UK).

### **2.1.5 Chemicals for bacterial culture**

Tryptone soy (TS) broth, tryptone soy agar (TSA), blood agar (BA) base and Mueller-Hinton (MH) broth were purchased from LabM (Bury, UK). Defibrinated horse blood was from TCS Biosciences (Botolph Claydon, UK). Resazurin sodium salt, mucin (II) from porcine stomach, deoxyribonucleic acid (DNA) from salmon fish sperm, RPMI 1640 amino acid solution, diethylenetriaminepentaacetic acid (DTPA), egg yolk emulsion and ethylenediaminetetraacetic acid (EDTA) were from Sigma Aldrich (Poole, UK). MaxSignal<sup>®</sup> colistin enzyme-linked immunosorbent assay (ELISA) test kit was from Bioo Scientific Corp. (Austin, USA).

### **2.1.6 Chemicals for cell culture**

Keratinocyte serum-free (K-SFM) medium (with L-glutamine), bovine pituitary extract (BPE, 0.05 mg/ml), human recombinant epidermal growth factor (EGF, 5 ng/ml), 0.05% w/v trypsin-0.53 mM EDTA were from Invitrogen Life Technologies (Paisley, UK). Trypan blue, DMSO (cell culture grade) and 3-(4,5-dimethylthiazol-2-yl)-2,5-diphenyltetrazolium bromide (MTT) were from Sigma Aldrich (Poole, UK). Human tumour necrosis factor alpha (TNF $\alpha$ ) ELISA kit was from Thermo Fisher Scientific (Loughborough, UK).

## **2.2 Cell line**

Human kidney proximal tubule cell line (HK-2, CRL-2190) was purchased from American Type Culture Collection (ATCC) (Manassas, USA). HK-2 cells were confirmed to be free of mycoplasma contamination. Typical morphology of the cells is shown in **Figure 2.1**.

## **2.3 Bacterial isolates**

Clinical bacterial isolates and *Escherichia coli* ATCC 25922 were provided by

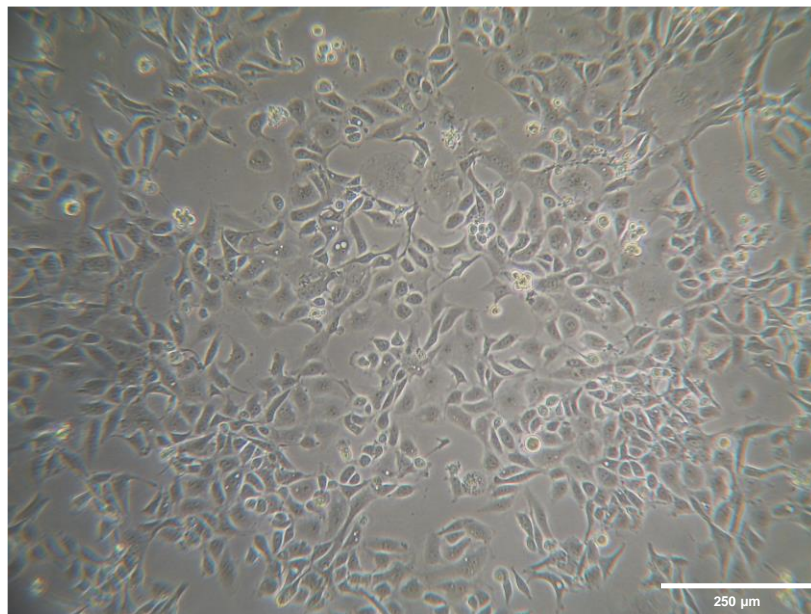


**Figure 2.1** Morphology of the HK-2 cells. Picture was taken using the Nikon Eclipse TS100 inverted microscope equipped with Moticam® digital camera (magnification x10).

Prof Tim Walsh (Department of Medical Microbiology and Infectious Disease, Cardiff University, UK), except for MDR *Acinetobacter baumannii* 7789, *Pseudomonas aeruginosa* PAO1 ATCC 15692, *Pseudomonas aeruginosa* National Collection of Type Culture (NCTC) 10662 and *Escherichia coli* NCTC 10418 which were donated by Dr Robin Howe (Public Health Wales Microbiology Department, University Hospital of Wales, Cardiff, UK). Multiple drug resistance was confirmed by the referring laboratories. The origin of pathogens and resistance genotypes are provided in **Table 4.1**.

## **2.4. Equipment**

### **2.4.1 General equipment for bacterial and cell culture**

Sterile general consumables: flat-bottom 96-well plates, universal containers, centrifuge tubes (15 and 50 ml), 7 ml bijoux containers, petri dishes, tissue culture flasks (25 and 75 cm<sup>2</sup>), pipettes (5, 10 and 25 ml) and cryovials were purchased from Starstedt (Leicester, UK). Low protein binding sterile polyvinylidene fluoride (PVDF) syringe filters (0.22 µm) were purchased from Merck Millipore (Watford, UK). Sterile needles were purchased from BD Microlance (Fraga, Spain) and sterile syringes were from BD Plastipak (Madrid, Spain). Spectra/Por<sup>®</sup> 7 regenerated cellulose dialysis tubing was from Spectrum Laboratories Inc. (California, USA). Slide-A-Lyzer sterile dialysis cassettes were from Thermo Fisher Scientific (Loughborough, UK). Microbank vials were from Pro-Lab (Birkenhead, UK). Sterile Transwell (0.4 µm pore polycarbonate membrane) plates and sterile flat-bottom black 96-well plates were from Corning Inc. (New York, USA). Sterile 96-well flat glass bottom black plates were from Greiner Bio-One (Stonehouse, UK) and sterile surgical thread was from Ethicon Inc. (Somerville, USA).

### **2.4.2 Analytical equipment**

#### **2.4.2.1 Gel permeation chromatography (GPC)**

An aqueous GPC system comprised of JASCO pump (PU-4180), two TSK gel columns (5000 PW<sub>XL</sub> followed by 3000 PW<sub>XL</sub>), a guard column (Progel PW<sub>XL</sub>)

and PL Datastream monitor was from Polymer Laboratories (Church Stretton, UK). A Gilson 133 differential refractometer (Middleton, USA) was used to study the elution profile. The Cirrus GPC software (version 3.2) from Polymer Laboratories (Church Stretton, UK) was used for data collection and analysis.

#### **2.4.2.2 Fast protein liquid chromatography (FPLC)**

An ÄKTA Purifier FPLC system connected to a prepacked Superdex 75 (10/300 or 16/600) GL size exclusion column and a fraction collector (Frac-950) was from GE Healthcare (Amersham, UK). The Unicorn software (version 5.31) from GE Healthcare (Amersham, UK) was used for UV absorbance data collection and analysis.

#### **2.4.2.3 Spectrophotometry: Ultraviolet/visible (UV/vis)**

A Fluostar Optima microplate reader with Optima software (version 3.00 R2) from BMG Labtech (Aylesbury, UK) was used for UV/vis absorbance and fluorescence intensity measurements. A Du 800 UV/Vis Spectrophotometer and Du 800 software (version 2.0.83) were from Beckman Coulter (High Wycombe, UK).

#### **2.4.2.4 Confocal laser scanning microscopy (CLSM)**

A Leica TCS SP5 system equipped with Leica DMI6000B microscope and Leica Application Suite Advanced Fluorescence (LAS AF) software (version 1.6.2) was from Leica Microsystems (Milton Keynes, UK). CLSM images were processed using image analysis software Imaris (version 8.1.2) from Bitplane (Concord, USA). Biofilm structural changes were quantified using COMSTAT image analysis software (Heydorn et al., 2000).

#### **2.4.2.5 Miscellaneous equipment**

A Hanna HI2210 pH meter was from Hanna Instruments (Leighton Buzzard, UK). A Scanvac freeze-dryer was from Thistle Scientific (Uddingston, UK) connected to a high vacuum pump from Vacuubrand (Brackley, UK). PD-10

desalting columns (Sephadex G-25) were purchased from GE Healthcare (Amersham, UK).

## **2.5 Sterilisation**

To ensure workspace sterility and avoid contamination of the samples, for microbiological experiments, working surfaces were sprayed with 1% w/v Virkon™ disinfectant solution and the experiments were performed under a Bunsen burner flame or in a laminar flow cabinet. Except for centrifugation steps, all cell culture was performed in a Microflow Class II laminar flow cabinet. For tissue culture experiments, materials and equipment placed in the safety cabinets and incubators were sprayed with a 70% v/v ethanol solution. Those items not supplied pre-sterilised were sterilised by (a) autoclaving (120°C, 15 lb/m<sup>2</sup>, 15 min) for glassware, certain plastics, phosphate buffered saline (PBS) and distilled water (dH<sub>2</sub>O) or (b) microfiltration (0.22 µm) for solutions.

## **2.6 General methods**

This section gives a detailed description of the general methods used in these studies. Those specific methods used in each chapter are described in full there. Methods used for conjugate synthesis are described in detail in Chapter 3 (Section 3.3.1) and the methods used for conjugate characterisation are described below.

### **2.6.1 Purification of OligoG-antibiotic conjugates**

FPLC was used to purify the reaction mixture of OligoG-antibiotic conjugate by removal of unreacted protein and crosslinking agents. To begin with, a prepacked Superdex 75 (16/600) column was washed with one column volume (~120 ml) of filtered (0.22 µm) and degassed dH<sub>2</sub>O at a flow rate of 0.3 ml/min. The column was then equilibrated with two column volumes of filtered and degassed PBS (pH 7.4) at a flow rate of 0.5 ml/min and calibrated (1 ml/min flow rate) using standardised proteins of various molecular weights: aprotinin (6,500 g/mol), cytochrome C (12,400 g/mol), carbonic anhydrase (29,000

g/mol), albumin (66,000 g/mol) and alcohol dehydrogenase (150,000 g/mol) (3 mg/ml in PBS, pH 7.4) by injection of 200  $\mu$ l of sample into a 100  $\mu$ l loop. Blue dextran (10 mg/ml in PBS, pH 7.4) was used as a void volume marker. The calibration curve is shown in **Figure 2.2**. Then, samples of the conjugation reaction mixture (2 ml) were injected into a 2 ml loop using PBS buffer (pH 7.4) as eluent at a flow rate of 1 ml/min. Fractions corresponding to OligoG-antibiotic conjugates were collected, pooled (~40-45 ml in total) and lyophilised. The resultant products were redissolved in a minimal volume of dH<sub>2</sub>O, then dialysed using the dialysis membrane of 1,000 g/mol molecular weight cut-off against 1 L of dH<sub>2</sub>O to remove PBS salts. Dialysis was carried out for 5 h, changing the water hourly, before the desalted conjugates were lyophilised and stored at -20°C.

## **2.6.2 Characterisation of OligoG-antibiotic conjugates**

After purification, physicochemical characterisation of OligoG-antibiotic conjugates was performed by GPC, FPLC, BCA assay and ninhydrin assay.

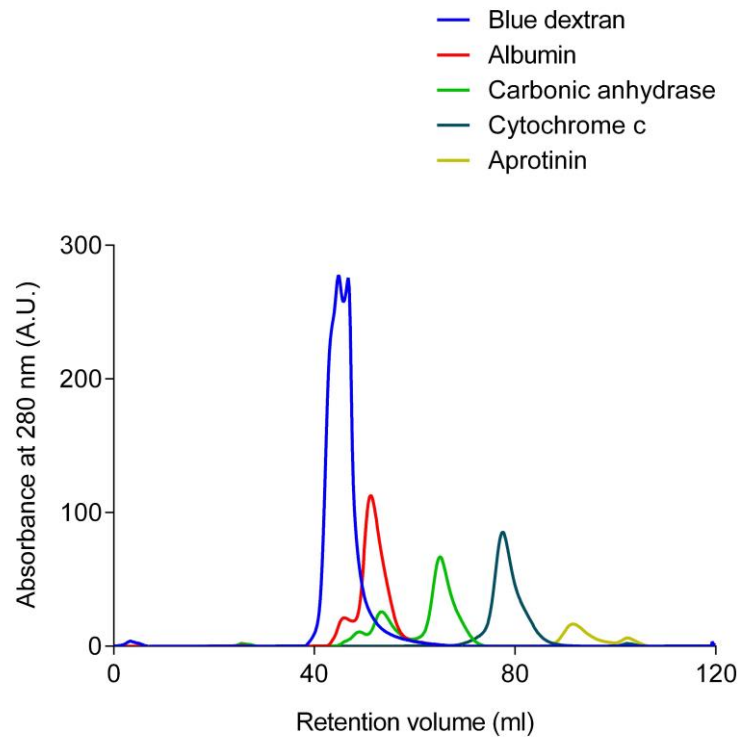
### **2.6.2.1 Characterisation by GPC**

The approximate molecular weight and polydispersity of the OligoG-antibiotic conjugates was determined according to their hydrodynamic radius using an aqueous GPC system. First, TSK gel columns were equilibrated using filtered (0.22  $\mu$ m) and degassed PBS (pH 7.4) at a flow rate of 1 ml/min. Then, polysaccharide (pullulan) molecular weight standards (molecular weight from 180 to 788,000 g/mol) were used to produce a calibration curve, as shown in **Figure 2.3**. Samples were prepared at 3 mg/ml in PBS (pH 7.4) and approximately 80  $\mu$ l was injected into the system (20  $\mu$ l loop at a flow rate of 1 ml/min).

### **2.6.2.2 Characterisation by FPLC**

FPLC (as previously described) was also used to estimate proportion (%) of free and bound antibiotic. Equilibration and calibration of a Superdex 75 column (10/300 GL) was performed as previously described in Section 2.6.1.

(a)



(b)

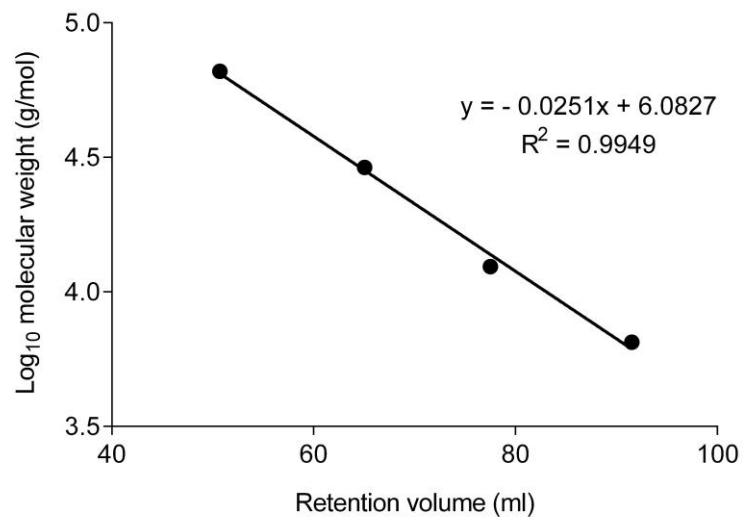
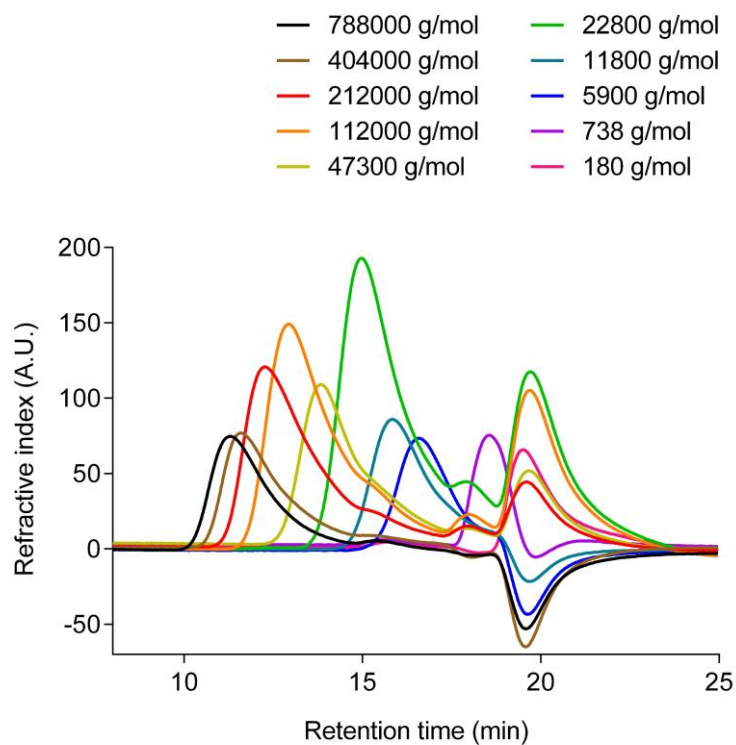


**Figure 2.2** Typical FPLC calibration using Superdex 75 (16/600) column. (a) Chromatogram of various protein molecular weight standards. (b) Calibration curve for estimation of molecular weight.  $V_0$  (void volume) = 45 ml,  $V_b$  (bed volume) = 120 ml.

(a)



(b)

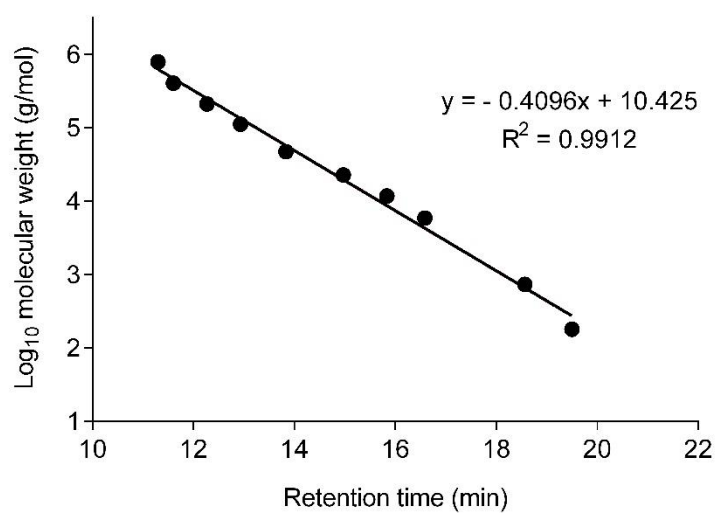


**Figure 2.3** Typical GPC calibration using pullulan molecular weight standards. (a) Chromatogram of various pullulan standards. (b) Calibration curve for estimation of molecular weight.  $V_0$  (void volume) = 13 ml,  $V_b$  (bed volume) = 20 ml.

A typical calibration curve can be seen in **Figure 2.4**. Purified OligoG-antibiotic conjugates were dissolved in PBS (pH 7.4) (3 mg/ml) and 200  $\mu$ l of the sample was injected into a 100  $\mu$ l loop using PBS (pH 7.4) as the mobile phase at a flow rate of 0.5 ml/min. The area under the curve corresponding to free and conjugated antibiotic was calculated and used to estimate the percentage of free drug in the conjugate.

### **2.6.2.3 Characterisation by BCA**

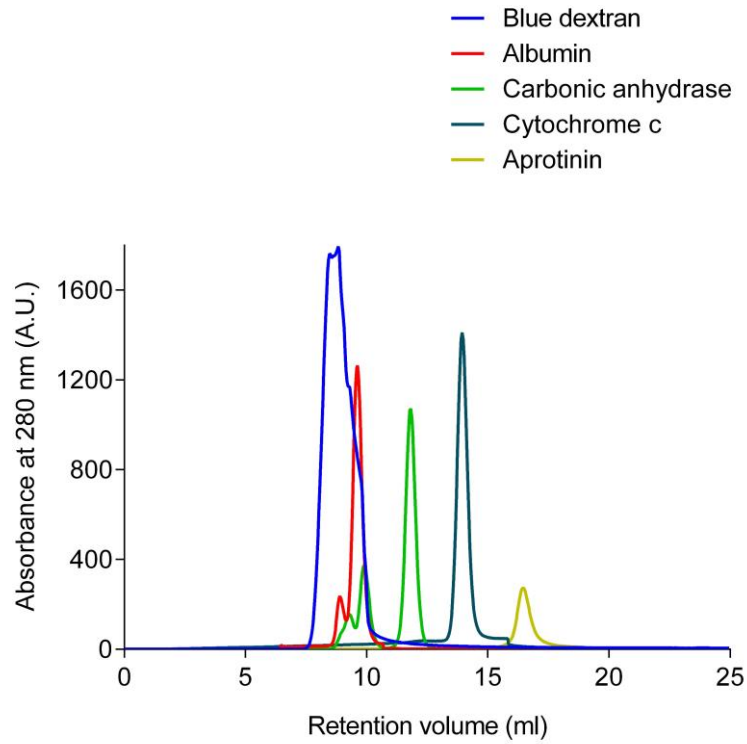
The BCA assay was used to determine the total protein content in the OligoG-antibiotic conjugates (Smith et al., 1985). Colorimetric detection of proteins is achieved when the peptide bonds in the protein reduce cupric ion ( $\text{Cu}^{2+}$ ) to cuprous ion ( $\text{Cu}^+$ ) by the biuret reaction, which then chelates with two BCA molecules. This complex formation produces a purple coloured solution, whereby the intensity of the colour is proportional to the protein concentration in the sample.

The BCA assay was carried out in a 96-well microtitre plate. Calibration curves were produced using colistin sulfate, polymyxin B or bacitracin (20  $\mu$ l, 0-1 mg/ml in PBS, n = 3) and used to determine the protein content of the corresponding conjugate. Typical calibration curves are shown in **Figure 2.5**. Sample wells contained OligoG-antibiotic conjugate (20  $\mu$ l, 1 and 3 mg/ml in PBS, n = 8). BCA reagent (1 ml of BCA: 20  $\mu$ l Cu (II) sulfate) was added to each well (200  $\mu$ l), then, the microtitre plate was gently agitated and incubated in the dark at 37°C for 20 min. The absorbance values were then read spectrophotometrically at 550 nm and used to calculate the protein content in the OligoG-antibiotic conjugates (% w/w).

### **2.6.2.4 Characterisation by ninhydrin assay**

Prior to conjugation to OligoG, it was considered important to determine the number of available primary amine groups on the antibiotic molecules using the ninhydrin assay. Ninhydrin is a powerful oxidising agent, which reacts with the primary amine groups at pH 4-8, resulting in a Ruhemann's purple product (Friedman, 2004).

(a)



(b)

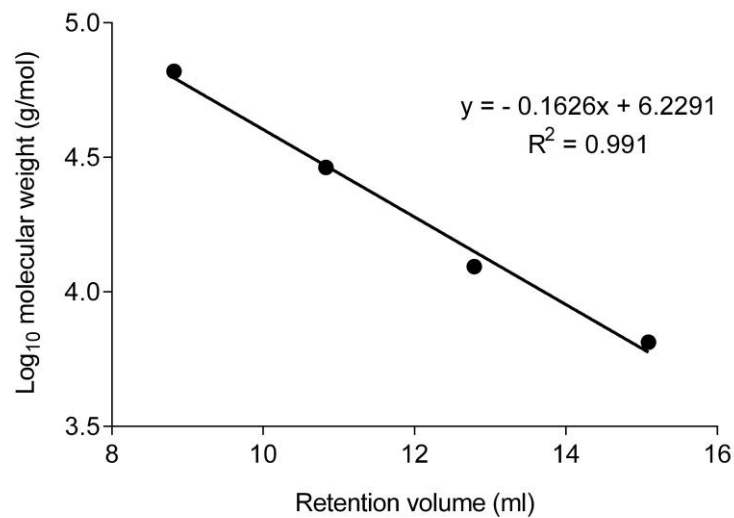


**Figure 2.4** Typical FPLC calibration using Superdex 75 column (10/300 GL) column. (a) Chromatogram of various protein molecular weight standards. (b) Calibration curve for estimation of molecular weight.  $V_0$  (void volume) = 7.7 ml,  $V_b$  (bed volume) = 24 ml.

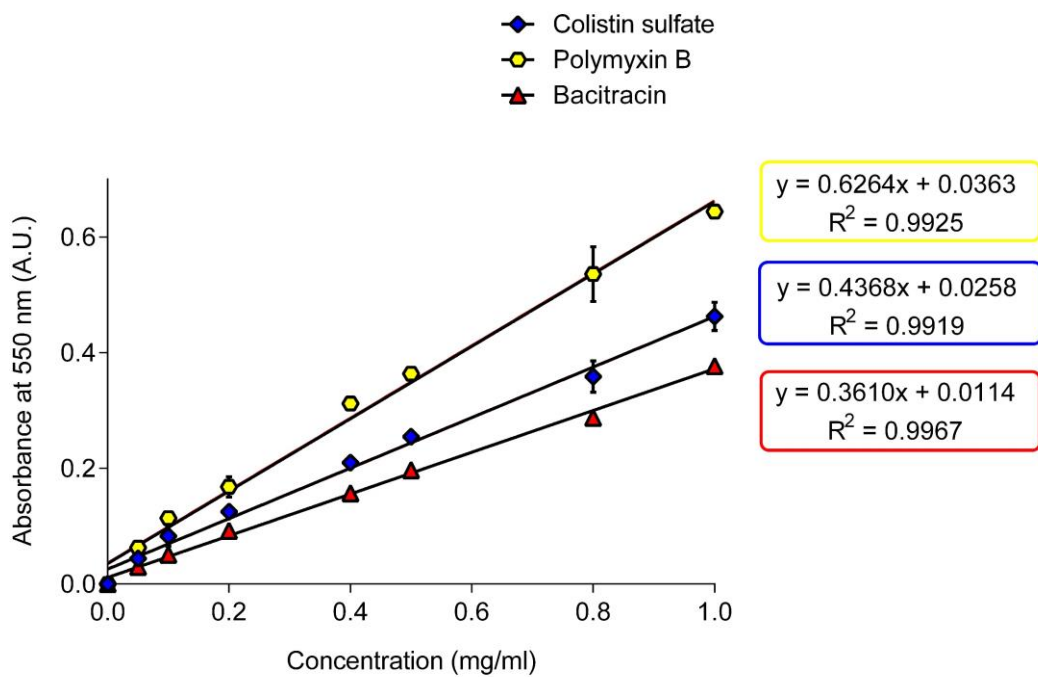


**Figure 2.5** Typical BCA assay calibration curves using colistin sulfate, polymyxin B and bacitracin as protein standards. Data is expressed as mean  $\pm$  SD (n = 3).

First, a lithium acetate buffer (4 M) was prepared by dissolving lithium acetate dihydrate (40.81 g) in 60 ml of dH<sub>2</sub>O. The pH of the buffer was adjusted to 5.2 with the addition of acetic acid (glacial) and made up to a final volume of 100 ml with dH<sub>2</sub>O. Then, ninhydrin reagent was prepared by dissolving ninhydrin (0.2 g) and hydrindantin (0.03 g) in 7.5 ml of DMSO and 2.5 ml of lithium acetate buffer. Ethanolamine calibration standards (0.0165-0.1158 mM in PBS, pH 7.4) and of test compounds (86 µl) were diluted with an equal volume of ninhydrin reagent and heated in a water bath (100°C) for 15 min. The solutions were cooled to room temperature then 50% v/v ethanol solution (130 µl) was added to each tube. Aliquots (200 µl) were transferred into the wells of a 96-well microtitre plate and analysed spectrophotometrically at 570 nm. A typical calibration curve is shown in **Figure 2.6**.

### **2.6.3 Biological characterisation of OligoG-antibiotic conjugates**

#### **2.6.3.1 Cell maintenance**

HK-2 cells were grown in K-SFM, containing 0.05 mg/ml BPE and 5 ng/ml human recombinant EGF in a humidified 37°C/5% CO<sub>2</sub> incubator. Cell culture medium was changed on alternate days.

#### **2.6.3.2 Defrosting cells**

Cells were grown from frozen stocks (1 ml of cell suspension/vial). First, cells were rapidly thawed in a water bath (37°C), transferred into a universal tube containing 9 ml of K-SFM and centrifuged at 226 g (20°C) for 5 min. The supernatant was then removed by aspiration and the cell pellet was resuspended in K-SFM (5 ml). The cell suspension was then transferred into a 25 cm<sup>2</sup> flask and placed in an incubator. After 24 h, the culture medium was replaced with fresh K-SFM and cells were grown until ~80% of confluency was reached.

#### **2.6.3.3 Cell passaging**

Once ~80% of confluency was reached, the HK-2 cells were passaged at a

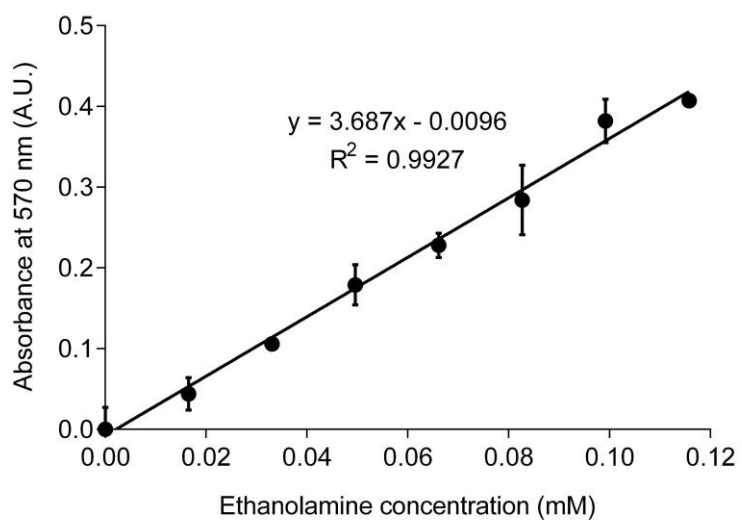


**Figure 2.6** Typical ninhydrin assay calibration curve using ethanolamine standards. Data is expressed as mean  $\pm$  SD (n = 3).

ratio of 1 to 4 and transferred to a 75 cm<sup>2</sup> flask. The old medium was aspirated and the cells were washed with sterile PBS (10 ml) to remove dead cells before addition of trypsin-EDTA solution (1 ml). Flasks were then incubated at 37°C for approximately 3 min or until the cells were detached from the surface. Next, 9 ml of K-SFM was added to the flask and the cell suspension was transferred into a universal tube and centrifuged at 226 g (20°C) for 5 min. The supernatant was removed and the cells were resuspended in fresh K-SFM (10 ml). This suspension was used to prepare new flasks after appropriate dilution.

#### **2.6.3.4 Cell counting**

Cells were washed with PBS, trypsinised and resuspended as described previously. To produce a homogenous single cell suspension, cells were first passed through a needle (23G). Then, an aliquot of cell suspension (100 µl) was mixed with an equal volume of trypan blue (0.2% in PBS) and transferred into a haemocytometer. Cells from ten 0.1 mm<sup>3</sup> squares (five taken from the top chamber, 5 taken from the bottom chamber) were counted. Viable cells were counted within a square and on the left and top boundary grid lines. Non-viable cells (stained dark blue) were not included in the cell count. Cell number was calculated using the following formula:

$$\text{Viable cell count (cells/ml)} = \text{Mean cell count} \times \text{dilution factor} \times 10^4$$

where mean was the arithmetic mean of the 10 squares, the dilution factor was 2 (to account for dilution with trypan blue) and 10<sup>4</sup> accounted for conversion from 0.1 mm<sup>3</sup> to 1 ml). The cell suspension was subsequently diluted with K-SFM to achieve a cell density of 1 x 10<sup>5</sup> cells/ml.

#### **2.6.3.5 Characterisation by MTT**

An MTT assay was used to measure viability and proliferation of cells in the presence of OligoG-antibiotic conjugates. The yellow tetrazolium MTT reagent is reduced to purple insoluble formazan in metabolically active cells by mitochondrial dehydrogenase enzymes, resulting in the production of insoluble

formazan crystals which correlates with the number of viable cells (Mosmann, 1983).

HK-2 cells were seeded (100 µl/well) in a sterile 96-well microtitre plate at  $1 \times 10^5$  cells/ml and allowed to adhere for 24 h at 37°C. Subsequently, the old medium was removed and replaced with fresh medium containing test compounds dissolved in K-SFM (0.22 µm filter-sterilised) and serially diluted across the plate. The plate was then incubated for 67 h at 37°C. Next, MTT solution (20 µl, 5 mg/ml in PBS and 0.22 µm filter-sterilised) was added to each well and incubated for a further 5 h at 37°C. Finally, medium from each well was carefully removed and the formazan crystals were solubilised in DMSO (100 µl) for 30 min, before measuring absorbance at 550 nm using a plate reader. The results were expressed as a percentage of the cell viability compared to untreated control cells ( $\pm$  SEM, n = 18).

#### **2.6.3.6 Characterisation by TNF $\alpha$ ELISA**

Release of the cytokine, TNF $\alpha$ , by HK-2 cells after exposure to free- and OligoG-conjugated antibiotic (72 h) was assessed using an ELISA kit, according to the manufacturer's instructions (Section 3.3.4). Plates were analysed spectrophotometrically at 450 nm. A typical calibration curve is shown in **Figure 2.7**.

#### **2.6.4 Microbiological characterisation of OligoG-antibiotic conjugates**

##### **2.6.4.1 Preparation of microbiological growth media and agar**

Agars (BA and TSA) and broths (MH and TS) were prepared according to the manufacturer's instructions. BA was supplemented with 5% v/v defibrinated horse blood. The prepared agar plates were then stored at 4°C until required.

##### **2.6.4.2 Bacterial cultures maintenance**

Bacterial isolates were grown from -80°C frozen stocks (on Microbank beads). One bead of each bacterial strain was used to streak the isolate on BA plates. The plates were incubated overnight at 37°C then stored at 4°C until required.

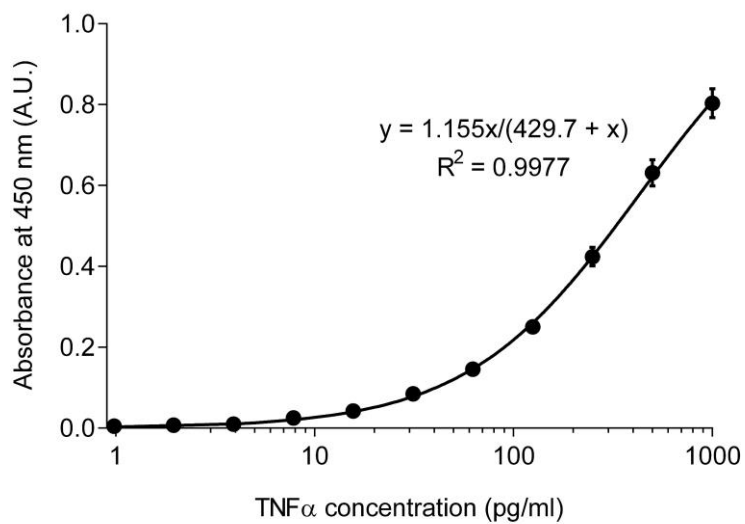


**Figure 2.7** Typical ELISA assay calibration curve using TNF $\alpha$  standards. Data is expressed as mean  $\pm$  SD (n = 6).

Bacterial cultures were re-plated every 4 weeks.

#### **2.6.4.3 Preparation of overnight bacterial culture**

A single bacterial colony was picked with a sterile loop, inoculated in TS broth (10 ml) and incubated overnight (37°C) in shaking incubator (120 rpm).

#### **2.6.4.4 Minimum inhibitory concentration (MIC) assay**

The susceptibility of a panel of Gram-negative bacteria to OligoG-antibiotic conjugates was tested using serial microdilutions in MH broth (100 µl/well) across a sterile 96-well microtitre plate (EUCAST, 2003). Overnight bacterial cultures were standardised in sterile PBS to achieve an optical density (OD<sub>625</sub>) between 0.08 and 0.10 (0.5 McFarland standard) and then further diluted in MH broth at a ratio of 1 to 10 and 5 µl was added to all wells containing test compound. Sterility (MH broth), growth (no antibiotic) and quality control strains were used in every study. Plates were wrapped in parafilm and incubated at 37°C for 20 h. The sterility control was accepted if no visible bacterial growth was noted, the growth control was considered acceptable if visible cloudiness and turbidity was observed. The MIC value was reported as the lowest concentration where no visible bacterial growth was observed. The results were expressed as median values (n = 3). MIC values were accepted if those of the quality control strains were within one serial dilution from published values (EUCAST, 2003). A significant difference between two MIC values was accepted if they differed by at least a two-fold dilution. A typical plate layout for MIC determination is shown in **Figure 2.8**.

#### **2.6.4.5 Colistin quantification**

The concentration of colistin in MH broth was measured using an ELISA kit. To extract colistin, 50 µl of the sample was mixed with 240 µl of 20% v/v acetonitrile solution in colistin extraction buffer, followed by 16 µl of clean up buffer I (vortexed for 10 s) and 16 µl of clean up buffer II (vortexed for 3 min and then centrifuged for 10 min, 4000 g, 21°C). Aliquots of extracted solution (75 µl) were assayed using the ELISA kit according to the manufacturer's

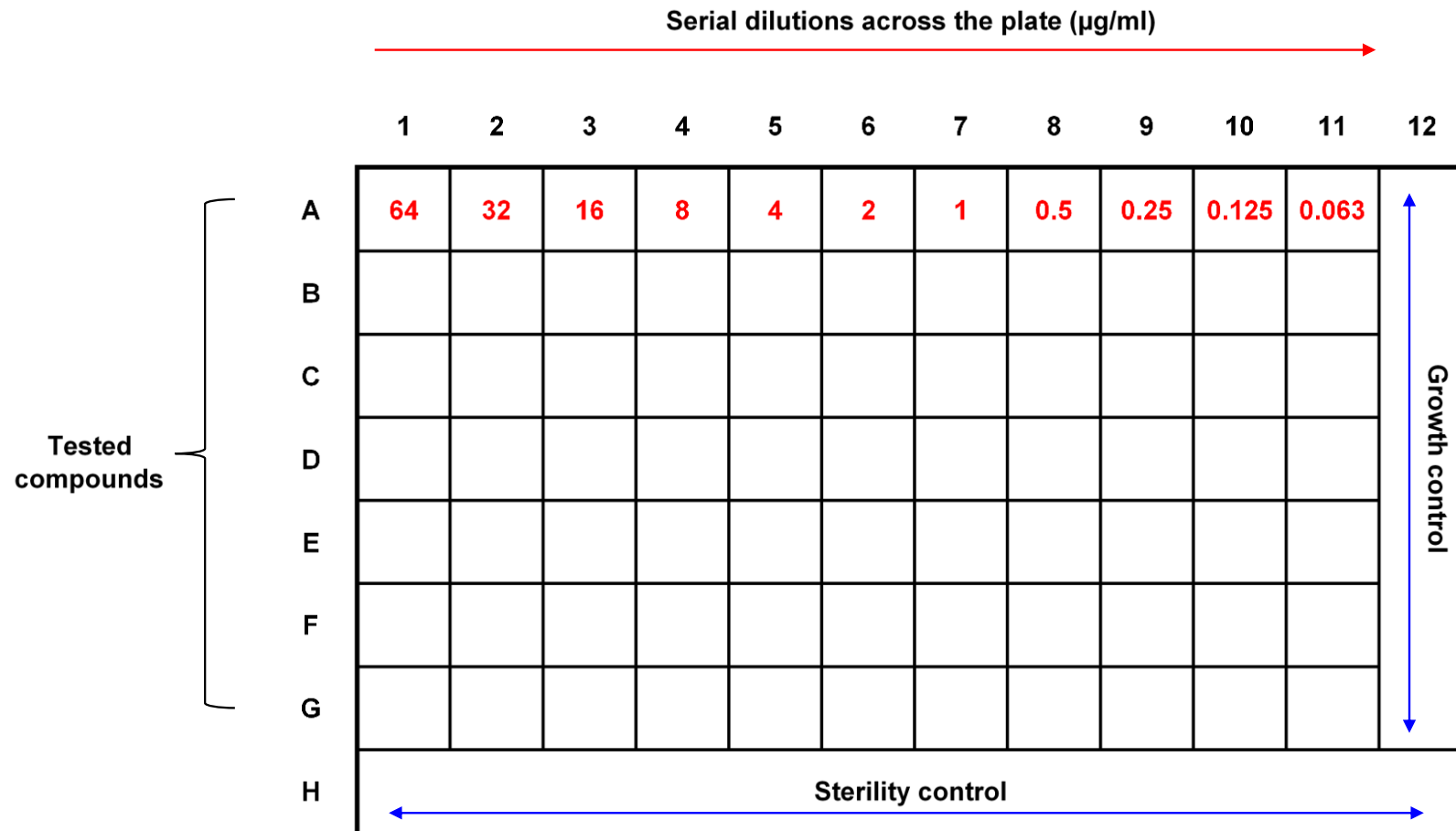


**Figure 2.8** Typical plate layout for susceptibility testing of OligoG-antibiotic conjugates using the MIC assay.

instructions. Plates were analysed spectrophotometrically at 450 nm. A calibration curve was constructed by plotting the mean relative absorbance of the calibration standards (%) against the corresponding colistin concentration (ng/ml). Data was expressed as mean  $\pm$  SD (n = 2). A typical calibration curve is shown in **Figure 2.9**.

## **2.7 Statistical analysis**

Data were presented as mean  $\pm$  standard deviation (SD, when  $n \leq 3$ ) or standard error of the mean (SEM, when  $n > 3$ ). GraphPad Prism (version 6.01, San Diego, USA) was used for statistical analysis. Statistical significance was indicated by \*, where \* $p < 0.05$ , \*\* $p < 0.01$ , \*\*\* $p < 0.001$  and \*\*\*\* $p < 0.0001$ . The coefficient of determination ( $R^2$ ) was used to analyse the fit of the regression models. To evaluate the significance between the two independent groups, Student's t-test was used. Analysis of variance (ANOVA) was used to evaluate multiple group comparisons ( $n > 2$ ) followed by Dunnett's (compares every sample mean to the control mean) or Tukey's (compares every sample mean to every other mean) *post hoc* tests to account for multiple comparisons.

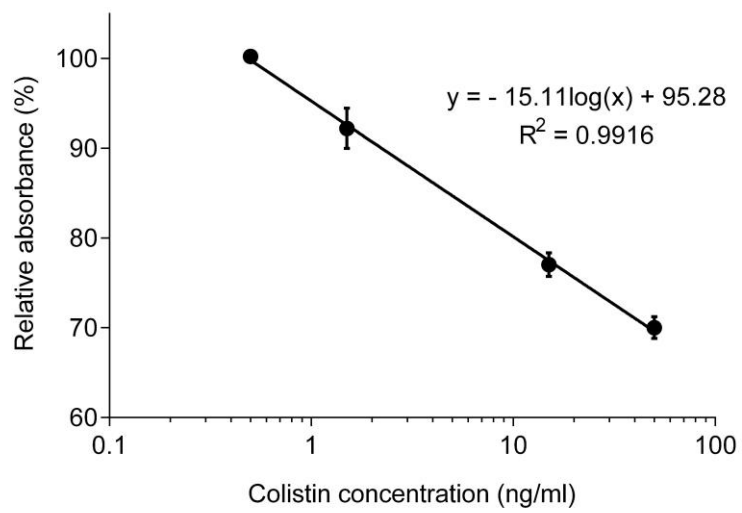


**Figure 2.9** Typical ELISA assay calibration curve using colistin standards. Data is expressed as mean  $\pm$  SD (n = 2).

# **Chapter 3**

## **Synthesis and Characterisation of OligoG- Polymyxin Conjugates**

### 3.1 Introduction

To develop the polymer-antibiotic conjugate as a successful candidate to treat multidrug-resistant (MDR) bacterial infections, it was important to select not only the most appropriate polymeric carrier, but also the best bioactive compound and conjugation chemistry. It was essential for the covalent linker between the polymeric backbone and the drug to be inert and stable in the bloodstream, without inhibiting antibiotic activity. This can be achieved by enzymatic biodegradation of the polymer or by selecting a linker that is enzymatically cleavable or sensitive to changes in pH, to facilitate liberation of the drug at the target site (Duncan, 2003). Conjugation of low molecular weight antibiotics to a water-soluble polymer can significantly improve efficacy and reduce immunogenicity and toxicity of the drug. The increased molecular weight of the conjugated drug can also reduce the renal clearance and enhance antibiotic bioavailability leading in improved biodistribution through the EPR effect (Vicent et al., 2008). Factors such as “batch-to-batch” reproducibility, toxicity and stability of the polymer-drug conjugate were also considered.

#### 3.1.1 Choice of polymer

Polysaccharides, such as hyaluronan, dextran and polysialic acid, have been widely used in drug delivery and other biomedical applications. They are comprised of long chains of saccharide units (typically > 10 monomers) bound together by glycosidic linkages to form polymeric carbohydrate molecules, which, on hydrolysis, yield the constituent mono- or oligosaccharides. Polysaccharides have the additional benefit of being able to adhere to mucosal surfaces via non-covalent interactions known as ‘mucoadhesion’ (Basu et al., 2015, Lee et al., 2000). This further supports the potential application of polysaccharides in drug delivery for chronic respiratory diseases. This chapter aimed to investigate whether alginates can also be successfully exploited in drug delivery as they possess many favourable features as discussed in Chapter 1. Numerous alginate conjugates have been described in the literature; these are summarised in **Table 3.1**.

**Table 3.1** Examples of alginate conjugates in clinical development.

<b>Alginate conjugate</b>	<b>Indication</b>	<b>Linker</b>	<b>Reference</b>
Alginate-graphene oxide	Novel non-toxic carrier for targeted/controlled drug-release. Alginate-graphene oxide polymer was used to encapsulate anticancer drug doxorubicin, showing high drug loading capacity and fast drug release in acidic conditions with high cytotoxicity towards HeLa cells.	Amide	(Fan et al., 2016)
Alginate-curcumin	As a potential treatment for various inflammatory diseases including cancer and Alzheimer's disease, curcumin conjugation to alginate (alginate mean molecular weight; $4 \times 10^5$ g/mol) increased water solubility, enhanced stability and improved bioavailability of the drug.	Ester	(Dey and Sreenivasan, 2014)
Alginate-rhodamine	Rhodamine attachment to alginate backbone facilitated the specific recognition and scavenging of biologically active and toxic metal ions such as $\text{Cr}^{3+}$ or $\text{Hg}^{2+}$ .	Amide	(Saha et al., 2012)
Alginate-cisplatin	Low water solubility and high systemic toxicity of cisplatin was overcome by conjugation to alginate. Further incorporation into epidermal growth factor modified liposomes significantly improved cisplatin targeting and efficacy at the site of ovarian tumours in mice.	Pt-O	(Wang et al., 2014)

Pt-O, platinum-oxygen bond.

OligoG is a low molecular weight alginate oligosaccharide, which is extracted as a sodium salt from the stem of brown seaweed (*Laminaria hyperbora*). It is composed of  $\alpha$ -L-guluronic acid (> 85%) and  $\beta$ -D-mannuronic acid (< 15%) residues, which contain suitable hydroxyl and carboxyl functional groups for drug attachment (Khan et al., 2012).

To date, it has been shown that OligoG inhibits bacterial growth and potentiates the efficacy of commonly used antibiotics against MDR Gram-negative pathogens (Khan et al., 2012). Inhibition of biofilm formation and physical disruption, or “clumping”, of established Gram-negative biofilms in the presence of OligoG has been reported (Khan et al., 2012). Previous studies have demonstrated that OligoG interacts with and modifies the cell surface of *P. aeruginosa* and effectively inhibits the motility and swarming of important CF pathogens such as *Burkholderia* spp., causing not only bacterial aggregation and reduction in virulence, but also weakening of the mechanical robustness of treated biofilms (Powell et al., 2013, Powell et al., 2014). In addition, OligoG interferes with, and alters, mucin hydrogel networks in sputum, thus allowing it to be used as a potential treatment in pathological respiratory diseases (Pritchard et al., 2016). Importantly, preliminary resistance studies indicated that daily sub-culturing of *P. aeruginosa* PAO1 with escalating concentrations of OligoG had no effect on antibiotic susceptibility (tested by MIC assay), indicating that resistance did not develop over a prolonged period of time (Khan et al., 2012).

Preclinical trials in rats have demonstrated that 82.6% of orally administered OligoG was eliminated by the gastrointestinal tract within the first 24 h (Pritchard et al., 2016). Additional studies revealed that after 24 h of intravenous administration of  $^3\text{H}$ -radio-labelled OligoG, 80.3% of the dose had been excreted via urine (Pritchard et al., 2016). Results from Phase I (Identifier: NCT00970346) and Phase IIa (Identifier: NCT01465529) clinical trials revealed that OligoG is safe and well-tolerated in healthy humans (demonstrated by inhalation studies using up to 540 mg/day over 3 days) and cystic fibrosis (CF) patients with no abnormal clinical signs or significant changes in respiratory, biochemical and hematological properties (Pritchard et

al., 2016). OligoG is currently undergoing Phase IIb clinical studies in patients with CF as an inhalation therapy.

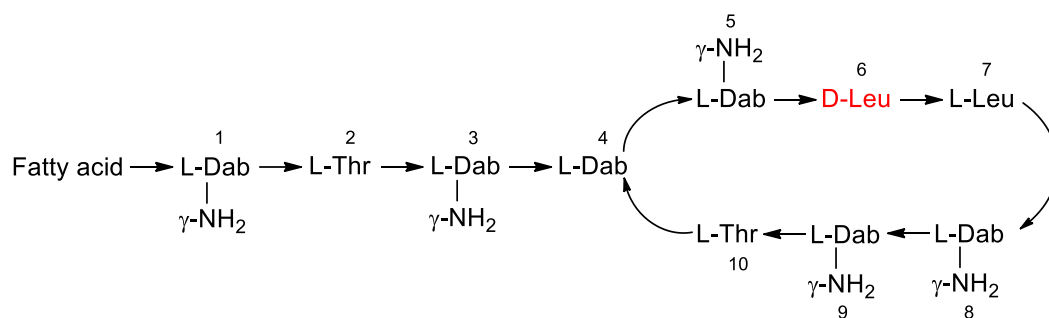
### 3.1.2 Selection of bioactive compound

Polymyxins, such as polymyxin B and colistin (also known as polymyxin E), are a class of polypeptide antibiotics that have poor oral absorption and, like other small molecule drugs, a lack of disease specific targeting. In addition, polymyxins have limited clinical use due to relatively high toxicity, thereby making polymyxins very promising candidates for polymer conjugation. It was hypothesised that polymer conjugation could significantly alter the biodistribution, reduce the toxicity and increase the efficacy of these antibiotics at the infected site.

Polymyxins are composed of a hydrophilic heptapeptide ring which is attached to a hydrophobic acyl tail through a tripeptide link, resulting in an amphiphilic structure (Azzopardi et al., 2013a). Under physiological conditions ( $pK_a \approx 10$ ), five amino groups per polymyxin molecule are positively charged and accessible for conjugation (Kwa et al., 2008). The only structural difference between polymyxin B and colistin molecules is a change in a single amino acid. Colistin contains a D-leucine residue at position 6, which is replaced by D-phenylalanine in polymyxin B, as shown in **Figures 3.1** and **3.2** (Kwa et al., 2008). Ordinarily, polymyxins are not homogenous compounds, but rather mixtures of closely related molecules. For example, colistin is composed of at least 30 different constituents. Colistin A and B (also known as polymyxin E<sub>1</sub> and polymyxin E<sub>2</sub>, respectively) are the main components, although only polymyxin E<sub>1</sub> is considered an active therapeutic ingredient (Kadar et al., 2013, Kline et al., 2001). Similarly, polymyxin B<sub>1</sub> and polymyxin B<sub>2</sub> are the main components in polymyxin B, accounting for more than 80% of the drug (Velkov et al., 2013). The major difference between the constituents is in the fatty acyl tail, which is composed of 6-methyloctanoic acid in polymyxin B<sub>1</sub> and E<sub>1</sub> or 6-methylheptanoic acid in polymyxin B<sub>2</sub> and E<sub>2</sub> (Kadar et al., 2013).

After administration to patients, more than 50% of the polymyxin dose becomes bound to human plasma proteins (Li et al., 2003a). Free amino acid

(a)



(b)

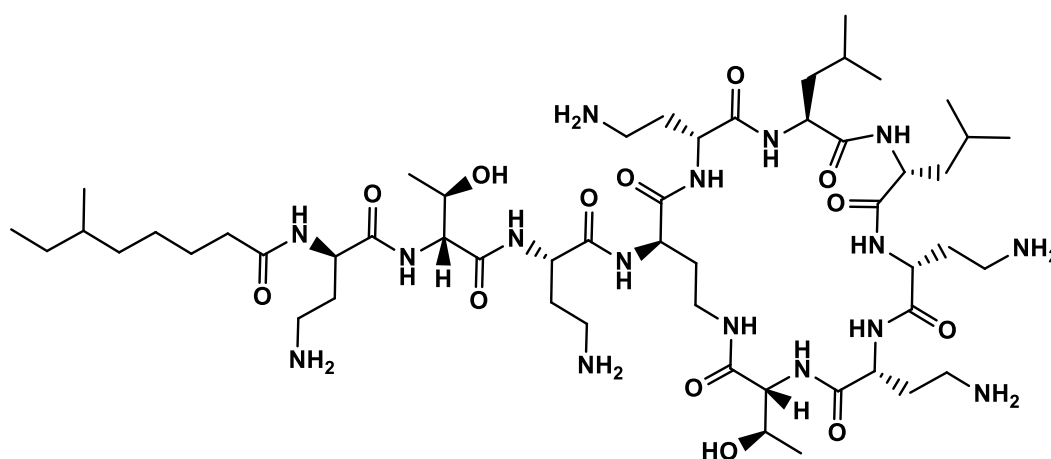
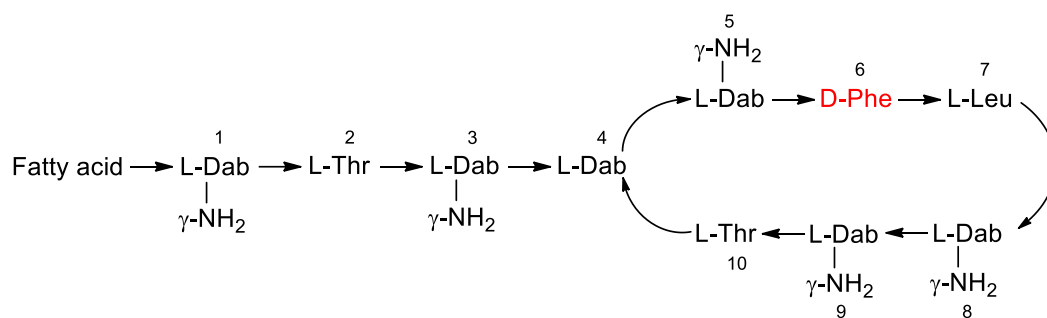


**Figure 3.1** (a) Graphic and (b) chemical structure of colistin. Amino acid components: Dab, diaminobutyric acid; Thr, threonine; Leu, leucine; Phe, phenylalanine.

(a)



(b)

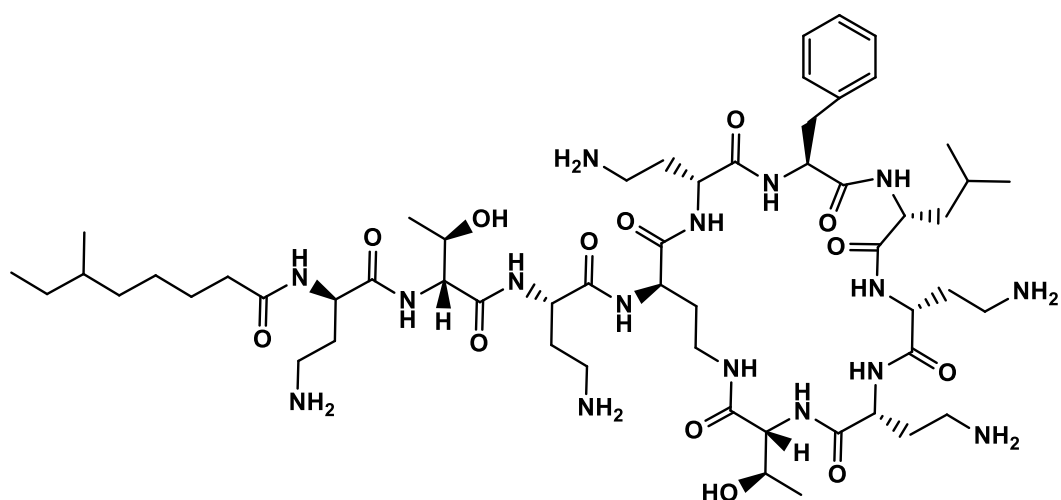


**Figure 3.2** (a) Graphic and (b) chemical structure of polymyxin B. Amino acid components: Dab, diaminobutyric acid; Thr, threonine; Leu, leucine; Phe, phenylalanine.

groups of polymyxins strongly interact with negatively charged membrane lipids of various tissues, including heart, brain, liver, lung, kidney or muscles cells (Kadar et al., 2013). Therefore, the release of tissue-bound polymyxin is relatively slow and the drug can persist in the body for over five days (Martin et al., 1999). Following IV administration of colistin to rats, only small amounts of unchanged drug was recovered in the urine (Li et al., 2003b). This suggests that extensive reabsorption of polymyxins occurs, from renal tubular cells into the blood. Likewise, after IV injection of polymyxin B in critically ill patients, up to 95% of the drug was reabsorbed by renal tubular cells (Sandri et al., 2013). Given that less than 1% of unchanged polymyxin B was recovered in urine, it is believed that polymyxin B is excreted by a non-renal clearance pathway (Abdelraouf et al., 2012).

The five positively charged amino groups of colistin or polymyxin B have been implicated in causing side-effects, such as neurotoxicity and nephrotoxicity. At the cellular level, accumulated polymyxins bind to acidic phospholipids and the glycoprotein, megalin, located on the apical membrane of renal proximal tubule cells to increase membrane permeability (Azzopardi et al., 2012). This causes an increased influx of water, anions and cations, which ultimately leads to cell swelling and lysis (Kadar et al., 2013). Acute tubular necrosis has been also reported due to increased levels of creatinine and urea, which are also associated with polymyxin-induced toxicity (Azad et al., 2013). Respiratory paralysis induced by neuromuscular blockade has also been observed in patients treated with polymyxins, which was attributed to them binding to the lipids of the nerve fibre membrane, resulting in impaired acetylcholine release from presynaptic neurons into the synaptic gap (McQuillen et al., 1968, Myint et al., 2016). Insufficient release of acetylcholine prevents sodium ion influx into postsynaptic muscle fibres, leading to inhibition of muscle contraction. Most of the cases described in the literature suggested an increased risk of neuromuscular blockade in patients with renal dysfunction (Lindesmith et al., 1968, Myint et al., 2016).

As a consequence of these toxicity issues, sulfomethylation of colistin free amino groups has been used to produce a less toxic pro-drug, colistimethate

sodium (CMS; Colomycin®), which hydrolyses in the body into active colistin (Beveridge and Martin, 1967). Although sulfomethylation decreases the efficacy of the drug (as well as its membrane-binding capacity), it is the only form of colistin currently used clinically for systemic administration. Unlike colistin, when CMS is administered IV to critically ill patients, ~60% is eliminated unchanged in the urine by glomerular filtration (Michalopoulos and Falagas, 2011). Prior to administration, lyophilised CMS is reconstituted in sterile water and hydrolysis occurs rapidly in human plasma at 37°C. Due to the unpredictable rate and extent of hydrolysis, reconstitution should be performed no more than 24 h prior to administration, since premature hydrolysis and formation of active drug may occur if the solution is made up in advance (Le et al., 2010). Indeed, in 2007, the FDA issued an alert after a patient died following inhalation of a pre-mixed Colomycin solution that was believed to have hydrolysed *in vitro* (FDA, 2007).

### **3.1.3 Selection of appropriate linker**

Selection of an appropriate linker for the attachment of the polymer to its payload is fundamental to being able to reproducibly generate a stable conjugate in high yields. The ability to achieve triggered drug release and reinstatement of its activity at the target site is also advantageous. Many linker groups have been used for polymer-drug conjugation including carbonate, urethane, anhydride, ester or amide bonds (Elvira et al., 2005). To improve the therapeutic index and decrease the systemic toxicity of antibiotics, amide, ester and urethane linkers have been used to attach the peptide and polyene antibiotics to PEG (Cal et al., 2017). PEGylated amphotericin B, linked via a stable amide bond, not only retained antifungal activity in a range of clinical isolates, but also exhibited significantly higher water solubility and markedly reduced toxicity (Halperin et al., 2016). Due to the lability of the ester bond, PEGylated colistin prodrug reverted back into its active form within the first 24 h *in vitro* and demonstrated a similar antimicrobial activity to CMS against several MDR bacterial pathogens and displayed no nephrotoxicity, as confirmed by histological analysis of mice kidneys (Zhu et al., 2017).

Carbodiimide compounds are so-called 'zero-length' cross-linking reagents that are used to facilitate direct conjugation of the bioactive molecule without becoming part of the final linker structure (Xu et al., 2003). Indeed, the majority of previously reported alginate conjugates were synthesised using EDC/NHS crosslinkers to form an amide bond, while DCC/DMAP coupling agents have been used for ester bond formation (Basu et al., 2015, Yang et al., 2011). In this study, amide and ester linkers were chosen for antibiotic conjugation to OligoG.

Amide linkage is a very common means of conjugating a polysaccharide to a protein drug and was previously used in dextrin-colistin conjugates (Ferguson et al., 2014). These conjugates are very stable and rely on degradation of the polymer's backbone by the enzyme alginate lyase. This leaves both sugar residues and the linker group still attached to the antibiotic, which may impact on its antimicrobial activity. Endolytic alginate lyase cleaves the glycosidic bonds using a  $\beta$ -elimination reaction, leading to depolymerisation of alginate into oligomers (Kim et al., 2011). Subsequently, exolytic oligoalginate lyase further degrades oligomers into unsaturated monosaccharides. To date, however, no enzymatic pathways capable of degrading alginates have been discovered in humans. However, some bacterial pathogens such as *P. aeruginosa* or *A. vinelandii* are able to synthesise, degrade and metabolise alginates. To form a stable amide bond, water-soluble EDC activates the carboxyl groups of OligoG polymer backbone forming an O-acylisourea intermediate, which then reacts with the primary amino groups of the polymyxin. In aqueous solutions, however, O-acylisourea is unstable and prone to hydrolysis, which results in regeneration of carboxyl groups and the liberation of unsubstituted urea (Hermanson, 2013). Therefore, to increase the efficacy of the reaction, sulfo-NHS is commonly combined with EDC to convert the O-acylisourea intermediate into a stable amine-reactive sulfo-NHS ester, which then rapidly reacts with amino groups on the target molecule. The reaction scheme can be seen in **Figure 3.3**.

In contrast to the amide linker, incorporation of an ester bond between the alginate oligomer and antibiotic would allow separation of the parent molecules

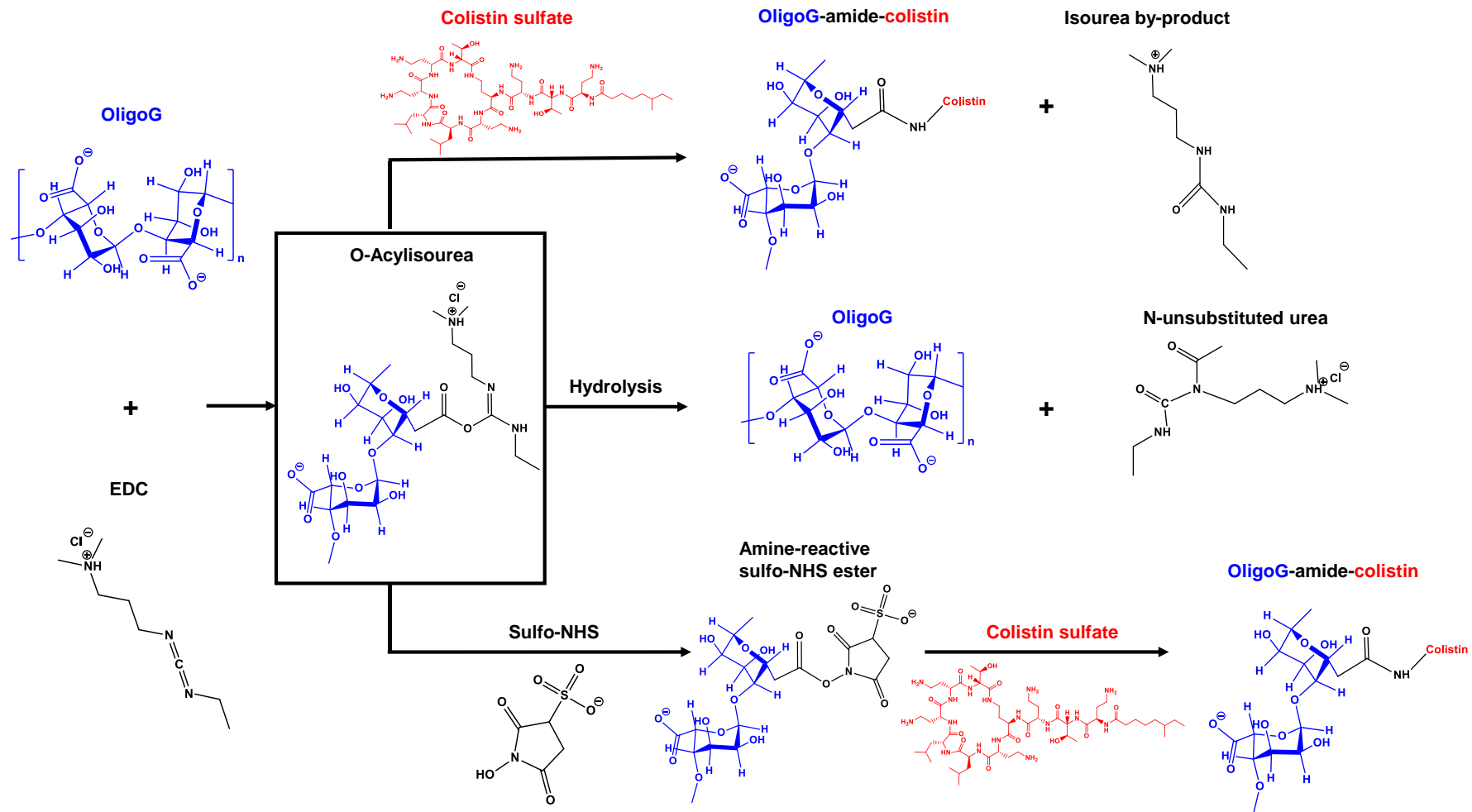


**Figure 3.3** Schematic diagram showing synthesis of the OligoG-amide-polymyxin conjugate.

by esterase enzymes and hydrolysis at sites of bacterial infection. Ongoing inflammation, overproduction of reactive oxygen and nitrogen species and an acidic pH would accelerate ester bond degradation (Liang and Liu, 2016, Pu et al., 2014). Additionally, hydrolytic enzymes such as esterases, catalyse the cleavage of the ester bond, forming alcohol and acid metabolites (Montella et al., 2012). The advantage of this approach is that conjugated antibiotics may benefit from passive targeting to sites of infection by the EPR effect (Section 1.6.2), and that full antibiotic activity of each component could be reinstated after separation. Hence, the potential “bifunctionality” of the conjugate (i.e. the antibiotic potentiation effect of OligoG alongside polymyxin efficacy) could also be exploited by this co-localisation of the antibiotic and intact alginate oligomer at the site of infection. Ester bond formation using DCC and DMAP was first reported by Neises and Steglich (Neises and Steglich, 1978). Here, DCC reacts with the carboxyl groups of OligoG to form an O-acylisourea intermediate, which then reacts with the hydroxyl groups of the polymyxins. However, since hydroxyl groups are much weaker nucleophiles than amines, potential side reactions can occur causing spontaneous rearrangement of the O-acylisourea intermediate into undesirable N-acylurea, which is unable to further react with hydroxyl groups (Tsakos et al., 2015). Therefore, to accelerate the DCC-mediated coupling and suppress the side product formation, DMAP is commonly used as a catalyst. The DMAP rapidly interacts with O-acylisourea forming acyl pyridinium species, which further react with hydroxyl groups of the target molecule to form the ester bond (Tsakos et al., 2015). This reaction scheme can be seen in **Figure 3.4**.

The main principle of conjugate synthesis and drug release can be seen in **Figure 3.5**.

### **3.2 Experimental aims and objectives**

**The specific aims of this study were:**

- To synthesise a library of polymer-polymyxin conjugates using the antimicrobial alginate OligoG.

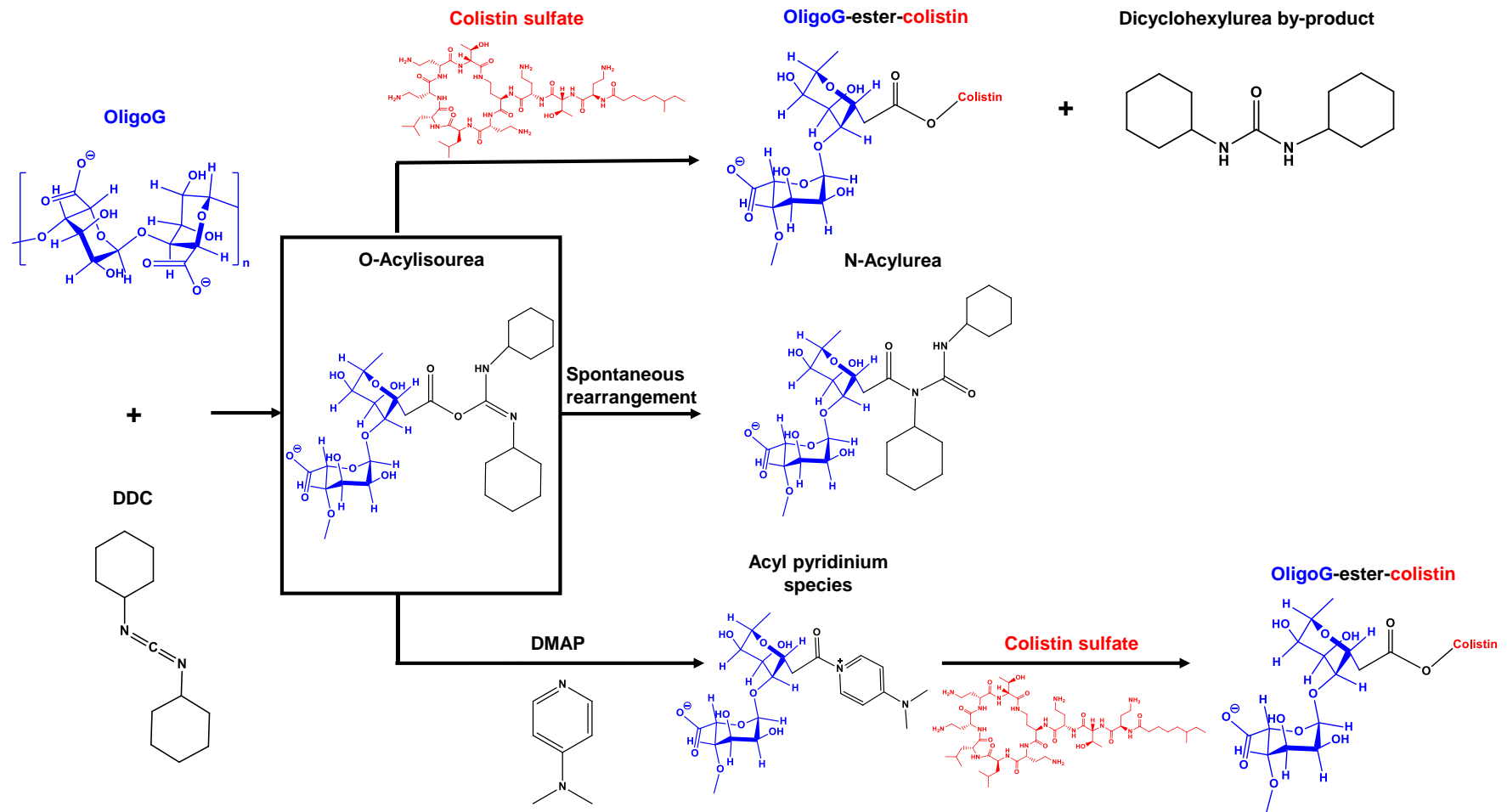
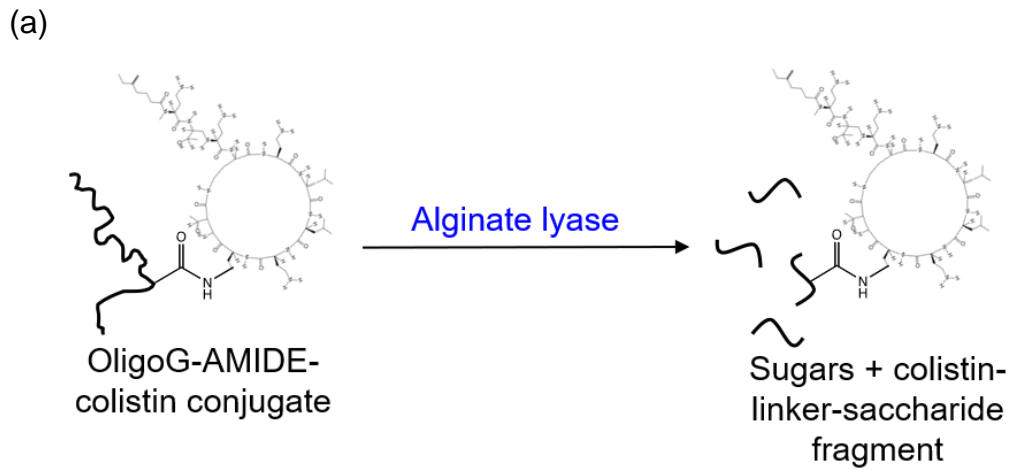
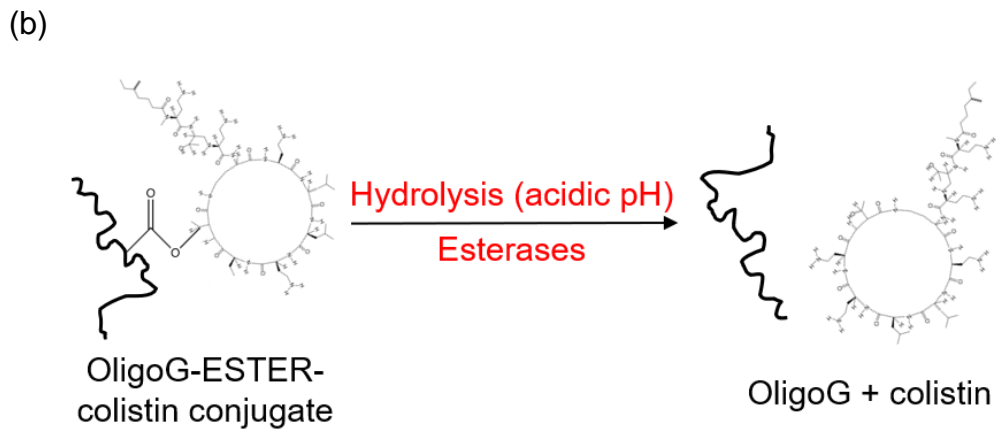


Figure 3.4 Schematic diagram showing synthesis of the OligoG-ester-polymyxin conjugate.



Amide conjugates rely on enzyme degradation of the polymer backbone, leaving sugar residues still attached to the antibiotic.



Allows separation of the parent molecules at the site of infection.

**Figure 3.5** Schematic diagram showing alginate antibiotic conjugation and drug release from the polymer of (a) the OligoG-AMIDE-colistin conjugate and (b) the OligoG-ESTER-colistin conjugate.

- To characterise polymer-drug conjugates in respect of their total protein content (drug loading), molecular weight and molecular weight distribution (polydispersity), purity (free protein content of the conjugate) and the number of amino groups in the polymyxins used for OligoG binding.
- To assess the *in vitro* cytotoxicity of the OligoG-antibiotic conjugates in human kidney (HK-2) cells.

### 3.3 Methods

Many general methods were used for physicochemical characterisation of OligoG-polymyxin conjugates including the BCA assay (Section 2.6.2.3), FPLC (Section 2.6.2.2), GPC (Section 2.6.2.1) and the ninhydrin assay (Section 2.6.2.4). Biological characterisation of OligoG-antibiotic conjugates was performed using a TNF $\alpha$  ELISA (Section 2.6.3.6) and the MTT assay (Section 2.6.3.5) as described in Chapter 2.

#### 3.3.1 Synthesis of OligoG-antibiotic conjugates

OligoG-polymyxin conjugates were synthesised using the zero-length cross-linking agents, EDC (with sulfo-NHS) or DCC (with DMAP), to create stable amide or ester bond formation, respectively. The reactions are described in detail below. In addition, OligoG-amide-bacitracin conjugate has been synthesised and characterised using the methods described below but due to relatively low drug loading, the results are provided as supplementary information (**Appendices 5.1-5.5**).

##### *a) Synthesis of OligoG-polymyxin conjugates using an amide (A) linker*

OligoG (1000 mg, 0.3 mmol), EDC (96.8 mg, 0.5 mmol) and sulfo-NHS (109.6 mg, 0.5 mmol) were dissolved in dH<sub>2</sub>O (10 ml) in a round-bottomed flask and stirred for 15 min at 21°C. To this mixture, colistin sulfate (146.7 mg, 0.1 mmol) or polymyxin B (144.4 mg, 0.1 mmol) was added followed by dropwise addition of NaOH (0.5 M) until pH 8 was reached. The reaction mixture was stirred for 2 h at 21°C, then stored at -20°C prior to purification by FPLC.

### *b) Synthesis of OligoG-polymyxin conjugates using an ester (E) linker*

OligoG (1000 mg, 0.3 mmol), DCC (64.5 mg, 0.3 mmol), DMAP (6.4 mg, 0.05 mmol) and colistin sulfate (146.7 mg, 0.1 mmol) or polymyxin B (144.4 mg, 0.1 mmol) were dissolved under stirring in anhydrous DMSO (10 ml) in a round-bottomed flask. The reaction mixture was left to stir overnight at 21°C. The reaction was stopped by pouring the mixture into excess chloroform (~50 ml). Formed precipitates were collected by filtration and dissolved in dH<sub>2</sub>O (10 ml), then stored at -20°C prior to purification by FPLC.

### **3.3.2 Purification and characterisation of OligoG-polymyxin conjugates**

FPLC was used to purify OligoG-polymyxin conjugates by removing unreacted linking agents and drug, as already described in Chapter 2 (Section 2.6.1). Collected fractions were desalted, lyophilised and stored at -20°C prior use. The final product was characterised by BCA assay to determine total protein content (Section 2.6.2.3); by GPC to define molecular weight and molecular weight distribution (Section 2.6.2.1); by FPLC to quantify the percentage of unconjugated drug (Section 2.6.2.2) and by ninhydrin assay to calculate the number of primary amines used for OligoG conjugation (Section 2.6.2.4).

### **3.3.3 Cytotoxicity of OligoG-antibiotic conjugates**

An MTT assay (Section 2.6.3.5) was used to measure HK-2 cell viability and proliferation after 72 h incubation with OligoG, OligoG-polymyxin conjugates or polymyxin alone. Cytotoxicity of OligoG-E-colistin and OligoG-E-polymyxin B conjugates had previously been assessed by E. L. Ferguson (for inclusion in a patent application). The concentration range of 0.004-1 mg/ml (polymyxin equivalent) was used to calculate the IC<sub>50</sub> (half maximal inhibitory concentration) values of the compounds (n = 18).

### **3.3.4 TNF $\alpha$ ELISA assay**

The release of the proinflammatory cytokine, TNF $\alpha$ , from HK-2 cells was assessed using an ELISA kit. Cells were treated with a range of concentrations of OligoG-polymyxin conjugates or polymyxin alone as

described in Chapter 2 (Section 2.6.3.5). After 72 h incubation, the 96-well microtitre plates were centrifuged (226 g, 3 min), the supernatant was transferred into a clean 96-well plate, then diluted in equal parts with reagent diluent and analysed with the TNF $\alpha$  ELISA according to the manufacturer's instructions. In parallel, 100  $\mu$ l of K-SFM was added to centrifuged cells and MTT assays were performed as described previously (Section 2.6.3.5). A standard curve was constructed by plotting the mean absorbance obtained from each standard solution versus the corresponding TNF $\alpha$  concentration (pg/ml). This curve was used to calculate the TNF $\alpha$  concentrations of the test samples, which were then multiplied by the dilution factor (x 2) and divided by cell viability for each drug concentration (from the MTT assay results). Data was expressed as mean  $\pm$  SEM (n = 6).

### **3.4 Results**

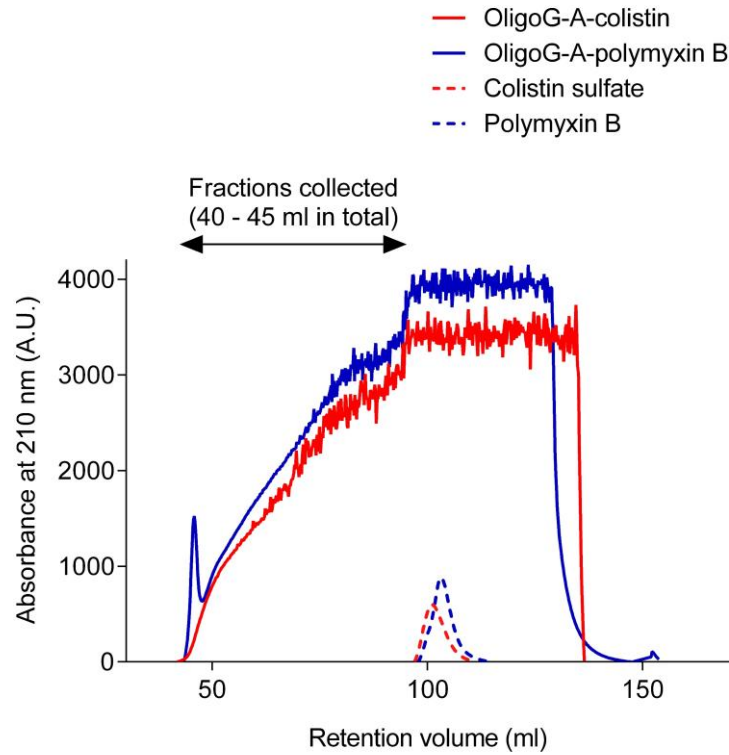
#### **3.4.1 Synthesis and purification of OligoG-polymyxin conjugates**

FPLC confirmed successful OligoG-polymyxin conjugate synthesis, with conjugates typically eluting between 40-95 ml. Polymyxins, which exhibited strong absorbance at 210 nm, eluted at ~100 ml. Since OligoG had no absorbance signal, unconjugated OligoG was not visible by FPLC. Fractions containing conjugates were collected, pooled and lyophilised. A typical elution profile of the conjugate reaction mixture can be seen in **Figure 3.6a** (OligoG-A-polymyxin conjugate) and **Figure 3.6b** (OligoG-E-polymyxin conjugate).

#### **3.4.2 Characterisation of OligoG-polymyxin conjugates**

GPC analysis revealed a shorter retention time, indicative of an increase in molecular weight and polydispersity of the OligoG-drug conjugates, compared with the free drugs (**Figure 3.7**). Typically, OligoG-polymyxin conjugates had an apparent molecular weight 2-3 times higher than that of the free drug, resulting in a range of 22,500-27,000 g/mol for amide-linked conjugates and slightly lower (15,500-20,000 g/mol) for ester-linked conjugates. The polydispersity index indicated a broad molecular weight distribution, which varied from 2.2-2.7 for amide-linked and 2.1-3.1 for ester-linked conjugates.

(a)



(b)

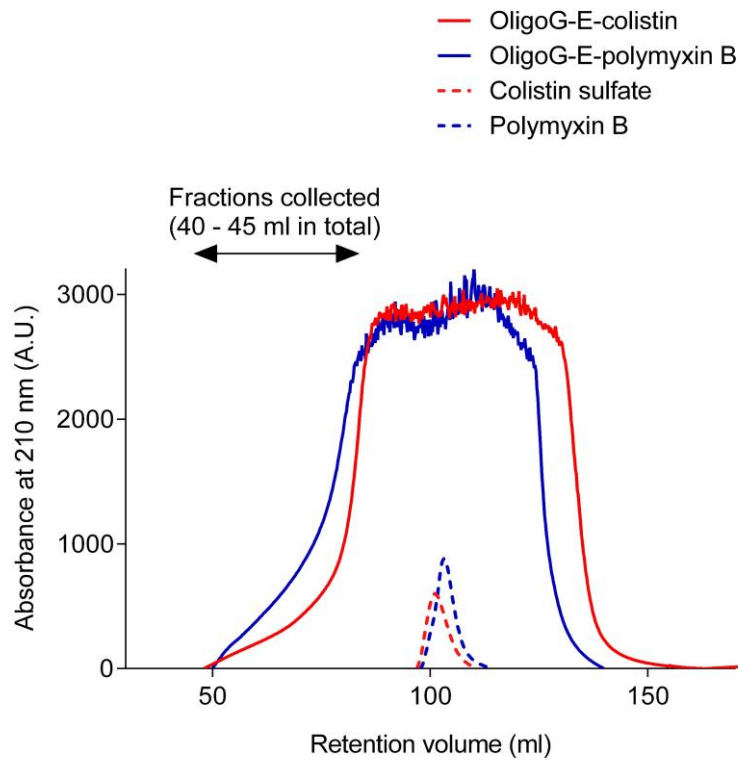


**Figure 3.6** Typical elution profile of conjugate reaction mixture before purification using a Superdex 75 (16/600) size exclusion column. (a) Chromatogram of the OligoG-A-polymyxin conjugate, (b) chromatogram of the OligoG-E-polymyxin conjugate.  $V_0$  (void volume) = 45 ml,  $V_b$  (bed volume) = 120 ml.

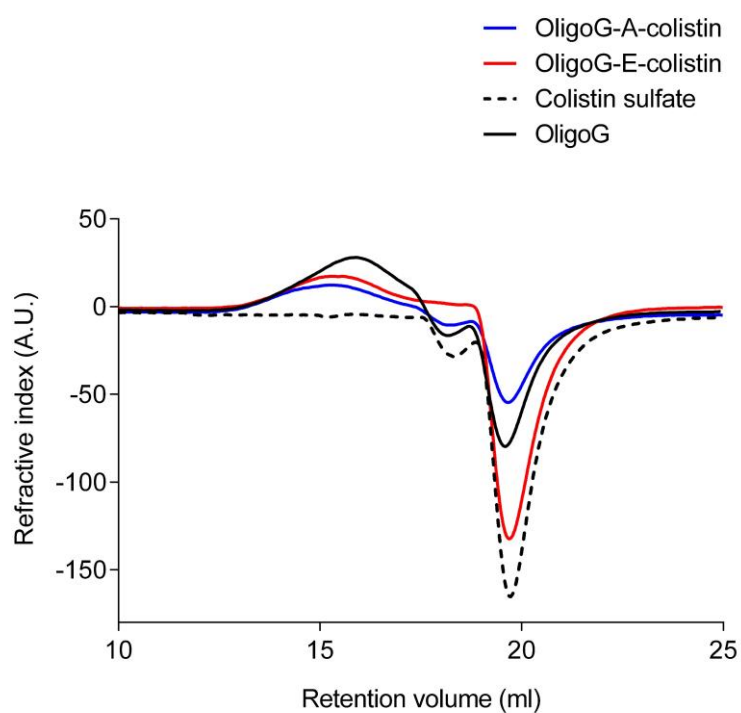


**Figure 3.7** Typical elution profile of OligoG-polymyxin conjugates using GPC analysis.  $V_0$  (void volume) = 13 ml,  $V_b$  (bed volume) = 20 ml.

A summary of the relative molecular weight average and polydispersity of each OligoG-polymyxin batch is presented in **Table 3.2**.

The presence of the high molecular weight conjugate with an elution peak at ~8-14 ml was verified by FPLC analysis. Free antibiotic eluted at ~17 ml, while a peak corresponding to unreacted cross-linking agents was observed at ~18-19 ml. The typical elution profile of OligoG-polymyxin conjugate and its unreacted components can be seen in **Figure 3.8a**. The chromatograms of purified conjugates are shown in **Figure 3.8b**, where the first peak shows the OligoG-antibiotic conjugate with an almost undetectable amount of free drug (circled peak). Analysis of the area under the curves indicated that the free drug content in the conjugates was always < 6% (**Table 3.2**). The drug loading, calculated by BCA assay, of OligoG-A-polymyxin conjugates varied from 6.1-12.5% (w/w), while OligoG-E-polymyxin conjugates contained 7-12.9 % (w/w) of the drug (**Table 3.2**). After conjugation, the ninhydrin assay revealed that OligoG-A-colistin conjugates used ~3-4 primary amino groups on the colistin molecule, while OligoG-A-polymyxin B conjugates used ~2 of these groups, as indicated in **Table 3.2**.

### 3.4.3 Biological characterisation of OligoG-antibiotic conjugates

The concentration-dependent cytotoxicity of free antibiotics, OligoG and OligoG-polymyxin conjugates in HK-2 cells is shown in **Figure 3.9**. **Table 3.3** summarises the IC<sub>50</sub> values derived from these plots. As expected, no cytotoxicity was observed when cells were treated with OligoG alone up to 10 mg/ml. While colistin and polymyxin B were cytotoxic to HK-2 cells in a dose-dependent manner (IC<sub>50</sub> = 0.026 ± 0.002 mg/ml and 0.011 ± 0.001 mg/ml, respectively), conjugation of OligoG markedly reduced their toxicity. Conjugates containing an amide linker increased colistin's IC<sub>50</sub> by 9.3-fold (IC<sub>50</sub> = 0.242 ± 0.066 mg/ml) whereas ester-linked conjugates reduced toxicity by 2.2-fold (IC<sub>50</sub> = 0.057 ± 0.014 mg/ml). Similarly, OligoG conjugation significantly reduced the toxicity of polymyxin B by 27.2-fold for OligoG-A-polymyxin B (IC<sub>50</sub> = 0.299 ± 0.033 mg/ml) and 2.9-fold for OligoG-E-polymyxin B (IC<sub>50</sub> = 0.032 ± 0.003 mg/ml) conjugates. There was a significant difference

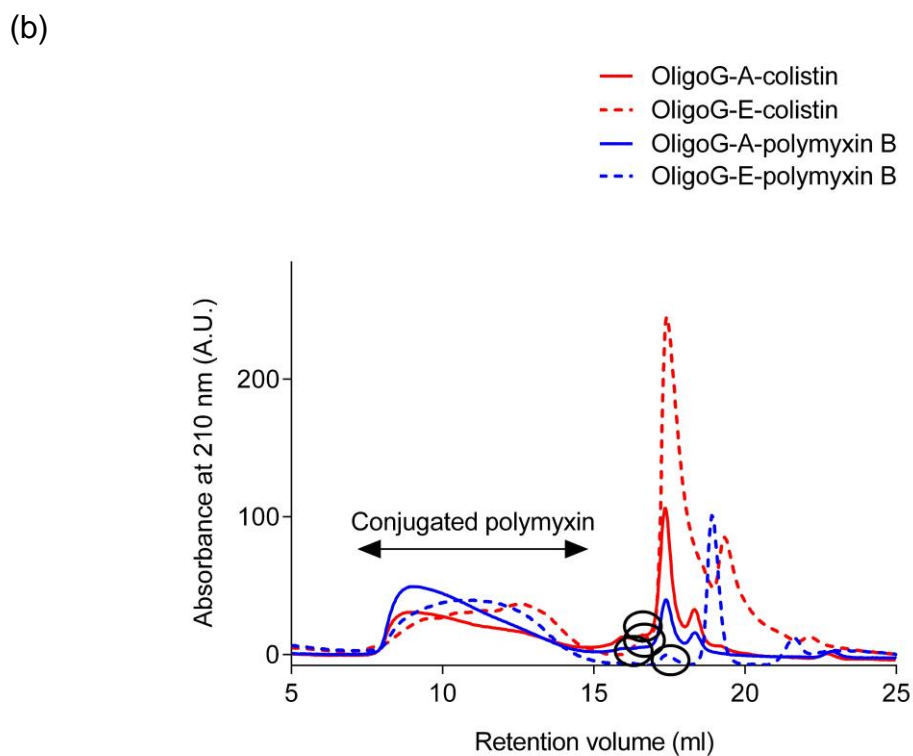
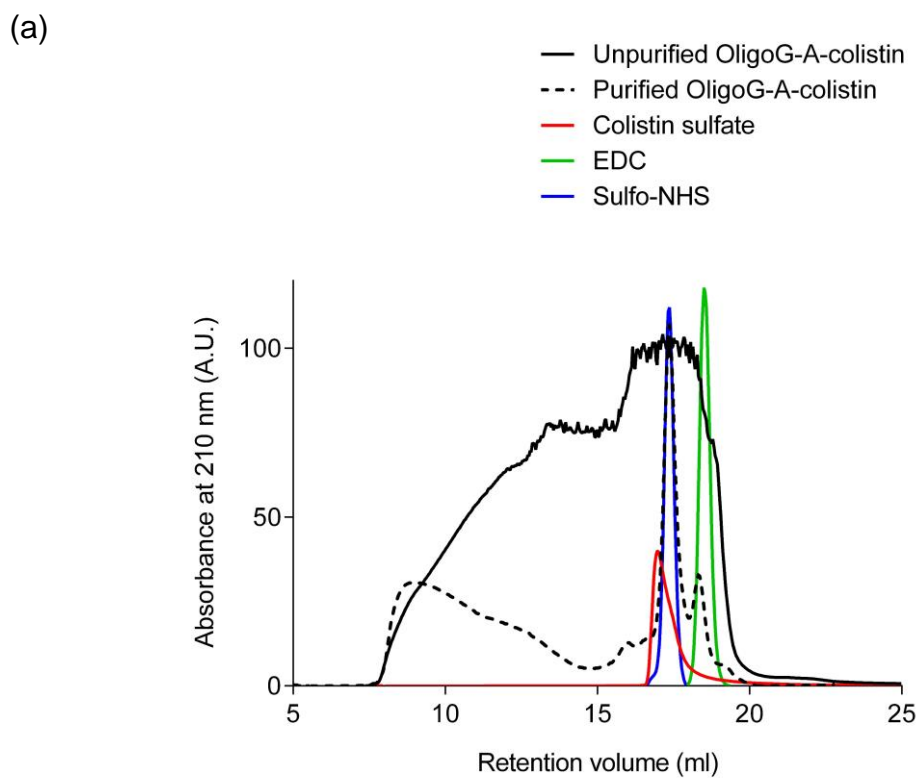


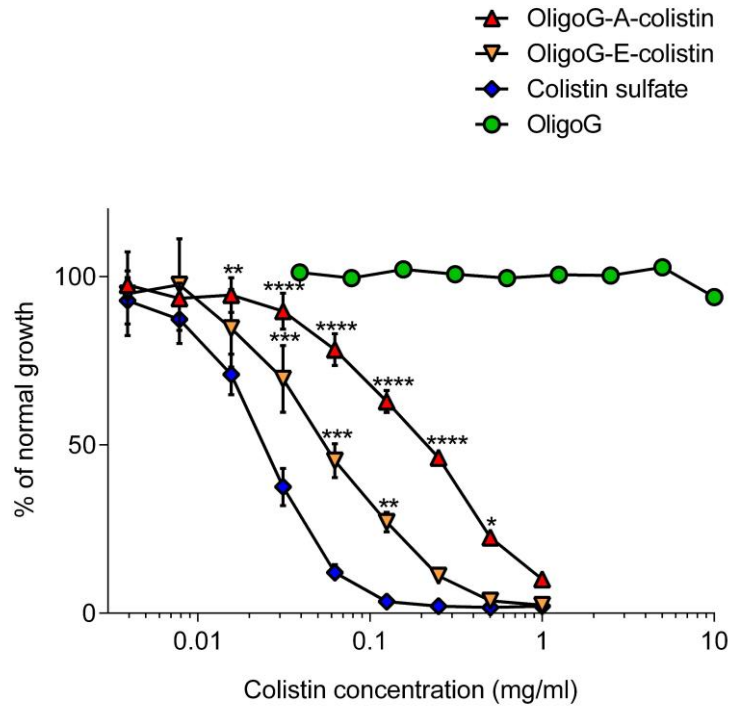
**Figure 3.8** Characterisation of OligoG-polymyxin conjugates using FPLC. (a) Typical analysis profile of OligoG-A-colistin conjugate. (b) Elution profiles of purified OligoG-drug conjugates. Elution peak of the free drug has been circled.  $V_0$  (void volume) = 7.7 ml,  $V_b$  (bed volume) = 24 ml.

**Table 3.2** Characterisation summary of OligoG-polymyxin conjugates.

Tested compound	Mw (g/mol) (PDI) by GPC	Mw (g/mol) (PDI) by SEC-MALLS	Protein content (% w/w)	Molar ratio (per colistin)	Conjugated NH <sub>2</sub> per molecule	Free protein (%)
OligoG-A-colistin	25,500 (2.6)	12,300 (1.4)	8.7	4.6	2.8	5.7
OligoG-A-colistin	22,500 (2.3)	9,100 (1.3)	8.8	4.6	2.7	1.5
OligoG-A-colistin	24,500 (2.3)	-	9.1	4.4	3.6	2.5
OligoG-A-colistin	27,000 (2.5)	-	12.5	3.1	3.3	2.4
OligoG-A-colistin	24,500 (2.2)	-	8.1	5.0	4.6	4.0
OligoG-E-colistin	14,500 (2.3)	5,900 (1.2)	12.9	3.0	-	2.0
OligoG-E-colistin	16,500 (2.2)	-	11.5	3.4	-	3.5
OligoG-E-colistin	20,000 (3.1)	-	8.3	4.9	-	2.7
OligoG-A-polymyxin B	23,000 (2.7)	12,800 (1.5)	8.0	5.1	1.9	1.6
OligoG-A-polymyxin B	23,500 (2.2)	9,100 (1.3)	6.1	6.8	2.0	1.6
OligoG-E-polymyxin B	15,500 (2.1)	6,200 (1.2)	7.0	5.9	-	2.7

Molecular weight was estimated by GPC relative to pullulan standards or by size exclusion chromatography with multi-angle laser light scattering (SEC-MALLS). Mw, molecular weight average of the weight; PDI, polydispersity index.

(a)



(b)

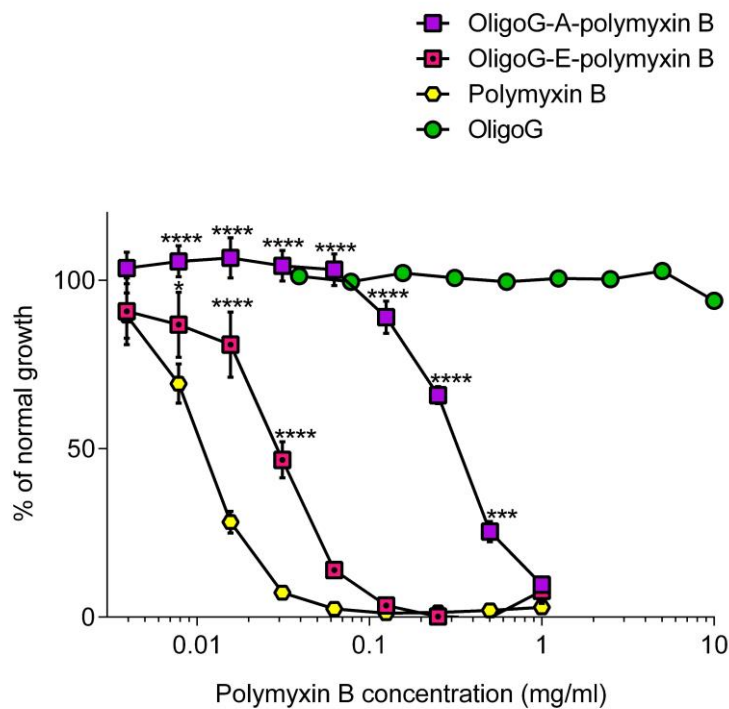


**Figure 3.9** *In vitro* cytotoxicity of OligoG-polymyxin conjugates in HK-2 cells. Cell viability after incubation with a range of (a) colistin and (b) polymyxin B concentrations. Data is presented as % of normal growth compared with the untreated control cells  $\pm$  SEM ( $n = 18$ ). Significant difference is indicated by \*, where \* $p < 0.05$ , \*\* $p < 0.01$ , \*\*\* $p < 0.001$ , \*\*\*\* $p < 0.0001$  compared to colistin sulfate or polymyxin B. (Two-way ANOVA and Dunnett's multiple comparisons tests).

**Table 3.3** IC<sub>50</sub> values ( $\pm$  SEM) and fold-change of OligoG-polymyxin conjugates derived from MTT assay in HK-2 cells.

<b>Compound</b>	<b>IC<sub>50</sub> (mg/ml)</b>	<b>Fold-change</b>
OligoG-A-colistin	0.242 $\pm$ 0.066	9.3
OligoG-E-colistin	0.057 $\pm$ 0.014	2.2
Colistin sulfate	0.026 $\pm$ 0.002	-
OligoG-A-polymyxin B	0.299 $\pm$ 0.033	27.2
OligoG-E-polymyxin B	0.032 $\pm$ 0.003	2.9
Polymyxin B	0.011 $\pm$ 0.001	-
OligoG	> 10	-

between cytotoxicity of the treatment combinations tested ( $p < 0.05$ ).

Concentration-dependent release of TNF $\alpha$  is presented in **Figure 3.10a**. However, as the previous MTT assays had shown that the different treatments used had different effects on cell viability, the TNF $\alpha$  release data was adjusted to account for cell viability of each drug concentration as shown in **Figure 3.10b**. The outliers were identified and removed using Robust regression and Outlier removal (ROUT) method (Q coefficient was set to 0.2%) specified by GraphPad Prism software. Both Polymyxin B and colistin alone induced greater TNF $\alpha$  release compared to the conjugates, where TNF $\alpha$  release was very low or undetectable, except for OligoG-E-polymyxin B, although this was still lower than free polymyxin B. At the highest drug concentration, significant differences were observed between free and OligoG-conjugated antibiotics at equivalent drug concentrations ( $p < 0.05$ ).

### 3.5 Discussion

The limited therapeutic options available to treat MDR infections, particularly those caused by Gram-negative pathogens, has forced the clinical use of last resort antibiotics, such as polymyxins in humans. However, the misuse and overuse of polymyxins (especially in animal husbandry) has greatly contributed to antimicrobial resistance. Therefore, this Chapter aimed to synthesise a library of OligoG-polymyxin conjugates to (i) select the best linker for use in polymer conjugate chemistry, and (ii) characterise their *in vitro* toxicity and antimicrobial activity (addressed in subsequent chapters).

The fate of alginates after systemic administration has been studied in mice by covalent incorporation of tyrosinamide into the polymer chains and subsequent radioiodination (Al-Shamkhani and Duncan, 1995). After IV administration of the polymer conjugate for 24 h, larger fractions ( $> 48,000$  g/mol) remained in the circulation without any tissue accumulation, while low molecular weight fractions ( $< 48,000$  g/mol) were excreted in the urine. After systemic administration, many polysaccharides, such as hyaluronan and dextran are degraded by physiological enzymes, which can be harnessed to release the drug payload at the target site using polymer-masked unmasked protein

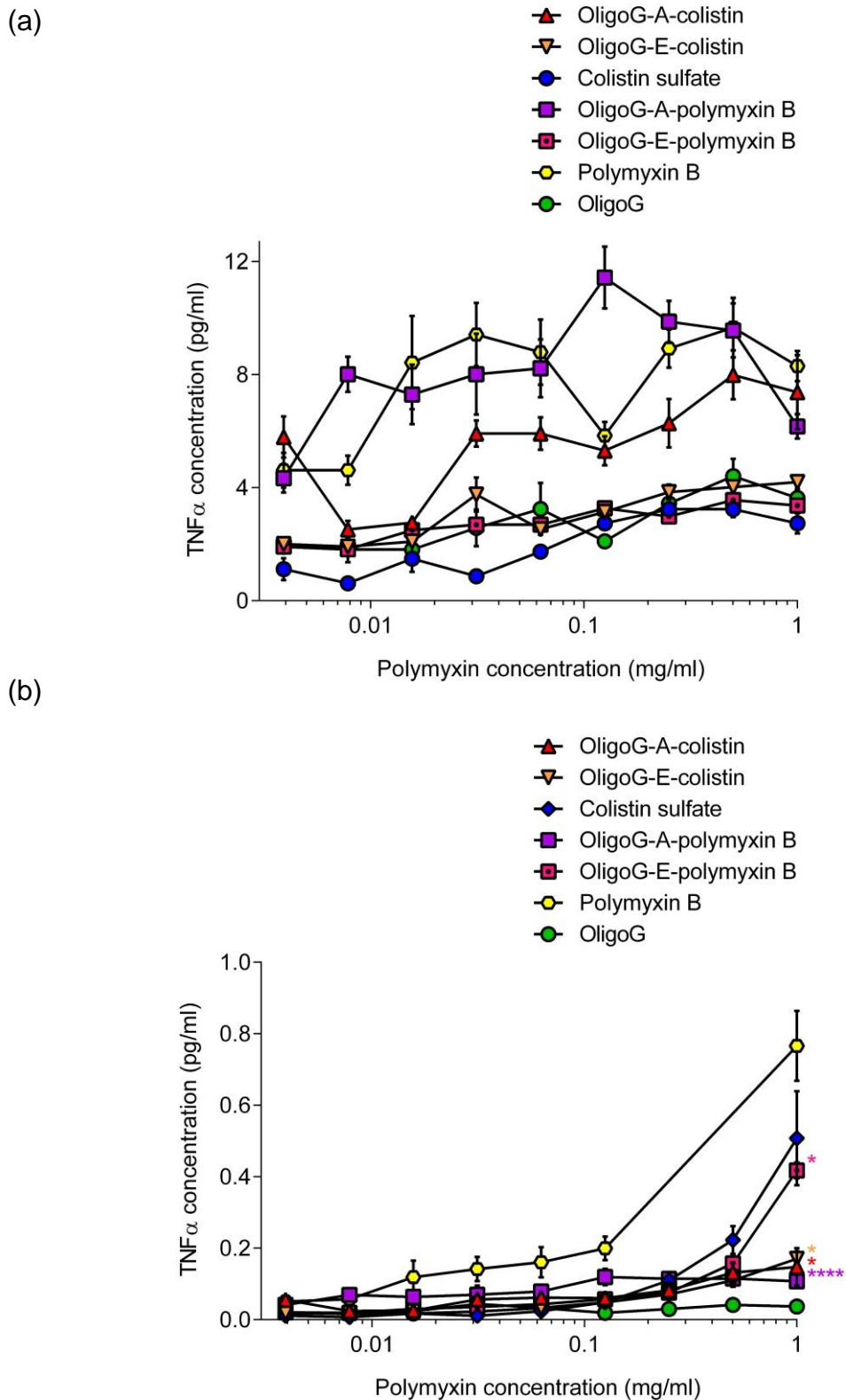


**Figure 3.10** TNF $\alpha$  release in HK-2 cells after incubation with OligoG-polymyxin conjugates for 72 h. (a) TNF $\alpha$  release for a range of polymyxin concentrations ( $\pm$  SEM;  $n = 6$ ). (b) TNF $\alpha$  release adjusted to cell viability for each drug concentration ( $\pm$  SEM;  $n = 6$ ). Significant difference is indicated by \*, where \* $p < 0.05$ , \*\*\*\* $p < 0.0001$  compared to the colistin or polymyxin B controls. (Two-way ANOVA and Dunnett's multiple comparisons tests).

therapy (PUMPT). Unfortunately, alginate conjugates are not suitable for PUMPT, since alginates such as OligoG are not degraded by mammalian enzymes. Instead, it is necessary to rely on bacterial alginate lyase, secreted by certain bacteria, to break down the polymer.

Preliminary experiments, using GPC to analyse the change in molecular weight of OligoG in the presence of alginate lyase isolated from *Sphingobacterium multivorum* (1-1000 U/ml) had revealed a concentration-dependent reduction in molecular weight (Ferguson et al., 2016). Similarly, incubation of OligoG-polymyxin conjugates with bacterial alginate lyase (1 U/ml) had effectively decreased apparent molecular weight of the conjugate, triggering ~30% of colistin and ~90% of polymyxin B release within 24 h. Interestingly, no notable difference between amide or ester-linked conjugates was observed. While amide-linked conjugates rely on degradation of the polymer backbone, incorporation of an ester bond would render the conjugates susceptible to degradation and drug release due to acidic pH, esterase enzymes and overproduction of reactive oxygen species in the infected tissues, as well as secreted alginate lyase from bacterial infection. It is widely accepted that non-biodegradable polymers with a molecular weight lower than the renal threshold (< 40,000 g/mol) can be excreted without accumulating in the body (Greco and Vicent, 2008), so the conjugates synthesised here would be readily excreted by the kidney, regardless.

*P. aeruginosa* is one of the leading pathogens responsible for high morbidity and mortality in patients with cystic fibrosis due to overproduction of exopolysaccharide composed of guluronic and mannuronic acids, by predominantly mucoid isoforms. Co-administration of bacterial alginate lyase with antibiotics has been shown to significantly improve biofilm eradication in patients colonised with alginate-producing, mucoid bacteria (Alkawash et al., 2006). When mucoid *P. aeruginosa* biofilms were treated with gentamicin at 64 mg/ml (2-fold higher than its minimum bactericidal concentration) for 1 week, eradication was not achieved. However, when alginate lyase (20 U/ml) was co-administered with gentamicin, significant elimination of the mucoid biofilm was accomplished. These results validate the future potential of

developing a “two-step therapy”, whereby OligoG-antibiotic conjugates and alginate lyase are administered sequentially to target sites of infection by the EPR effect, thereby triggering localised drug release by polymer degradation.

Unlike well-defined conventional small molecule drugs, polysaccharide-protein and -peptide conjugates are complex mixtures that are not easily separated, identified or characterised. Indeed, many potential polymeric carriers, especially polysaccharides, lack structural uniformity. It has been demonstrated that molecular weight, chemical structure or morphological differences in the polymer, may have a profound effect on the physicochemical and biological properties of the whole polymer-drug conjugate (Ali and Brocchini, 2006, Godwin et al., 2001). While the lack of polymer uniformity may not be an issue for oral and topical formulations, its influence on biodistribution, metabolism and elimination of the conjugate after systemic administration is expected to be more significant. Polymer non-uniformity could also potentially impede batch-to-batch reproducibility for pharmaceutical development. What is more, previous reports have indicated the propensity for polysaccharides to become non-biodegradable and immunogenic after chemical modification such as drug conjugation (Vercauteren et al., 1990). It was therefore extremely important to fully characterise the OligoG-polymyxin conjugates used in these studies.

A major disadvantage of SEC methods employing a single concentration detector, is that they provide only comparative measurements derived from a calibration curve of molecular weight markers, as a function of time. While this method can provide accurate molecular weights for samples with the same chemistry as the calibration standards, when the chemical structure of the sample and standards are different, (as is the case with polysaccharide-peptide conjugates which are neither a protein or polymer), the results are only comparative. Also, since alginate molecular weight standards are not available for GPC calibration, pullulan molecular weight standards had to be used to produce the calibration curve. Pullulan is a polysaccharide that forms random coils in aqueous solution (Shingel, 2004), whereas alginates exhibit an expanded macromolecular structure due to repulsion between the negative

charges along its chain. Due to the effect on hydrodynamic volume, pullulan standards are known to overestimate alginate molecular weight by up to 6 times (Andersen et al., 2012). Nevertheless, GPC showed that the conjugates were a polydisperse mixture of species, it being well-known that polysaccharides are highly polydisperse ( $PDI > 2$ ), which presents a particular challenge for pharmaceutical development (Duncan, 2003). Ideally, drugs developed for pharmaceutical applications should have a narrow polydispersity, since high polydispersity can affect biological activity of the drug and hinder conjugate characterisation. Consequently, SEC with multi-angle laser light scattering (SEC-MALLS) detection is used as an international standard method for determining molecular weight and molecular weight distribution of alginates (American Society for Testing and Materials; ASTM, 2016). The principle of the technique is based on the Rayleigh theory, which shows that the intensity of the scattered light by a molecule is proportional to its molecular weight (Andersson et al., 2003). Therefore, multiple light scattering measurements can be made (at a range of different angles) to calculate absolute molecular mass. To validate the results obtained in these studies, OligoG-polymyxin conjugates developed in this chapter were also analysed using SEC-MALLS (carried out by Dr Olav Aarstad at the Norwegian University of Science and Technology, NTNU, Trondheim, Norway). As expected, notably lower molecular weights and molecular weight distributions of the OligoG-polymyxin conjugates were measured using this technique.

FPLC could not be used to determine the molecular weight of purified conjugates because OligoG-polymyxin conjugates eluted in the void volume of the column. It is also important to note that FPLC was not capable of distinguishing between free OligoG and the OligoG-polymyxin conjugate, since they both elute at the same point. Although it is not ideal to include free OligoG in the product, clinical trials have shown the polymer to be safe and non-immunogenic (at concentrations up to 60 mg/ml) and its inherent biological activity may yield additional clinical benefit. In the longer term, to facilitate thorough characterisation of the active species, this issue will ultimately need to be addressed. Nevertheless, FPLC showed that only a small fraction of the free drug was present in the conjugate suggesting that OligoG-polymyxin

conjugates would have a beneficial therapeutic index *in vivo*.

OligoG-polymyxin conjugates were reproducibly synthesised to contain 6.1-12.9% (w/w) protein with < 6% free drug. The choice of linker did not appear to significantly affect drug loading, although the OligoG-polymyxin B conjugates typically contained less drug than the colistin conjugates. The ninhydrin assay indicated a decrease in available primary amines in the OligoG-conjugated amide-linked polymyxins, suggesting that 2-4 amino groups were used for binding to the polymer. Although colistin and polymyxin B are known to contain 5 primary amines, the ninhydrin assay only detected ~4 of them. This may be due to one of the amines being inaccessible. It has also been shown that some amines react with ninhydrin at a much slower rate, affecting Ruhemann's purple colour yield formation (Friedman, 2004), which could also help explain the difference between the actual and measured amine groups seen here.

Since polymyxins have been reported to cause severe nephrotoxicity in up to 53.5% of patients (Spapen et al., 2011), it was important to determine the *in vitro* toxicity of the conjugates in kidney cells. As previously shown in the literature, polymyxin B was 2-3 times more nephrotoxic than colistin sulfate in HK-2 cells (Vaara and Vaara, 2013). Importantly here, OligoG conjugation significantly decreased the cytotoxicity of both colistin and polymyxin B in human kidney cells. Previous studies reported an IC<sub>50</sub> value for dextrin-colistin conjugates to be 0.06 mg/ml (Ferguson et al., 2014), while in this study, the OligoG-colistin conjugates had IC<sub>50</sub> values of 0.24 mg/ml and 0.06 mg/ml (for amide- and ester-linked conjugates, respectively), suggesting that OligoG conjugates may be better tolerated *in vivo*. As expected, OligoG-E-polymyxin conjugates exhibited higher toxicity towards HK-2 cells compared with the amide-linked conjugates. Since 2-4 of the polymyxin's primary amines were used for irreversible amide bond formation with OligoG, and these groups being known to mediate polymyxin toxicity, it was not surprising that the amide-linked conjugates were less toxic than ester-bound conjugates. Previous studies have investigated structure of the polymyxin molecule with the major colistin and polymyxin B components shown to exhibit similar antimicrobial

activity in a range of clinical Gram-negative pathogens (Roberts et al., 2015). However, polymyxin B1 and colistin A induced 3-fold higher apoptotic effects in HK-2 cells compared to polymyxin B2 and colistin B, suggesting that individual lipopeptide components might be reabsorbed differently by HK-2 cells. This further highlights the need to standardise the composition of commercially available colistin and polymyxin B products, to improve the safety profile of OligoG-polymyxin conjugates.

Immunogenicity of the polymer-drug conjugates can cause severe clinical issues, affecting both the biodistribution and efficacy of the drug *in vivo*. It has been suggested that polymers might induce B cell activation leading to antibody production (Jiskoot et al., 2009). For example, previous studies have shown the presence of anti-PEG antibodies in patients treated with PEG-asparaginase, which led to rapid clearance of the conjugate from the bloodstream (Armstrong et al., 2007). It is known that drug delivery systems (including polymer-drug conjugates) can be immunogenic, causing recognition and binding of the drug by opsonin proteins (Owens and Peppas, 2006). Opsonins can be components of the blood serum, such as albumin or fibrinogen, as well as complement proteins and immunoglobulins (Markovsky et al., 2012). As a result, macrophages of the mononuclear phagocytic system, can recognise opsonin proteins bound to foreign material, leading to fast conjugate clearance from the bloodstream and its accumulation, mainly in the spleen and liver (Markovsky et al., 2012). As previously highlighted nano-sized agents with hydrodynamic diameters larger than 20 nm, might not be able to avoid recognition by mononuclear phagocytic system (Duncan and Vicent, 2010). In addition, activated macrophages produce pro-inflammatory mediators such as TNF $\alpha$  or interleukin-1 (IL-1) that play a crucial role in inflammation (Parameswaran and Patial, 2010). In this study, OligoG conjugation was shown to markedly reduce the release of inflammatory cytokines in HK-2 cells at concentrations higher than > 0.5 mg/ml. A previous study had already shown a significant and dose-dependent reduction in systemic inflammatory responses in mice infected with *P. aeruginosa* NH57388A following OligoG treatment, with levels of IL-1 $\alpha$  dropping from 30.8 pg/ml (in untreated mice) to 4.5 pg/ml after receiving 5% OligoG (Hengzhuang

et al., 2016). Mild alveolar macrophage accumulation has been observed in rats after 28 days of daily administration of 6% nebulised OligoG, but this was not considered a toxicological effect, but rather, a normal adaptive response to inhaled material (Myrvold et al., 2010). Detailed immunological analysis of alginates and their components (G-blocks, M-blocks and MG-blocks) revealed that high G (64%) content alginates were ~10 times less immunogenic compared to low G (46%) alginates, indicating that M- and MG-, but not the G-blocks were potent cytokine stimulators, inducing human monocytes to produce high levels of IL-1, IL-6 and TNF $\alpha$  (Otterlei et al., 1991). All the data provided from the studies above suggests that OligoG (G > 85%) conjugation to antibiotics might be advantageous *in vivo* by reducing the inflammatory responses provoked by cytotoxic antibiotics.

### 3.6 Conclusions

Here, successful conjugation of OligoG to polymyxin antibiotics was achieved via amide and ester linkage. OligoG-polymyxin conjugates containing 6.1-12.9% (w/w) antibiotic and possessing a molecular weight between 14,500-27,000 g/mol were reproducibly synthesised. Conjugation of OligoG to polymyxins was also shown to significantly reduce *in vitro* toxicity and immunogenicity in a kidney cell line. These preliminary studies confirmed the potential of these OligoG-polymyxin conjugates as an antibacterial therapy and a library of OligoG-polymyxin conjugates was developed for further analysis. The following studies assessed *in vitro* antimicrobial activity of the conjugates in a range of bacterial pathogens (Chapter 4).

# **Chapter 4**

## **Antimicrobial Activity of OligoG-Polymyxin Conjugates**

## 4.1 Introduction

Promisingly, as described in Chapter 3, OligoG conjugation was shown to significantly reduce the cytotoxicity of the antibiotics colistin and polymyxin B. Hence, to show clinical utility to these conjugates, it was necessary to demonstrate that they still retained antimicrobial activity towards multidrug-resistant (MDR) Gram-negative bacteria. It was also important to characterise the ability of alginate oligomers to potentiate antibiotic treatment and impede biofilm development when conjugated to the antibiotic, both important properties of OligoG (Khan et al., 2012). Therefore, in these studies, the antibacterial efficacy of OligoG-polymyxin conjugates was assessed against a range of pathogens to ensure clinical efficacy.

In addition, this study was designed to investigate how the conjugates might behave when used clinically. For example, colistin is known to bind strongly to mucin and plasma proteins, leading to reduced activity (Huang et al., 2015, Sivanesan et al., 2017), but polymer-protein conjugation has been previously shown to prevent this interaction due to steric hindrance (Gao and He, 2014, Verhoef and Anchordoquy, 2013).

### 4.1.1 Mechanism of action of polymyxin antibiotics

As relatively “old” drugs, polymyxin antibiotics were not subjected to the rigours of contemporary drug development and regulatory procedures. As a result, their mode of action of interacting with the lipid A moiety of lipopolysaccharide (LPS) in the outer membrane of Gram-negative bacteria has only recently been elucidated (Hancock, 1997). Electrostatic interactions between the anionic phosphate groups of lipid A and cationic amino groups of polymyxin has been shown to displace divalent cations, such as magnesium and calcium, which are required for bacterial outer membrane stabilisation (Velkov et al., 2010). Following this, the incorporation of N-terminal fatty acyl chain and hydrophobic regions, such as D-Phe<sup>6</sup>-L-Leu<sup>7</sup> of polymyxin B or D-Leu<sup>6</sup>-L-Leu<sup>7</sup> of colistin, into the bacterial outer membrane then causes further expansion and distortion of the membrane (Yu et al., 2015). Eventually, polymyxins cross the outer membrane by self-mediated uptake and straddle the hydrophilic

heads and hydrophobic fatty acyl tails of the phospholipid inner membrane bilayer, disrupting the physical integrity of the membrane (Velkov et al., 2010). A secondary target for the bactericidal activity of polymyxin suggested by Deris et al., (2014) showed that polymyxin B and colistin inhibit the efficacy of a respiratory enzyme called NADH-quinone oxidoreductase (NDH-2) in the inner membrane of Gram-negative bacteria. As a result, enhanced membrane permeability and leakage of intracellular contents facilitates cell lysis and death (Evans et al., 1999).

It has also been proposed that polymyxins in the periplasmic space could form molecular contacts between the outer and inner membranes of Gram-negative bacteria (Cajal et al., 1995, Cajal et al., 1996). The binding of polymyxins to the negatively-charged phospholipid layer of outer and inner membranes triggers lipid exchange, thus disturbing their phospholipid composition, which results in osmotic imbalance and cell lysis (Clausell et al., 2007, Velkov et al., 2010, Yu et al., 2015).

The bactericidal antibiotics such as aminoglycosides,  $\beta$ -lactams and quinolones have been shown to induce hydroxyl radical production in both Gram-positive and Gram-negative bacteria, which contributes to rapid cell death (Kohanski et al., 2007). Rapid polymyxin B and colistin-induced killing of MDR *A. baumannii* has also been associated with hydroxyl radical production and accumulation via the Fenton reaction, which could be delayed by radical quenching (Sampson et al., 2012). It is believed that when polymyxins cross the outer and inner bacterial membranes, an increase in NADH consumption and hyper-stimulation of the electron transport chain induces superoxide generation, which is converted into hydrogen peroxide by superoxide dismutase located in the cells (Yu et al., 2017). As a result, both superoxide and hydrogen peroxide radicals inactivate the iron-sulphur (Fe-S) clusters, leading to ferrous iron ( $\text{Fe}^{2+}$ ) conversion into ferric iron ( $\text{Fe}^{3+}$ ) along with hydroxyl radical production from hydrogen peroxide by the Fenton reaction (Yu et al., 2017, Yu et al., 2015). Eventually, overproduction of reactive oxygen species triggers oxidative damage to proteins, lipids and DNA leading to rapid cell death (Yu et al., 2017). A summary of the antibacterial

mechanisms mediated by polymyxin antibiotics is shown in **Figure 4.1**.

Given the key role of charged groups on the polymyxin molecule to its antimicrobial activity, it was extremely important to establish whether reversible (ester-linked) or irreversible (amide-linked) conjugation of OligoG to polymyxin B and colistin would affect its ability to kill bacteria.

#### **4.1.2 Antimicrobial susceptibility testing**

A significant increase in polymyxin use in hospitalised and critically ill patients has necessitated the development of a reliable method to determine the susceptibility of bacteria to polymyxin B and colistin in these patients. Recently, the European Committee on Antimicrobial Susceptibility Testing (EUCAST) and Clinical and Laboratory Standards Institute (CLSI) recommended the use of broth micro-dilution as a standard method for minimum inhibitory concentration (MIC) determination of polymyxins (EUCAST, 2016, Vasoo, 2017). An MIC assay defines the lowest concentration required to inhibit visible growth of a bacterial pathogen after overnight incubation (EUCAST, 2003). However, several technical issues regarding accuracy of susceptibility testing for colistin and polymyxin B have been reported. Firstly, due to the cationic nature of polymyxins, their adherence and binding to negatively-charged surfaces of commonly-used laboratory tools made of glass, polystyrene or polypropylene has been widely observed (Vasoo, 2017). Even though the joint CLSI-EUCAST group suggests performing MIC assays in microtitre plates made of plain polystyrene, a recent report by Karvanen et al. (2017) highlighted a significant loss of colistin from solutions prepared in polystyrene test tubes, compared with other materials, such as polypropylene or glass. Previously, addition of the surfactant, polysorbate 80, had been recommended by CLSI to prevent lipoglycopeptide adherence to plastics (CLSI, 2012). However, susceptibility testing of *E. coli*, *K. pneumoniae*, *P. aeruginosa* and *Acinetobacter* species to polymyxins subsequently showed a decrease in MIC values (by up to 8-fold) in the presence of polysorbate 80 (Sader et al., 2012). Synergy between polysorbate 80 and polymyxin B has also been reported in *P. aeruginosa*, showing that the

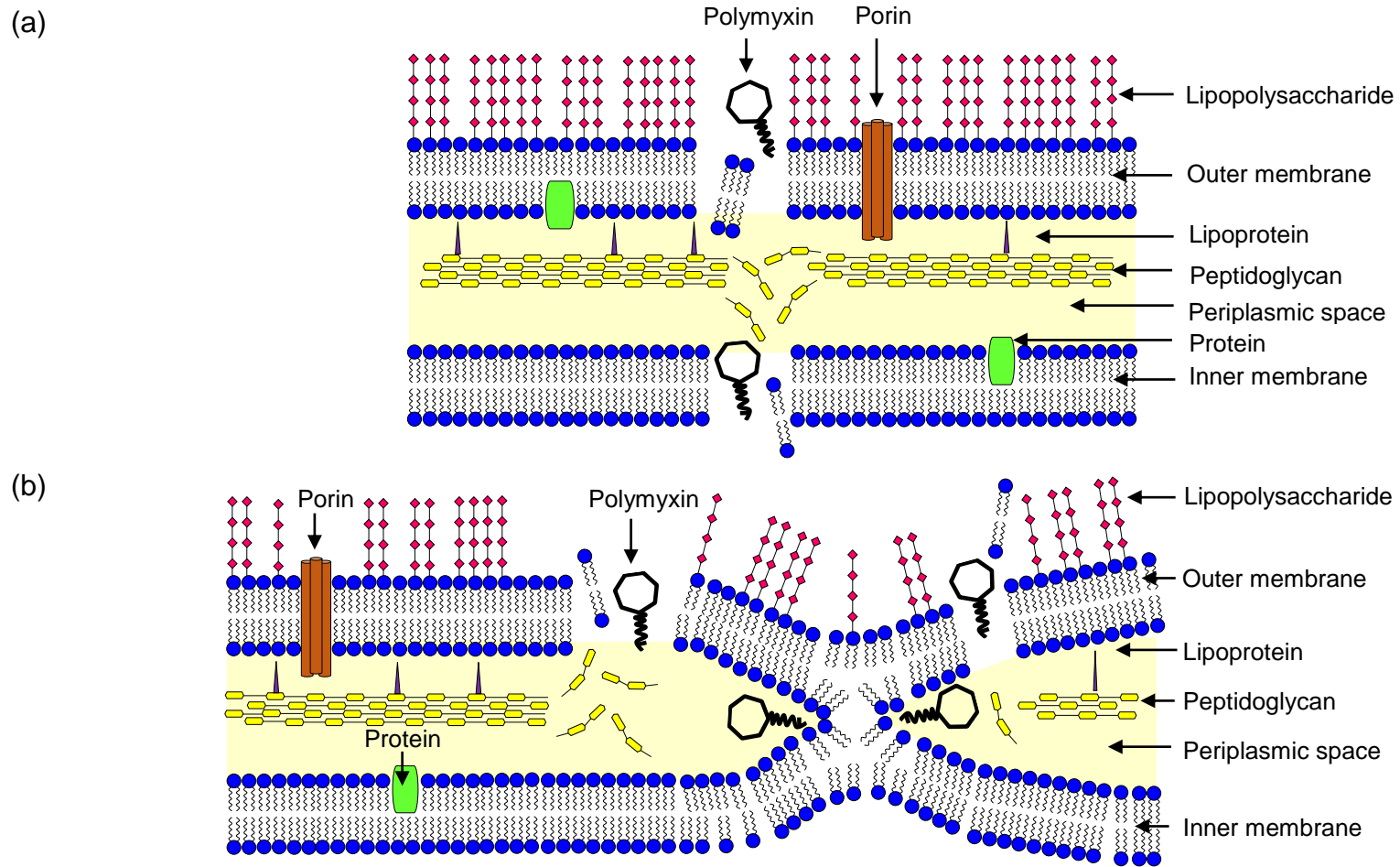


**Figure 4.1** Antibacterial mechanisms mediated by polymyxins. Panel (a) shows membrane lysis death pathway. Panel (b) indicates vesicle-vesicle contact pathway. Panel (c) represents hydroxyl radical death pathway. (Adapted from Yu et al., 2015).

(c)

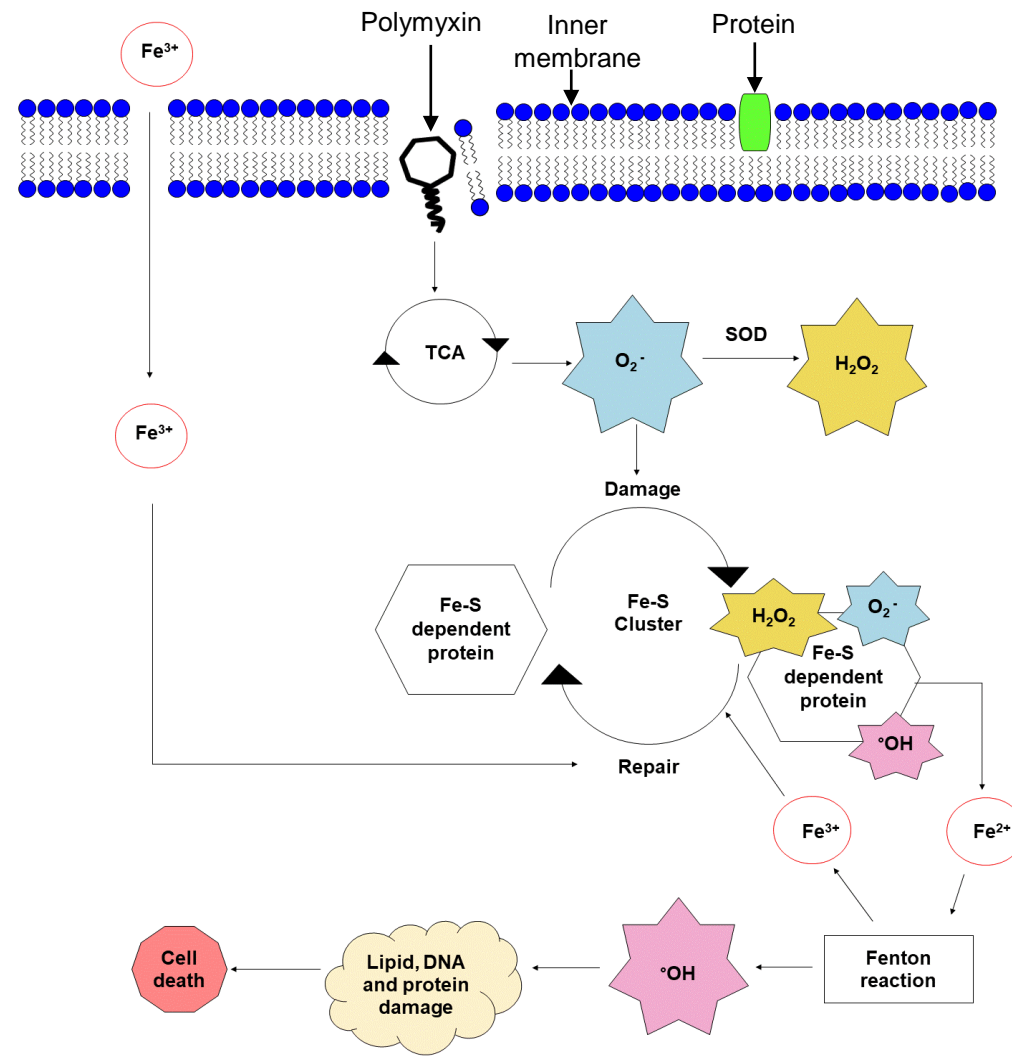


Figure 4.1 (continued).

surfactant modified the outer membrane lipid structure to facilitate entry of polymyxin (Brown et al., 1971). Furthermore, polysorbate 80 itself was shown to possess weak antimicrobial activity (Brown et al., 1979). As a result, CLSI and EUCAST no longer recommend polysorbate 80 for use in susceptibility testing of polymyxins (EUCAST, 2016). Additionally, heterogeneity in the composition of polymyxin B and colistin formulations, as well as variation in the calcium and magnesium content of Mueller-Hinton broth, have also led to misleading MIC results (Bakthavatchalam et al., 2018, Vasoo, 2017).

Alternative susceptibility testing methods have been reported in the literature, but due to their relatively high molecular weight, polymyxins diffuse poorly in agar, which compromises the reliability of the Etest and disk diffusion techniques (Chew et al., 2017, Humphries, 2015, Lo-Ten-Foe et al., 2007). The agar dilution method has been suggested as a means of overcoming the adsorption of polymyxins to the surface of plastic (Humphries, 2015). Studies by Hogardt et al. (2004) demonstrated that agar dilution produced higher MIC values compared to those obtained using the broth microdilution method, suggesting higher resistance frequency to polymyxins in agar. Likewise, while automated systems such as VITEK 2 employ turbidimetric analysis of bacterial growth, they exhibit low sensitivity towards heteroresistant subpopulations of bacteria (Lo-Ten-Foe et al., 2007, Vasoo, 2017). Consequently, susceptibility of a range of laboratory and clinical strains of bacteria to OligoG-polymyxin conjugates was determined using the broth microdilution method according to the instructions provided by the joint CLSI-EUCAST group (EUCAST, 2016).

Additionally, given that drug-resistant *E. coli* is predicted to kill an extra 40,000 people a year by 2026 (O'Neill, 2016), the effectiveness of the OligoG-polymyxin conjugates against colistin resistant *E. coli* (plasmid-encoded *mcr-1* colistin resistance) was also studied to determine whether polymyxin conjugation to OligoG could overcome antibiotic resistance. Plasmids (IncHI2, IncI2, IncX4 and IncP) carrying *mcr-1* has been identified in *Enterobacteriaceae* and is the first polymyxin resistance gene known to be capable of spreading between bacterial strains and species by horizontal gene transfer (Liu et al., 2016, Zhao et al., 2017b). The *mcr-1* gene encodes an

intramembrane enzyme (phosphatidylethanolamine transferase) that is responsible for phosphoethanolamine residue transfer to the lipid A moiety in the Gram-negative bacterial cell membrane. This structural modification of lipid A leads to a lower affinity for polymyxins and reduced ability to activate the innate immune response, culminating in reduced antimicrobial efficacy (Xu et al., 2018, Yang et al., 2017).

Since the OligoG-polymyxin conjugates were expected to display different pharmacokinetics to the unmodified antibiotic, in addition to using conventional MIC tests, bacterial growth patterns in the presence of prolonged exposure to antibiotic treatments were also studied. One of the main advantages of the growth curve is the ability to demonstrate bacterial regrowth which is commonly associated with the presence of resistant (persister) sub-populations (Yourassowsky et al., 1985).

Additionally, as a third model of bacterial susceptibility testing, confocal laser scanning microscopy (CLSM) was employed to evaluate biofilm formation in the presence of OligoG-polymyxin conjugates or polymyxin alone, to specifically determine biofilm thickness, roughness coefficients and biomass. CLSM is a commonly used tool for generating high resolution images of the three-dimensional structure of biofilms (Lawrence and Neu, 1999).

#### **4.1.3 Combination therapy for Gram-negative infections**

Since many bacterial infections are commonly treated with combination therapies, the antimicrobial efficacy of OligoG-polymyxin conjugates was also tested in combination with azithromycin using a two-directional checkerboard assay. Checkerboard assays are commonly used to assess the interaction of different antimicrobial agents and the efficacy of drug combinations at clinically relevant concentrations (Saiman, 2007). The fractional inhibitory concentration index (FICI) is derived by comparing the MIC values of the individual agents with the MIC value of the combined treatments (Hsieh et al., 1993). Azithromycin was selected for these studies since it had been previously shown that azithromycin can exhibit synergistic activity with polymyxin derivatives against *E. coli*, *Enterobacter cloacae*, *K. pneumoniae* and *A.*

*baumannii* strains (Vaara et al., 2010) and *P. aeruginosa* (Landman et al., 2005). Synergism has also been demonstrated between polymyxin B and imipenem or rifampicin in polymyxin-resistant *P. aeruginosa* isolates (Landman et al., 2005). Azithromycin acts by interfering with protein synthesis inside the cell, therefore it must cross the cell wall to exert its antimicrobial effect (Parnham et al., 2014). It has been proposed that co-administered polymyxins could permeabilise the bacterial outer membrane, thereby enhancing internalisation of azithromycin and allowing the use of lower antibiotic doses, which would cause less side effects. Indeed, it has further been shown that colistin facilitated and synergistically enhanced the efficacy and entry of azithromycin into *P. aeruginosa*, *K. pneumoniae* and *A. baumannii* (Lin et al., 2015).

#### **4.1.4 Environmental factors affecting Minimum Inhibitory Concentration**

In contrast to standard *in vitro* models of antimicrobial susceptibility which routinely employ Mueller-Hinton (MH) medium to optimise bacterial growth, when antibiotics are administered to patients, they are exposed to a wide range of proteins and destructive environments. For example, mucins are high molecular weight glycoproteins that regulate the rheological properties of the airway mucus and thus, contribute to mucociliary clearance of foreign particles and pathogens (Lillehoj and Kim, 2002, Ma et al., 2017). However, hypersecretion and overproduction of mucin in sputum, along with bacterial debris and inflammatory cells, is commonly seen in chronic respiratory infections and pathological airway conditions, including cystic fibrosis and chronic obstructive pulmonary disease (Ma et al., 2017, Voynow and Rubin, 2009). Colistin is commonly used in patients with chronic airway infections caused by *P. aeruginosa*. Huang et al. (2015) demonstrated that colistin binds strongly to mucin, causing > 100-fold increase in colistin MIC in a range of Gram-negative bacteria. The authors proposed that binding of colistin to secretory mucin in sputum or airway epithelium, would lead to reduced *in vivo* free colistin concentrations and hence reduced antibacterial efficacy. In addition, these sub-MIC concentrations of antibiotic may also lead to increased development of antibiotic resistance. Consequently, it was deemed pertinent

to establish whether attachment of OligoG to the antibiotic could inhibit these mucin-polymyxin interactions and improve antibacterial efficacy.

Given its potential therapeutic use, it was also considered interesting to study the microbiological activity of OligoG-polymyxin antibiotics in CF sputum itself. However, its high heterogeneity, high variability between patients, excessive therapeutic use of antibiotics, an abundance of resistant yeasts and changes in consistency during sterilisation, make CF sputum unreliable and impractical for the susceptibility testing (Fung et al., 2010). Consequently, an alternative medium to mimic the nutritional composition of the CF lung was sought. Palmer et al. (2007) had previously developed a defined, synthetic CF sputum medium (SCFM) to mimic the composition of CF sputum. However, it did not contain important components, such as the mucin, lipids, nucleotides or intact proteins, that are usually present in CF sputum (Palmer et al., 2007). More applicable to these studies, Sriramulu et al. (2005) established an artificial sputum (AS) medium that closely resembles the unique composition of CF sputum, containing, not only amino acids and salt ions, but also DNA, mucin, lecithin and surfactants. Adaptations of this AS medium have since been used in several studies (Fung et al., 2010, Kirchner et al., 2012, Pritchard et al., 2017), supporting the decision to use this medium to study the antimicrobial efficacy of OligoG-polymyxin conjugates in a more clinical relevant model of the lung environment.

## **4.2 Experimental aims and objectives**

**The specific aims of this study were:**

- To investigate the antimicrobial activity of OligoG-polymyxin conjugates and polymyxin antibiotics in a range of MDR Gram-negative pathogens, including colistin-resistant *E. coli* strains, in conventional MH as well as mucin-supplemented and AS medium.
- To characterise the *in vitro* pharmacokinetic profiles of bacteria grown in the presence of OligoG-colistin conjugates or colistin sulfate using bacterial growth curves.

- To visually assess how the presence of OligoG-colistin conjugates or colistin sulfate altered the development of *P. aeruginosa* (24 h) biofilms.
- To compare the antimicrobial activity of azithromycin in the presence of OligoG-polymyxin conjugates and polymyxins alone as a possible combination treatment for Gram-negative infections.

### **4.3 Methods**

Various general methods including preparation of agars, broths and bacterial cultures were used as reported in Chapter 2 (Sections 2.6.4.1 and 2.6.4.3). OligoG-polymyxin conjugates were synthesised and prepared as detailed in Section 3.3.1. OligoG-polymyxin conjugates used in this Chapter were synthesised by myself as described previously in Chapter 3 while conjugates containing acid hydrolysed high molecular weight alginate (Pronova) (2.5k AHG-A-colistin and 2.5k AHG-E-colistin) were synthesised by E. L. Ferguson.

#### **4.3.1 Bacterial strains**

The Gram-negative bacterial isolates used for susceptibility testing included reference bacterial strains and clinical isolates. The origin and relevant resistance genotypes are listed in **Table 4.1** (Khan et al., 2012, Yang et al., 2017).

#### **4.3.2 Susceptibility testing using MIC assays**

Susceptibility testing of OligoG-polymyxin conjugates, colistin and polymyxin B was performed using conventional broth microdilution MIC assays as described in Chapter 2 (Section 2.6.4.4). The MIC susceptibility breakpoints defined by CLSI and EUCAST for colistin and polymyxin B are summarised in **Table 4.2**.

#### **4.3.3 Susceptibility testing using MIC assays modified with mucin**

In addition, to study the antimicrobial activity of antibiotic treatments and OligoG (0.2% and 2% w/v) in the presence of mucin, MH broth was also

**Table 4.1** Bacterial isolates used for characterisation of OligoG-antibiotic conjugates.

Strain code	Bacterial isolate	Genotype	Origin
V1	<i>Pseudomonas aeruginosa</i> R22	VIM-2	China
V2	<i>Pseudomonas aeruginosa</i> MDR 301	VIM-2	Poland
X11	<i>Pseudomonas aeruginosa</i> NH57388A	-	Denmark
V13	<i>Pseudomonas aeruginosa</i> PAO1, ATCC 15692	-	Reference strain
E69	<i>Pseudomonas aeruginosa</i> NCTC 10662	-	Reference strain
V3	<i>Klebsiella pneumoniae</i> KP05 506	NDM-1	India
V6	<i>Klebsiella pneumoniae</i> IR25	NDM-1	India
V4	<i>Acinetobacter baumannii</i> MDR ACB	MDR	Libya
V19	<i>Acinetobacter baumannii</i> 7789	MDR	United Kingdom
V5	<i>Escherichia coli</i>	AIM-1	Australia
V7	<i>Escherichia coli</i> IR57	NDM-1	India
V11	<i>Escherichia coli</i> 5702	-	United Kingdom
V24	<i>Escherichia coli</i> 7273	-	United Kingdom
E70	<i>Escherichia coli</i> NCTC 10418	-	Reference strain
THAI 21	<i>Escherichia coli</i> PN21	<i>mcr-1</i>	Thailand
THAI 25	<i>Escherichia coli</i> PN25	<i>mcr-1</i>	Thailand
THAI 26	<i>Escherichia coli</i> PN26	-	Thailand
	<i>Escherichia coli</i> ATCC 25922	-	Reference strain
E68	<i>Staphylococcus aureus</i> NCTC 6571	-	Reference strain
E75	<i>Staphylococcus aureus</i> NCTC 12493	-	Reference strain

Resistance genotype: VIM-2, carbapenem-hydrolyzing metallo- $\beta$ -lactamase; NDM-1, New Delhi metallo- $\beta$ -lactamase; MDR, multidrug resistant; AIM-1, metallo- $\beta$ -lactamase; *mcr-1*, plasmid-encoded colistin resistance.

**Table 4.2** MIC breakpoints ( $\mu\text{g/ml}$ ) for colistin sulfate and polymyxin B recommended by the Clinical and Laboratory Standards Institute (CLSI) and the European Committee on Antimicrobial Susceptibility Testing (EUCAST) in 2018.

Polymyxin	MIC breakpoints ( $\mu\text{g/ml}$ )																	
	<i>Pseudomonas</i> spp.						<i>Acinetobacter</i> spp.						<i>Enterobacteriaceae</i>					
	CLSI			EUCAST			CLSI			EUCAST			CLSI			EUCAST		
	S	I	R	S	I	R	S	I	R	S	I	R	S	I	R	S	I	R
Colistin sulfate	$\leq 2$	-	$\geq 4$	$\leq 2$	-	$> 2$	$\leq 2$	-	$\geq 4$	$\leq 2$	-	$> 2$	-	-	-	$\leq 2$	-	$> 2$
Polymyxin B	$\leq 2$	4	$\geq 8$	-	-	-	$\leq 2$	-	$\geq 4$	-	-	-	-	-	-	-	-	-

Interpretative indices: S, susceptible; I, intermediate; R, resistant.

supplemented with 0.2% and 2% w/v porcine stomach (type II) mucin. A stock solution of mucin was prepared (12.5% w/v in MH broth) and used to set up the 96-well plates according to the standard MIC protocol. It was noted that addition of mucin to the MH medium produced a cloudy solution, which made it impossible to distinguish differences between bacterial growth or no growth after the overnight incubation step. Therefore, at the end of the incubation period, 30 µl of resazurin, an oxidation-reduction agent, was added to the wells of the plate (stock solution prepared at 0.01% w/v in sterile dH<sub>2</sub>O) and incubated for a further 3 h at 37°C. The results were then determined visually; blue colouration indicating no bacterial growth and a pink colour signifying live cells or bacterial growth. A typical plate set-up using resazurin for MIC assay determination can be seen in **Figure 4.2**.

#### **4.3.4 Susceptibility testing using MIC assays modified with artificial sputum medium**

To study the antimicrobial efficacy of antibiotic treatments under more clinically relevant conditions, the standard MIC assay was employed using AS medium instead of MH medium.

RPMI 1640 medium was made up in dH<sub>2</sub>O according to the manufacturer's instructions consisting of (10.4 g/L) and 3-(N-morpholino) propanesulfonic acid (MOPS) (0.165 M final concentration) and the pH adjusted to 7.0 with 0.5 M NaOH. The solution was filter sterilised, then stored at 4°C prior to use.

AS medium was prepared by dissolving deoxyribonucleic acid (DNA) from salmon fish sperm (4 g/L) and porcine stomach (type II) mucin (5 g/L) in sterile dH<sub>2</sub>O by stirring overnight at 4°C. The remaining components of the AS medium were then subsequently added to the DNA/mucin solution including, RPMI 1640 medium (2% v/v), diethylenetriaminepentaacetic acid (DTPA) (5.9 mg/L), egg-yolk emulsion (0.5% v/v), NaCl (5.0 g/L) and KCl (2.2 g/L). After mixing, the pH was adjusted to 7.0 by the addition of NaOH (0.5 M) and the medium made up to a final volume of 1 L. Finally, the AS medium was filter-sterilised using a barrel filter (0.22 µm pore size), stored at 4°C in the dark and used within 4 weeks.

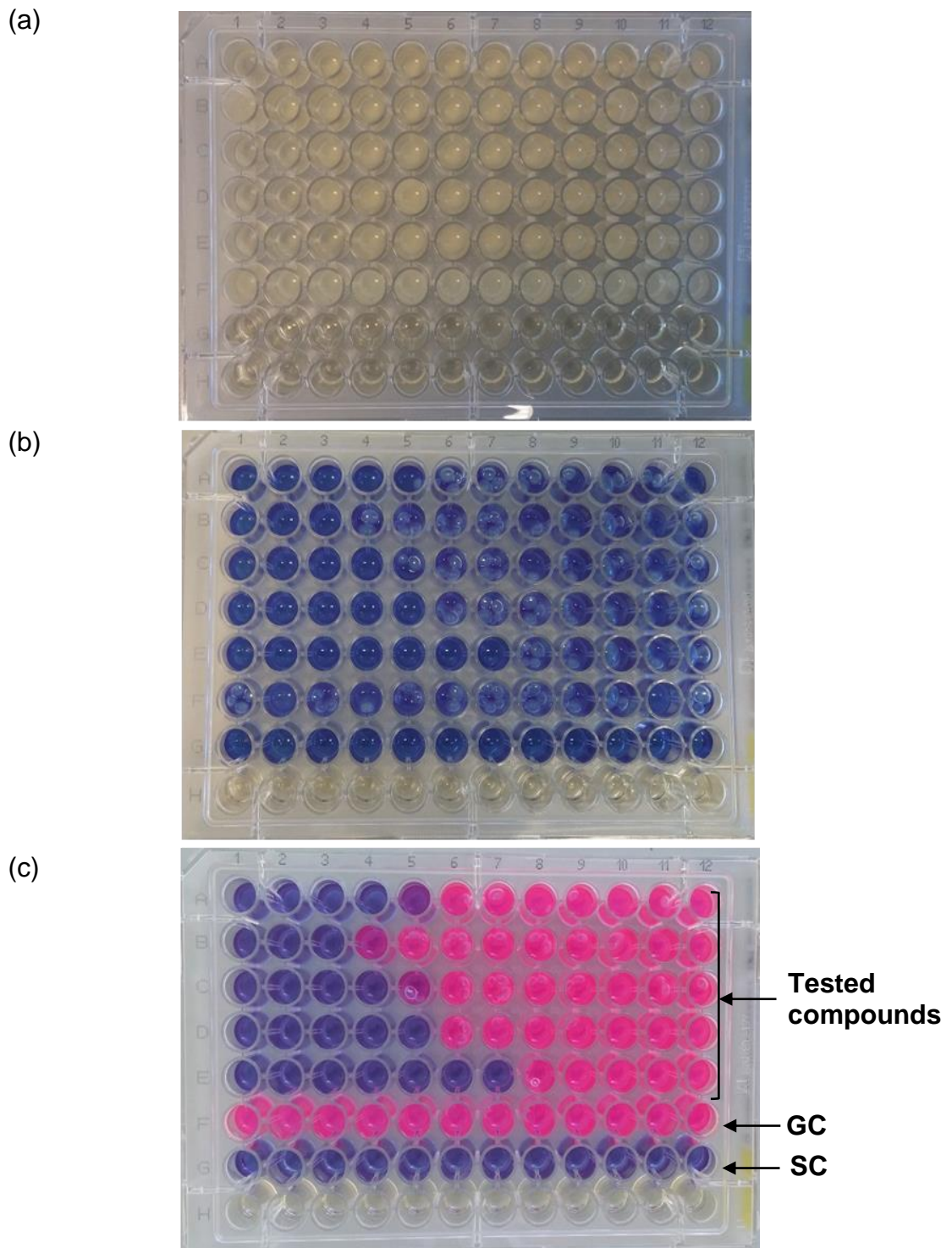


**Figure 4.2** Typical MIC plate set up. (a) The MIC plate after 20 h incubation with tested compounds and mucin. (b) Plate after addition of resazurin indicator (pink, bacterial growth; blue, no bacterial growth). (c) Plate after 3 h incubation with resazurin. Row F, positive growth control (GC); Row G, sterility control (SC). Rows A-E tested compounds.

### 4.3.5 Bacterial growth curves

To study the pharmacokinetic profiles of bacteria during antibiotic treatment, 96-well microtitre growth curve plates were set up according to methods previously described in Section 2.6.4.4 (used at concentrations ranging from 16 x MIC to MIC/16). Plates were then wrapped in parafilm and placed in a microtitre plate reader at 37°C, and absorbance at 600 nm was measured hourly for 48 h. For comparison, bacterial growth in the presence of i) OligoG, ii) PRONOVA (high molecular weight alginate) and iii) OligoG plus colistin, at equivalent concentrations to those used in the corresponding conjugates, was measured. Experiments were conducted in triplicate and results were presented as mean values (n = 3).

### 4.3.6 Checkerboard assay

Following MIC determinations against the various test bacteria, checker board MIC assays were performed to test the interaction and potency of two antimicrobials concurrently i.e. OligoG-colistin conjugates and colistin sulfate against azithromycin. For this, stock solutions of OligoG-colistin conjugates and colistin (used at 8 x the MIC value) and serial two-fold dilutions of azithromycin (used at concentrations ranging from 16 x MIC to MIC/16) were freshly prepared in MH medium. MH medium (50 µl) was placed in each well of rows B-H (columns 1-10) of a 96-well microtitre plate. Solutions of OligoG-colistin conjugate or colistin (100 µl) were placed in row A (columns 1-10) of the plate and serially diluted down the plate by transfer of 50 µl, stopping at row G so that row H contained MH medium only. Serially diluted azithromycin solutions (50 µl) were added in decreasing concentrations across the plate (rows A-H), stopping at column 9, so that column 10 contained conjugate or colistin solution only. Columns 11 (growth control) and 12 (sterility control) contained MH medium only (100 µl). Each microtitre well (except column 12) was inoculated with bacteria as previously described (Section 2.6.4.4), then the plate was wrapped in parafilm and incubated at 37°C for 20 h. A typical plate set up for checkerboard assay can be seen in **Figure 4.3**. Assays were performed in triplicate and results were expressed as median values. Then,

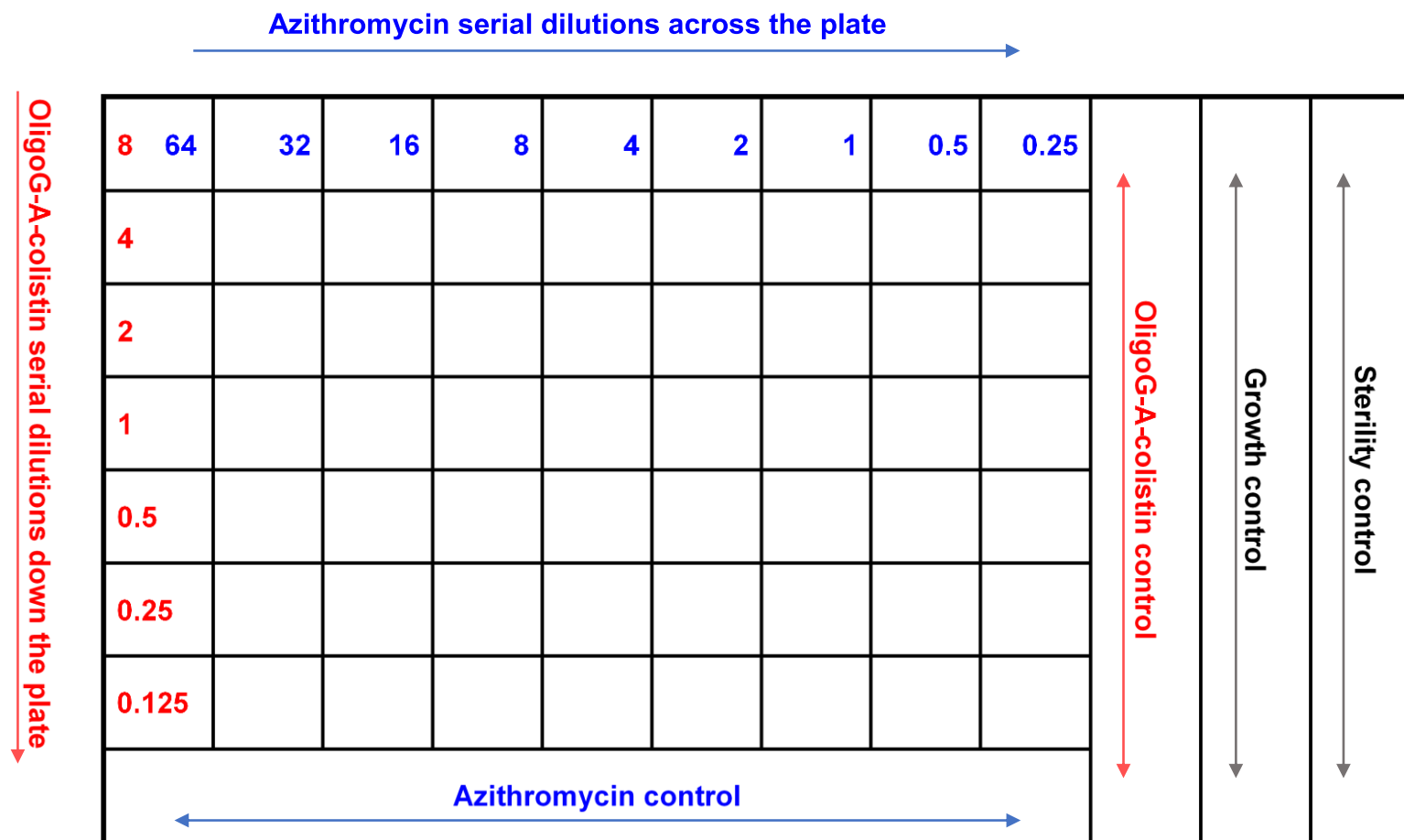


**Figure 4.3** Typical plate layout for checkerboard MIC assay using OligoG-A-colistin and azithromycin in combination against *P. aeruginosa* MDR 301 (MIC = 1 and 8 µg/ml, respectively).

the FICI was calculated by using the concentration of the first non-turbid well in each row along the turbid/non-turbid interface as follows:

$$\text{FIC index}_{A/B} = \frac{\text{MIC (A combination)}}{\text{MIC (A alone)}} + \frac{\text{MIC (B combination)}}{\text{MIC (B alone)}}$$

The combined therapy was considered synergistic when the mean FICI was  $\leq 0.5$ , additive when the FICI was between 0.5-2, indifferent when the FICI was between 2-4, and antagonistic when the FICI was  $\geq 4$  (Bonapace et al., 2002).

#### **4.3.7 Biofilm formation assay**

The effect of antibiotic and conjugate treatments on biofilm formation was then determined. For this, serially diluted antibiotic solutions (ranging from 2 x MIC [of antibiotic/conjugate] to MIC/4) in MH broth were added to the wells of a Greiner glass-bottomed optical 96-well plate (90  $\mu\text{l}$  per well). *Pseudomonas* cultures (*P. aeruginosa* R22) from overnight inoculums were standardised to  $10^7$  CFU/ml and added to the wells of 96-well plate (10  $\mu\text{l}$  per well). The plate was wrapped in parafilm and incubated for 24 h on a rocker (20 rpm) at 37°C. Sterility (MH only) and growth (no antibiotic) controls were included in each plate. After 24 h, the supernatant was carefully removed and 5  $\mu\text{l}$  of LIVE/DEAD stain (LIVE/DEAD Bacterial Viability kit; prepared by mixing 5  $\mu\text{M}$  of SYTO 9 [LIVE] and 30  $\mu\text{M}$  of propidium iodide [DEAD] in PBS) was added. The plate was wrapped in foil and kept in the dark for 10 min, then PBS (45  $\mu\text{l}$ ) was added to the wells and CLSM was performed immediately using objective magnification of x63 under oil, resolution of 512 x 512, line averaging of 1 and a step size of 0.79  $\mu\text{m}$ . The excitation/emission ranges used in this study were 480/500 nm for SYTO 9 and 490/635 for propidium iodide. Experiments were performed in triplicate and biofilm stack images ( $n = 15$ ) were quantified by Comstat image analysis programme that applies a fixed binary thresholding to distinguish the biofilm biomass from the background (Heydorn et al., 2000). Thus, the changes in biofilm thickness, roughness coefficient and biomass were reliably assessed.

## 4.4 Results

### 4.4.1 Microbiological characterisation of OligoG-polymyxin conjugates

Conjugation of OligoG slightly reduced the antimicrobial activity of colistin and polymyxin B against a panel of Gram-negative bacteria, typically increasing the MIC to 1-2-fold compared to that of the free drug (**Table 4.3**). OligoG-ester-polymyxin conjugates showed the best equivalence to the free drug's activity, while an increase in the antibiotic's MIC of 2-fold or more was most commonly seen for amide-linked conjugates, especially those containing polymyxin B. Nevertheless, the OligoG-A-colistin conjugates had significantly higher antimicrobial activity compared to previously published dextrin-A-colistin conjugates as indicated in **Table 4.4**. Minimal batch-to-batch variability in the antimicrobial activity of the OligoG-colistin conjugates was observed in several Gram-negative strains (**Table 4.5**).

When antimicrobial activity was tested in colistin-resistant strains, it was observed that OligoG alone had no antibacterial activity (MIC > 1280 µg/ml) and that conjugation did not improve the bactericidal efficacy of colistin (**Table 4.3**). As observed in the other (colistin-sensitive) strains, ester-linked antibiotic conjugates exhibited slightly better antimicrobial activity compared to amide-linked ones and displayed similar MIC values to those of the free drug.

When the antimicrobial activity of OligoG-polymyxin conjugates was tested in the presence of 0.2% or 2% mucin, MIC values increased in a dose-dependent manner, with increasing concentration of mucin, and there was a clear decrease in antimicrobial efficacy (**Table 4.6**). The inhibitory effect of mucin was greatest for *K. pneumoniae*, where MIC values increased > 10-fold in the presence of mucin. Also, when bacteria were treated with OligoG (0.2% or 2%) with colistin or polymyxin B without conjugation antibiotic activity was similar to that of equivalent concentrations of the free drug.

Similarly, the antimicrobial activity of the antibiotics in AS medium was also reduced compared to in MH medium (**Table 4.7**). Typically, MIC values were around 2-4-fold higher in the AS medium. Interestingly, OligoG-colistin conjugates retained their efficacy towards the *E. coli* IR57 isolate in AS

**Table 4.3** MIC determinations of OligoG-polymyxin conjugates against a range of Gram-negative bacterial pathogens.

Drug	MIC ( $\mu\text{g/ml}$ )															
	<i>P. aeruginosa</i> R22	<i>P. aeruginosa</i> MDR 301	<i>P. aeruginosa</i> NH57388A	<i>P. aeruginosa</i> NCTC 10662	<i>K. pneumoniae</i> KP05 506	<i>K. pneumoniae</i> IR25	<i>A. baumannii</i> MDR ACB	<i>A. baumannii</i> 7789	<i>E. coli</i> AIM-1	<i>E. coli</i> IR57	<i>E. coli</i> 5702	<i>E. coli</i> NCTC 10418	<i>E. coli</i> PN21	<i>E. coli</i> PN25	<i>E. coli</i> PN26	<i>E. coli</i> ATCC 25922
OligoG-A-colistin	2	1	0.5	1	0.125	1	1	0.125	0.008	0.125	0.063	0.25	32	32	0.5	1
OligoG-E-colistin	1	0.5	0.25	0.25	0.125	0.125	0.25	0.125	0.008	0.25	0.031	0.5	16	8	0.25	1
Colistin sulfate	0.5	0.5	0.25	0.125	0.125	0.063	0.5	0.25	< 0.008	0.125	0.031	0.125	8	8	0.125	0.25
OligoG-A-polymyxin B	4	2	1	4	0.5	4	2	0.5	0.063	2	0.25	4	32	32	0.5	16
OligoG-E-polymyxin B	0.25	0.5	0.25	0.25	0.25	0.125	0.063	0.5	0.016	0.5	0.063	0.25	8	4	0.25	0.5
Polymyxin B	0.25	0.5	0.25	0.063	0.125	0.125	0.125	0.125	< 0.004	0.5	0.063	0.25	8	4	0.125	0.5

Decreased antimicrobial activity of conjugated polymyxin, where the MIC was at least 2-fold higher compared to colistin sulfate or polymyxin B controls, is shown in red.

**Table 4.4** Comparison of the antimicrobial activity MIC ( $\mu\text{g/ml}$ ) of OligoG-A-colistin and dextrin-A-colistin conjugates.

Drug	MIC ( $\mu\text{g/ml}$ )								
	<i>P. aeruginosa</i> R22	<i>P. aeruginosa</i> MDR 301	<i>K. pneumoniae</i> KP05 506	<i>K. pneumoniae</i> IR25	<i>A. baumannii</i> MDR ACB	<i>A. baumannii</i> 7789	<i>E. coli</i> AIM-1	<i>E. coli</i> IR57	<i>E. coli</i> 5702
OligoG-A-colistin	2	1	0.125	1	1	0.125	0.008	0.125	0.063
Dextrin-A-colistin	128	512	4	8	8	8	1	4	8
<b>Fold-change</b>	<b>6</b>	<b>9</b>	<b>5</b>	<b>3</b>	<b>3</b>	<b>6</b>	<b>7</b>	<b>5</b>	<b>7</b>

**Table 4.5** Batch-to-batch reproducibility of MIC determinations of OligoG-colistin conjugates against a range of Gram-negative bacterial pathogens.

Drug	Batch number	MIC (µg/ml)			
		<i>P. aeruginosa</i> MDR 301	<i>K. pneumoniae</i> KP05 506	<i>E. coli</i> IR57	<i>A. baumannii</i> 7789
OligoG-A-colistin	1	1	0.25	0.5	0.5
	2	1	0.125	0.125	0.125
	3	2	0.125	0.125	0.063
	4	2	0.125	0.125	0.063
	5	2	0.125	0.25	0.125
OligoG-E-colistin	1	0.5	0.125	0.25	0.125
	2	0.5	0.063	0.125	0.063
Colistin sulfate	-	0.5	0.125	0.125	0.25

**Table 4.6** Microbiological efficacy (MICs) of antibiotics in the absence and presence of mucin against Gram-negative

Drug ↓	Mucin (%) →	MIC (µg/ml)											
		<i>P. aeruginosa</i> R22			<i>A. baumannii</i> MDR ACB			<i>K. pneumoniae</i> IR25			<i>E. coli</i> IR57		
		0	0.2	2	0	0.2	2	0	0.2	2	0	0.2	2
OligoG-A-colistin		4	4	64	0.125	4	64	0.125	8	> 128	0.063	2	8
OligoG-E-colistin		1	16	64	1	16	64	0.063	32	> 128	0.063	4	64
2.5k AHG-A-colistin		2	4	64	1	16	64	0.125	16	> 128	0.25	2	4
2.5k AHG-E-colistin		1	4	64	1	4	32	0.063	4	128	0.25	2	4
0.2% OligoG + colistin		0.25	2	32	ND	ND	ND	ND	ND	ND	< 0.063	2	4
2% OligoG + colistin		1	4	32	ND	ND	ND	ND	ND	ND	0.25	0.5	2
<b>Colistin sulfate</b>		<b>0.5</b>	<b>2</b>	<b>16</b>	<b>0.5</b>	<b>1</b>	<b>16</b>	<b>0.063</b>	<b>1</b>	<b>64</b>	<b>0.125</b>	<b>1</b>	<b>2</b>
OligoG-A-polymyxin B		2	64	> 128	4	16	128	2	16	> 128	2	16	32
OligoG-E-polymyxin B		0.5	2	32	0.25	1	16	0.125	2	128	0.125	0.5	1
0.2% OligoG + polymyxin B		0.5	4	64	ND	ND	ND	ND	ND	ND	0.125	2	4
2% OligoG + polymyxin B		1	4	32	ND	ND	ND	ND	ND	ND	< 0.063	0.5	2
<b>Polymyxin B</b>		<b>0.25</b>	<b>4</b>	<b>64</b>	<b>0.125</b>	<b>1</b>	<b>16</b>	<b>0.125</b>	<b>4</b>	<b>64</b>	<b>0.5</b>	<b>1</b>	<b>4</b>

ND, not determined.

**Table 4.7** Comparison of the effect of growth medium (AS medium and MH broth) on antimicrobial activity (MIC determinations) of antibiotics.

Drug ↓	Medium →	MIC (µg/ml)											
		<i>P. aeruginosa</i> MDR 301		<i>P. aeruginosa</i> NH57388A		<i>K. pneumoniae</i> KP05 506		<i>E. coli</i> IR57		<i>E. coli</i> 5702		<i>A. baumannii</i> 7789	
		AS	MH	AS	MH	AS	MH	AS	MH	AS	MH	AS	MH
OligoG-A-colistin		4	1	2	0.5	2	0.125	0.125	0.125	0.25	0.063	2	0.125
OligoG-E-colistin		4	0.5	1	0.25	1	0.125	0.063	0.25	0.125	0.031	1	0.125
Colistin sulfate		2	0.5	1	0.25	1	0.125	0.125	0.125	0.125	0.031	1	0.25
OligoG-A-polymyxin B		16	2	4	1	8	0.5	0.5	2	1	0.25	4	0.5
OligoG-E-polymyxin B		8	0.5	2	0.25	2	0.25	0.125	0.5	0.25	0.063	1	0.5
Polymyxin B		4	0.5	1	0.25	1	0.125	0.125	0.5	0.25	0.063	0.5	0.125

medium, showing equivalent or lower MICs than in MH broth.

#### 4.4.2 Characterisation of bacterial growth curves

Bacterial growth curves (**Figure 4.4**) showed that the OligoG-colistin conjugates delayed bacterial growth in a concentration-dependent manner and slowed the rate of regrowth compared to untreated bacteria. On the other hand, colistin sulfate alone showed more rapid bacterial regrowth. Overall, at the median of previously determined MIC values across all batches, OligoG-colistin conjugates typically showed the longest inhibition of bacterial regrowth, while colistin sulfate showed the shortest inhibition of bacterial regrowth (indeed, equivalent to the no antibiotic control for *K. pneumoniae* KP05 506 and *A. baumannii* 7789 (**Appendices 2.1** and **2.3**). OligoG-colistin conjugates inhibited bacterial regrowth for up to 48 h at  $\geq 2 \times$  MIC, while colistin sulfate inhibited bacterial regrowth for up to 48 h at  $\geq 8 \times$  MIC (i.e. higher equivalent concentrations of colistin alone were required to achieve the equivalent growth inhibition obtained for the OligoG-colistin conjugates). There was no difference in time to onset of bacterial regrowth between the amide- and ester-linked conjugates. The combination of OligoG plus colistin at equivalent concentrations to the OligoG and colistin in the corresponding conjugates showed concentration-dependent growth inhibition. Typically, colistin that was covalently conjugated to OligoG showed equivalent activity to unconjugated colistin plus OligoG at equivalent concentrations. Furthermore, OligoG or Pronova, at an equivalent concentration to the OligoG in the OligoG-colistin conjugates (amide- and ester-linked), had no significant effect in reducing bacterial growth.

#### 4.4.3 Checkerboard assays with azithromycin

MIC values for OligoG-colistin conjugates, colistin and azithromycin are summarised in **Table 4.8**. In most cases, combining azithromycin with OligoG- colistin or colistin sulfate resulted in an indifferent or additive effect on the organisms tested here. Generally, OligoG conjugation did not alter the efficacy of the antibiotic combination, except in *A. baumannii* 7789, where the

(a)

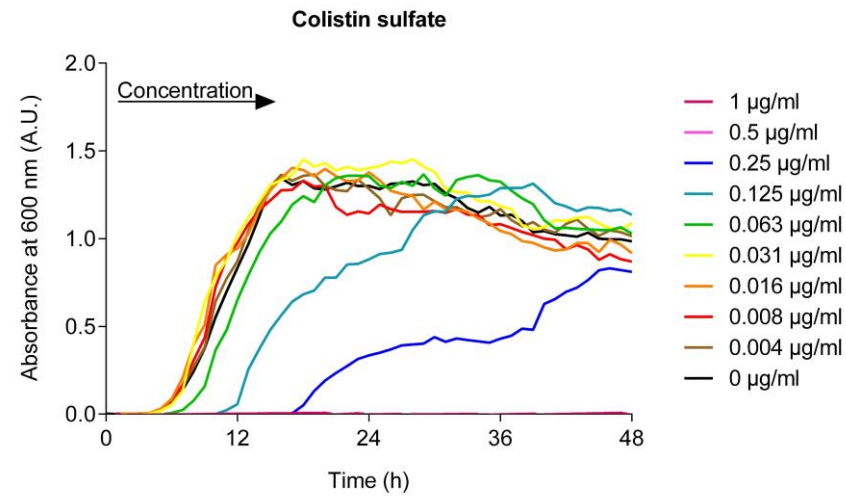


**Figure 4.4** Bacterial growth curves for *P. aeruginosa* MDR 301 (48 h) in the presence of (a) colistin sulfate, (b and f) OligoG-colistin conjugates (amide and ester linked). Controls used included (c and g) unconjugated colistin plus OligoG, (d and h) OligoG and (e and i) the high molecular weight alginate, PRONOVA, all at equivalent concentrations used in corresponding conjugates (n = 3).

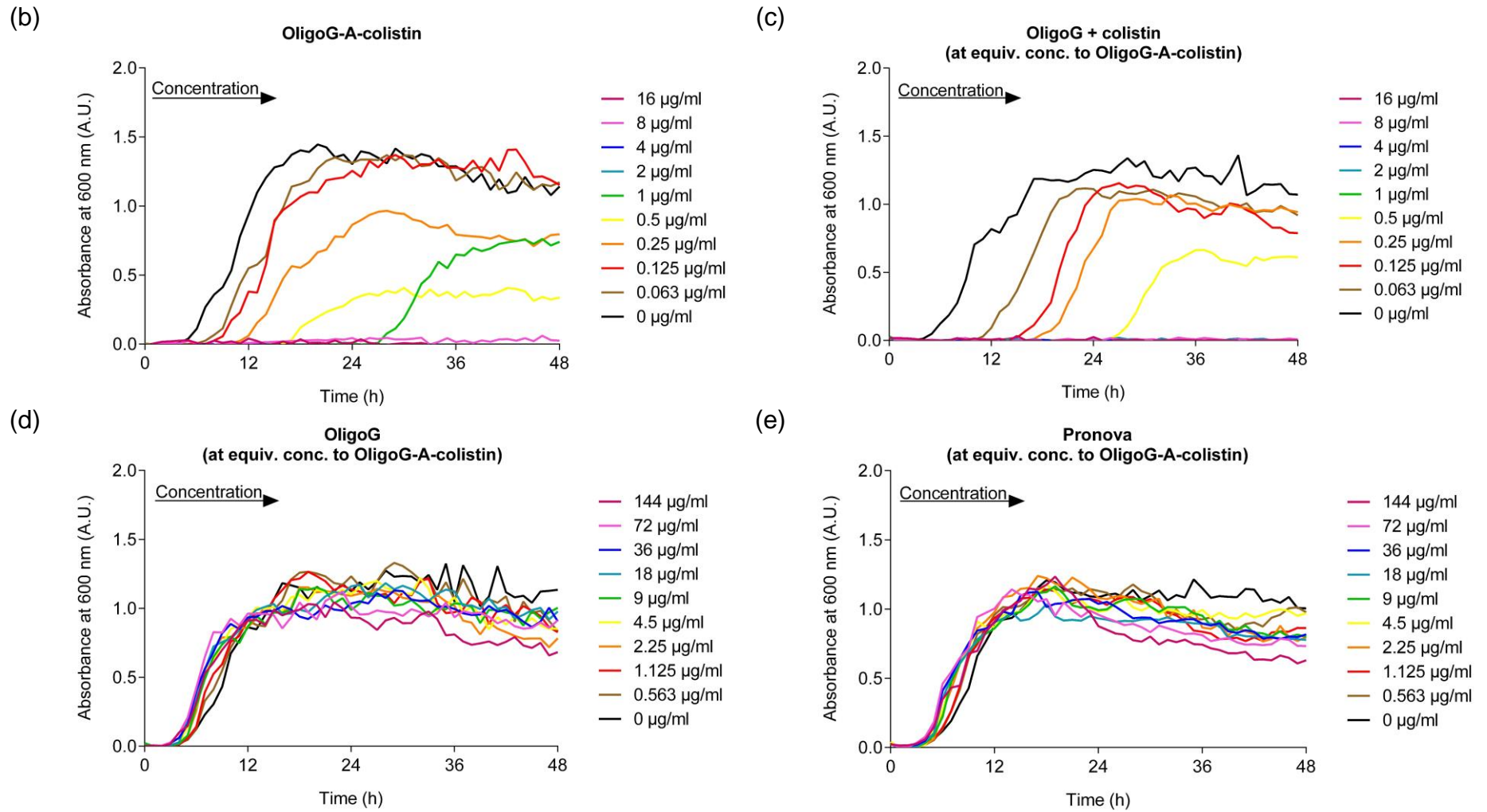


Figure 4.4 (continued).

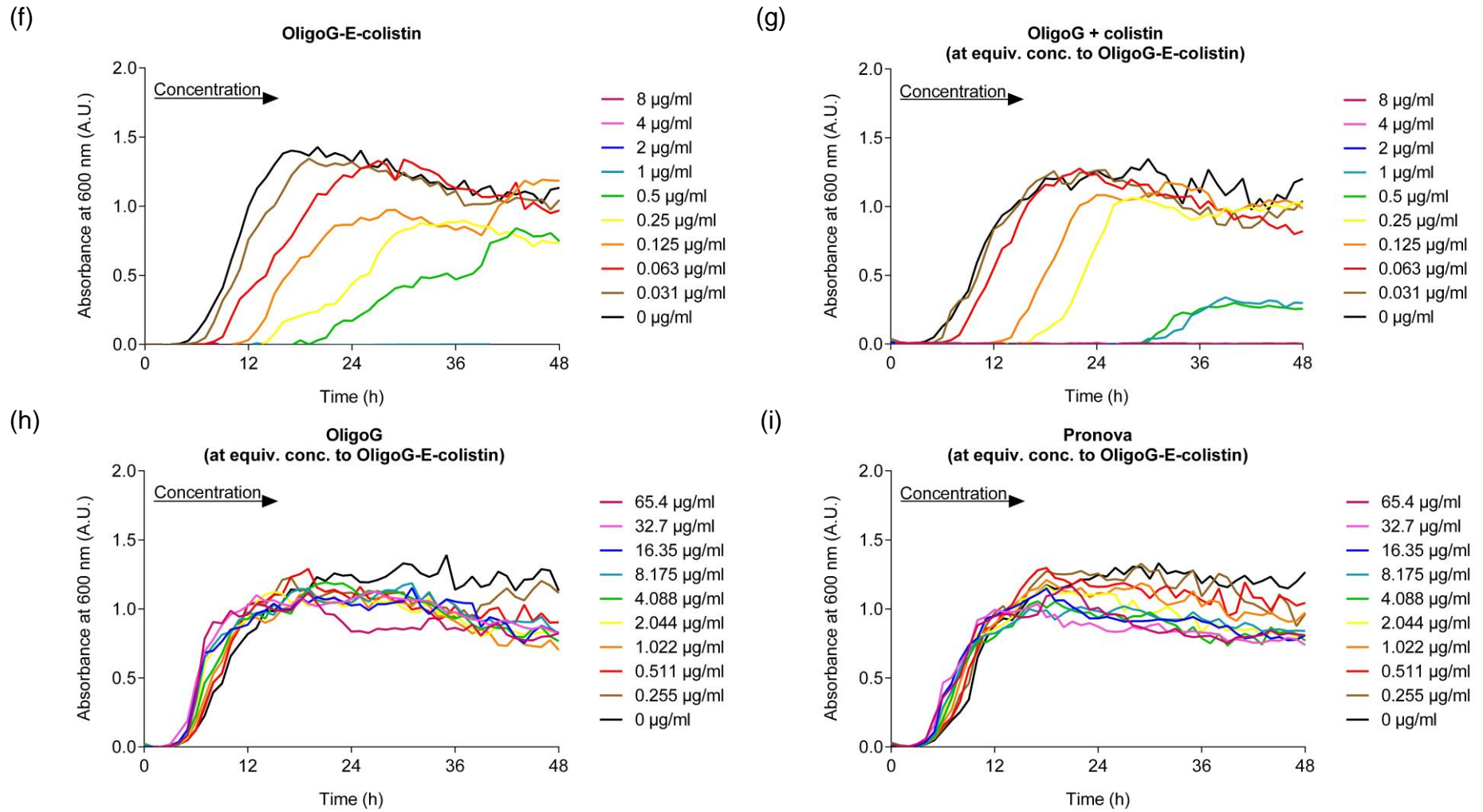


Figure 4.4 (continued).

**Table 4.8** MIC and FICI values of OligoG-colistin conjugates, colistin and azithromycin, alone and in combination.

Drug		<i>P. aeruginosa</i> MDR 301	<i>K. pneumoniae</i> KP05 506	<i>A. baumannii</i> 7789	<i>E. coli</i> NCTC 10418
MIC (µg/ml)	OligoG-A-colistin	1	0.125	0.125	0.25
	OligoG-E-colistin	0.5	0.125	0.125	0.125
	Colistin sulfate	0.5	0.125	0.25	0.125
	Azithromycin	8	32	32	4
FICI	OligoG-A-colistin + Azithromycin	1.35 (Additive)	3.15 (Indifferent)	3.40 (Indifferent)	0.64 (Additive)
	OligoG-E-colistin+ Azithromycin	1.45 (Additive)	2.43 (Indifferent)	2.53 (Indifferent)	0.46 (Synergy)
	Colistin sulfate + Azithromycin	1.51 (Additive)	2.20 (Indifferent)	1.14 (Additive)	0.83 (Additive)

combination with colistin resulted in an additive effect (FICI = 1.14) but the conjugates' effect was indifferent (FICI > 2.5). Synergy was only observed when azithromycin was combined with OligoG-E-colistin in the *E. coli* NCTC 10418 isolate (FICI = 0.46).

#### **4.4.4 The effect of OligoG-colistin conjugates on biofilm formation**

In the biofilm formation assay, CLSM images of LIVE/DEAD stained Pseudomonal biofilms demonstrated homogeneous growth in the untreated control. However, addition of OligoG-colistin conjugates or colistin sulfate markedly disrupted biofilm formation and induced bacterial death at  $\geq$  MIC, as shown in **Figure 4.5**. At the MIC (1  $\mu$ g/ml), the OligoG-E-colistin conjugate caused bacterial clumping, disruption of biofilm structure, and cell death. In all cases, Comstat analysis of the images revealed a significant reduction in biofilm thickness at  $\geq$  MIC ( $p < 0.05$ ; **Figure 4.6**). Also, OligoG-A-colistin and OligoG-E-colistin conjugates at  $\geq$  MIC, and colistin sulfate at MIC, significantly increased the biofilm roughness ( $p < 0.05$ ). In addition, both the OligoG-A-colistin and OligoG-E-colistin conjugates at 2 x MIC markedly reduced the biofilm biomass compared to untreated control ( $p < 0.05$ ), although no significant activity was observed with colistin sulfate alone at up to 2 x MIC (**Figure 4.6**). In all cases, the ratio of dead to live bacterial cells was significantly higher at MIC compared to the untreated control ( $p < 0.05$ ). On the other hand, a substantially larger biofilm biomass and thickness, as well as lower biofilm roughness and the ratio of dead to live cells was observed for all tested compounds at  $\leq$  MIC/2 which was more evident with OligoG-A-colistin conjugate and colistin sulfate.

#### **4.5 Discussion**

Here, the antimicrobial activity of OligoG-polymyxin conjugates was assessed in a range of Gram-negative MDR pathogens. Susceptibility testing using MIC assays is an extensively used technique allowing the determination of the lowest effective dose of an antimicrobial agent and identification of resistant bacterial pathogens based on clinical breakpoints. Indeed, suboptimal doses

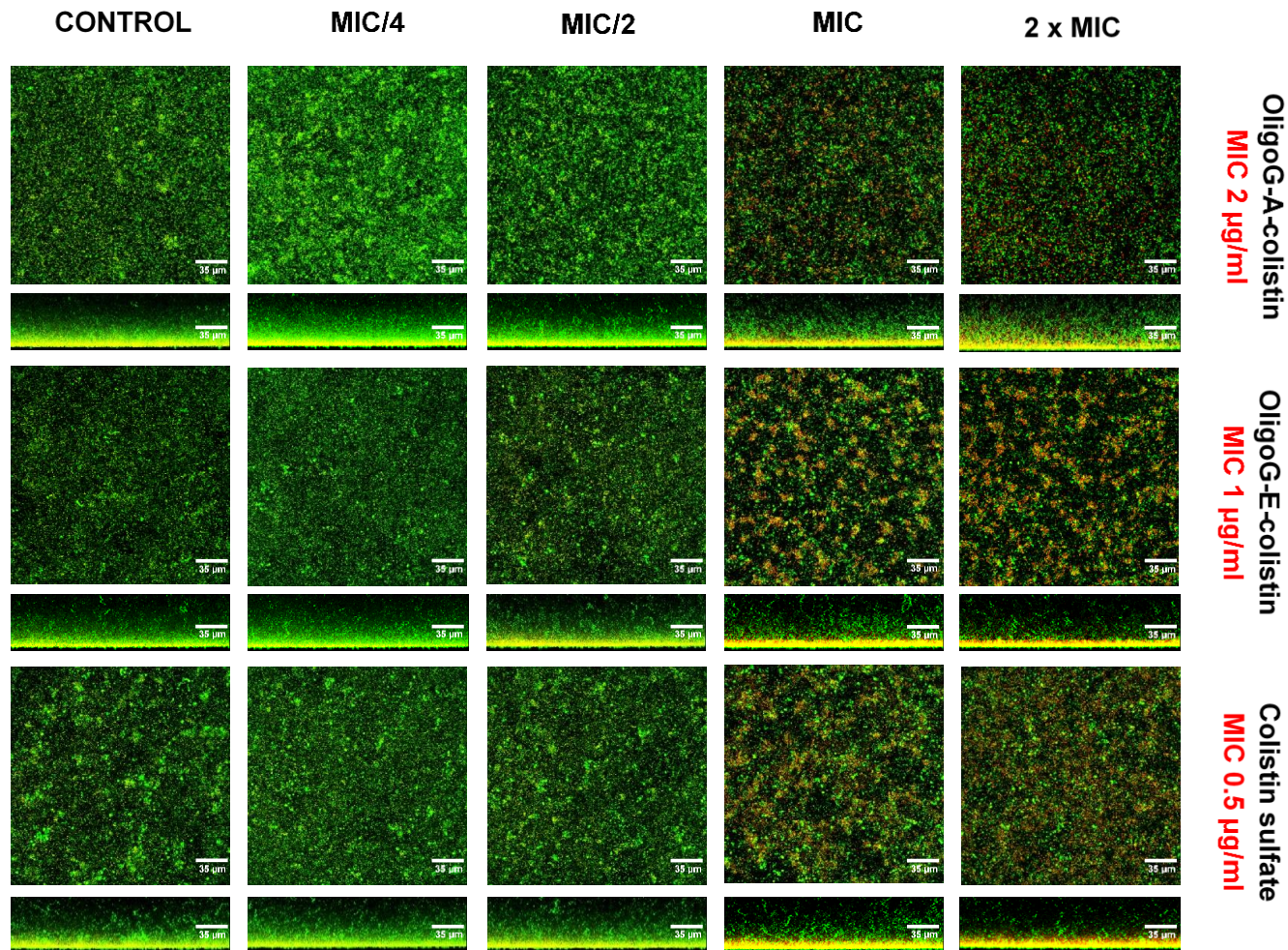


**Figure 4.5** Biofilm formation assay showing LIVE (green)/DEAD (red) stained CLSM (aerial and cross-sectional views) of *P. aeruginosa* R22 biofilms grown for 24 h in the presence of free- and OligoG-conjugated colistin.

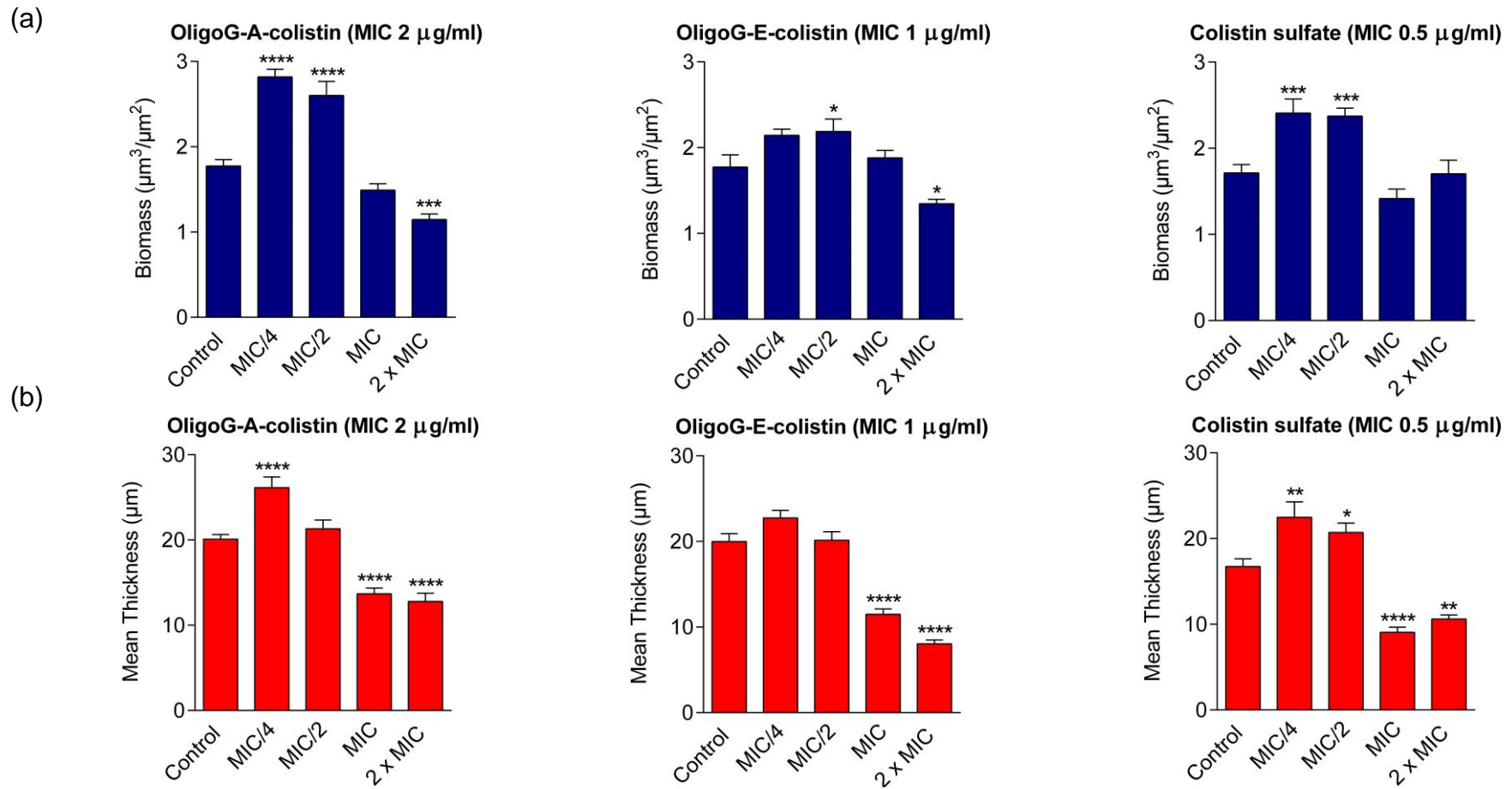
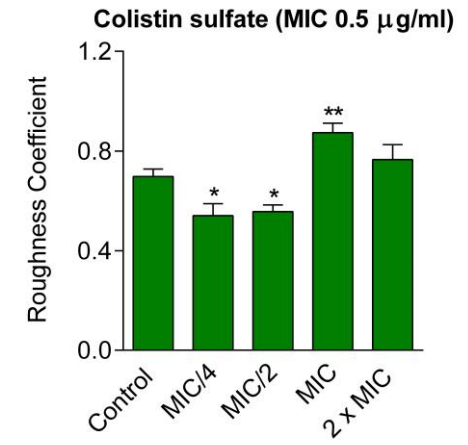
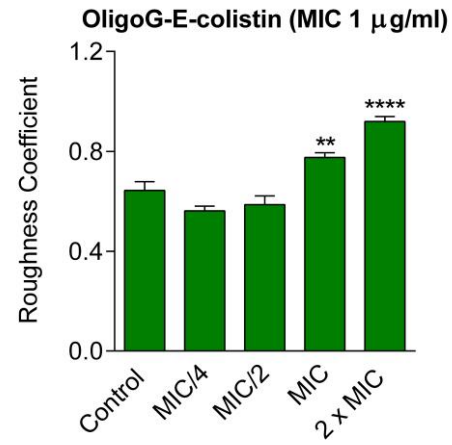
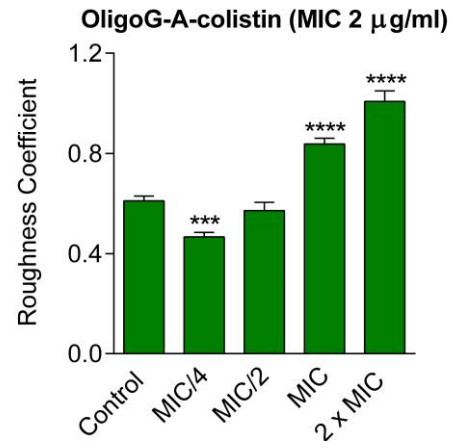


**Figure 4.6** Comstat image analysis of *P. aeruginosa* R22 biofilms grown for 24 h in the presence of free- and OligoG-conjugated colistin. (a) Bio-volume ( $\mu\text{m}^3/\mu\text{m}^2$ ); (b) mean thickness ( $\mu\text{m}$ ); (c) roughness coefficient and (d) DEAD/LIVE bacteria ratio ( $\pm$  SEM;  $n = 15$ ). Significant difference is indicated by \*, where \* $p < 0.05$ , \*\* $p < 0.01$ , \*\*\* $p < 0.001$ , \*\*\*\* $p < 0.0001$  compared to untreated control. (One-way ANOVA and Dunnett's multiple comparisons tests).

(c)



(d)

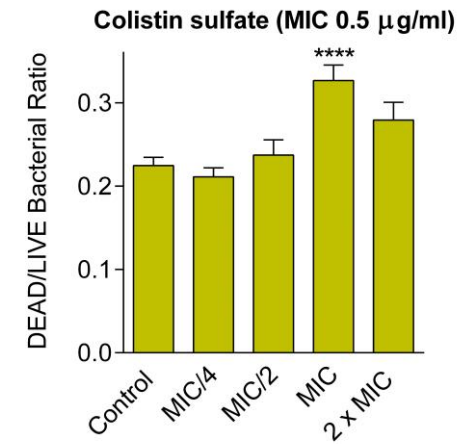
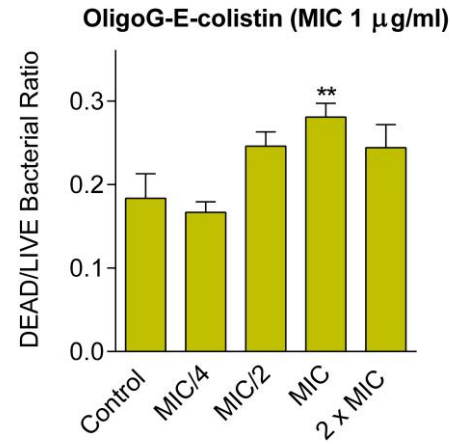
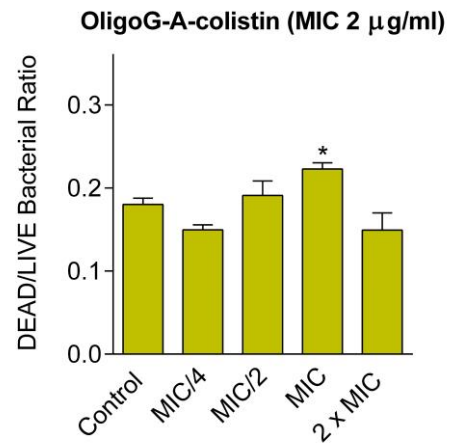


Figure 4.6 (continued).

of antibiotic, poor absorption and extensive clearance of the drug from the body, as well as high MIC values are associated with narrow pharmacodynamic index and poor clinical outcome (Macgowan, 2008). Conflicting recommendations for polymyxin MIC susceptibility breakpoints between the Clinical and Laboratory Standards Institute (CLSI) and the European Committee on Antimicrobial Susceptibility Testing (EUCAST), have been reported. While the CLSI guidelines (CLSI, 2018) state MIC breakpoints for colistin and polymyxin B against *P. aeruginosa* and *Acinetobacter* spp., but not for the *Enterobacteriaceae* family, susceptibility breakpoints for polymyxin B are not identified at all in the EUCAST report (EUCAST, 2018). Consequently, interpretation of breakpoints using CLSI and EUCAST guidelines may cause difficulties in identifying resistant bacterial pathogens. Then again, there are no current susceptibility breakpoints defined for polymer-antibiotic conjugates, so the cut-off guidelines for polymyxins were used for comparison/guidance.

Although the polymyxins had already been shown to exhibit significantly higher *in vitro* cytotoxicity, compared to the OligoG-polymyxin conjugates, colistin and polymyxin B demonstrated potent antimicrobial activity against a range of MDR Gram-negative pathogens. In this study, OligoG-polymyxin conjugates retained equivalent antimicrobial efficacy to the unconjugated antibiotic. Typically, OligoG-polymyxin conjugates were below the susceptibility breakpoints, except for OligoG-A-polymyxin B, which had MIC values of 4 µg/ml against four *P. aeruginosa*, *K. pneumoniae* and *E. coli* isolates.

Since alginates are degraded by bacterial alginate lyase and reinstatement of protein bioactivity following enzymatic degradation has already been described. Ferguson et al. (2016) assessed the antimicrobial activity of OligoG-polymyxin conjugates in the presence of alginate lyase. They observed no significant change with either amide- or ester-linked conjugates, suggesting that, either OligoG degradation was not necessary for antibiotic activity, or that the alginate oligomers were degraded by bacterial enzymes or those contained within the MH medium. As polymyxins exhibit their antimicrobial activity using cationic amino groups, this might explain why ester-

linked conjugates are more biologically active compared to amide-linked ones. A reduction in the overall cationic charge of polymyxins following conjugation of two to four positively charged amino groups to OligoG through amide linkage, might contribute to the slightly reduced activity of OligoG-A-polymyxin conjugates compared to free drug. In addition, enhanced vascular permeability at sites of infection is expected to promote the accumulation of macromolecular conjugates at higher local concentration than in plasma (Azzopardi et al., 2013b), suggesting that the stable and controlled release of drug from the polymer might achieve better therapeutic activity at a lower dose, contributing to reduced toxicity and emergence of resistant bacteria.

The unique tripartite structure of polymyxin antibiotics is crucial for their interaction with bacterial LPS and their antimicrobial efficacy. Previous studies have shown that modification of the cyclic ring or N-terminal fatty acyl chain, as well as masking of the cationic amino groups, resulted in complete or partial loss of antibacterial activity (Velkov et al., 2010). For example, sulfomethylation of the free polymyxin amino groups yielded less toxic colistin and polymyxin B derivatives, but with significant loss of activity (Barnett et al., 1964). Furthermore, administration of a dextran 70-polymyxin B conjugate with imipenem was effective in reducing lethality in mice modelling *E. coli* or *P. aeruginosa* septic shock but retained minimal antimicrobial activity by itself that might be caused by steric hindrance due to high molecular weight polymer binding and blocking of the active sites of the drug (Bucklin et al., 1995, Fuchs et al., 1998). In addition, covalent conjugation of colistin to dextrin was shown to significantly reduce the antimicrobial activity of the antibiotic, even after amylase triggered release of the drug, in a range of Gram-negative bacteria (Ferguson et al., 2014). It has also been demonstrated that by increasing the molecular weight and degree of succinylation to incorporate carboxyl groups in dextrin, the antimicrobial efficacy of dextrin-colistin conjugates markedly decreased (Ferguson et al., 2014). OligoG is a low molecular weight and an inherently bioactive polymer, which might explain the substantially improved antimicrobial activity of the OligoG-polymyxin conjugates. Indeed, comparison of the MIC values of the OligoG-A-colistin conjugate with previously published values for dextrin-A-colistin conjugates (Ferguson et al., 2014), showed that

the OligoG-A-colistin conjugates were significantly more active than the dextrin-A-colistin conjugates, resulting in 3 to 9-fold lower MIC values.

The emergence of plasmid-mediated resistance to the polymyxin antibiotics may limit the treatment options available to tackle severe clinical infections, especially those caused by *Enterobacteriaceae*, and therefore, may contribute to the spread of pan-drug-resistant bacteria (Jeannot et al., 2017). To date, twelve variants of the colistin resistance gene *mcr-1* have been identified in *Enterobacteriaceae* from over forty different countries (Wang et al., 2018). Particularly disquieting is their spread to IncP plasmids, as IncP plasmids are self-transferable and broad host range, so could transfer colistin to many other genera outside *Enterobacteriaceae* including *Pseudomonas* (Liu et al., 2017, Lu et al., 2017). Unfortunately, OligoG conjugation did not improve the antimicrobial activity of colistin and polymyxin B in colistin-resistant *E. coli* strains. Since polymyxins exert their antimicrobial activity by interacting with the lipid A component of LPS located in the outer membrane of Gram-negative bacteria, it is not surprising that modifying the structure of the lipid A moiety decreased the initial binding between the OligoG-polymyxin conjugates and bacteria. Yang et al. (2017) demonstrated that overexpression of the *mcr-1* gene in *E. coli* not only had a detrimental effect on the growth rate and viability of the host bacteria, but also induced significant morphological changes and compromised the structural integrity of the outer membrane (Yang et al., 2017). This suggests that these *mcr-1* positive *E. coli* were evidently challenged in terms of fitness to find a balance between overcoming colistin mediated toxicity and cell survival (MIC = 4-8 µg/ml). Therefore, other studies have explored alternative combination treatment possibilities. Bulman et al. (2017) assessed the antimicrobial activity of commercially available antibiotics combined with polymyxin B against an *E. coli* isolate carrying *mcr-1* and *NDM-5* resistance in time-kill studies. The combination of polymyxin B, amikacin and aztreonam completely eradicated the polymyxin and carbapenem resistant *E. coli* pathogen after 26 h, with undetectable bacterial counts for up to 240 h. An alternative approach against *Enterobacteriaceae* pathogens expressing *mcr-1* resistance by MacNair et al., (2018) demonstrated that colistin could potentiate the activity of conventionally used antibiotics against

Gram-positive bacteria, thereby inhibiting bacterial (Gram-negative) growth below the clinical susceptibility breakpoints. In this way, the administration of OligoG-polymyxin conjugates might disrupt the bacterial outer membrane sufficiently to induce antibiotic uptake and increase the susceptibility to e.g. Gram-positive antibiotics such as macrolides, and thus, prevent the emergence of resistance due to the absence of selective pressure.

It was initially hypothesised that conjugation of OligoG to polymyxin would prevent the interaction of mucin with the antibiotic. However, when MIC assays were performed in the presence of mucin, the MIC values for OligoG-polymyxin conjugates and unconjugated OligoG plus polymyxin increased significantly showing that OligoG conjugation was unable to prevent mucin from binding to and neutralising the polymyxin antibiotics. These results correlated with those of Huang et al., (2015) who showed that addition of mucin to the culture medium increased the MIC values of colistin and polymyxin B by over 100-fold. They also demonstrated that antibiotics with a high primary amine content and overall polybasic positive charge such as colistin sulfate, polymyxin B and tobramycin, had the strongest interaction with mucin compared to less basic antibiotics such as ciprofloxacin and daptomycin. It was, therefore, surprising that OligoG conjugation to the polymyxin amine groups did not inhibit this interaction. Previous studies have shown that OligoG binds and significantly increases the negative surface charge of respiratory mucins via hydrogen bonding (Pritchard et al., 2016) which might contribute to the increased attraction of polymyxins to mucins and thus, reduced efficacy. While colistin is active against MDR Gram-negative bacteria, mucin binding in the airways might reduce its antimicrobial activity and availability, while exposure to suboptimal doses of antibiotic could contribute to the development of colistin resistance. Previous studies have shown that high molecular weight DNA is highly abundant in sputum constituting up to 10% of its dry weight and that it can also interact with antibiotics such as tobramycin, which could lead in further reduction of antibiotic potency (Hunt et al., 1995). Polymer conjugation has previously been shown to prevent binding of drugs to plasma proteins (Banerjee et al., 2012), therefore it remains to be determined whether OligoG might enhance drug efficacy in more complex *in vivo* systems.

OligoG-polymyxin conjugates exhibited a 4-fold decrease in antimicrobial activity in AS medium compared to MH broth. Previous studies have also reported 4-fold greater MIC values for colistin in AS medium compared to MH broth that has been attributed to altered growth of bacteria, modification of LPS structure or direct colistin-mucin interactions (Pritchard et al., 2017). Recently, Schneider-Futschik et al. (2018) investigated the antimicrobial efficacy of a series of polymyxin lipopeptides against *P. aeruginosa* CF isolates grown in AS medium and their interaction with sputum biomolecules, including DNA, mucin, surfactant, F-actin, LPS and phospholipids. This study indicated the propensity of sputum biomolecules to diminish the antimicrobial activity of natural and synthetic polymyxin lipopeptides, but also highlighted the potential antibacterial efficacy of an octapeptin A<sub>3</sub> lipopeptide carrying four positively charged amino groups against *P. aeruginosa* isolates. Since two to four primary polymyxin amino groups were used for binding to OligoG and stable amide bond formation, this might explain the reduced antimicrobial activity observed in AS medium of the OligoG-A-polymyxin conjugates. Both, OligoG-ester-colistin and OligoG-ester-polymyxin B conjugates exhibited 2-fold improved efficacy in AS medium compared to MH broth against the *E. coli* IR57 isolate, suggesting that ester-linked colistin would have a better therapeutic index *in vivo*. Other studies have also looked at colistin and LPS interactions. It is known that polymyxins bind to and neutralise bacterial LPS (Davies and Cohen, 2011). Even though Roberts et al. demonstrated ~50% reduction in the interaction of LPS with dextrin-colistin conjugates compared to colistin alone, concentration-dependent inhibition of LPS-induced TNF $\alpha$  secretion by human kidney cells and reduced hemolysis of rat erythrocytes was observed (Roberts et al., 2016). The interaction between LPS and OligoG-polymyxin conjugates still needs to be explored for their potential use in the treatment of systemic sepsis. Overall, the antimicrobial activity of inhaled colistin is highly affected by sputum binding in the airways, but it remains unclear whether intravenously administered OligoG-polymyxin conjugates, exhibiting sustained and controlled release of antibiotic at the site of infection, could be more effective in reducing sputum binding than a rapid and high concentration of colistin achieved via inhalation.

Studies of the bacterial growth kinetics indicated a dose-dependent response to OligoG-colistin conjugates (amide- and ester-linked) and a decreased rate of bacterial regrowth. These results might suggest that the conjugates produced a more stable and controlled release of colistin, thereby maintaining its concentration within the therapeutic window and prolonging its activity at the site of infection. The sustained release of colistin from PEG due to labile ester bonding, lead to similar or improved antimicrobial activity against *P. aeruginosa* and *A. baumannii* isolates (Zhu et al., 2017). In this study, higher concentrations of free colistin, compared to OligoG-colistin conjugates, were required to inhibit bacterial regrowth for up to 48 h. At the previously determined MIC, both OligoG-colistin conjugates showed the longest inhibition of bacterial regrowth compared to colistin. However, the ester-linked conjugate delayed the onset of bacterial regrowth for a much longer time compared to amide-linked conjugates. Previous studies have analysed the growth pattern of several *P. aeruginosa* isolates from CF patients in the presence of sub-MIC concentrations of individual components or combined mixtures of antimicrobial lipopeptide and colistin (De Gier et al., 2016). They revealed that lipopeptide alone (at 4 µg/ml) was ineffective in reducing the growth of colistin sensitive and resistant *P. aeruginosa*, whereas colistin (at concentrations of 0.25 and 2 µg/ml respectively), prolonged the lag growth phase for up to 4 hours. The successful synergistic inhibition of bacterial growth for > 18 h was achieved when both components were used at the individually tested concentrations. Similarly, OligoG-amide-colistin (1 µg/ml, colistin equivalent) and OligoG-ester-colistin (0.5 µg/ml, colistin equivalent) conjugates used at their MIC concentrations, delayed the lag phase of *P. aeruginosa* MDR 301 for > 24 h and > 18 h, respectively and changed the rate of bacterial growth, suggesting that OligoG-colistin conjugates would have better and prolonged therapeutic activity *in vivo*.

The combination therapy of two synergistic antimicrobial agents can simultaneously enhance the efficacy of each compound and thus, reduce the required dosage and toxicity or even broaden the antimicrobial spectrum (Riahifard et al., 2017). Even though OligoG conjugation did not enhance the efficacy of colistin in combination with azithromycin, synergistic activity was

observed for the OligoG-E-colistin conjugates with azithromycin in an *E. coli* isolate. It is proposed that colistin may increase the permeability of the bacterial outer membrane to azithromycin, which may explain the synergy observed between the OligoG-E-colistin conjugate and azithromycin in this *E. coli* pathogen. Importantly, colistin conjugation to OligoG did not induce an antagonistic activity with azithromycin, suggesting that OligoG-colistin conjugates and azithromycin could be used clinically in combination with no deleterious effects. Previous studies have demonstrated the ability of OligoG to potentiate the antimicrobial efficacy of colistin against the mucoid *P. aeruginosa* NH57388A CF isolate (Hengzhuang et al., 2016). In this case, OligoG alone was also able to enhance the efficacy of azithromycin. However, since it has no MIC value, the FICI cannot be calculated. Similarly, low molecular weight ( $M_w < 10$  kDa) oligosaccharides of alginate and chitosan have previously been combined with azithromycin, demonstrating additive and synergistic effects against *P. aeruginosa*, respectively (He et al., 2014). This correlates with the results obtained in this study with the OligoG-colistin conjugates which also demonstrated additive activity between OligoG-colistin conjugates and azithromycin against the *P. aeruginosa* MDR 301 isolate. Importantly, the therapeutic benefits of OligoG-colistin conjugates, in combination with azithromycin, might have been underestimated by the checkerboard assay, as passive accumulation of conjugates at the site of infection due to the EPR effect, and controlled release of the drug from the polymer, might enhance the efficacy of azithromycin and thus, reduce the doses required to eradicate the pathogen.

Both amide- and ester-linked OligoG-colistin conjugates markedly disrupted the formation of *P. aeruginosa* biofilms, although, only the OligoG-E-colistin conjugate caused actual bacterial clumping (at MIC concentrations and above). Comstat analysis of z-stack images revealed that both OligoG-colistin conjugates and colistin sulfate at concentrations below or equal to the MIC, were unable to inhibit biofilm growth, leading to a marked increase in biofilm biomass and thickness and a decrease in roughness coefficient. The presence of persister cells within the biofilm due to exposure of sub-MIC concentrations of antibiotics might explain this phenomenon (Lewis, 2006).

Alternatively, OligoG might be broken down by bacterial enzymes and used as a carbon source to increase bacterial respiration rate and efficiency of growth (Passalacqua et al., 2016). In addition, Powell et al. (2018) have previously shown that OligoG, at concentrations  $\geq 0.5\%$  induced bacterial aggregation, and at  $\geq 2\%$  significantly disrupted *P. aeruginosa* biofilm formation and growth as confirmed by decreased biofilm biomass and thickness, and increased roughness coefficient.

In this Chapter, the antimicrobial efficacy of OligoG-polymyxin conjugates has been characterised *in vitro*, highlighting a potential new clinical therapy for the treatment of multidrug resistant bacterial infections.

#### **4.6 Conclusions**

Multi-drug resistance is one of the leading causes of morbidity and mortality worldwide. The recent emergence of resistance to colistin, encoded by mobile genetic elements, highlights an urgent need for improved antimicrobials that can be delivered to sites of infection. OligoG-polymyxin conjugates exhibited substantial or full retention of antimicrobial activity and controlled release of the antibiotic from OligoG resulting in sustained inhibition of bacterial growth. OligoG conjugation was unable to inhibit the deleterious effects of mucin binding or nutrient-deficient media, nor could it overcome *mcr-1* colistin resistance. However, targeted delivery of the antibiotic to sites of infection through the EPR effect would potentially maximise its local bioavailability and efficacy, while at the same time, minimising any side effects and drug resistance. To investigate further the controlled release of antibiotic, an *in vitro* pharmacokinetic-pharmacodynamic model was developed to compare the activity of free- and OligoG-conjugated colistin (Chapter 5).

# **Chapter 5**

## ***In vitro* Pharmacokinetic-Pharmacodynamic Model**

## 5.1 Introduction

Characterisation of the pharmacokinetic-pharmacodynamic (PK-PD) profile of a drug is an essential step in optimising dosing and predicting its behaviour *in vivo*. Since polymer conjugation substantially alters the PK-PD properties of the attached antibiotic, this chapter aimed to develop an *in vitro* two-compartment PK-PD model to characterise drug release from the conjugate and compare the antimicrobial efficacy of free- and OligoG-conjugated colistin against the MDR *A. baumannii* 7789 clinical isolate. *A. baumannii* is an opportunistic pathogen that causes a broad range of clinical infections that are associated with significant antibiotic resistance and mortality rates of 8.4-36.5% (Falagas and Rafailidis, 2007). Thus, it provided a clinically relevant organism to characterise the antimicrobial profile of the OligoG-colistin conjugates.

### 5.1.1 PK-PD models described in the literature

While MIC susceptibility testing is an important and useful tool for defining the potential therapeutic activity of new antimicrobial agents, the static concentrations of antibiotic used do not always correlate with the efficacy of the drug *in vivo*. MIC values are also unable to distinguish between bacteriostatic and bactericidal activity, nor can they tell us whether bactericidal activity is concentration- or time-dependent or if it has a post-antibiotic effect when drug concentrations fall below MIC (Lister, 2006). Additionally, MIC assays are unable to quantify the rate of bacterial killing or identify the pharmacodynamic target. Although animal models have been widely used to imitate the characteristics of infection in humans and determine the relationships between antibiotic concentrations found in tissue, plasma or serum, the differences in animal and human metabolisms and the impact of the immune system, complicate the evaluation of antibiotic interactions with bacteria (Andes and Craig, 2002). These limitations have led researchers to develop *in vitro* PK-PD models to predict concentration-time profiles and correlate them to antibiotic efficacy at the site of infection. One of the main advantages of employing *in vitro* PK-PD models is that they simulate human

pharmacokinetic properties, allowing the effect of various antibiotic concentrations on the rate and extent of bacterial eradication to be determined using time-to-kill (TTK) assays (Budha et al., 2009). Typically, the change in viable bacterial counts is monitored over time and quantified at different time intervals by various methods (summarised in **Table 5.1**), thus enabling analysis of bacterial growth patterns during drug exposure. Most *in vitro* PK-PD models described in the literature can be classified into one of two models: static models (constant antibiotic exposure) that simulate the drug concentration at a steady state, or single/multiple compartment models (changing antibiotic concentrations) attained by diffusion or dilution to simulate multiple dosing (Gloede et al., 2010).

Conventional static TTK models have been extensively used to study the effect of fixed antibiotic concentrations on bacterial growth. However, these approaches are not clinically relevant, as the antibiotic concentration remains unchanged throughout the experiment (Owen et al., 2007). To reflect the situation *in vivo*, and to mimic the elimination half-life of a drug, single compartment PK-PD models have been developed, where the systematic loss and dilution of the antibiotic is achieved by the continuous pumping of sterile media into a central reservoir containing bacteria and the antimicrobial agent (Grasso et al., 1978). Filter membranes and magnetic stirrers have been incorporated into these one-compartment models to maintain homogenous mixing and prevent bacterial loss from the system, which can cause experimental bias (Budha et al., 2009). Unfortunately, filter membrane blockage is common in these modified models, especially when antibiotics with short elimination half-lives were analysed (Vaddady et al., 2010). To overcome the loss of viable bacteria from the system, two-compartment PK-PD models have been constructed, whereby the antibiotic contained in the central compartment is physically separated from the bacterial pathogen in the peripheral compartment (usually by dialysis membrane) and distributed through the compartments using peristaltic pumps (White, 2001). The concentration gradient between the central and peripheral compartments induces passive diffusion of the antibiotic across the dialysis membrane, exposing the bacteria to fluctuating drug concentrations over time (Ba et al.,

**Table 5.1** Examples of bacterial quantification methods used in time-to-kill assays.

<b>Method</b>	<b>Description</b>	<b>Limitations</b>	<b>Reference</b>
Viable bacterial counts	Incubation of bacterial samples on agar plates by spiral plating or the Miles-Misra method followed by bacterial colony counting.	Caution must be taken to avoid an antibiotic carry-over effect.	(Jönsson et al., 2018, Tam et al., 2005)
Turbidimetric measurements	Determination of turbidity or cloudiness (optical density) of bacterial samples spectrophotometrically. Measurements can be directly correlated to bacterial concentration.	Not reliable if bacteria form clumps in the liquid medium. Cannot distinguish between live and dead bacteria.	(Li et al., 1993)
Microscopic counts	Determination of bacterial cell numbers using Petroff-Hausser counting chambers by phase-contrast microscopy. Trypan blue can be used to distinguish between live and dead bacteria.	Small cells might be missed or miscounted. Labour intensive.	(Dever et al., 1992)
Bioluminescence assays	Quantification of bacterial intracellular ATP content (as a measure of bacterial respiration) and correlation to bacterial concentration.	Difficult to differentiate the intracellular and extracellular bacterial ATP.	(Hanberger et al., 1993)

2001). The main drawback of the multi-compartment model has been that they can be technically challenging to set up, since they require special equipment and software to interpret the results.

Selecting the most appropriate PK-PD model to characterise the antimicrobial profile and controlled release properties of antibiotics contained in complex drug delivery systems such as polymer-drug conjugates has been challenging. Due to the limitations of conventional PK-PD systems, Azzopardi et al. (2015) developed a novel two-compartment dialysis bag model to investigate the antimicrobial properties, (including degradation and antibiotic release patterns of the dextrin-colistin conjugates), whose content of unmasked colistin changed with time. This model offered a simple and effective way of analysing and modifying the composition of the individual compartments. For example, to mimic the pathological conditions of infected tissue, infected wound fluid or physiological concentrations of amylase was placed in the outer compartment, enabling the pharmacokinetics of enzyme-triggered activation of the dextrin-colistin conjugate to be studied.

This study, therefore, aimed to develop a similar *in vitro* PK-PD model for the characterisation of OligoG-colistin conjugates, that allowed differentiation of free- and OligoG-conjugated colistin. Separation of the species was achieved by diffusion through a dialysis membrane, using either a Slide-a-lyzer dialysis cassette or a dialysis membrane bag, as previously used to study the PK-PD parameters of dextrin-colistin conjugates (Azzopardi et al., 2015). The two-compartment dialysis bag model was employed to assess the TTK profile of a single OligoG-colistin (amide- and ester-linked) conjugate dose. As previously discussed, the concentration gradient between the two compartments was used as a driving force to achieve the required fluctuations in drug concentrations (Gloede et al., 2010).

## **5.2 Experimental aims and objectives**

**The specific aims of this study were:**

- To determine whether complete release of the antibiotic from OligoG

was required for full re-instatement of the antibacterial activity of the individual components of the alginate-conjugate.

- To develop an *in vitro* two-compartment PK-PD model to compare the diffusion profiles of colistin sulfate, OligoG-A-colistin and OligoG-E-colistin conjugates.
- To compare the antimicrobial activity and TTK profile of colistin sulfate, OligoG-A-colistin and OligoG-E-colistin conjugates against MDR *A. baumannii* 7789.

### 5.3 Methods

OligoG-A-colistin (8.8% w/w colistin content, Mw ~22,500 g/mol) and OligoG-E-colistin (12.9% w/w colistin content, Mw ~14,500 g/mol) conjugates tested in this chapter were synthesised and characterised as previously described in Chapter 3. For details of bacterial strain used in this study refer to **Table 4.1**.

#### 5.3.1 Development of the two-compartment PK-PD model using the Slide-a-lyzer dialysis cassettes

Initially, sterile Slide-a-lyzer dialysis cassettes (molecular weight cut-off; MWCO: 2,000 and 10,000 g/mol) were used to compare the PK-PD profile of free- and OligoG-conjugated colistin. The model consisted of a sealable sampling port, an inner compartment (IC; 3 ml) and an outer compartment (OC; 200 ml) separated by regenerated cellulose membrane as shown in **Figure 5.1**. All model systems were prepared and maintained under aseptic conditions. A summary of the model development is presented in **Table 5.2**.

##### 5.3.1.1 Phase 1: Method validation using the dialysis cassettes

A dialysis cassette was filled with PBS containing either the OligoG-colistin conjugate or colistin sulfate (10 mg/ml colistin equivalent). The cassette was then suspended in sterile PBS (200 ml) in a sterile beaker, sealed with parafilm wiped in ethanol and equilibrated under gentle stirring at room temperature for 5 min. Samples (100 µl) were collected from the IC or OC at different time points (0, 2, 4, 6, 8, 24 and 48 h) and stored at -20°C prior to analysis by BCA

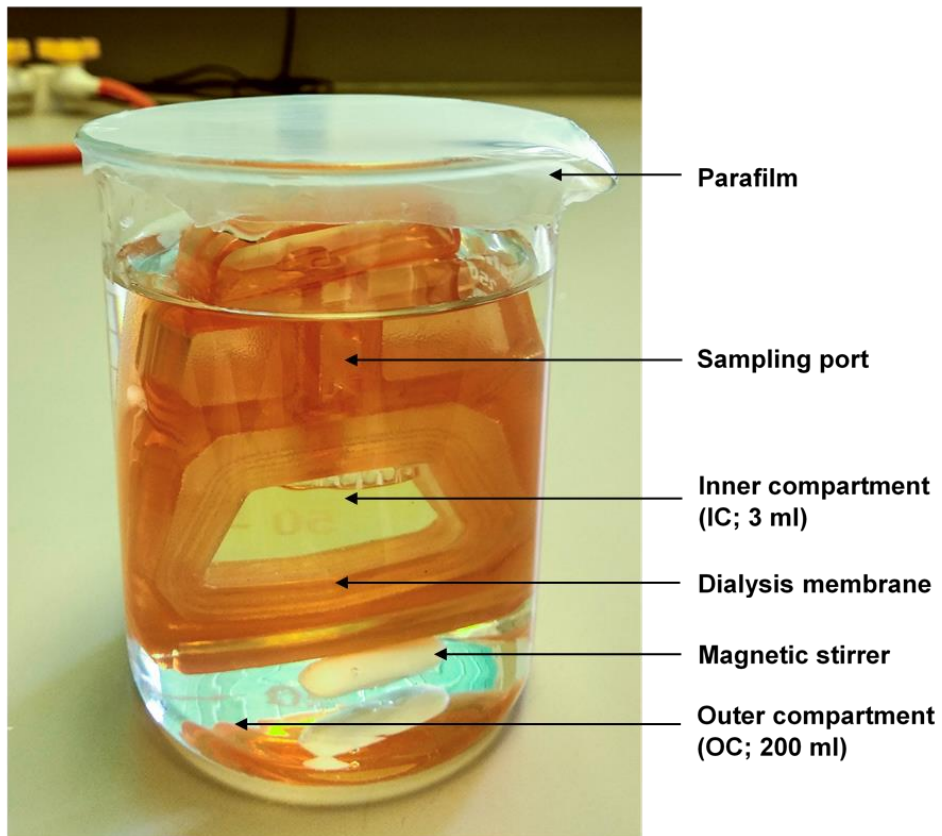


**Figure 5.1** Representative picture of the two-compartment PK-PD model using a Slide-a-lyzer dialysis cassette.

**Table 5.2** Developmental phases of the PK-PD model using the Slide-a-lyzer dialysis cassettes.

Method development	Inner compartment (IC; 3 ml)	Outer compartment (OC; 200 ml)	Sampling method used
<b>Phase 1:</b> Method validation	OligoG-colistin conjugates or colistin sulfate in PBS (10 mg/ml colistin equivalent).	PBS	Sample IC and OC; protein determination by BCA assay.
<b>Phase 2:</b> Method validation	MH broth	OligoG-colistin conjugates or colistin sulfate in MH broth (1 µg/ml colistin equivalent).	Sample IC; colistin determination by ELISA. Sample OC; sterility testing.
<b>Phase 3:</b> Time-to-kill (TTK) model	<i>A. baumannii</i> 7789 in MH broth (1 x 10 <sup>7</sup> or 5 x 10 <sup>5</sup> CFU/ml).	OligoG-colistin conjugates or colistin sulfate in MH broth (1 or 2 x MIC).	Sample IC; CFU/ml determination by colony count. Sample OC; sterility testing.

assay as previously described (Section 2.6.2.3).

### **5.3.1.2 Phase 2: Method validation using the dialysis cassettes**

To validate and determine the feasibility of the model for TTK studies, total colistin content in the IC after 24 h was determined by colistin ELISA as described in Chapter 2 (Section 2.6.4.5). In this instance, the IC contained MH broth and the OC contained OligoG-A-colistin, OligoG-E-colistin or colistin sulfate (1 µg/ml colistin equivalent) in MH broth. Sterility of the OC was confirmed by sampling a 5 µl drop of the liquid phase and plating it onto a TSA plate. No visible growth following overnight incubation at 37°C was considered acceptable.

### **5.3.1.3 Phase 3: TTK model using the dialysis cassettes**

To analyse the antimicrobial activity of a single dose of free- and OligoG-conjugated colistin over 8 or 24 h, *A. baumannii* 7789 ( $1 \times 10^7$  or  $5 \times 10^5$  CFU/ml) was added to MH broth in the IC, while the OC contained OligoG-A-colistin, OligoG-E-colistin or colistin sulfate at 1 or 2 x MIC in MH broth. The colistin equivalent concentrations used were:

- OligoG-A-colistin: 0.125, 0.25 µg/ml
- OligoG-E-colistin: 0.125, 0.25 µg/ml
- Colistin sulfate: 0.25, 0.5, 4 µg/ml (16 x MIC)

A growth control, with MH broth in the OC, was analysed for up to 24 h. A range of dialysis cassettes with MWCOs of 2,000, 10,000 and 20,000 g/mol were tested in the model to facilitate diffusion across the membrane. Sterility of the OC was monitored over 48 h (as described in Section 5.3.1.2). Samples collected at various time points from the IC were characterised for the number of colony forming units (CFU/ml) according to the Miles and Misra method (Miles et al., 1938). Briefly, TSA plates were dried in a laminar air flow cabinet for 15 min prior to use. Aliquots of the IC were serially diluted (1:10 in PBS) up to  $10^{-8}$  and 20 µl of each dilution was dropped onto the surface of the dried TSA plates in triplicate, allowing the drop to spread naturally. The TSA plates

were left undisturbed to dry, then inverted and incubated at 37°C for 18-20 h. The dilution sector with the highest number of discrete, full size colonies (usually 2-20 colonies) was recorded and the colony count calculated using the formula below:

$$\text{CFU/ml} = \text{Mean number of colonies counted} \times 50 \times \text{dilution factor}$$

### **5.3.2 Development of a two-compartment PK-PD model using a dialysis bag**

A second PK-PD model was constructed using a regenerated cellulose dialysis membrane (MWCO 10,000 g/mol; 24 mm flat width) instead of the Slide-analyzer cassette. The dialysis membrane was washed and pre-soaked in dH<sub>2</sub>O for 10 min, one end was secured with sterile surgical thread then filled with the IC solution (5 ml) before tying the open end in the same way. The dialysis bag was then suspended in a 25 ml beaker containing the OC solution (15 ml) and sealed with parafilm, as shown in **Figure 5.2**. The beaker was placed in a shaking incubator using an orbital agitation of 70 rpm, at 37°C for 48 h. Samples (100 µl) were collected from the IC or OC at different time points (0, 2, 4, 6, 8, 24 and 48 h) and stored at -20°C prior to analysis. All model systems were prepared and maintained under aseptic conditions. A summary of the model development is presented in **Table 5.3**.

#### **5.3.2.1 Phase 1: Method validation using the dialysis bag model**

To validate the model set-up, a modified version of the method described in 5.3.1.1 was used. The model was set up as described in **Table 5.3** and samples were analysed over 48 h for protein content by BCA assay (Section 2.6.2.3).

#### **5.3.2.2 Phase 2: TTK model using the dialysis bag**

To assess TTK, *A. baumannii* 7789 ( $5 \times 10^5$  CFU/ml) was added to the MH broth in the OC, while the IC contained OligoG-A-colistin or OligoG-E-colistin at 1 or 2 x MIC or colistin sulfate at 1 x MIC (considering the total volume in

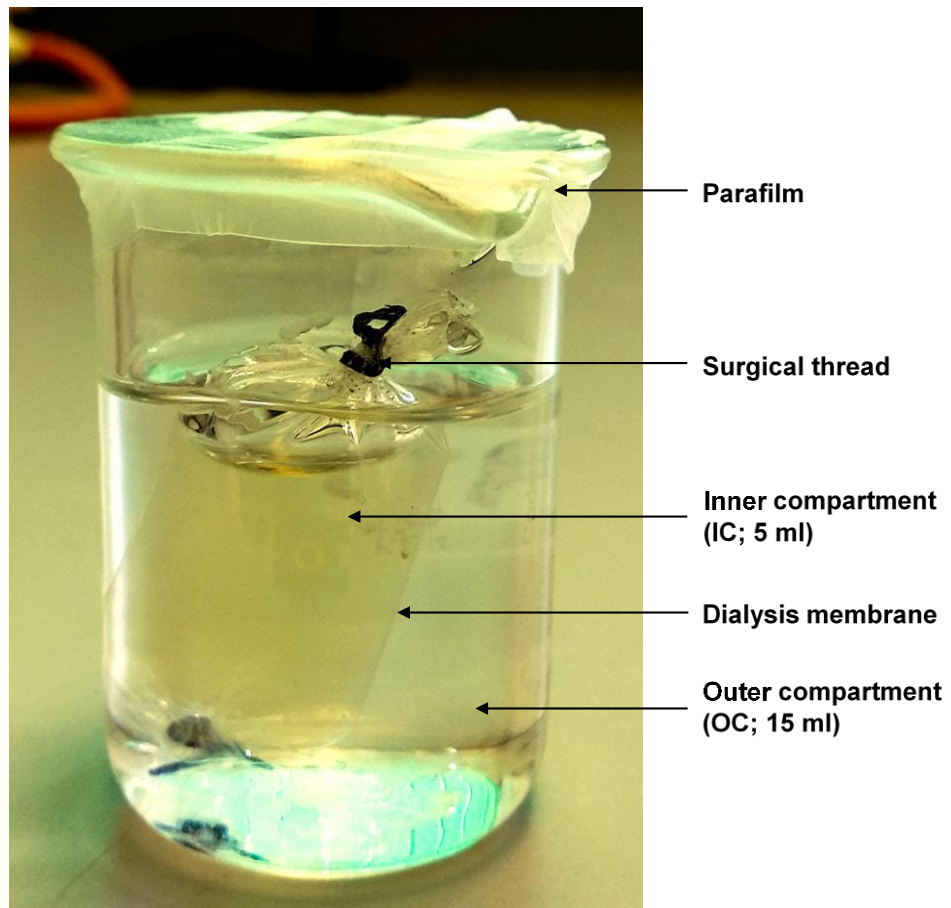


**Figure 5.2** Representative picture of the two-compartment PK-PD model using a dialysis bag.

**Table 5.3** Developmental phases of the PK-PD model using the dialysis bag.

<b>Method development</b>	<b>Inner compartment (IC; 5 ml)</b>	<b>Outer compartment (OC; 15 ml)</b>	<b>Sampling method used</b>
<b>Phase 1:</b> Method validation	OligoG-colistin conjugates or colistin sulfate in PBS (10 mg/ml colistin equivalent).	PBS	Sample IC and OC; protein determination by BCA assay.
<b>Phase 2:</b> Time-to-kill (TTK) model	OligoG-colistin conjugates or colistin sulfate in PBS (1 or 2 x MIC).	<i>A. baumannii</i> 7789 in MH broth ( $5 \times 10^5$ CFU/ml).	Sample OC; CFU/ml determination by colony count.

the system) in PBS. The colistin equivalent concentrations used were:

- OligoG-A-colistin: 0.125, 0.25 µg/ml
- OligoG-E-colistin: 0.125, 0.25 µg/ml
- Colistin sulfate: 0.25 µg/ml

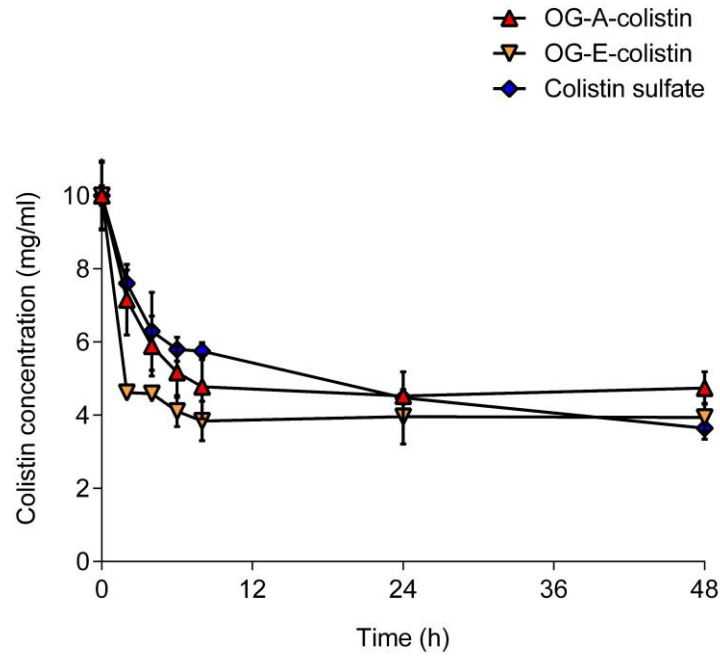
A growth control, with PBS in the IC, was analysed for up to 48 h. Sterility of the OC was tested over 48 h (as described in Section 5.3.1.2). Samples collected at various time points from OC were characterised for the bacterial number of colony forming units (CFU/ml) as described in Section 5.3.1.3. Antibiotics were considered bactericidal if the reduction in viable bacterial counts was  $\geq 3 \log_{10}$  CFU/ml (equivalent to 99.9% of the initial inoculum) and bacteriostatic if the decrease was  $< 3 \log_{10}$  CFU/ml (CLSI, 1999, Levison and Levison, 2009).

## 5.4 Results

### 5.4.1 Characterisation of the two-compartment PK-PD model using Slide-a-lyzer dialysis cassettes

*Phase 1:* Typically, the protein concentration in the IC markedly decreased over the 48 h time period which mostly correlated with a reciprocal increase of the protein concentration in the OC (**Figures 5.3** and **5.4**). As expected, the diffusion of free colistin was faster and greater than that of the (much larger) conjugates. When OligoG-colistin conjugates were placed inside the 2,000 g/mol MWCO dialysis cassettes, the protein content in the OC remained below the limit of quantification throughout the experiment. In contrast, while conjugate diffusion using the 10,000 g/mol MWCO dialysis cassette was greater, it still failed to reach the same levels as that of the free colistin, and neither the ester- or amide- linked colistin conjugates caused a substantial increase in protein concentration in the OC (**Figures 5.3b** and **5.4b**). Also, the levels of both conjugates failed to fall below 4 mg/ml using the 2,000 g/mol MWCO dialysis cassettes from the 8 h time point onwards, (possibly suggestive of membrane saturation or blockage) whilst levels using the larger 10,000 g/mol MWCO dialysis cassette continued to fall over the duration of

(a)



(b)

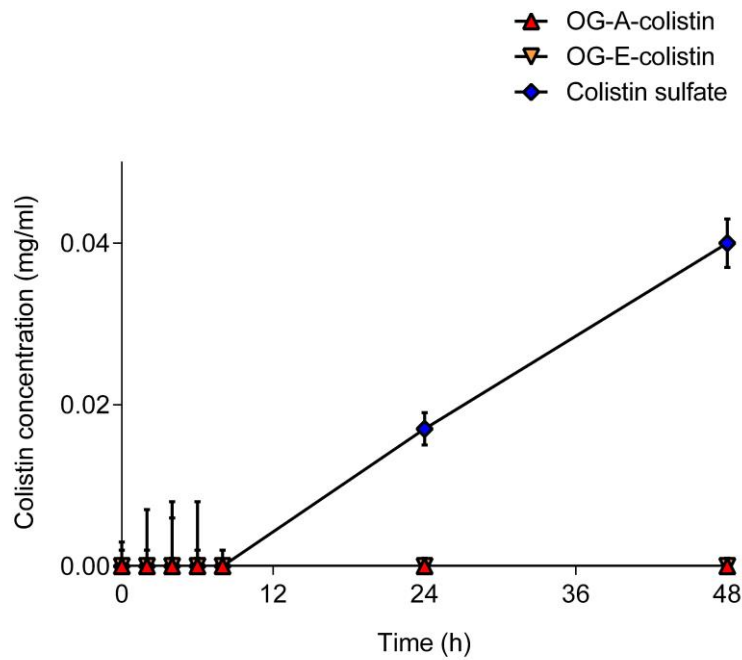
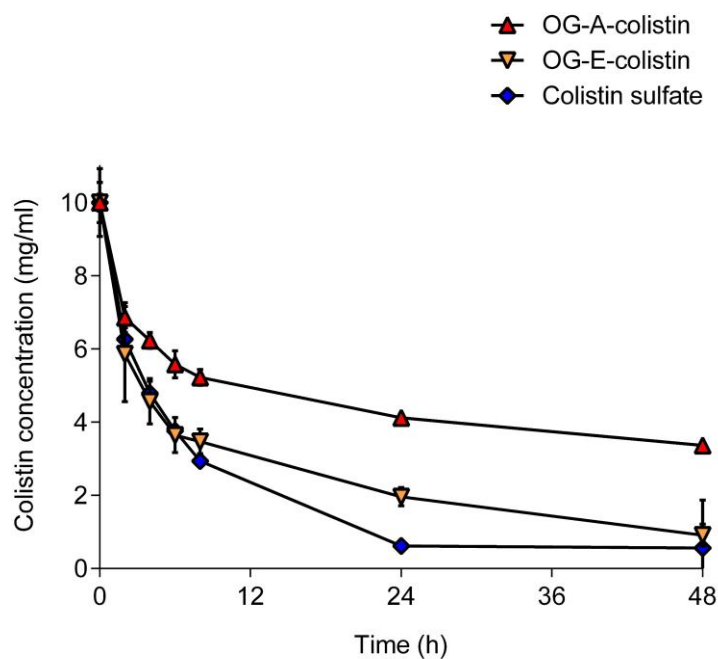


**Figure 5.3** Phase 1 method validation: Colistin concentration, measured by BCA assay, in the (a) IC and (b) OC following diffusion through 2,000 g/mol MWCO dialysis cassettes over 48 h. Data represents mean colistin concentration  $\pm$  SD ( $n = 3$ ).

(a)



(b)

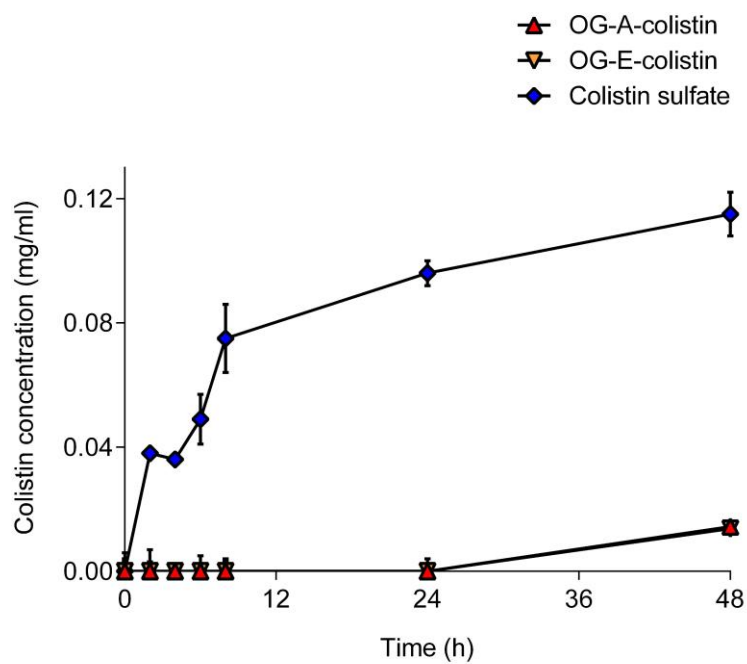


**Figure 5.4** Phase 1 method validation: Colistin concentration, measured by BCA assay, in the (a) IC and (b) OC following diffusion through 10,000 g/mol MWCO dialysis cassettes over 48 h. Data represents mean colistin concentration  $\pm$  SD ( $n = 3$ ).

the 48 h experiment.

*Phase 2:* Colistin content in the IC was only determined at the 24 h time point, as formation of a large pellet after centrifugation of the samples during colistin extraction caused substantial variation in the colistin concentrations detected by the ELISA (**Figure 5.5**). Despite these issues however, up to ~73% of the original dose was detected in the IC after 24 h (**Table 5.4**).

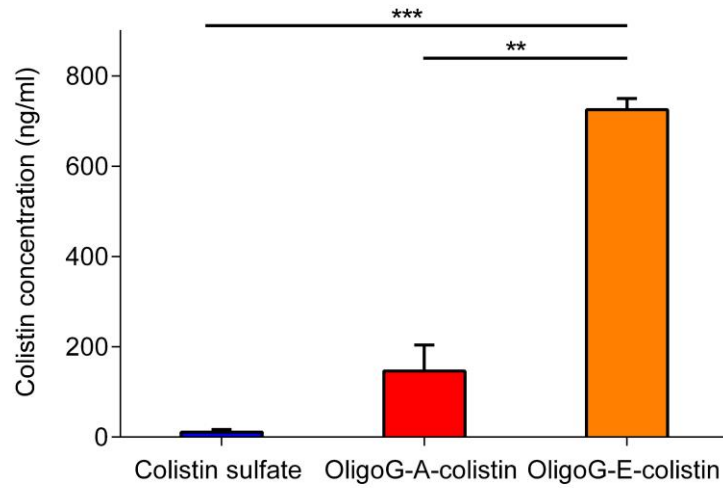
**Table 5.4** Summary of the percentage of the original colistin dose detected in the IC after 24 h.

Treatment	% of original dose in IC at 24 h	
	2,000 MWCO	10,000 MWCO
OligoG-A-colistin	14.7	34.3
OligoG-E-colistin	72.6	65.6
Colistin sulfate	1.1	4.9

Diffusion of colistin into the IC was significantly lower than that of the OligoG-E-colistin conjugate for both MWCO membranes ( $p < 0.05$ ). When the OligoG-A-colistin conjugate was placed in the OC, the colistin concentration in the IC at 24 h was greater than seen with colistin sulfate, but still less than with the ester-linked conjugate. While the MWCO of the membrane (2,000 or 10,000 g/mol) did not greatly alter the colistin concentration in the IC in the experiments using either OligoG-E-colistin or colistin, markedly more colistin was detected in the IC when OligoG-A-colistin was tested using the 10,000 MWCO cassette however this was not significant, ( $p > 0.05$ ), according to an unpaired t-test.

*Phase 3:* When *A. baumannii* 7789 were added to the IC, growth in the IC and sterility of the OC was maintained for up to 48 h. However, as previously determined using either 1 or 2 x MIC, OligoG-colistin conjugates (amide and ester linked) or colistin sulfate had no effect in reducing viable bacterial colony counts using either the 2,000 or 10,000 g/mol MWCO dialysis cassettes with a starting bacterial inoculum of  $1 \times 10^7$  CFU/ml (**Figures 5.6** and **5.7**). Even when the starting inoculum was reduced to  $5 \times 10^5$  CFU/ml and colistin sulfate

(a)



(b)

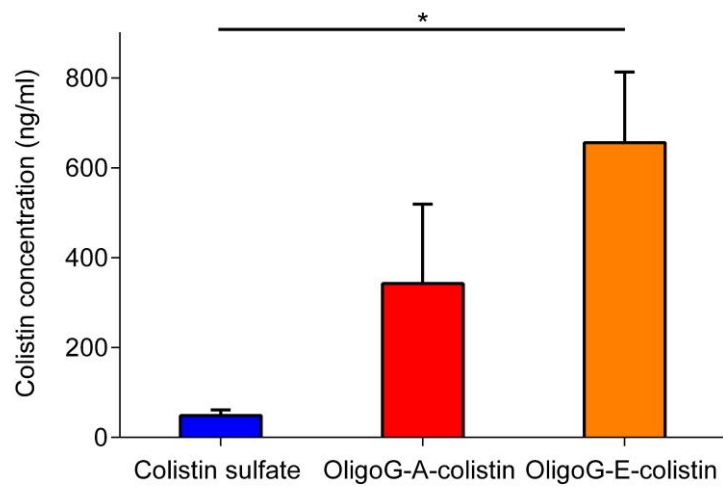
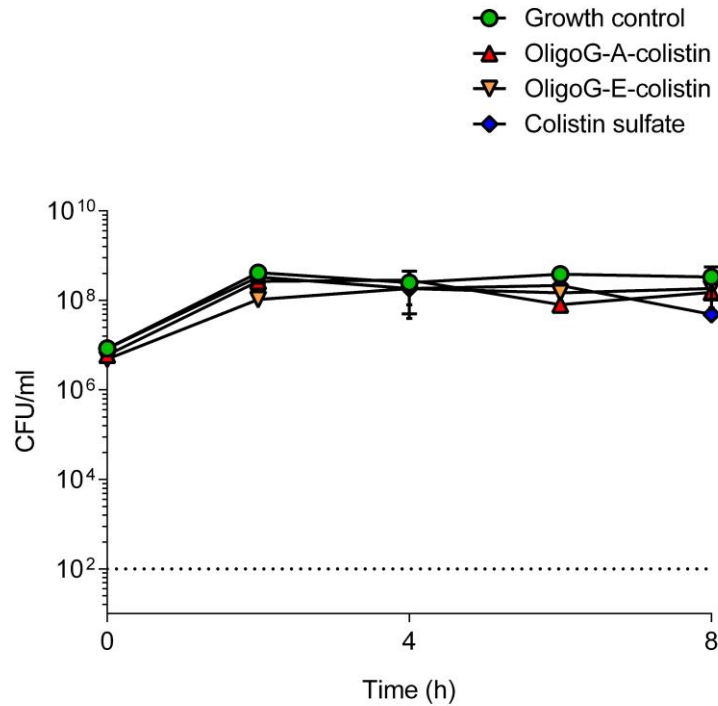


**Figure 5.5** Phase 2 method validation: Quantification of colistin concentration, measured by ELISA, in the IC after 24 h using (a) 2,000 and (b) 10,000 g/mol MWCO dialysis cassettes. Data represents mean  $\pm$  SD ( $n = 2$ ). Significant difference is indicated by \*, where \* $p < 0.05$ , \*\* $p < 0.01$ , \*\*\* $p < 0.001$ . (One-way ANOVA and Tukey's multiple comparisons tests).

(a)



(b)

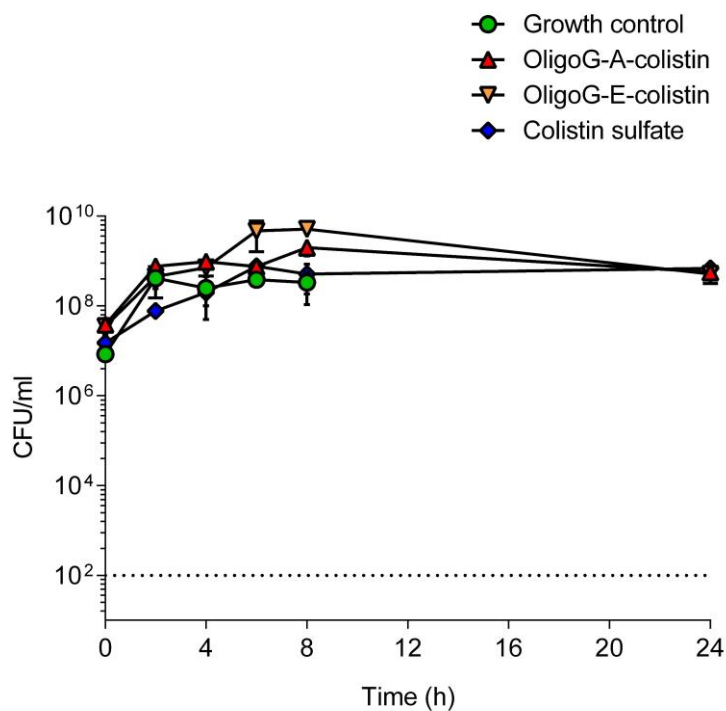


**Figure 5.6** Phase 3: Effect of antibiotic treatments (at 1 x MIC) on the cell viability of *A. baumannii* 7789 in a TTK model using (a) 2,000 g/mol and (b) 10,000 g/mol MWCO dialysis cassettes. Data represents mean bacterial colony count  $\pm$  SD ( $n = 3$ ). The lower limit of detection ( $10^2$  CFU/ml) is represented by the dotted line.

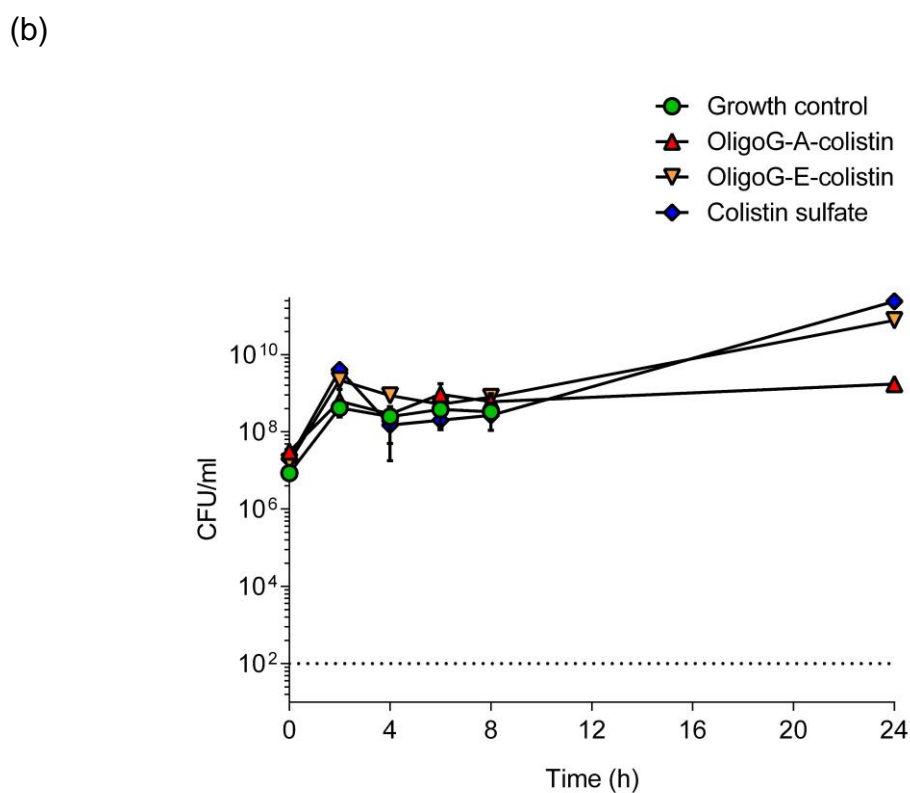
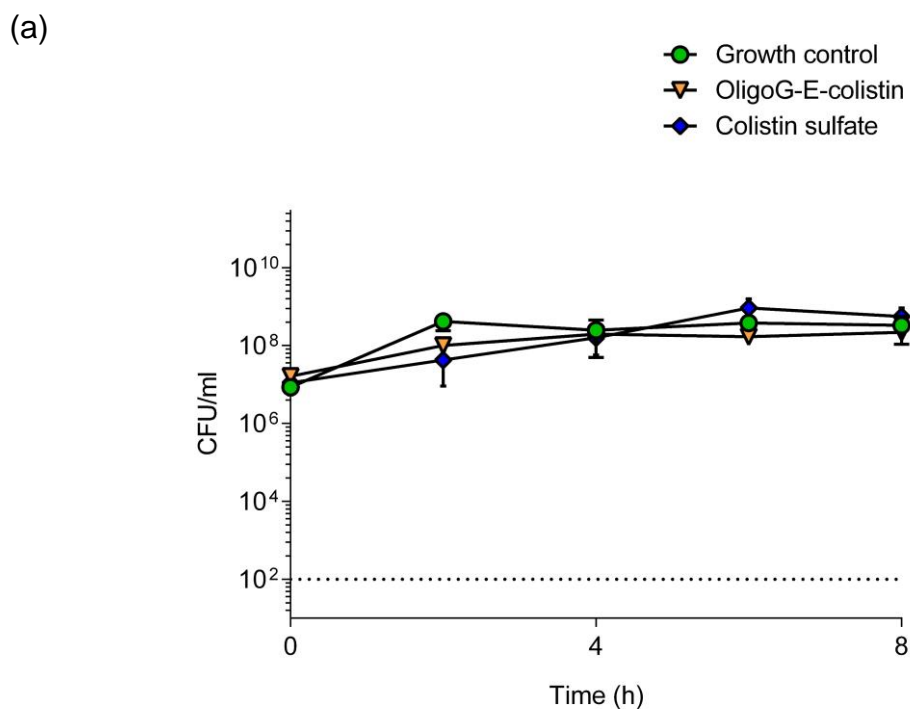


**Figure 5.7** Phase 3: Effect of antibiotic treatments (at 2 x MIC) on the cell viability of *A. baumannii* 7789 in a TTK model using (a) 2,000 g/mol and (b) 10,000 g/mol MWCO dialysis cassettes. Data represents mean bacterial colony count  $\pm$  SD ( $n = 3$ ). The lower limit of detection ( $10^2$  CFU/ml) is represented by the dotted line.

was tested using dialysis cassettes with a MWCO of up to 20,000 g/mol, no difference in bacterial viability counts was observed (**Figure 5.8**). Interestingly, no viable bacterial colonies were detected over 24 h when colistin sulfate was tested at 16 x MIC using the 10,000 MWCO cassette, proving that the model was effective when the antibiotic concentration used was sufficiently high (**Figure 5.8**).

#### **5.4.2 Characterisation of the two-compartment PK-PD model using dialysis tubing**

*Phase 1:* As observed in previous experiments, an increase in the concentration of colistin in the OC was mirrored by a decrease in its concentration in the IC and this was also true of the PK-PD model using dialysis tubing described here (**Figure 5.9**). The concentration of colistin detected in the OC was significantly higher than that detected in experiments using dialysis cassettes ( $p < 0.05$ , according to unpaired t-test). In addition, using the dialysis bag model, the colistin concentration increased faster when colistin sulfate was placed in the IC, compared to the OligoG-colistin conjugates (time to reach 1 mg/ml in the OC: 2.83 h [colistin] < 10.47 h [OligoG-E-colistin] < 17.35 h [OligoG-A-colistin]).

*Phase 2:* When *A. baumannii* 7789 were added to the OC, growth in the IC and sterility of the IC was maintained for up to 48 h. Colistin sulfate, at its previously determined MIC (0.25 µg/ml) and OligoG-E-colistin conjugate at 2 x MIC (0.25 µg/ml) showed rapid bacterial killing that reached a maximum reduction in viable bacterial counts after 4 h. For both treatments, colony counts were ~5-fold lower than the control and ~2-fold lower than the initial starting bacterial concentration (**Figure 5.10**). No significant effect on bacterial growth was observed with OligoG-A-colistin conjugates, even at 2 x MIC.

### **5.5 Discussion**

An *in vitro* two-compartment PK-PD model was developed and validated to compare the diffusion and antimicrobial effectiveness of free- and OligoG-conjugated colistin. The two conjugates resulting from the different

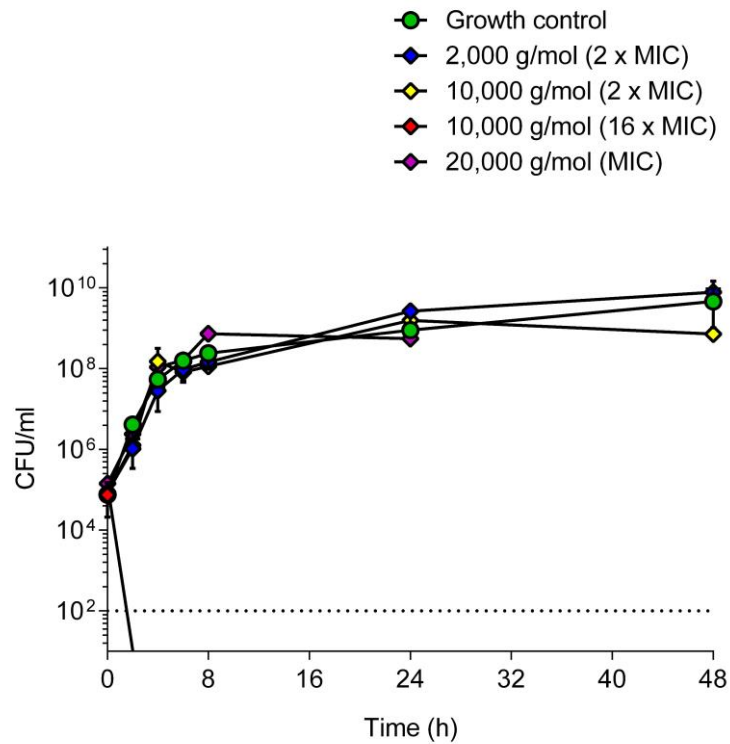
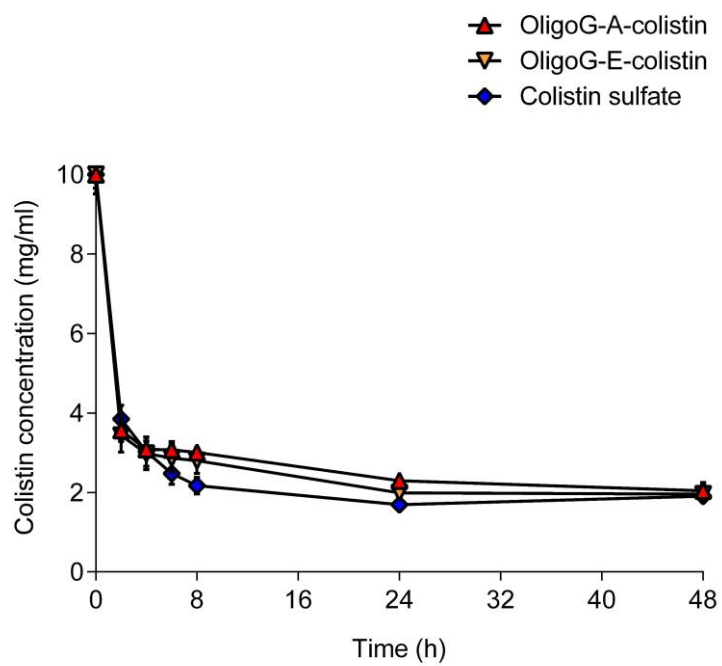


**Figure 5.8** Phase 3: Effect of colistin sulfate on the viability of *A. baumannii* 7789 in a TTK model using 2,000-20,000 g/mol MWCO dialysis cassettes. All experiments were performed using 2 x MIC or 16 x MIC, except for the 20,000 g/mol MWCO experiment, which used colistin at 1 x MIC. Data represents mean bacterial colony count  $\pm$  SD (n = 3). The lower limit of detection ( $10^2$  CFU/ml) is represented by the dotted line.

(a)



(b)

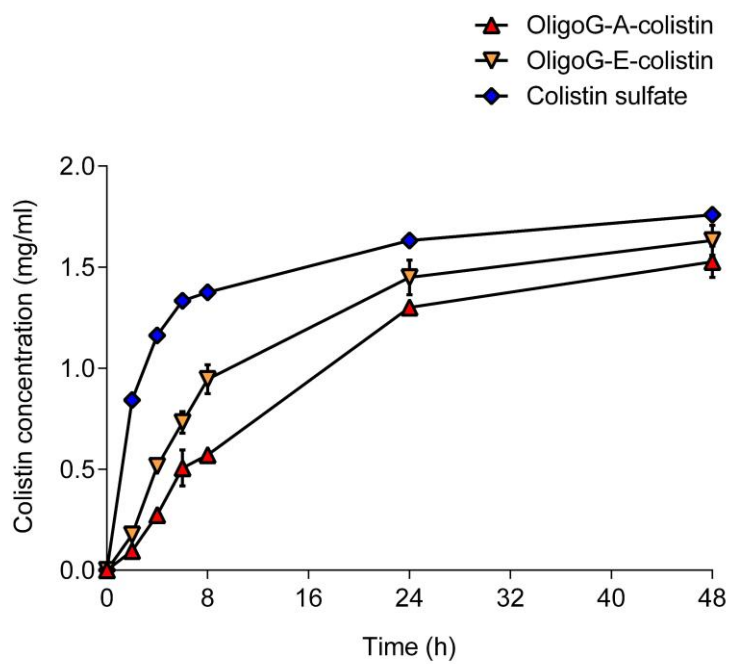


**Figure 5.9** Phase 1 method validation: Colistin concentration, measured by BCA assay, in the (a) IC and (b) OC following diffusion through dialysis tubing over 48 h. Data represents mean colistin concentration  $\pm$  SD ( $n = 3$ ).

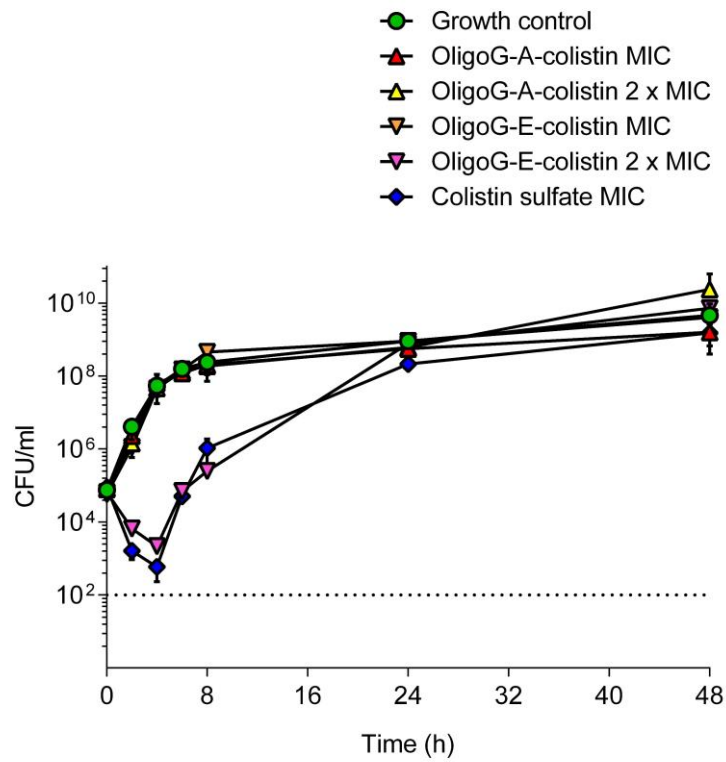


**Figure 5.10** Phase 2: Effect of antibiotic treatments on the viability of *A. baumannii* 7789 in a TTK model using dialysis tubing. Data represents mean bacterial colony count  $\pm$  SD ( $n = 3$ ). Lower limit of detection ( $10^2$  CFU/ml) is presented as dotted line.

conjugation chemistries using the reversible (ester) or irreversible (amide) linkers were analysed to determine whether complete release of colistin at the site of infection is required for full re-instatement of antibacterial activity.

Initially, dialysis cassettes were employed for studying the PK-PD profile of free- and OligoG-conjugated colistin. However, it soon became apparent that they presented specific limitations compared to the dialysis bag model. A major issue observed in these studies was potential binding of colistin to the dialysis cassette. Although the dialysis membrane used in Slide-a-lyzer cassettes is made of low binding regenerated cellulose, (which is the same material as that used in the dialysis tubing), the casing of the cassettes is made of acrylonitrile butadiene styrene (ABS) plastic. Previous studies have shown that colistin adsorbs to the surface of a wide range of plastics, which can significantly alter the accuracy of susceptibility testing, including MIC and TTK assays (Karvanen et al., 2017). The extent of colistin adherence to the surface of the plastics is highly dependent on the nature of the plastic, as well as the coating and the surface charge applied during the manufacturing processes (Albur et al., 2014). Colistin quantification in a “sham” TTK assay in the absence of bacteria performed using liquid chromatography-tandem mass spectrometry (LC-MS/MS), had previously shown substantial binding and loss of antibiotic activity in polystyrene test tubes (Karvanen et al., 2017). The addition of a surfactant, such as polysorbate 80, has been shown to counter such effects, reducing polymyxin adherence to the surface of polystyrene plates, and leading to 4-8-fold lower estimation of MIC values against *Enterobacteriaceae*, *Acinetobacter* spp. and *P. aeruginosa* pathogens (Hindler and Humphries, 2013, Sader et al., 2012). Polysorbate 80 was not used in these studies. Due to the amphiphilic structure and cationic charge of polymyxins, it is not surprising that colistin readily adheres to the negatively-charged surfaces of commonly used laboratory materials made from polystyrene or polypropylene. As expected, a reduction in the cationic charge of colistin by covalent attachment of OligoG did not improve the diffusion of the antibiotic or neither there was a difference between the ester- and amide-linked conjugates during the validation phase.

Another challenge encountered in these studies was the large quantity of sediment produced following centrifugation during the colistin extraction process, which affected not only the accuracy but also the reliability of the results from the colistin ELISA. MH broth is a complex medium containing a high concentration (17.5 g/L) of proteins and peptides, which may account for the precipitate. Quantification of polymyxins in biological fluids using conventional methods has proved to be limited due to their lack of sensitivity, weak UV absorption and the absence of intrinsic fluorescence requiring the derivatisation of the molecule (Li et al., 2001). Previous studies have established a high-performance liquid chromatography (HPLC) method, based on the formation of fluorescent derivatives of polymyxin B, colistin sulfate or CMS, for reproducible and rapid antibiotic quantification in human plasma or urine (Cao et al., 2008, Li et al., 2002, Li et al., 2001). Recently, a liquid chromatography-mass spectrometry method was developed and validated for polymyxin B quantification in MH and tryptone soya broths (Cheah et al., 2014). The accuracy and reliability of the method was not affected by the presence of high bacterial numbers of *A. baumannii*, *P. aeruginosa* or *K. pneumoniae* or by co-administration of different classes of antibiotics with polymyxin B, all factors indicative of the better applicability and higher sensitivity of this method compared to the MaxSignal® ELISA kit that was actually used here. Nevertheless, significantly less colistin was detected in the IC in the colistin sulfate experiments, compared to the OligoG-colistin conjugates, perhaps due to higher protein binding in the MH broth. Also, the concentration of colistin detected in the IC from OligoG-E-colistin was markedly higher than with OligoG-A-colistin, presumably due to colistin release by hydrolysis of the ester bond.

Non-specific binding to the dialysis cassette housing, as well as the low MIC values (< 0.25 µg/ml) of colistin and both of the conjugates, might explain the lack of activity observed in the TTK assays against *A. baumannii* 7789. In addition, premature degradation of colistin sulfate or OligoG-colistin conjugates, as well as the decreased surface area to volume ratio due to sampling, might further have caused a significant loss of activity of free- and OligoG-conjugated colistin. Even though the dialysis cassettes offered a

simple and fast method for a PK-PD characterisation of OligoG-colistin conjugates, these studies have proved the lack of feasibility of the model for microbiological use.

Several technical aspects such as the volume, time, MWCO of the dialysis membrane, temperature and agitation rate were considered for reproducible and reliable PK-PD model development. For instance, the volume ratio of 1:4 between the inner and outer compartments created a concentration gradient for passive diffusion and maximised the surface area/volume ratio (White, 2001). An incubation time of 48 h was chosen for determination of viable bacterial counts to allow sufficient time to observe whether the OligoG-colistin conjugates exhibited the prolonged efficacy and controlled release of colistin that was previously observed with dextrin-colistin conjugates (Azzopardi et al., 2015). A dialysis membrane with a MWCO of 10,000 g/mol was chosen to allow efficient diffusion of colistin between compartments, but that was also able to restrict the transfer of bacteria to the IC (Nielsen and Friberg, 2013). Bacterial infections are commonly characterised by disrupted “leaky” vasculature at sites of infection which occur due to large gaps between the endothelial cell junctions that vary from 20 to 200 kDa (Markovsky et al., 2012). Thus, the 10 kDa MWCO dialysis membrane provided a clinically-relevant pore size that would model a key aspect of infected tissues. Many different types of the dialysis membranes (artificial and natural) have been used in the development of the PK-PD models (Gloede et al., 2010), but due to better chemical compatibility, heat stability, hydrophilicity and high purity, Spectra/Por® 7 regenerated cellulose membrane was selected to prevent loss and non-specific binding of the antibiotic (Li et al., 2003b). A temperature of 37°C and agitation rate of 70 rpm was selected to ensure homogenous mixing and optimum bacterial growth, while preventing bacterial attachment and blockage of the membrane (Azzopardi et al., 2015, Schwartz et al., 2008).

As expected, due to its lower molecular weight, diffusion of colistin was considerably faster than that of either of the OligoG conjugates and was mirrored by an increase in drug concentration in the OC over 48 h. Also, the diffusion of colistin when OligoG-E-colistin conjugate was contained in the IC

was more pronounced than that of the amide linked conjugate, presumably due to the lability of the ester bond. The suitability of the dialysis bag model for characterisation of the TTK profile of OligoG-colistin conjugates and colistin sulfate was confirmed by the growth control of *A. baumannii* 7789 over the time-course of the experiment, reaching the stationary growth phase between  $10^8$ - $10^9$  CFU/ml. The TTK curves demonstrated rapid and substantial bacterial killing in the presence of colistin sulfate at its MIC (0.25 µg/ml) and the OligoG-E-colistin conjugate at 2 x MIC (0.25 µg/ml), although marked bacterial regrowth was observed at 24 h. Previous TTK studies demonstrated heteroresistance of *A. baumannii* clinical isolates to colistin that contributed to significant bacterial regrowth at 24 h at 32 x MIC (Li et al., 2006) and 64 x MIC (Owen et al., 2007). In these studies, the maximum efficacy of colistin sulfate and OligoG-E-colistin conjugate was achieved at 4 h, however, since the viable bacterial counts were reduced by  $< 3 \log_{10}$  CFU/ml compared to the initial inoculum, this was indicative of bacteriostatic activity only. Similarly, previous TTK studies have also demonstrated the bacteriostatic activity of colistin at its MIC in *A. baumannii* clinical isolates, showing a 2-fold decrease in CFU/ml 4-6 h post-dose (Tan et al., 2007). Colistin only becomes bactericidal at higher drug concentrations (Owen et al., 2007), for instance, significant bactericidal activity was observed when carbapenem-resistant *A. baumannii* isolates were treated with colistin at  $\geq 4$  x MIC (Song et al., 2007). These observations support the clinical limitations of conventional colistin dosing due to concentration-dependent nephrotoxicity, which may limit the amount of drug that can safely be administered.

The findings of this study suggest that the OligoG-E-colistin conjugate may be more suitable clinically as it exhibited equivalent antimicrobial activity to colistin at 0.25 µg/ml, but with significantly lower cytotoxicity in human kidney cells (Chapter 3). After systemic administration of CMS, plasma colistin concentration at steady-state is typically between 0.5 to 4 µg/ml (Garonzik et al., 2011, Nation et al., 2016). As nephrotoxicity is the clinically limiting factor in colistin dosing, a plasma concentration of 2 µg/ml has been recommended as a target for bacterial pathogens with MIC values  $\leq 1$  µg/ml (Landersdorfer and Nation, 2015). Similarly, a plasma concentration threshold of 2.42 µg/ml

has been defined to avoid acute kidney injury (Horcajada et al., 2016, Sorlí et al., 2013). Meanwhile, the clinical susceptibility breakpoint for *Acinetobacter* spp. against colistin is 2 µg/ml (CLSI, 2018, EUCAST, 2018), which suggests a very narrow therapeutic index *in vivo*. Since the OligoG-E-colistin conjugates are expected to accumulate to higher concentrations within infected tissues due to the EPR effect, higher bactericidal concentrations (> 0.25 µg/ml, equivalent to > 2 x MIC) could theoretically be achieved more readily than the conventional antibiotic. Moreover, prolonged antimicrobial activity of the conjugate, as well as reduced cytotoxicity and emergence of resistance support the suitability of OligoG-conjugated antibiotics for therapeutic use.

Using a similar two-compartment PK-PD model, sustained release of colistin over 48 h as well as a concentration-dependant effect was also reported for dextrin-colistin conjugates (Azzopardi et al., 2015). As the dextrin-colistin conjugate contained an amide bond, 'unmasking' of colistin relied on  $\alpha$ -amylase-mediated degradation of dextrin. The  $\alpha$ -amylase triggered activation of dextrin-EGF conjugate has also been shown to cause controlled release of growth factor in chronic wound fluid over 48 h (Hardwicke et al., 2010). Since alginate lyase is only secreted by specific bacteria and was not added to this PK-PD model, this might explain the lack of antimicrobial efficacy observed with the OligoG-A-colistin conjugate. These findings suggest that 'unmasking' or release of colistin is required for, and indeed a pre-requisite for, reinstatement of antibiotic activity. Nevertheless, alginate lyase, isolated from cystic fibrosis patients infected with *K. pneumoniae* and *P. aeruginosa*, was able to degrade alginate (Simpson et al., 1993), suggesting that locally-triggered degradation of OligoG at sites of bacterial infection could readily release colistin from the conjugate at the target site. While these findings confirm the potential suitability of these conjugates for therapeutic utility, they also demonstrate that colistin release from amide-linked conjugates relies on passive targeting to sites of infection by the EPR effect and the existence of alginate lyase-producing bacteria in these infected tissues. What is more, the OligoG-A-colistin conjugate might also exhibit reduced activity due to remaining sugar residues attached to the antibiotic, which would not be present on colistin released from the ester-linked conjugates.

## 5.6 Conclusions

The two-compartment PK-PD dialysis bag system has been developed and validated, showing the compatibility and reproducibility of the model to characterise OligoG-colistin conjugates in respect of *in vitro* drug release and antimicrobial activity. Although no significant activity was observed with OligoG-A-colistin conjugates, up to 2 x MIC, a substantial reduction in viable *A. baumannii* 7789 was observed in the presence of OligoG-E-colistin at 2 x MIC (0.25 µg/ml). Furthermore, whilst OligoG-E-colistin exhibited equivalent antimicrobial efficacy to conventional colistin, conjugates have the added advantage of reduced nephrotoxicity. Passive targeting and accumulation of OligoG-colistin conjugates at sites of infection, followed by release of the antibiotic would maximise therapeutic effectiveness and minimise systemic side effects. Due to its intrinsic antimicrobial activity, Chapter 6 aimed to investigate the diffusion, distribution and efficacy of OligoG in bacterial biofilms.

# **Chapter 6**

## **Diffusion Modelling and Antimicrobial Activity of OligoG in Bacterial Biofilms**

## 6.1 Introduction

According to the Centers for Disease Control and Prevention, more than 65% of human bacterial infections are associated with biofilm formation (Potera, 1999). Chronic respiratory diseases are commonly characterised by colonisation of opportunistic pathogens such as *P. aeruginosa*, which further contributes to inflammation and severity of the disease and eventually, accelerates the decline in pulmonary function (Bhagirath et al., 2016). Since OligoG exhibits intrinsic antibacterial activity, this chapter aimed to develop a diffusion model to investigate the ability of OligoG to alter biofilm structure and architecture. Initial experiments examined biofilm formation of a cystic fibrosis isolate *P. aeruginosa* NH57388A using a Transwell model.

Secretion of extracellular polymeric substance (EPS) by bacterial pathogens such as *E. coli* facilitates, not only the adhesion of bacteria to solid surfaces, but also plays an important role in biofilm development and maturation (Tsuneda et al., 2003). In additional experiments, confocal microscopy was employed to visualise the localisation, antimicrobial activity and interaction of the alginate oligomers with EPS using fluorescently-labelled OligoG in *E. coli* IR57 biofilms.

### 6.1.1 Extracellular polymeric substance (EPS)

Genotypic adaptations in bacteria that result in transition from acute to chronic infection are associated with phenotypic alterations in a number of factors, including biofilm formation, EPS production, antibiotic resistance, quorum sensing, virulence factors production, hypermutability and formation of small colony variants (Cullen and McClean, 2015). The EPS is a complex, highly heterogeneous biopolymer whose secretion is initiated by bacteria during the attachment stage of biofilm formation and continues throughout maturation of the biofilm (Vu et al., 2009). Water accounts for up to 97% of the composition of EPS and plays a major role in nutrient distribution within the biofilm matrix (Sutherland, 2001b). The remaining constituents of EPS, such as proteins, polysaccharides, glycolipids and nucleic acids, provide structural stability and rigidity for the biofilm. The proportion of bacterial cells in a biofilm typically

varies from 5% to 35% while the remaining 65% to 95% of the volume constitutes the EPS matrix (Jamal et al., 2018). The chemical composition of EPS in Gram-negative bacteria is composed of various functional groups such as amino, phosphate or carboxyl, which contribute to the neutral or polyanionic nature of the matrix (Tsuneda et al., 2003). In addition, the abundance of ketal-linked pyruvates and uronic acids such as D-glucuronic, D-galacturonic or mannuronic acid in EPS further enhances the negative charge of the structure (Vu et al., 2009). EPS chelates divalent cations such as calcium and magnesium and facilitates cross-linking in the biofilm (Aslam et al., 2008). Conversely, the EPS in Gram-positive bacteria such as *Staphylococci* is mostly cationic in nature (Donlan, 2002). Importantly, EPS acts as a protective barrier against antimicrobial agents, environmental stress and the host immune response, and also promotes the sorption of organic compounds or inorganic ions, facilitates the exchange of genetic information within the biofilm and provides a source of carbon, nitrogen and phosphorus for energy (Flemming, 2016, Flemming et al., 2016).

Previous studies have shown the ability of OligoG to bind to the cell surface of Gram-negative bacteria (Powell et al., 2014) and facilitate the disruption of mucoid *P. aeruginosa* NH57388A biofilms EPS matrix (Powell et al., 2018). Therefore, it was interesting in these studies to establish whether OligoG can also interact with the EPS component and thus, initiate the disruption of other Gram-negative biofilms such as *E. coli*.

### **6.1.2 Selection of fluorescent probes**

Fluorescent labelling has been used extensively to analyse real-time bacterial responses to antimicrobial agents and to monitor actual localisation of these antibiotics within biofilms (Stone et al., 2018). Previously, intrinsically fluorescent antibiotics such as tetracyclines or fluoroquinolones were employed to study the movement of drugs across the bacterial membrane and determine their intracellular accumulation (Du Buy et al., 1964, Kaščáková et al., 2012). However, for antibiotics with no intrinsic fluorescence, the covalent coupling of a fluorophore to the antimicrobial agent is required. Selection of

an appropriate fluorescent probe is essential to ensure successful visualisation of OligoG within the bacterial biofilm. Several important characteristics such as initial brightness, photostability, molecular weight, availability of functional groups and hydrophilicity of the fluorescent probe need to be considered. Ideally, conjugation of a fluorophore to an antimicrobial agent should not alter its physicochemical features, conformation, cellular distribution or efficacy (Stone et al., 2018).

Previous studies have shown the propensity of hydrophobic probes to adhere to the cell surface by non-specific interactions (Zanetti-Domingues et al., 2013) which could significantly modify the localisation and anti-biofilm effectiveness of the antimicrobial to which they are coupled. Therefore, in the case of OligoG, Texas Red (TxRd) and Oregon Green (OrGr) (**Table 6.1**) were chosen for conjugation as they have been extensively used to study the cellular internalisation of various polymers and therapeutic drugs (Chvatal et al., 2008, Richardson et al., 2008, Seib et al., 2007). To study the effect of polymer architecture on cellular pharmacokinetics, OrGr-labelled linear and branched polyethylenimines (PEIs) and cationic polyamidoamine (PAMAM) dendrimers were analysed in B16F10 murine melanoma cells using flow cytometry and confocal microscopy (Seib et al., 2007). The localisation and intracellular fate of OrGr-labelled dextrin, HPMA and PEG has been studied in several different cell lines (Richardson et al., 2008). Additionally, the internalisation and endocytic fate of OrGr-labelled dextrin-phospholipase A<sub>2</sub> conjugate in the breast cancer cell line, MCF-7, was also analysed using confocal microscopy and flow cytometry (Ferguson et al., 2010b).

In addition, TxRd labelling has previously been used to analyse gentamicin uptake and intracellular accumulation in *S. aureus* biofilms (Henry-Stanley et al., 2014) and *E. coli* (Cui et al., 2016). In addition, TxRd-labelled dextran was used to confirm the localisation and trafficking of highly-fluorescent nanoparticles to lysosomes in a mouse macrophage cell line (Fernando et al., 2010). Binding of TxRd-labelled lectin to specific sugar residues within the EPS structure of *Sphingomonas* biofilms has also been demonstrated (Johnsen et al., 2000).

**Table 6.1** Characteristics of Texas Red (TxRd) and Oregon Green (OrGr) fluorescent probes and their use in previous polymer-labelling studies.

Fluorescent probe properties	Texas Red	Oregon Green
Molecular weight (g/mol)	690.87	496.47
Molecular formula	C <sub>36</sub> H <sub>42</sub> N <sub>4</sub> O <sub>6</sub> S <sub>2</sub>	C <sub>26</sub> H <sub>22</sub> F <sub>2</sub> N <sub>2</sub> O <sub>6</sub>
Reactive group	Primary amine	Primary amine
Solubility	DMSO or DMF	DMF
Molar extinction coefficient (cm <sup>-1</sup> M <sup>-1</sup> )	90,000	75,000
Excitation/emission (nm)	596/615	485/520
Fluorescent quenching	Minimal concentration- and pH-dependent fluorescent quenching	Minimal concentration- and pH-dependent fluorescent quenching
Previous studies using labelled polymers	Alginate (Powell et al., 2018), pentosan polysulphate (Anees, 1996), poly(methyl methacrylate) (Roth et al., 2009), dextran (Lin et al., 2017, Lou et al., 2016), poly(tert-butyl acrylate)-block-poly[(2-hydroxyethyl methacrylate)-random-(succinyloxyethyl meth acrylate) (Li et al., 2002)	Dextrin, PEG, HPMA (Richardson et al., 2008, Barz et al., 2010a), poly(β-amino ester) (Bechler and Lynn, 2011), PGA (Eldar-Boock et al., 2011), PEIs, PAMAM dendrimers (Morris et al., 2017, Seib et al., 2007), p(HPMA)-b-poly(L-lactide) copolymers (Barz et al., 2010b)

DMF, N,N-dimethylformamide.

To investigate localisation of the fluorescently-labelled OligoG within the biofilm structure, it was important for selected probes to display both minimal concentration- and pH-dependence of fluorescent output, which otherwise, could trigger fluorescent quenching of the probe. Previous studies have shown a less than optimal bell-shaped concentration-dependent fluorescent quenching of free- and HPMA copolymer-bound doxorubicin which on the other hand, was independent of pH 5.4-7.4 (Seib et al., 2006). In contrast, minimal concentration- and pH-dependent fluorescent quenching was reported for both OrGr-labelled linear and branched PEIs and cationic PAMAM dendrimers (Seib et al., 2007). Furthermore, a linear correlation between TxRd concentration and fluorescence yield was demonstrated which was unaffected at both pH 5 and 7 (Pritchard, 2014).

Fluorescent stains can also be used to target different, specific components of the biofilm structure including metabolic enzymes, DNA, proteins or polysaccharides to, for example, assess bacterial viability after exposure to various antimicrobial agents (Baudin et al., 2017, Palmer and Sternberg, 1999, Zhou et al., 2014). Here, to more fully elucidate the role of OligoG in biofilm disruption, SYTO-9 (green fluorescent nucleic acid stain) and Concanavalin A (ConA; red fluorescent  $\alpha$ -D-mannose and  $\alpha$ -D-glucose EPS stain) were used to evaluate the localisation and disruption of *E. coli* IR57 biofilms by TxRd-OligoG or OrGr-OligoG, respectively, using confocal laser scanning microscopy (CLSM).

## **6.2 Experimental aims and objectives**

**The specific aims of this study were:**

- To develop a Transwell diffusion model to assess the disruption of *P. aeruginosa* NH57388A biofilms after OligoG treatment.
- To synthesise and characterise TxRd- and OrGr-labelled OligoG.
- To assess the disruption of *E. coli* IR57 biofilms after exposure to OligoG.
- To study the localisation of TxRd-OligoG conjugate in *E. coli* IR57 biofilms.

- To study the interaction of OrGr-OligoG conjugate with the EPS component of *E. coli* IR57 biofilms.

### 6.3 Methods

For details of strains used in this study refer to Chapter 4 (**Table 4.1**).

#### 6.3.1. Development of a Transwell diffusion model

A Transwell model system was constructed to measure the diffusion of rhodamine through a biofilm after exposure to an antimicrobial agent where greater diffusion of the fluorescent probe corresponded to greater disruption of the biofilm. The model used 6.5 mm Transwell inserts, where the upper (donor) and lower (acceptor) compartments (wells) were separated by a microporous membrane (0.4  $\mu\text{m}$  pore size) as shown in **Figure 6.1**.

##### 6.3.1.1 Validation of the Transwell diffusion model

To begin with, the feasibility of using the Transwell model for biofilm disruption studies was analysed. Overnight bacterial cultures (Section 2.6.4.3) of *P. aeruginosa* NH57388A were adjusted to  $1 \times 10^8$ ,  $1 \times 10^6$ ,  $1 \times 10^4$  and  $1 \times 10^2$  CFU/ml in MH broth and added to the upper donor well (100  $\mu\text{l}$  per well). After incubating the plate at room temperature for 1 h, 150  $\mu\text{l}$  of MH broth was placed into the donor well and 1.1 ml into the acceptor well. The plate was wrapped in parafilm and incubated statically at 37°C for 48 h. After incubation, the Transwell inserts were moved to clean wells. The supernatant from the donor wells was removed, biofilms were then washed with 200  $\mu\text{l}$  of PBS and 1.1 ml of PBS was added to the acceptor wells. Finally, 140  $\mu\text{l}$  of rhodamine solution (30  $\mu\text{g}/\text{ml}$  in PBS; prepared from 5 mg/ml stock solution in  $\text{dH}_2\text{O}$ ) was added to the upper donor wells and the plate was incubated statically at 37°C. Samples (100  $\mu\text{l}$ ) were taken from the lower acceptor wells at various time points (1, 2, 4, 6, 24 and 48 h) and placed into a Grenier glass-bottom 96-well black plate for fluorescence reading (excitation: 534 nm, emission: 547 nm, gain 1000). After each sample was taken/removed, 100  $\mu\text{l}$  of PBS was added to the lower acceptor well. In addition to these test samples, the fluorescence

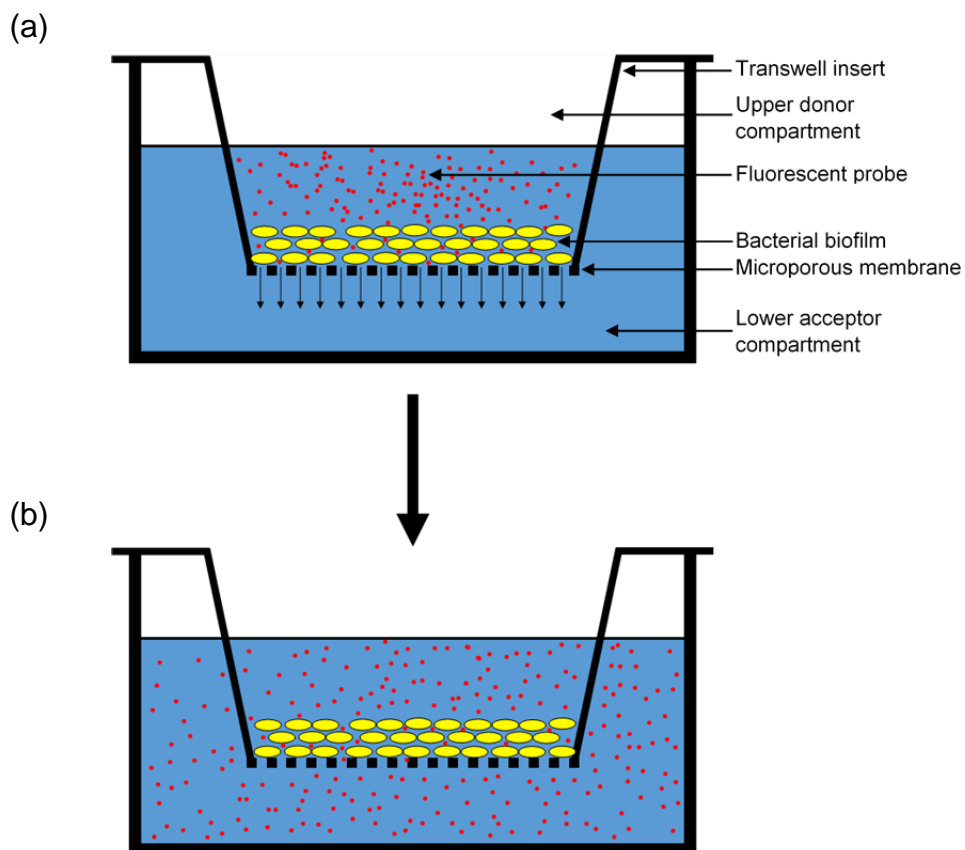


**Figure 6.1** Schematic diagram of the Transwell biofilm diffusion model, indicating (a) start (with the fluorescent probe added to the donor compartment) and (b) end (with the fluorescent probe diffused throughout the acceptor well) of the experiment.

of rhodamine at the initial concentration used in the experiment (diluted 1:10) and at 0.125-4 µg/ml (to prepare a calibration graph) were also measured. Rhodamine diffusion (%) through the biofilm was calculated using the formula below:

$$\% = \left( \frac{\text{t} \times (\text{conc. of rhodamine} \times \text{total volume}) + \text{t-1} \times (\text{conc. of rhodamine} \times \text{sampling volume})}{\text{initial conc. of rhodamine} \times \text{volume of rhodamine added}} \right) \times 100$$

where concentration of rhodamine in the samples collected at different time points was calculated from the calibration curve; the total volume in the system was 1.24 ml; sampling volume was 0.1 ml; initial concentration of rhodamine was 30 µg/ml and volume of rhodamine solution added to the upper donor well was 0.14 ml.

As a control, it was important to ensure that rhodamine diffusion through the microporous membrane (without biofilm) was not affected by the presence of OligoG or EDTA alone. For this, 1.1 ml of PBS was placed in the lower acceptor well and 140 µl of rhodamine (30 µg/ml in PBS) with and without OligoG (0.5% or 1%) or EDTA (1 mM, 50 mM or 100 mM) was added to the upper donor well. Rhodamine diffusion was again calculated as described above.

### **6.3.1.2 Transwell biofilm diffusion model using rhodamine**

The Transwell biofilm model system was set up as described in Section 6.3.1.1 using an overnight culture of *P. aeruginosa* NH57388A adjusted to  $1 \times 10^8$  CFU/ml in MH broth. After 48 h growth, 150 µl of MH broth alone or containing 1% OligoG, 1 mM, 50 mM or 100 mM EDTA was added to the upper donor well. The plate was incubated statically at 37°C for 4 h. After treatment, the supernatant was removed. Biofilms treated with EDTA were washed once, while OligoG-treated biofilms were tested with and without the washing step. After addition of the rhodamine solution, samples were collected for up to 24 h, as previously described.

### 6.3.2 Biofilm disruption assay

To study the ability of OligoG to disrupt established biofilms, overnight bacterial cultures of *E. coli* IR57 were standardised to  $10^7$  CFU/ml and 10  $\mu$ l was added to the wells of a Greiner glass-bottomed optical 96-well plate containing 90  $\mu$ l of MH broth. The plate was wrapped in parafilm and incubated for 24 h on a rocker (20 rpm) at 37°C. Subsequently, half the supernatant was removed (50  $\mu$ l) and replaced with MH broth containing OligoG (0.5%, 2% or 6%). The plate was then re-wrapped in parafilm and incubated for 4 or 24 h on a rocker (20 rpm) at 37°C. Sterility and growth controls were also included in the plate. After the treatment, the supernatant was carefully removed and biofilms were stained for 10 min with either LIVE/DEAD viability stain (as described in Chapter 4; Section 4.3.7) or ConA ( $\alpha$ -D-glucose and  $\alpha$ -D-mannose specific; red) and SYTO 9 (the nucleic acid specific LIVE component of the LIVE/DEAD viability stain; green). For the latter, 50  $\mu$ l of ConA was added per well (0.15 mg/ml in PBS) and left for 1 h. The ConA solution was subsequently removed and 5  $\mu$ l of SYTO 9 (7.5  $\mu$ M in PBS) was added and the plate incubated for a further 10 min. Finally, the biofilms were washed and 50  $\mu$ l of PBS added. CLSM was performed immediately using x63 objective magnification under oil, a resolution of 512 x 512, line averaging of 1 and a step size of 0.69  $\mu$ m. In addition, zoom factor 2 was used for EPS visualisation in *E. coli* IR57 biofilms. The excitation/emission ranges used were 485/498 nm for SYTO 9 and 632/647 nm for ConA. Experiments were performed in triplicate and 5 images per well were taken. The fluorescence intensity of the biofilm z-stack images was quantified using the image analysis software Imaris.

### 6.3.4 Fluorescent labelling of OligoG

The conjugation methods used for synthesis of the TxRd- or OrGr-OligoG conjugates are summarised in **Figure 6.2**. **Table 6.2** summarises the quantities of reactants used for each conjugation. OligoG was dissolved in 1 ml of PBS (pH 7.4) in a 10 ml round-bottomed flask. To this, EDC and sulfo-NHS were added and the mixture was stirred for 15 min. Next, 1 ml of

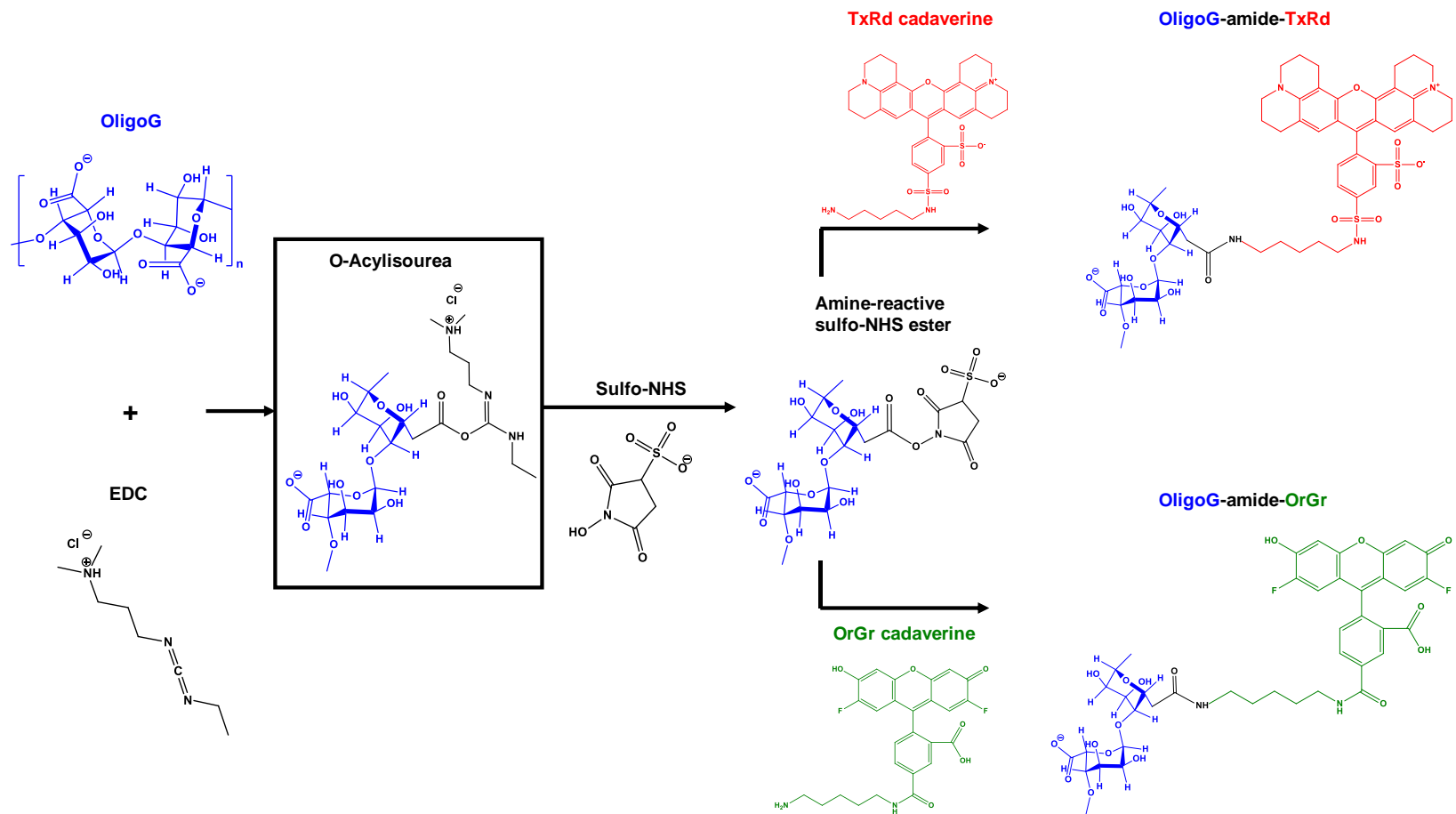


**Figure 6.2** Schematic diagram showing synthesis of the TxRd- or OrGr-OligoG conjugates.

**Table 6.2** Quantities (mg) of reactants used for TxRd-OligoG and OrGr-OligoG conjugation.

Reactant	Weight (mg) of reactant	
	TxRd-OligoG	OrGr-OligoG
OligoG	139.2	193.6
EDC (10 molar equiv.)	13.9	19.3
Sulfo-NHS (10 mol equiv.)	15.7	21.9
TxRd or OrGr cadaverine (2 mol equiv.)	5.0	5.0

Next, 1 ml of fluorescent probe solution was added (5 mg/ml; TxRd in DMSO, OrGr in PBS), followed by dropwise addition of NaOH (0.5 M) to raise the pH to 8.0. The reaction mixture was left stirring in the dark for 5 h at room temperature. Samples (5  $\mu$ l) were collected hourly, made up to 50  $\mu$ g/ml in PBS and stored at -20°C prior to analysis by size exclusion chromatography (SEC; PD-10 column). The final conjugate was purified by SEC using PD-10 desalting columns (containing Sephadex G-25 medium). Briefly, the PD-10 column was equilibrated with 25 ml dH<sub>2</sub>O before the entire reaction mixture was added and 4.5 ml (TxRd conjugate) or 5 ml (OrGr conjugate) of the eluted dH<sub>2</sub>O was collected, lyophilised and stored at -20°C. Due to the high residual content of OrGr after the initial purification, a second purification step was necessary for OligoG-OrGr (4.5 ml elution).

### 6.3.5 Characterisation of the fluorescently labelled OligoG

To monitor the reaction progress and estimate the proportion of free and bound fluorescent probe present in the conjugates, samples of crude reaction mixture and purified conjugates (prepared at 5 mg/ml in PBS) were characterised by SEC using PD-10 columns. The PD-10 desalting columns were equilibrated with 25 ml PBS prior to placing the sample onto the column. Fractions (0.5 ml) were collected in 0.5 ml microcentrifuge tubes (total 47 fractions). A sample of each fraction (100  $\mu$ l) was placed in duplicate into a black 96-well microtitre plate and fluorescence measured using a fluorescent plate reader. The excitation/emission wavelengths used were 596/615 nm for TxRd and 485/520

nm for OrGr (gain 1000). Fluorescence intensity was then plotted against retention volume (ml) and the percentage of bound TxRd or OrGr was expressed as percentage of total fluorescence measured for all fractions.

UV spectroscopy was used to quantify the total TxRd or OrGr content. Fluorescently labelled conjugates were prepared at 5 mg/ml in PBS and analysed by UV spectroscopy. TxRd or OrGr loading was determined from interpolation of the calibration curves (0.1-10 µg/ml in PBS). Specific activity (µg TxRd/OrGr per mg of TxRd-/OrGr-labelled conjugate) was calculated as follows:

$$\text{Specific activity} = \frac{\mu\text{g TxRd (or OrGr) from UV} \times \% \text{ TxRd (or OrGr) bound}}{100 \times \text{mg TxRd (or OrGr) – labelled conjugate}}$$

### **6.3.6 The effect of fluorescently labelled OligoG on biofilm disruption**

CLSM was employed to study localisation of TxRd-OligoG in *E. coli* IR57 biofilms and to study the interaction of OrGr-OligoG with the EPS components. Biofilms were prepared as previously described in Section 6.3.2. After 24 h of growth, biofilms were treated with TxRd-OligoG (0.5% and 6%) or OrGr-OligoG (4.8%) for a further 24 h by application to the surface of the biofilm. Control wells were prepared containing TxRd (0.841 µg/ml; equivalent to that contained in a 6% solution of TxRd-OligoG) or OrGr (0.123 µg/ml; equivalent to that contained in a 4.8% solution of OrGr-OligoG) alone. Subsequently, biofilms treated with TxRd-OligoG were stained with 5 µl of SYTO 9 (1.5 µl/ml in PBS) for 10 min followed by the addition of 45 µl of PBS. Biofilms treated with OrGr-OligoG were stained with 50 µl of ConA (30 µl/ml in PBS) for 1 h. Biofilms were then washed with 50 µl of PBS before adding 50 µl of PBS to each well. CLSM was performed immediately as described in Section 6.3.2. In addition, single optical section images from the bottom of the biofilm were taken for TxRd-OligoG conjugate samples using a zoom factor of 4.5, line average of 2, a resolution of 1024 x 1024 and a step size of 0.1 µm. For TxRd-OligoG, experiments were performed in triplicate (n = 3), taking 5 images per well, but only once for OrGr-OligoG, due to the low yield of the conjugate. To confirm the stability of fluorescently labelled OligoG in bacterial culture

medium, free TxRd or OrGr content in the supernatant at the end of the experiment was analysed using PD-10 columns as described in Section 6.3.5.

## 6.4 Results

### 6.4.1 Transwell biofilm diffusion assay

First, the concentration of rhodamine present in the lower acceptor well at the different time points was calculated using a rhodamine calibration curve (**Figure 6.3**). As expected, as the bacterial numbers in the inoculum decreased, rhodamine diffusion through *P. aeruginosa* NH57388A biofilms increased with time, reaching a maximum at 48 h (**Figure 6.4**). Rhodamine diffusion in the absence of biofilm was not affected by the presence of 0.5 and 1% OligoG (**Figure 6.5a**) or 1, 50 and 100 mM EDTA (**Figure 6.5b**). However, after treatment of the biofilm with 1% OligoG, rhodamine diffusion was lower over the 24 h period compared to that in the untreated control (at every time point tested), irrespective of whether a washing step was performed or not (**Figure 6.6a**). Significantly more rhodamine diffused to the lower compartment after 24 h when the biofilms were washed with PBS compared to the unwashed controls for both OligoG-treated and untreated biofilms ( $p < 0.05$ ). Addition of EDTA caused a concentration-dependent decrease in rhodamine diffusion over 24 h (**Figure 6.6b**) although at the 24 h time point, these differences were minimal.

### 6.4.2 Confocal Laser Scanning Microscopy of *E. coli* IR57 biofilm disruption studies

In the biofilm disruption assay, CLSM images of LIVE/DEAD stained *E. coli* IR57 biofilms demonstrated a well-structured, homogeneous growth in the untreated controls grown for both 24 h and 48 h. After 4 and 24 h treatment, no substantial decrease in biofilm thickness was observed with increasing OligoG concentration (0.5%-6%) (**Figure 6.7**). However, following 4 h treatment, 2% and 6% OligoG caused a significant reduction in SYTO 9 fluorescence intensity ( $p < 0.05$ ; **Figure 6.8a**). Surprisingly, following 24 h treatment, only 6% OligoG caused disruption and disorganisation of the biofilm

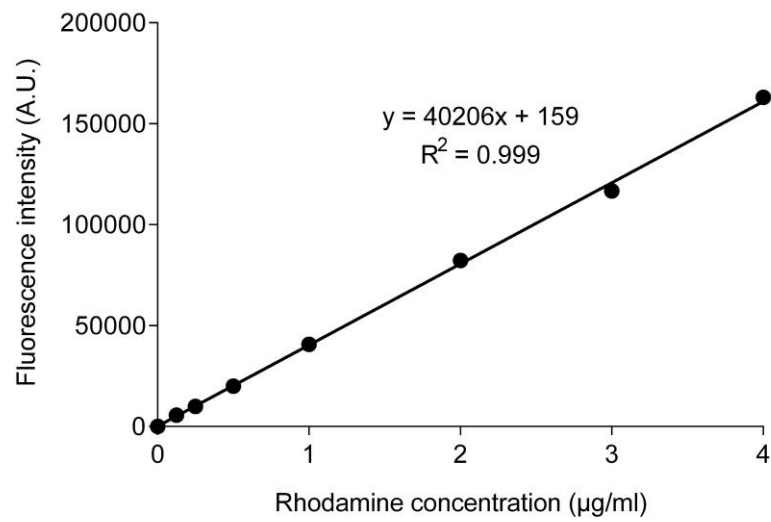


**Figure 6.3** Typical Transwell assay calibration curve for rhodamine. Data is expressed as mean  $\pm$  SD ( $n = 3$ ). Error bars are within the size of data points.

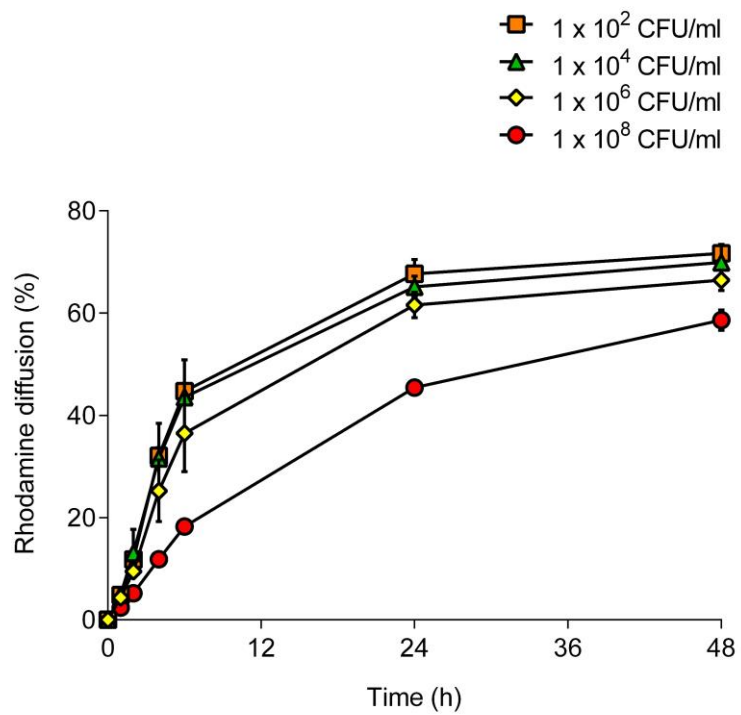
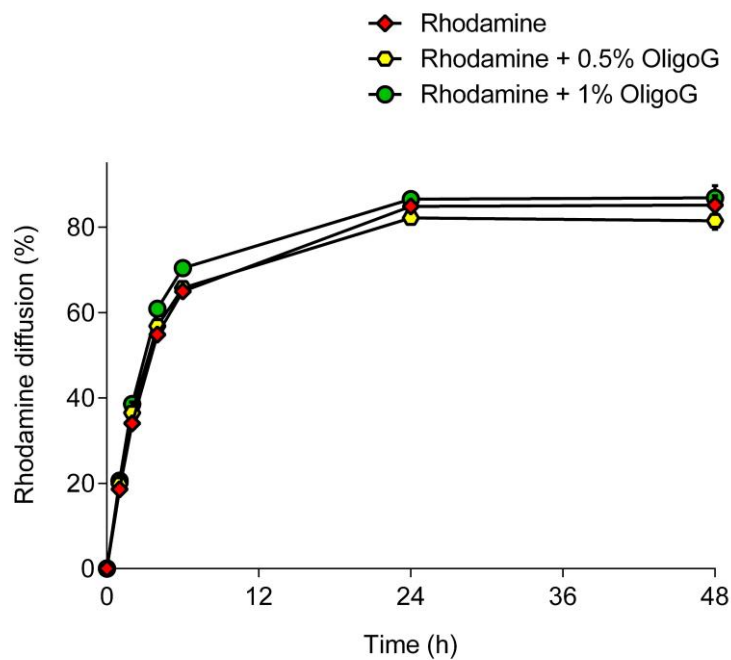


**Figure 6.4** Rhodamine diffusion through *P. aeruginosa* NH57388A biofilms grown at different seeding densities ( $1 \times 10^2$  to  $1 \times 10^8$  CFU/ml). Data represents mean rhodamine diffusion  $\pm$  SD (n = 3).

(a)



(b)

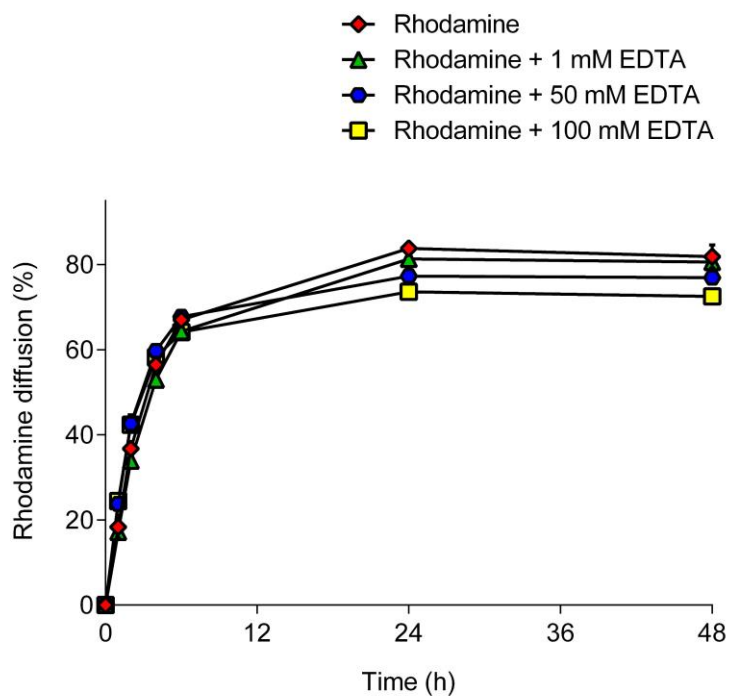
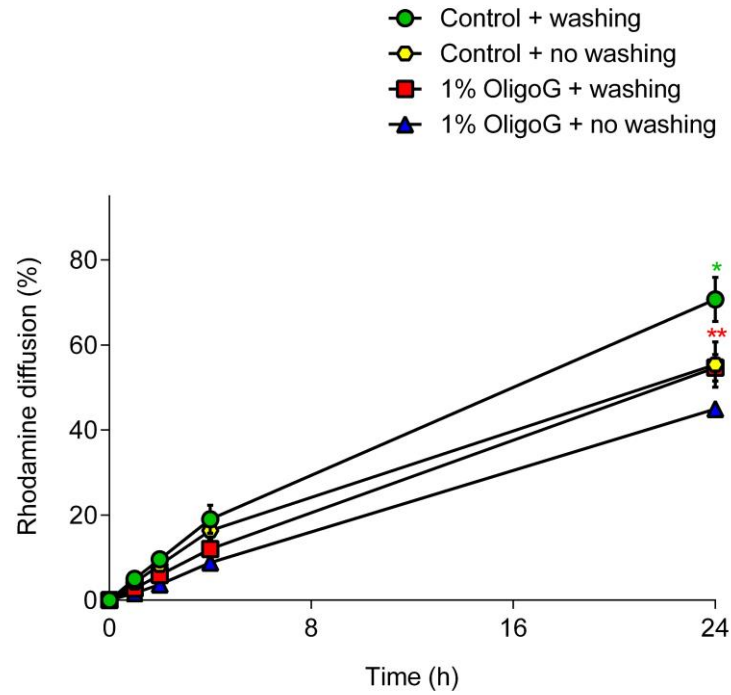


**Figure 6.5** Rhodamine diffusion through a microporous membrane in the presence of (a) OligoG (0%, 0.5% or 1%) or (b) EDTA (0 mM, 1 mM, 50 mM or 100 mM). Data represents mean Rhodamine diffusion  $\pm$  SD ( $n = 3$ ).

(a)



(b)

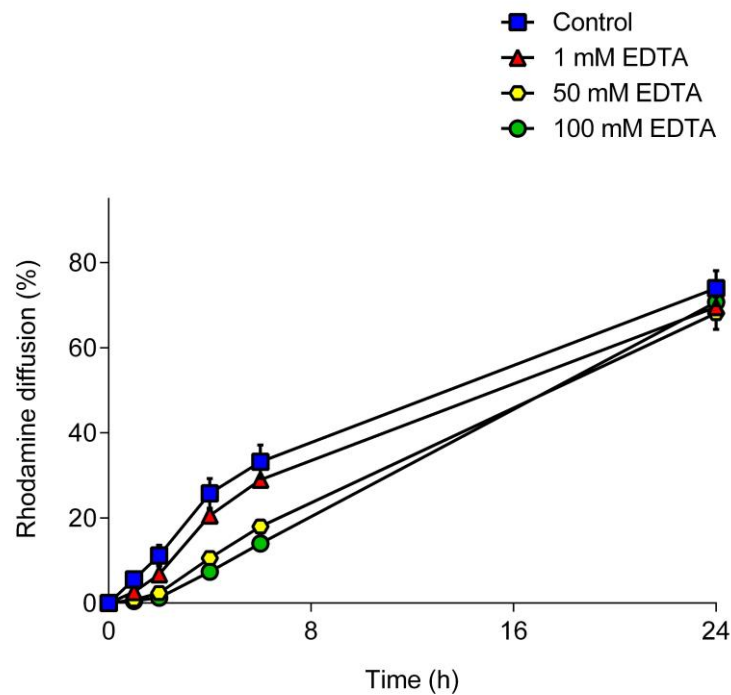


**Figure 6.6** Rhodamine diffusion through the *P. aeruginosa* NH57388A biofilms after (a) OligoG treatment with and without a washing step or (b) cell permeabiliser EDTA. Data represents mean rhodamine diffusion  $\pm$  SD ( $n = 3$ ). Significant difference is indicated by \*, where  $*p < 0.05$  and  $**p < 0.01$  compared to the equivalent unwashed control. (Unpaired t-test.).

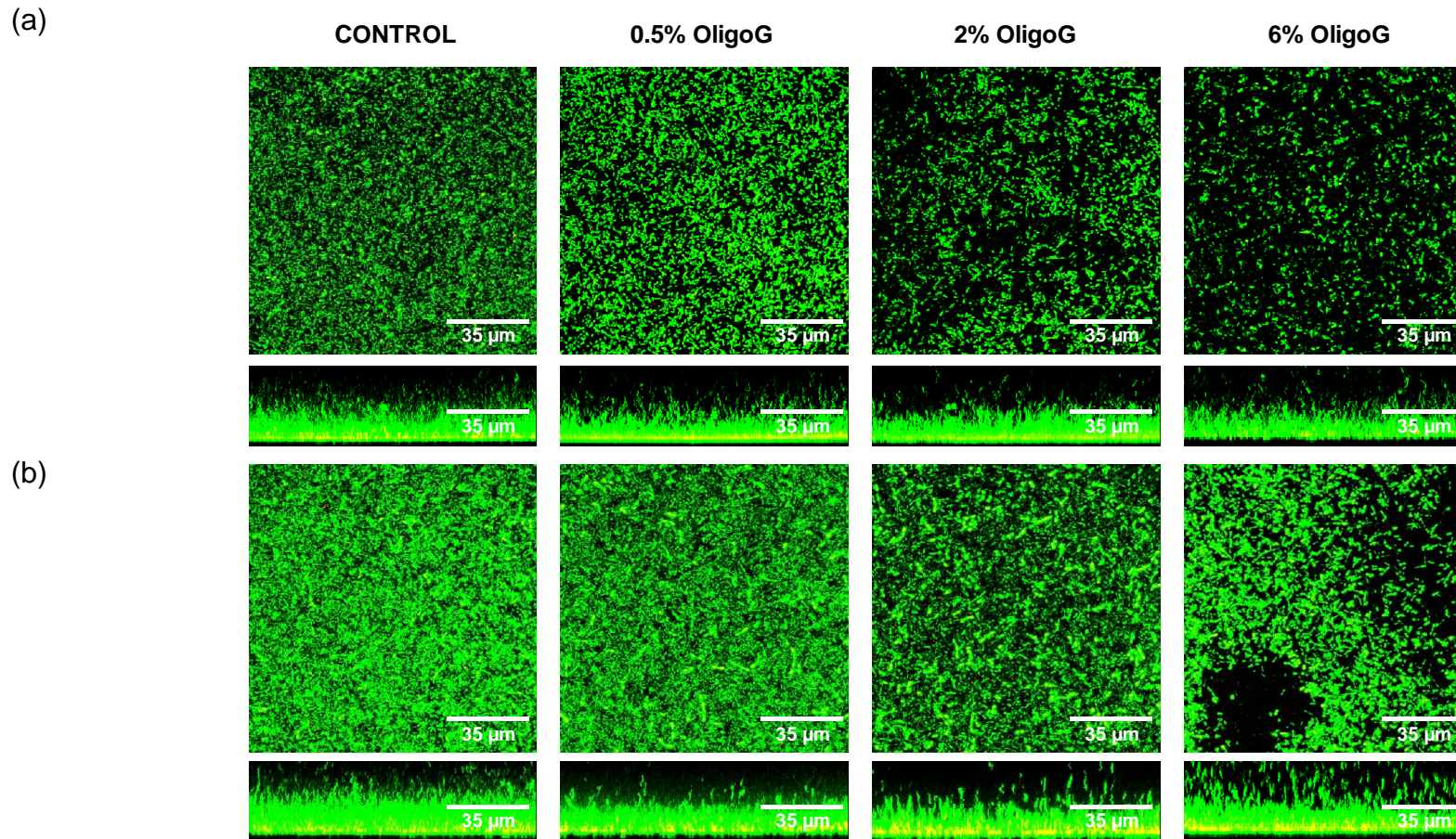
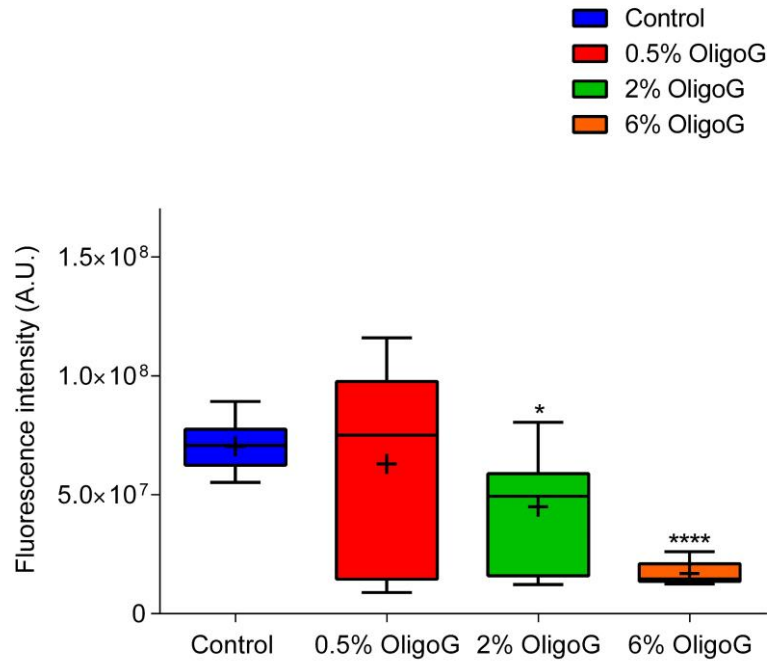


**Figure 6.7** Biofilm disruption assay showing LIVE (green)/DEAD (red) stained CLSM (aerial and cross-sectional views) of *E. coli* IR57 biofilms grown for 24 h, followed by (a) 4 h and (b) 24 h treatment with OligoG.

(a)



(b)

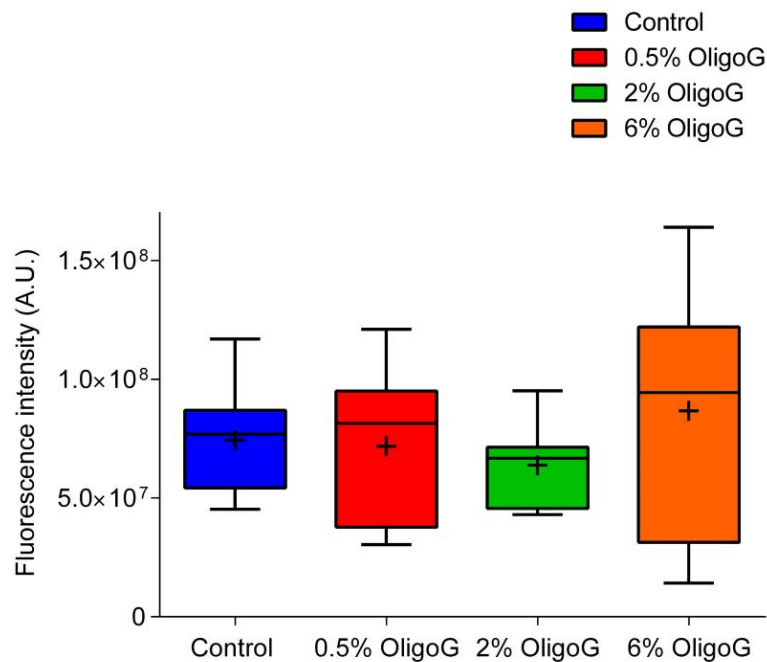


**Figure 6.8** Median fluorescence intensity and interquartile ranges obtained from CLSM imaging of the *E. coli* IR57 biofilms stained with SYTO 9 (**Figure 6.7**). Biofilms were grown for 24 h, followed by (a) 4 h and (b) 24 h treatment with OligoG. Mean fluorescence intensity is indicated by +. Significant difference is indicated by \*, where \* $p < 0.05$  and \*\*\*\* $p < 0.0001$  compared to untreated control. (One-way ANOVA and Dunnett's multiple comparisons tests).

structure, although this was rather uneven and not statistically significant ( $p > 0.05$ ; **Figure 6.8b**). Furthermore, only a few dead bacterial cells were present within the biofilm structure after OligoG treatment, indicative of bacteriostatic rather than bactericidal effects.

CLSM imaging of SYTO 9/ConA stained *E. coli* IR57 biofilms demonstrated no obvious change in EPS components (polysaccharides or nucleic acid) following 4 or 24 h OligoG treatment (**Figure 6.9**). However, a significant decrease in the fluorescence intensity of ConA (red channel only) was observed after 24 h treatment with 0.5% OligoG ( $p < 0.05$ ; **Figure 6.10b**), but not when tested at the higher concentrations (2 or 6%).

#### **6.4.3 Characterisation of TxRd or OrGr labelled OligoG**

Analysis of time versus yield of the TxRd-OligoG and OrGr-OligoG conjugates showed that the highest fluorescence output of the conjugation reaction was observed after 5 h (**Figure 6.11**). Typical elution profiles of the crude reaction mixtures and purified fluorescently-labelled OligoG can be seen in **Figure 6.12**. Typically, fluorescently labelled OligoG eluted in the void volume of the PD-10 column (1.5-4 ml) whereas free TxRd or OrGr eluted at  $> 5$  ml. Analysis of total fluorescence indicated that following the first purification step, the TxRd-OligoG conjugate had 6.9% of free TxRd and OrGr-OligoG contained 54.4% of free OrGr. After repeating the purification step for OrGr-OligoG, the free OrGr content was reduced to 11.6%. Typical calibration curves for the fluorescent probes are shown in **Figure 6.13**. The characteristics of the fluorescently-labelled OligoG synthesised are summarised in **Table 6.3**.

#### **6.4.4 *E. coli* IR57 biofilm disruption studies using fluorescently labelled OligoG**

CLSM imaging following 24 h treatment, showed that 0.5% TxRd-OligoG did not cause any disruption of the biofilm, although at 6%, TxRd-OligoG demonstrated a noticeable decrease in biofilm thickness and caused bacterial clumping (**Figure 6.14a**). CLSM images of the bottom of the biofilm confirmed the diffusion and penetration of TxRd-OligoG throughout the whole biofilm,

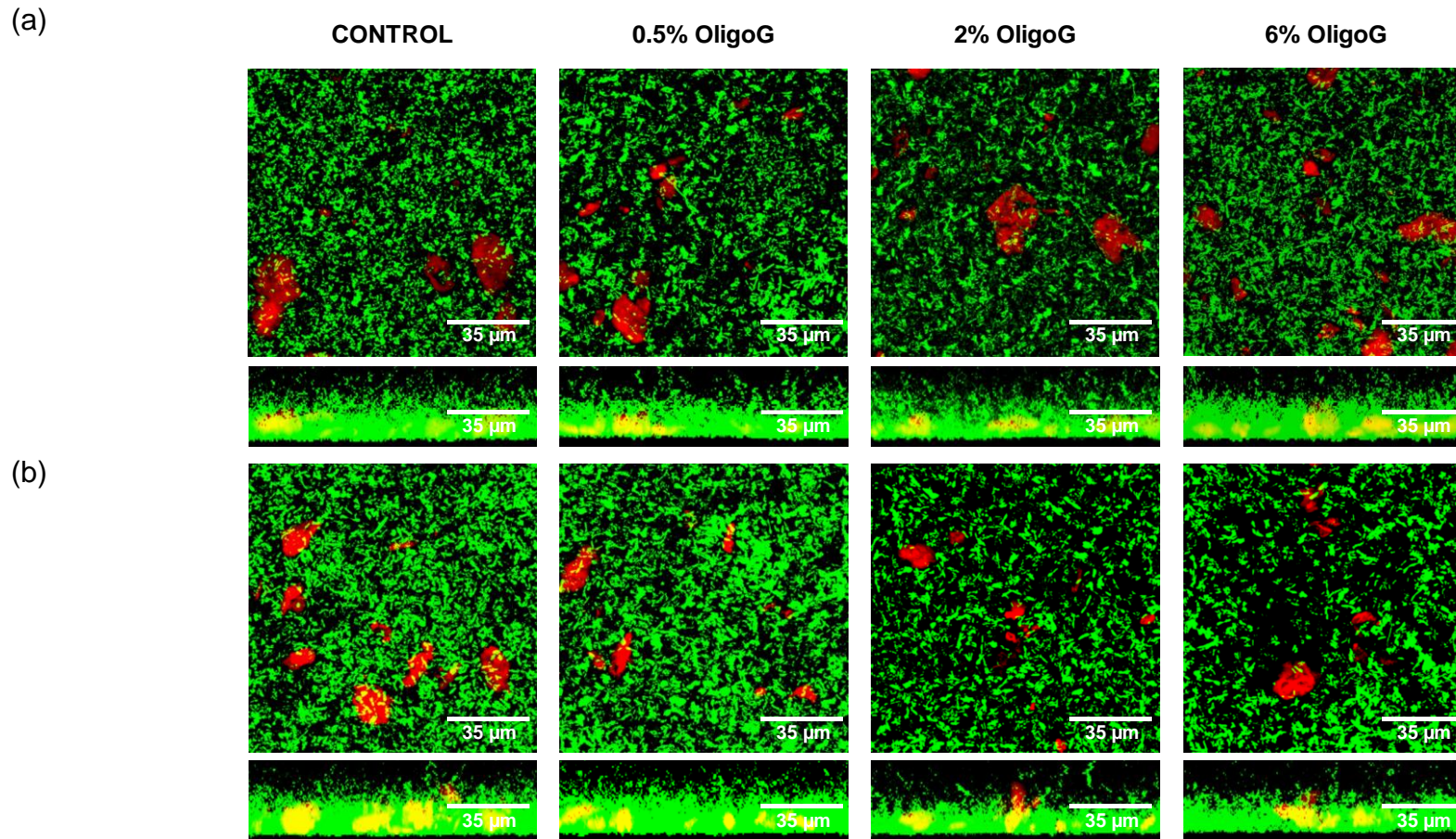
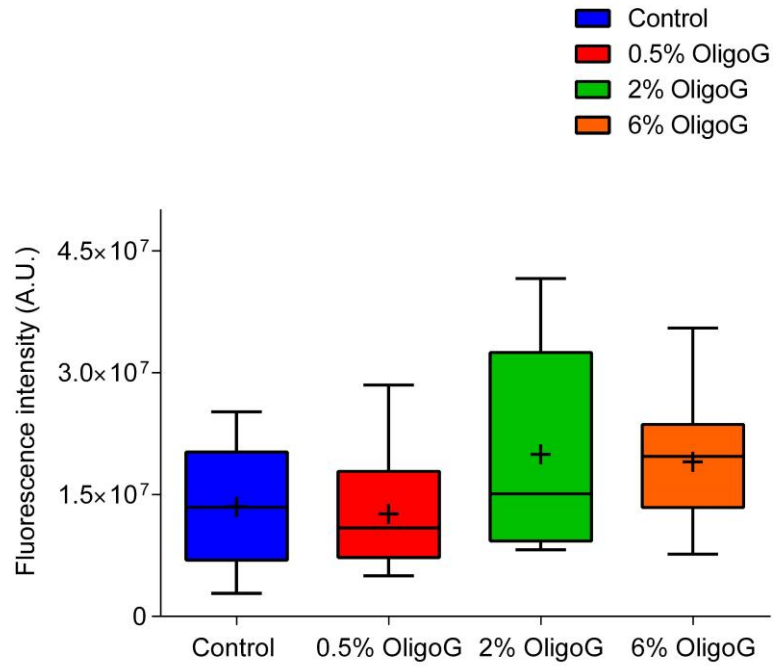


**Figure 6.9** Biofilm disruption assay showing SYTO 9 and ConA stained (nucleic acid [green] and EPS polysaccharides [red], respectively) CLSM imaging (aerial and cross-sectional views) of *E. coli* IR57 biofilms grown for 24 h, followed by (a) 4 h and (b) 24 h treatment with OligoG (zoom factor 2).

(a)



(b)

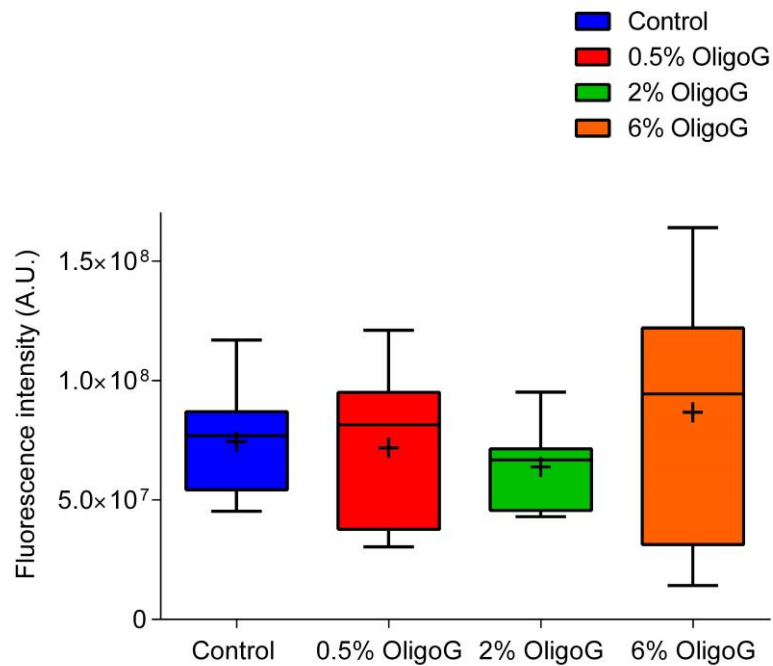


**Figure 6.10** Median fluorescence intensity and interquartile ranges obtained from CLSM imaging of the *E. coli* IR57 biofilms stained with ConA (**Figure 6.9**). Biofilms were grown for 24 h, followed by (a) 4 h and (b) 24 h treatment with OligoG. Mean fluorescence intensity is indicated by +. Significant difference is indicated by \*, where  $*p < 0.05$  compared to untreated control. (One-way ANOVA and Dunnett's multiple comparisons tests).

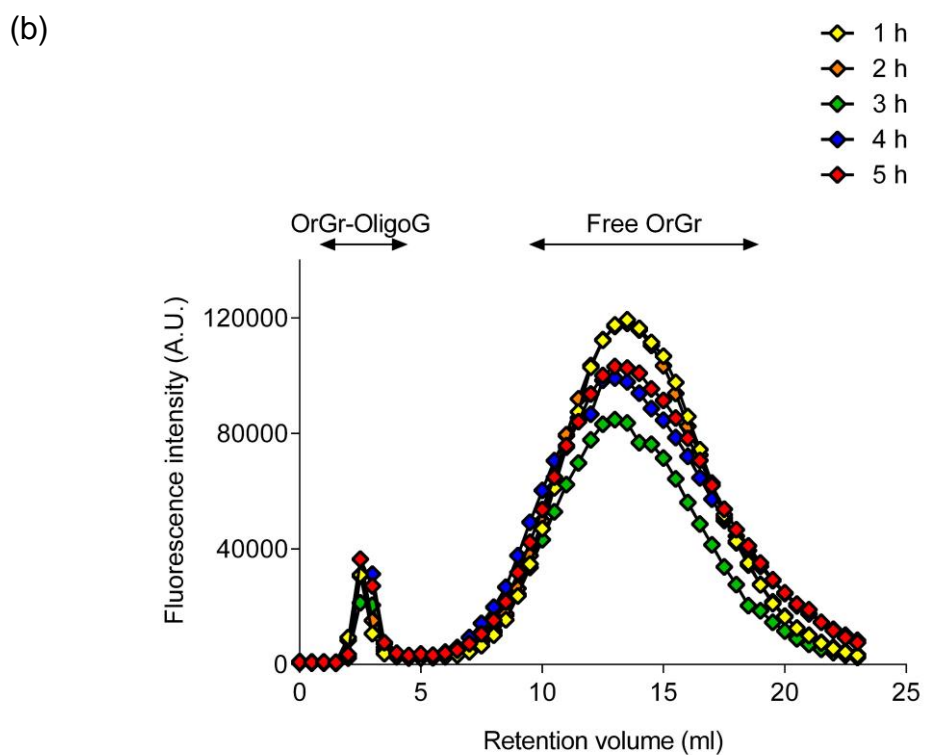
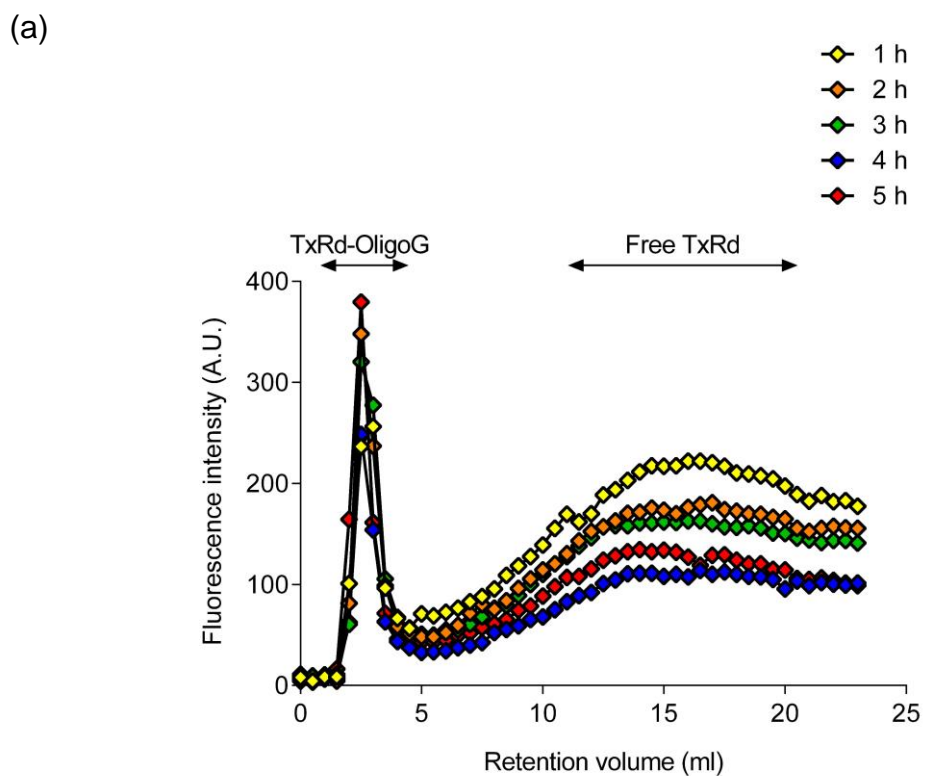


**Figure 6.11** Analysis of the reaction time on the reaction yield of (a) TxRd-OligoG and (b) OrGr-OligoG conjugates using a PD-10 column.

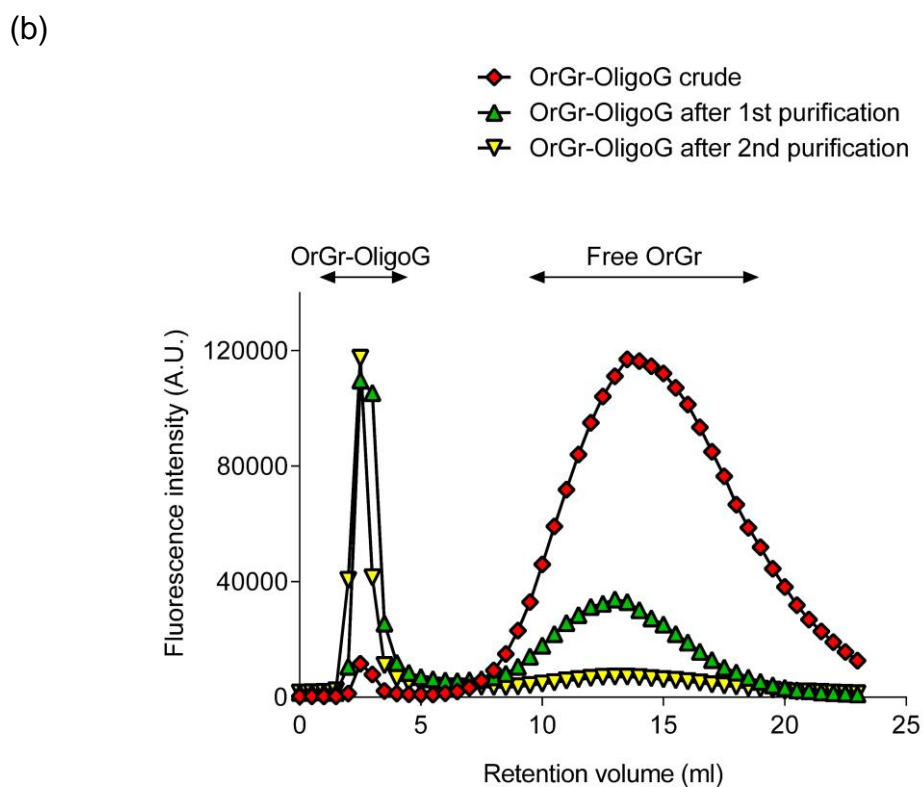
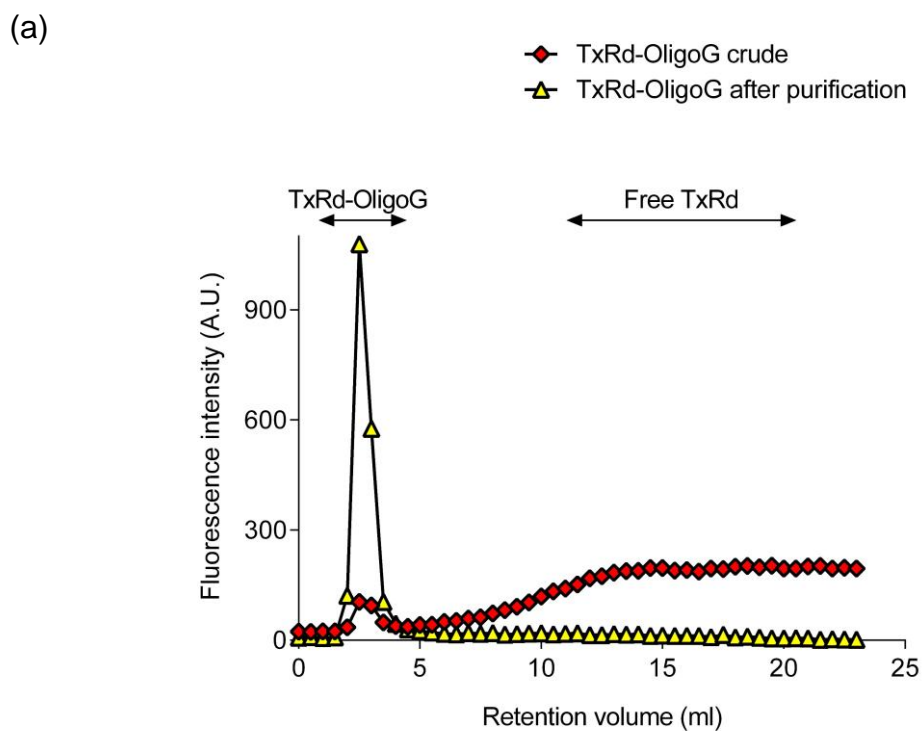
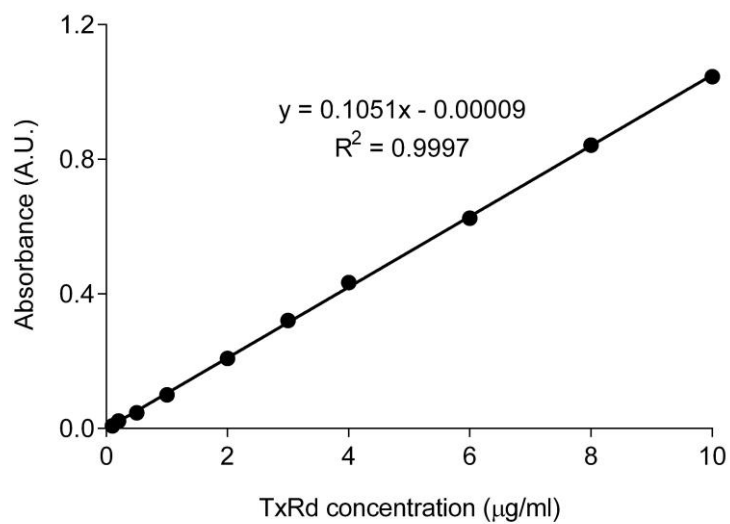


**Figure 6.12** Characterisation of the elution profile of crude and purified mixtures of (a) TxRd-OligoG and (b) OrGr-OligoG conjugates using a PD-10 column.

(a)



(b)

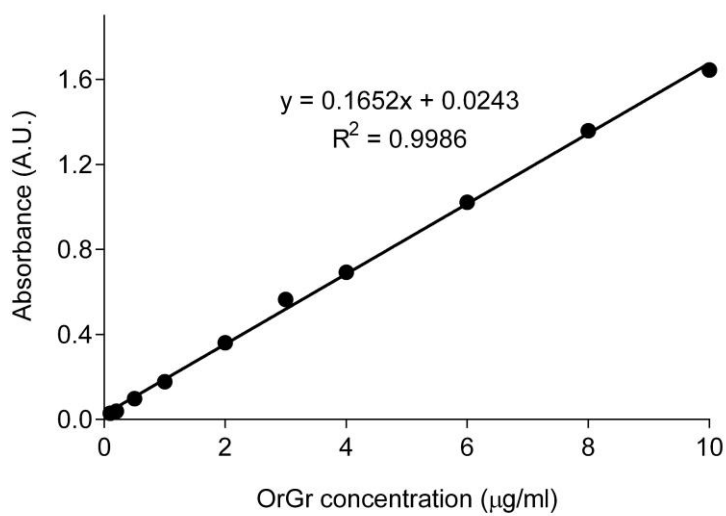


**Figure 6.13** Calibration curve for (a) TxRd cadaverine absorbance at a wavelength of 587 nm and (b) OrGr cadaverine absorbance at a wavelength of 493 nm.

**Table 6.3** Characterisation of TxRd- or OrGr-labelled OligoG.

<b>Conjugate</b>	<b>Molar ratio (TxRd or OrGr: OligoG)</b>	<b>Labelling efficiency (<math>\mu\text{g}</math> TxRd or OrGr/ mg conjugate)</b>	<b>Free TxRd or OrGr (%)</b>
TxRd-OligoG	0.01	1.39	6.9
OrGr-OligoG	0.02	2.55	11.6

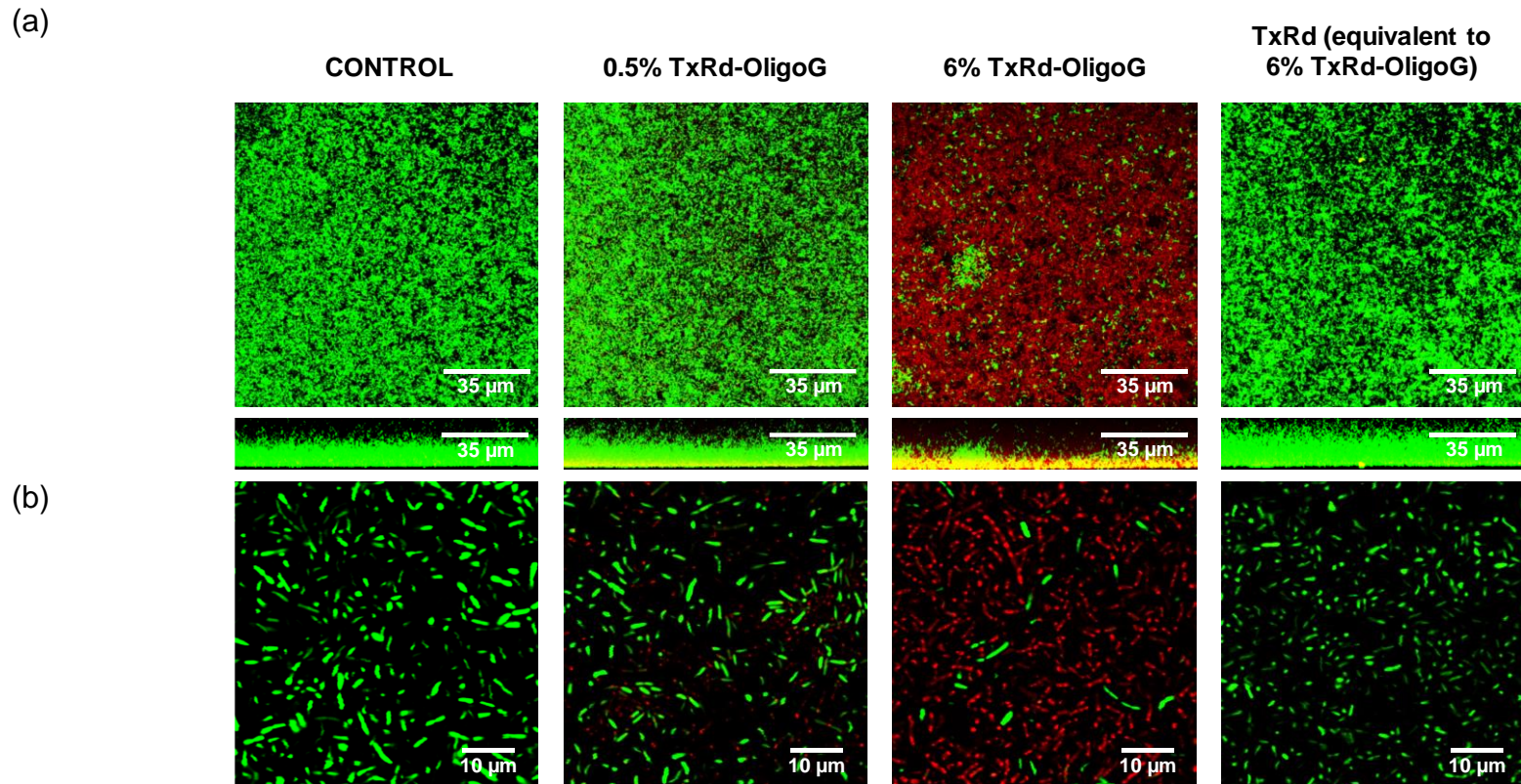


**Figure 6.14** Biofilm disruption assay showing SYTO 9 (green) stained CLSM of *E. coli* IR57 biofilms grown for 24 h, followed by 24 h treatment with TxRd-OligoG. (a) CLSM 3D imaging (aerial and cross-sectional views), (b) single optical section from the base of the biofilm (zoom factor 4.5).

even at 0.5%, although clearly there was considerably more Tx-Rd in the 6% sample (**Figure 6.14b**).

Due to the low yield of OrGr-OligoG conjugate, insufficient material was available for analysis, so only preliminary results could be obtained (n = 1). No change in the EPS component was observed following 24 h treatment with 4.8% OrGr-OligoG (**Figure 6.15**). However, it was noted that localisation of OrGr-labelled OligoG was more pronounced around the smaller clusters of EPS.

In controls, both TxRd and OrGr fluorescent probes, added at equivalent concentrations to those contained in the corresponding conjugate, lacked fluorescence intensity and were more susceptible to photobleaching. In each case, no change in biofilm or EPS structure was observed compared to the untreated control.

After incubation of biofilms with the TxRd-OligoG conjugate, analysis of the biofilm supernatants on a PD-10 column estimated low free TxRd levels of 7.2 and 7.4%, for 0.5% and 6% TxRd-OligoG, respectively (**Figure 6.16a**). In contrast, a substantial increase in free OrGr content (57.9%) was observed for biofilms incubated with OrGr-labelled OligoG (**Figure 6.16b**).

## 6.5 Discussion

In this study, the anti-biofilm efficacy and localisation of OligoG was assessed using both a Transwell diffusion assay of *P. aeruginosa* NH57388A biofilms and by CLSM imaging of fluorescently-labelled OligoG in *E. coli* IR57 biofilms.

The Transwell diffusion model has previously been employed to study the permeability of drugs and nanoparticles across the mucus barrier (Friedl et al., 2013, Lock et al., 2018), as well as the dissolution behaviour and diffusion of inhaled corticosteroids (Rohrschneider et al., 2015). Recently, a Transwell system was also used to study the diffusion of PEGylated tobramycin across the mucus network and determine its anti-biofilm activity in a *P. aeruginosa* biofilm (Bahamondez-Canas et al., 2018). Since chronic and persistent pulmonary infections, especially those colonised with mucoid *P. aeruginosa*

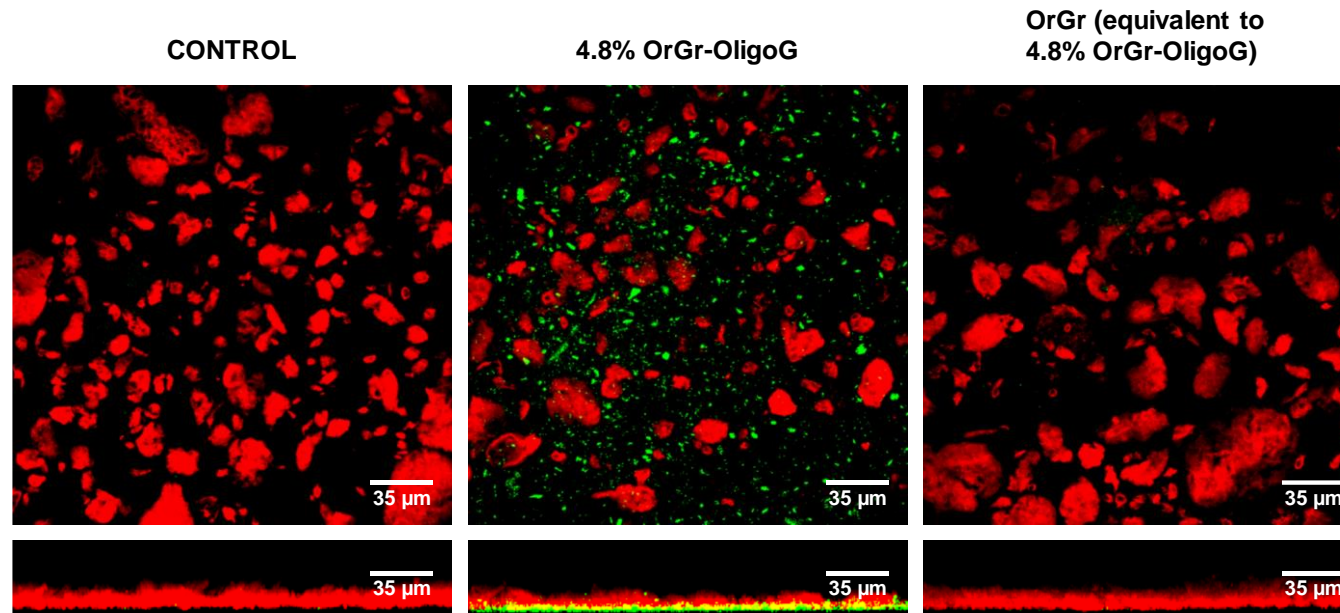
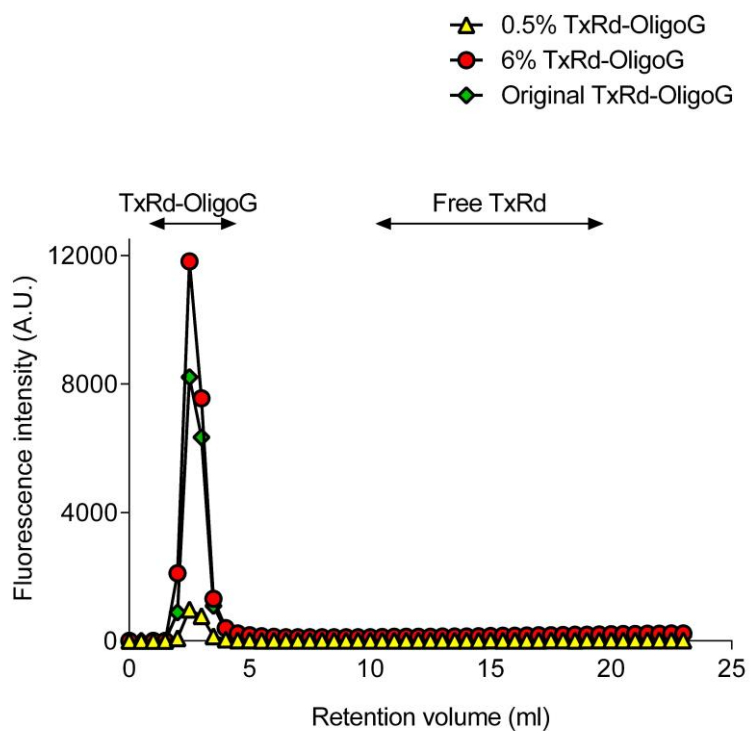


**Figure 6.15** CLSM image analysis (aerial and cross-sectional views) of *E. coli* IR57 biofilms grown for 24 h , followed by 24 h treatment with 4.8%OrGr-OligoG (green). The EPS polysaccharide component of the biofilms was stained with ConA (red).

(a)



(b)

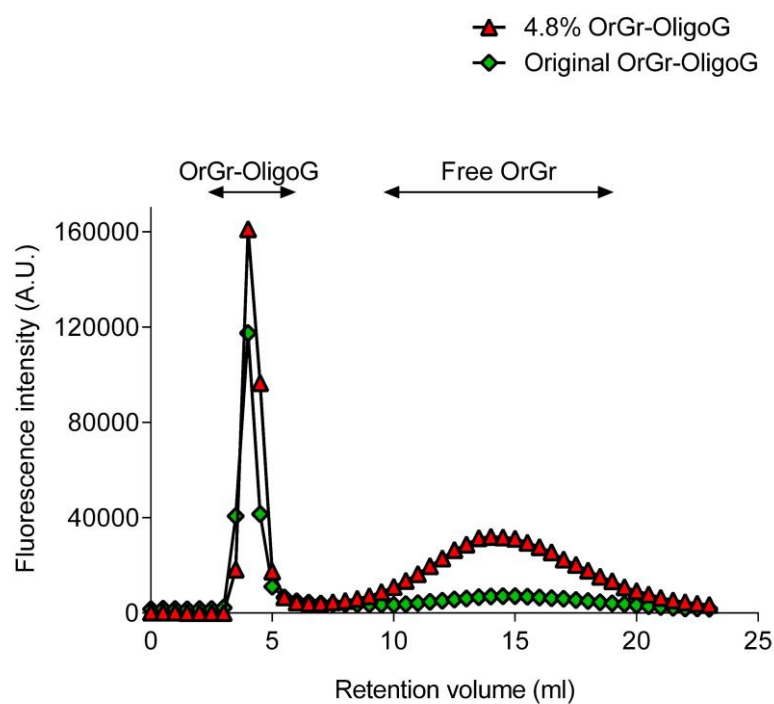


**Figure 6.16** Characterisation of supernatant from *E. coli* IR57 biofilms grown for 24 h, followed by 24 h treatment with (a) TxRd-OligoG and (b) OrGr-OligoG using a PD-10 column.

strains are a primary concern in patients with compromised lung function, it was interesting to study whether OligoG was able to disrupt and penetrate the whole structure of the biofilm or whether it would remain predominantly on the biofilm surface.

Several technical aspects needed to be considered for the development of a Transwell diffusion model using a highly fluorescent probe. For instance, Transwells with 0.4  $\mu\text{m}$  pore sizes were selected to both facilitate the formation of a thick *P. aeruginosa* NH57388A biofilm on the top of the membrane, while also preventing bacterial growth (and “seepage”) within/through the pores. In addition, the duration of biofilm growth (48 h to achieve thick biofilm development) and seeding density used ( $1 \times 10^8$  CFU/ml) were chosen to more closely mimic the environment of severe infection. Although the EPS matrix contains various functional groups which produce an overall negative charge in the biofilm (Sutherland, 2001a), diffusion coefficients of negatively charged fluorescent probes through a *Streptococcus mutans* biofilm have previously been shown to decrease as the negative charge of the probe increased (Zhang et al., 2011). Therefore, in this study, it was hypothesised that the positively charged rhodamine probe would effectively be ‘pulled’ through the *P. aeruginosa* NH57388A biofilm structure due to decreased electrostatic repulsion between the fluorescent probe and the biofilm itself.

The Transwell biofilm model system developed here demonstrated that rhodamine diffusion (up to 72% of initial concentration) through the un-treated biofilm network increased with time, proving the suitability of the model to study the anti-biofilm activity of OligoG. Previous studies have shown bacterial clumping and disruption of established biofilms following OligoG treatment ( $\geq 0.5\%$ ) in models of both non-mucoid *P. aeruginosa* PAO1 (Khan et al., 2012) and mucoid *P. aeruginosa* NH57388A (Powell et al., 2018). It was, therefore, highly surprising to observe a decrease in rhodamine diffusion after treatment with 1% OligoG in these studies. An interaction between the positively-charged rhodamine and negatively-charged OligoG was excluded as the possible cause, since diffusion through the microporous membrane was not affected by either component. Interestingly, a recent study by Powell et al.,

(2018) employed a Transwell system (3.0  $\mu\text{m}$  pore size) to study the diffusion of negatively-charged FluoSpheres through *P. aeruginosa* NH57388A biofilms grown for 24 h, followed by 4 h treatment with OligoG. Results revealed that only the 2% OligoG treatment was able to produce a significant increase in fluorescence intensity in the lower acceptor well 1 h after addition of the FluoSpheres, with no effect noted for the 0.5 % OligoG dose. It was, therefore, hypothesised that, as alginate oligomers are known to bind to divalent cations such as  $\text{Mg}^{2+}$  and  $\text{Ca}^{2+}$  (Borgogna et al., 2013), OligoG interaction with divalent cations in the MH broth may have caused cross-linking in the biofilm, which may in turn may have slowed down diffusion of the fluorescent probe. To test this, EDTA was employed to facilitate disruption of biofilm structure and thus, enhance diffusion of rhodamine. Previous studies have shown that while 1 mM EDTA prevented *P. aeruginosa* biofilm formation (Alakomi et al., 2006) at 50 mM, EDTA decreased the number of *P. aeruginosa* biofilm-associated cells by more than 99% (Banin et al., 2006). Despite this however, in these studies, rhodamine diffusion after treatment with EDTA (1 mM, 50 mM and 100 mM) was similar to that of OligoG. In fact, increasing the concentration of EDTA appeared to decrease rhodamine penetration through the biofilm, although the actual structure of the biofilm architecture was visibly disrupted.

The data collected in this study suggested that both chelating agents, OligoG and EDTA, might substantially disrupt and alter the biofilm network of *P. aeruginosa* NH57388A. However, the release of planktonic bacteria, along with release of cell debris/cellular contents, might then cause clogging of the Transwell membrane pores, and thus, interfere with, and actually impede rhodamine diffusion. Hence, although the Transwell diffusion model appeared to offer a simple and fast method to analyse the efficacy of anti-biofilm agents such as OligoG, the heterogeneity of the biofilms and issues with the experimental set-up (such as charge and membrane pore blockage) suggest a need to re-evaluate the benefits of the model used in this study.

Several other techniques have been described in the literature to quantify the diffusion of drugs, proteins, antibodies and fluorescent particles (Groo and Lagarce, 2014), including fluorescence recovery after photobleaching (FRAP)

(Nordgård et al., 2014, Pincet et al., 2016) or side-by-side diffusion cell systems (Bhat et al., 1996). To assess the mechanical and micro-rheological properties of the biofilm, single or multiple particle tracking systems have also been described, which allows simultaneous tracking of particles undergoing Brownian motion using microscopy, without disturbing the actual EPS/biofilm structure (Alona et al., 2014, Cheng et al., 2017). Importantly, these systems allow precise determination of the trajectory of a particle and calculation of the effective diffusion coefficient. For example, the mobility and diffusion of differently charged nanoparticles has been studied using single particle tracking in CF sputum, as well as in *Burkholderia multivorans* and *P. aeruginosa* biofilms (Forier et al., 2012). Thus, these might be better models to use to study bulk biofilm properties than the Transwell model actually used here.

Biofilm-associated infections, especially those caused by Gram-negative opportunistic pathogens are a major cause of persistent chronic infection, leading to increased tolerance to antimicrobial agents, and are thus a significant threat to public health (Bowler, 2018). Previous studies have shown the effectiveness of OligoG in *P. aeruginosa* biofilms (Powell et al., 2018, Pritchard et al., 2017). Hence in this study, it was interesting to also investigate the anti-biofilm properties of OligoG against other bacterial pathogens, such as *E. coli*. In this case, even though OligoG treatment apparently had no effect in reducing biofilm thickness in established multi-drug resistant *E. coli* IR57 biofilms, a significant and dose-dependent reduction in fluorescence intensity using SYTO 9 staining was observed indicative of biofilm growth inhibition. In addition, bacterial clumping, increased porosity and disorganisation of the biofilm structure were all clearly evident following OligoG treatment. This study, alongside the work of (Pritchard et al., 2017), who reported synergistic potentiation of colistin activity in the presence of OligoG against *P. aeruginosa* NH57388A biofilms), supports the potential therapeutic benefit of OligoG use in combination with antibiotics, where OligoG disruption of the tight and compact biofilm network into a looser structure, may facilitate and enhance the diffusion and effectiveness of antibiotics.

Dose-dependent disruption of an established *P. aeruginosa* NH57388A biofilm was previously reported after treatment with OligoG, which corresponded to a decrease and disruption in both eDNA and polysaccharide content of the EPS matrix (Powell et al., 2018). However, surprisingly in this study no significant changes in fluorescence intensity of ConA were observed following either 4 h or 24 h treatment with OligoG. Nevertheless, smaller clusters of EPS were apparent after treatment with 4.8% OrGr-OligoG or 6% OligoG, which might indicate the ability of OligoG, especially at higher concentrations, to interact with and disrupt the larger sugar components of the EPS matrix. This correlated with the reduced SYTO 9 fluorescence intensity observed after 4 h OligoG treatment and the disorganised biofilm structure observed after 24 h treatment, suggesting that its chelation of divalent cations might alter the EPS matrix and weaken the mechanical robustness of the biofilm. Then again, the difference in OligoG efficacy observed in *P. aeruginosa* and *E. coli* biofilms might also be due to their significantly different exopolysaccharide compositions. Analysis of the glycosyl composition of *P. aeruginosa* exopolysaccharides revealed that it is comprised of 80-90% mannose and 4-7% glucose, while *E. coli* exopolysaccharides contain ~10% mannose and ~40% glucose (Bales et al., 2013). Hence, the suitability of ConA stain for this study may not have been ideal since the EPS of *E. coli* biofilms contains fairly low amounts of  $\alpha$ -D-mannose and  $\alpha$ -D-glucose residues, to which the probe predominantly binds, and this might explain the lack of significant efficacy observed following OligoG treatment. It seems likely, therefore, that there may have been a considerable underestimate of EPS sugars in these samples. More specific probes are clearly required that unambiguously target the other EPS sugars present in *E. coli* biofilms such as galactose and glucuronic acid (Limoli et al., 2015). Surprisingly, analysis of the bacterial growth medium revealed liberation of high proportion of free OrGr. Although amide linkage is considered to be biologically stable, degradation of OligoG by bacterial enzymes would still leave the sugar residues attached to OrGr, which might have a similar elution profile to free OrGr. Also, OrGr might only be bound to OligoG by electrostatic interactions, which might be separated in bacterial culture medium, resulting in release of free OrGr.

Following conjugation of TxRd or OrGr to OligoG the amount of free fluorescent probe in the conjugates should have been minimal. However, up to 11.6% of free probe was detected. A strong electrostatic interaction between the fluorescent probe and the negatively-charged OligoG, as well as nonspecific binding to the PD-10 column might explain the reduced conjugation efficiency and presence of free TxRd or OrGr following purification.

CLSM imaging confirmed penetration of the TxRd-OligoG conjugate from the top (point of treatment) to the bottom of an established *E. coli* IR57 biofilm, which was not observed with free TxRd alone. Surprisingly, a noticeable decrease in established *E. coli* IR57 biofilm thickness following 24 h treatment with 6% TxRd-OligoG was demonstrated. It has previously been reported that OligoG treatment was associated with an increase in overall negative surface charge of Gram-negative bacteria alongside irreversible binding of OligoG to the bacterial surface and cell aggregation (Powell et al., 2014). Therefore, TxRd conjugation might also increase the negative charge of OligoG and thus, enhance disruption of the structural assembly of the biofilm. CLSM imaging at the very base of the biofilm demonstrated close binding of TxRd-OligoG to the surface of the bacterial cells, perhaps indicative of interaction between the TxRd's positively-charged amino group and the negatively-charged bacterial membrane. The stability of the TxRd-OligoG conjugate in the bacterial growth medium was confirmed by analysis of the supernatant by SEC using PD-10 column. No statistical analysis was performed for the biofilms treated with TxRd-OligoG, since OligoG antimicrobial efficacy may have been altered by conjugation with the fluorophore.

## **6.6 Conclusions**

This study highlighted the limitations of the Transwell system for analysis of bacterial biofilm disruption. The usefulness of applying fluorescent probe conjugation to investigate anti-biofilm therapeutics in conjunction with CLSM was confirmed, although only minimal, preliminary results could be obtained for OrGr-OligoG. The biofilm disruption assays showed that OligoG was able to reorganise/disrupt the biofilm structure of *E. coli* IR57 in a dose-dependent

manner (> 0.5%), although unlike previous studies on OligoG disruption of *P. aeruginosa* biofilms, no real decrease in biofilm thickness was observed. These anti-biofilm effects were more obvious using the TxRd-OligoG conjugate treatment, higher reduction in biofilm thickness was noted at 6%. These inconclusive results could be due to altered activity of the OligoG-probe conjugates themselves. Further work is required to examine these issues further.

# **Chapter 7**

## **General Discussion**

## 7.1 Evaluation of the present study

The basis of this thesis was to design and study a group of OligoG-polymyxin conjugates using irreversible (amide) and reversible (ester) linkers to explore the feasibility of engineering novel nanomedicines to support the clinical demand for new antibiotics against Gram-negative bacteria.

Over recent years, polymer therapeutics has emerged as a promising strategy to combat Gram-negative infections (Cal et al., 2017). Since the early 1990s, when polymyxin B was covalently linked to PEG to improve its stability and cytotoxicity, PEG has been the primary focus for such antimicrobial conjugations (Groves et al., 1990, Stebbins et al., 2014). In subsequent years, penicillin V was conjugated to water-soluble poly(ether urethane), a derivative of PEG and L-lysine, which were attached via a hydrolytically-cleavable ester linkage. The resulting conjugate exhibited equivalent antimicrobial activity to that of the free drug in *S. aureus*, *Streptococcus pyogenes* group A and *Enterococcus faecalis* (Nathan et al., 1993). PEG-tobramycin conjugates also performed favourably, demonstrating 3.2-fold greater efficacy against Gram-negative *P. aeruginosa* biofilms than tobramycin alone (Du et al., 2015). More recently, a reversible, traceless PEGylated colistin conjugate showed potent antimicrobial activity against MDR *P. aeruginosa* and *A. baumannii*, with a corresponding absence of nephrotoxic side effects after systemic administration to mice (Zhu et al., 2017). This further suggested that covalent conjugation of polymyxin antibiotics to water-soluble polymers, such as OligoG, could be used as systemic alternatives to CMS or polymyxin B.

Although PEG is commonly employed as a polymeric carrier for bioactive molecules, its' non-biodegradability (Section 1.7) and the presence up to two terminal functional groups per chain has limited its' capacity for drug attachment (Khandare and Minko, 2006). Therefore, selection of OligoG as the polymeric carrier for antibiotic conjugation was ideal due to its biocompatibility (Section 1.7.1) and intrinsic antimicrobial activity (Section 3.1.1). This thesis aimed to create a bi-functional polymer therapeutic that combined the antimicrobial properties of both, OligoG and polymyxin antibiotics, while reducing the latter's systemic toxicity whilst increasing its

efficacy at sites of infection.

OligoG-polymyxin conjugates were produced containing either an amide or ester linker to study whether complete release of the antibiotic was required to achieve maximal reinstatement of the antimicrobial activity of the individual components. Both linking chemistries promoted reproducible synthesis of OligoG-polymyxin conjugates with similar antibiotic loading. Release of the amide-linked polymyxin relies on enzymatic degradation of OligoG. However, it is important to note that no alginate degrading mammalian enzymes have been reported, which might impose additional difficulties for clinical translation to patients requiring long-term treatment (Shen et al., 2017). Nevertheless, alginate lyase from *K. pneumoniae* and *P. aeruginosa* found in CF patient lungs has been shown to effectively degrade alginate (Simpson et al., 1993), highlighting the possibility of harnessing such bacteria at sites of infection to trigger site-specific and target-specific degradation of alginate and release of the therapeutic payload.

Previous studies have shown inefficient and incomplete conversion of the colistin prodrug, CMS into its active form, can result in a slow and/or delayed increase in colistin plasma concentration (Garonzik et al., 2011). Although polymyxin B is used clinically as an antibiotic of last resort, studies have shown that it exhibits higher nephrotoxicity compared to CMS (Akajagbor et al., 2013). This further highlights the potential benefits of polymer conjugation to cytotoxic antibiotics, such as the polymyxins.

Colonisation by MDR Gram-negative bacterial pathogens, especially *P. aeruginosa* and repeated exposure to antibiotics, can lead to reduced therapeutic options and a deterioration in lung function in patients with chronic respiratory diseases. In addition, binding of sputum biomolecules in the airways is known to diminish the antimicrobial effectiveness of inhaled colistin (Schneider-Futschik et al., 2018, Weers, 2015). Although OligoG conjugation did not inhibit mucin binding or alter the effect of nutrient-deficient media on colistin and polymyxin B (Chapter 4), the high local concentrations of inhaled OligoG-polymyxin conjugates may still drastically improve drug targeting and overcome the deleterious effects associated with systemic exposure to

polymyxins. Both, amide- and ester-linked colistin described in this thesis displayed a broad spectrum of activity against a range of Gram-negative bacteria and delayed bacterial growth in a concentration-dependent manner. However, colistin linked to OligoG via ester bonding was notably more effective, especially in biofilm formation studies characterised by CLSM, causing bacterial clumping and disruption of the *P. aeruginosa* R22 biofilm structure, as well as inducing significantly higher cell death compared to the amide-linked antibiotic (Chapter 4). It was also evident in the 'time to kill' (TTK) model using *A. baumannii* 7789, where only the OligoG-E-colistin conjugate exhibited an antimicrobial profile equivalent to that of colistin alone (Chapter 5), suggesting that ester conjugation was likely to be more clinically beneficial at infected sites since it achieved complete separation of the parent molecules by esterase enzyme degradation and hydrolysis.

Many polymer conjugates described in the literature have explored the feasibility of using enzymatic degradation of a polymer backbone to reinstate bioactivity of the masked payload, including dextrin-trypsin (Duncan et al., 2008), dextrin-colistin (Ferguson et al., 2014), dextrin-phospholipase A<sub>2</sub> (Ferguson and Duncan, 2009), dextrin-recombinant human epidermal growth factor (Hardwicke et al., 2008), polyacetal-trypsin (Escalona et al., 2018), hyaluronic acid-trypsin (Ferguson et al., 2010a) or PGA-lysozyme (Talelli and Vicent, 2014) conjugates. Considering that more than 90% of an established *P. aeruginosa* biofilm was eradicated after 1 h treatment with PEG-alginate lyase (Lamppa et al., 2011), the co-administration of OligoG-A-polymyxin with PEG-alginate lyase conjugate might provide additional therapeutic benefits as a novel antibiofilm treatment. Unfortunately, conventional antimicrobial susceptibility techniques, such as the MIC and TTK assays, may underestimate the real antimicrobial efficacy of OligoG-polymyxin conjugates due to the altered PK-PD profile of the antibiotic.

Targeted delivery and controlled release of antibiotics at the infected site due to EPR effect would significantly improve their therapeutic index *in vivo* and may reduce the total dose required for bacterial eradication. Previous studies have shown that exposure to high concentrations of colistin at the beginning

of treatment induced rapid bactericidal activity against *P. aeruginosa* within the first 24 h (Rao et al., 2014). Conversely, increasing the concentration of polymyxin B drastically amplified resistance in *A. baumannii* (Tsuji et al., 2016). Therefore, prolonged retention of bi-functional OligoG-polymyxin conjugates at the site of infection might maximise bacterial killing at lower doses, thereby minimising the emergence of resistance.

It was deemed essential in this study to investigate localisation and interaction of OligoG within the biofilm network, to better understand its biofilm disruption properties. The diffusion of TxRd-labelled OligoG through an *E. coli* IR57 biofilm was confirmed by CLSM which was associated with bacterial clumping and alteration of the biofilm structure (Chapter 6). Although TxRd conjugation was associated with non-specific interactions with the bacterial cell membranes themselves, pronounced bacterial aggregation was also clearly demonstrated with the OligoG-E-colistin conjugate (Chapter 4) in the biofilm formation assay. The significant reduction of the EPS polysaccharides (ConA staining) in OligoG treated established *P. aeruginosa* NH57388A biofilms was reported (Powell et al., 2018). However, the inconclusive results observed in this study could be due to insufficient specificity of the ConA dye to stain all of the *E. coli* EPS sugars leading to an incomplete “capture” of EPS polysaccharide disruption in these biofilms. Further studies using MIC assays would have been beneficial to confirm that fluorescent labelling (TxRd or OrGr) did not alter or enhanced the antimicrobial activity of OligoG.

## **7.2 Suggestions for future development of OligoG-polymyxin conjugates**

The results presented in this thesis underline the potential clinical usefulness of OligoG-polymyxin conjugates. However, some questions remain unanswered. Therefore, the most important outstanding experiments in developing the OligoG-polymyxin conjugates are described here.

Firstly, since OligoG-polymyxin conjugates comprise a polydisperse mixture of species (Chapter 3), establishing suitable, specific analytical techniques to characterise them would improve understanding of their structure/activity

relationships. In future studies, the physicochemical properties of OligoG-polymyxin conjugates, such as size, architecture and solution conformation should be investigated under physiologically-relevant conditions. Previous studies using small-angle neutron scattering (SANS) have shown that differences in molecular structure of diethylstilbestrol-polyacetal conjugates significantly affected the solution behaviour and altered the biological output *in vitro* (Giménez et al., 2012). SANS has also been employed to study the solution structure and conformation of polymer-drug conjugates including HPMA copolymer-doxorubicin (Paul et al., 2010) and PGA-doxycycline (Conejos-Sánchez et al., 2015) and therefore, would be a beneficial technique to use to further characterise both the amide and ester linked polymyxins.

Translation of OligoG-polymyxin conjugates to the clinic will require considerable further investigation especially of the metabolic fate and preferential accumulation at sites of infection of these polymers. Preliminary *in vivo* single or multiple dose-escalating animal (and ultimately human) studies would also be necessary for determining *in vivo* toxicity and pharmacokinetic profiles, as well as the maximum tolerated dose of the conjugates. Animal studies with other polymer conjugates have previously been described in the literature. For example, to identify an appropriate dosing interval, the pharmacokinetics of a single intravenous bolus dose of dextrin-colistin conjugate (0.1 mg/kg colistin equivalent) was analysed in rats (Ferguson et al., 2014). However, this study was limited by colistin-mediated adverse effects (0.5 mg/kg) during the first 2 h post-dose, which were not observed at the equivalent concentration of conjugate. In another study, subcutaneous administration of colistin sulfate in mice was performed using single (5, 10, 20, or 40 mg/kg) and repeat dosing (5 to 160 mg/kg/day) studies against *P. aeruginosa* in both thigh and lung infection models (Dudhani et al., 2010). However, due to acute toxicity, the largest dose of colistin used in the study at any given time was 40 mg/kg. Even when colistin at an accumulated dose of 40 mg/kg induced mild histological damage in mice kidney, no toxicity was observed using PEGylated colistin conjugate (40 mg/kg colistin equivalent) (Zhu et al., 2017). It would therefore be extremely interesting to perform similar *in vivo* studies to determine the most suitable route of

administration (and tolerability) of free and OligoG-conjugated polymyxin, especially at higher concentrations.

To obtain meaningful results about tissue distribution and drug pharmacokinetics from the preclinical studies, it will be important, and indeed essential, to develop sensitive and accurate methods for the quantification of free and conjugated antibiotic in biological samples. Typically, the detection of antimicrobial cationic peptides, CMS and colistin concentration in plasma or urine has been studied using high-performance liquid chromatography (HPLC) or liquid chromatography-mass spectrometry (LC-MS) techniques (Ali et al., 2009, Li et al., 2003a, Li et al., 2003b). However, it was previously found that dextrin conjugation hindered colistin interaction with HPLC column, necessitating the use of a commercial colistin ELISA kit to quantify the colistin content of plasma and infected burn wound samples (Azzopardi et al., 2015. Ferguson et al., 2014). Unfortunately, the ELISA kit can only detect the total colistin content of a sample, highlighting the real need for novel analytical detection methods to better characterise the pharmacokinetic profile of OligoG-polymyxin conjugates in both *in vitro* and *in vivo* studies.

Although the antimicrobial activity of the OligoG-polymyxin conjugates was tested against polymyxin-resistant bacterial strains in this study, to date, no investigation into the development of bacterial resistance following prolonged exposure to the conjugate has yet been performed. The limitations of conventional susceptibility testing methods have already been discussed in Chapter 4. Recently, the Nordmann/Poirel (NP) test was developed for rapid identification of polymyxin resistance in *Enterobacteriaceae*, which relies on glucose metabolism by growing bacteria in the presence of a defined concentration of polymyxin antibiotic (Bakthavatchalam et al., 2016, Nordmann et al., 2016). The formed acid metabolites can be detected within 2 h by a phenol red colour change from orange to yellow. This method was successfully employed to detect colistin-resistant *Enterobacteriaceae* collected directly from blood cultures (Jayol et al., 2016). Thus, it could be interesting to use the NP test to detect polymyxin sensitive and resistant *Enterobacteriaceae* isolates after treatment with OligoG-polymyxin

conjugates, to identify emergence of early resistance, especially in septic patients who require prolonged antibiotic therapies.

Considering the results obtained in these studies from a broader view, as well as recent developments in the chemistry of polymer/antibiotic conjugates in the literature, a number of potential avenues for extending these studies are clear. Due to lack of disease-specific targeting and toxicity in neutrophils, the antibiotic chloramphenicol has been attached via glutaric anhydride linker to the cationic antibacterial peptide fragment UBI<sub>29-41</sub> which exhibited a high affinity towards both Gram-negative and Gram-positive bacteria (Chen et al., 2015). Therefore, it would be extremely interesting to assess the efficacy of UBI<sub>29-41</sub> as a targeting ligand for OligoG-polymyxin conjugates to enhance their bacterial specificity. Also, previous studies have shown that OligoG potentiates the antimicrobial activity of several other classes of antibiotics, including macrolides, tetracyclines and  $\beta$ -lactams against a range of MDR Gram-negative bacteria (Khan et al., 2012). Thus, OligoG conjugation might be employed to improve the pharmacokinetics and efficacy of other toxic, water-insoluble or otherwise undeliverable drugs.

### **7.3 Contribution of this thesis to antibiotic development**

The work in this thesis has demonstrated the feasibility of using OligoG conjugation as a means of reducing antibiotic toxicity, while maintaining its antimicrobial efficacy against a panel of MDR Gram-negative bacteria. These studies have established, for the first time, that complete detachment of the polymer (via an ester linkage) from the bioactive agent is required to restore its full biological activity, and that residual sugars inhibit complete regeneration of activity.

In conclusion, OligoG-polymyxin conjugates have shown exciting antimicrobial activity. Not only has their inherent antimicrobial activity been demonstrated, but also the bi-functionality of these molecules, thanks to the intrinsic bactericidal activity of the antibiotic in conjunction with the bacteriostatic antimicrobial/anti-biofilm activity of OligoG. Furthermore, both individual components have already undergone considerable *in vivo* safety testing.

# **Bibliography**

- ABDELRAOUF, K., HE, J., LEDESMA, K. R., HU, M. and TAM, V. H. 2012. Pharmacokinetics and renal disposition of polymyxin B in an animal model. *Antimicrobial Agents and Chemotherapy*, 56, 5724-5727.
- AKAJAGBOR, D. S., WILSON, S. L., SHERE-WOLFE, K. D., DAKUM, P., CHARURAT, M. E. and GILLIAM, B. L. 2013. Higher incidence of acute kidney injury with intravenous colistimethate sodium compared with polymyxin B in critically ill patients at a tertiary care medical center. *Clinical Infectious Diseases*, 57, 1300-1303.
- ALAKOMI, H. L., PAANANEN, A., SUIHKO, M. L., HELANDER, I. M. and SAARELA, M. 2006. Weakening effect of cell permeabilizers on Gram-negative bacteria causing biodeterioration. *Applied and Environmental Microbiology*, 72, 4695-4703.
- ALBUR, M., NOEL, A., BOWKER, K. and MACGOWAN, A. 2014. Colistin susceptibility testing: time for a review. *Journal of Antimicrobial Chemotherapy*, 69, 1432-1434.
- ALI, M. and BROCCINI, S. 2006. Synthetic approaches to uniform polymers. *Advanced Drug Delivery Reviews*, 58, 1671-1687.
- ALI, F. E. A., CAO, G., POUDYAL, A., VAARA, T., NATION, R. L., VAARA, M. and LI, J. 2009. Pharmacokinetics of novel antimicrobial cationic peptides NAB 7061 and NAB 739 in rats following intravenous administration. *Journal of Antimicrobial Chemotherapy*, 64, 1067-1070.
- ALKAWASH, M. A., SOOTHILL, J. S. and SCHILLER, N. L. 2006. Alginate lyase enhances antibiotic killing of mucoid *Pseudomonas aeruginosa* in biofilms. *APMIS (Acta Pathologica, Microbiologica, et Immunologica Scandinavica)*, 114, 131-138.
- ALONA, B., NICOLE, B., ELIZABETH, N., JUSTIN, H., KATHARINA, R. and PATRICK, S. D. 2014. Single particle tracking reveals spatial and dynamic organization of the *Escherichia coli* biofilm matrix. *New Journal of Physics*, 16, 085014.
- AL-SHAMKHANI, A. and DUNCAN, R. 1995. Radioiodination of alginate via covalently-bound tyrosinamide allows monitoring of its fate *in vivo*. *Journal of Bioactive and Compatible Polymers*, 10, 4-13.
- ANDERSEN, T., STRAND, B., FORMO, K., ALSBERG, E. and CHRISTENSEN, B. E. 2012. Alginates as biomaterials in tissue engineering. *Carbohydrate Chemistry*, 37, 227-258.
- ANDERSSON, M., WITTEGREN, B. and WAHLUND, K. G. 2003. Accuracy in multiangle light scattering measurements for molar mass and radius estimations. Model calculations and experiments. *Analytical Chemistry*, 75, 4279-4291.
- ANDES, D. and CRAIG, W. A. 2002. Animal model pharmacokinetics and pharmacodynamics: a critical review. *International Journal of Antimicrobial Agents*, 19, 261-268.
- ANEES, M. 1996. Location of tumour cells in colon tissue by Texas Red labelled pentosan polysulphate, an inhibitor of a cell surface protease. *Journal of Enzyme Inhibition*, 10, 203-214.
- ARMSTRONG, J. K., HEMPEL, G., KOLING, S., CHAN, L. S., FISHER, T., MEISELMAN, H. J. and GARRATTY, G. 2007. Antibody against poly(ethylene glycol) adversely affects PEG-asparaginase therapy in acute lymphoblastic leukemia patients. *Cancer*, 110, 103-111.

- ASLAM, S. N., NEWMAN, M. A., ERBS, G., MORRISSEY, K. L., CHINCHILLA, D., BOLLER, T., JENSEN, T. T., DE CASTRO, C., IERANO, T., MOLINARO, A., JACKSON, R. W., KNIGHT, M. R. and COOPER, R. M. 2008. Bacterial polysaccharides suppress induced innate immunity by calcium chelation. *Current Biology*, 18, 1078-1083.
- ASTM. 2016. Standard test method for determining the molar mass of sodium alginate by size exclusion chromatography with multi-angle light scattering detection (SEC-MALS). *ASTM F2605-16*. ASTM, West Conshohocken, Pennsylvania, USA. Available at: <https://www.astm.org/Standards/F2605.htm> [Accessed: 13 April 2018].
- AZAD, M. A. K., FINNIN, B. A., POU DYAL, A., DAVIS, K., LI, J., HILL, P. A., NATION, R. L., VELKOV, T. and LI, J. 2013. Polymyxin B induces apoptosis in kidney proximal tubular cells. *Antimicrobial Agents and Chemotherapy*, 57, 4329-4335.
- AZZOPARDI, E., BOYCE, D., THOMAS, D. and DICKSON, W. 2012. Colistin in burn intensive care: back to the future? *Burns*, 39, 7-15.
- AZZOPARDI, E. A., FERGUSON, E. L. and THOMAS, D. W. 2013a. Colistin past and future: a bibliographic analysis. *Journal of Critical Care*, 28, 219.e13-219.e19.
- AZZOPARDI, E. A., FERGUSON, E. L. and THOMAS, D. W. 2013b. The enhanced permeability retention effect: a new paradigm for drug targeting in infection. *Journal of Antimicrobial Chemotherapy*, 68, 257-274.
- AZZOPARDI, E. A., FERGUSON, E. L. and THOMAS, D. W. 2015. Development and validation of an *in vitro* pharmacokinetic/pharmacodynamic model to test the antibacterial efficacy of antibiotic polymer conjugates. *Antimicrobial Agents and Chemotherapy*, 59, 1837-1843.
- BA, B. B., BERNARD, A., ILIADIS, A., QUENTIN, C., DUCINT, D., ETIENNE, R., FOURTILLAN, M., MAACHI-GUILLOT, I. and SAUX, M. C. 2001. New approach for accurate simulation of human pharmacokinetics in an *in vitro* pharmacodynamic model: application to ciprofloxacin. *Journal of Antimicrobial Chemotherapy*, 47, 223-227.
- BAHAMONDEZ-CANAS, T. F., ZHANG, H., TEWES, F., LEAL, J. and SMYTH, H. D. C. 2018. PEGylation of tobramycin improves mucus penetration and antimicrobial activity against *Pseudomonas aeruginosa* biofilms *in vitro*. *Molecular Pharmaceutics*, 15, 1643-1652.
- BAI, F., LI, X., NIU, B., ZHANG, Z., MALAKAR, P. K., LIU, H., PAN, Y. and ZHAO, Y. 2018. A *mcr-1*-carrying conjugative IncX4 plasmid in colistin-resistant *Escherichia coli* ST278 strain isolated from dairy cow feces in Shanghai, China. *Frontiers in Microbiology*, 9, 2833.
- BAKTHAVATCHALAM, Y. D., PRAGASAM, A. K., BISWAS, I. and VEERARAGHAVAN, B. 2018. Polymyxin susceptibility testing, interpretative breakpoints and resistance mechanisms: an update. *Journal of Global Antimicrobial Resistance*, 12, 124-136.
- BAKTHAVATCHALAM, Y., VEERARAGHAVAN, B., MATHUR, P., PURIGHALLA, S. and RICHARD, V. 2016. Polymyxin Nordmann/Poirel test for rapid detection of polymyxin resistance in *Enterobacteriaceae*: Indian experience. *Indian Journal of Medical Microbiology*, 34, 564-565.

- BALAZUC, A. M., LAGRANDERIE, M., CHAVAROT, P., PESCHER, P., ROSEEUW, E., SCHACHT, E., DOMURADO, D. and MARCHAL, G. 2005. *In vivo* efficiency of targeted norfloxacin against persistent, isoniazid-insensitive, *Mycobacterium bovis* BCG present in the physiologically hypoxic mouse liver. *Microbes and Infection*, 7, 969-975.
- BALES, P. M., RENKE, E. M., MAY, S. L., SHEN, Y. and NELSON, D. C. 2013. Purification and characterization of biofilm-associated EPS exopolysaccharides from ESKAPE organisms and other pathogens. *PLOS ONE*, 8, e67950.
- BANERJEE, S. S., AHER, N., PATIL, R. and KHANDARE, J. 2012. Poly(ethylene glycol)-prodrug conjugates: concept, design, and applications. *Journal of Drug Delivery*, 2012, 103973.
- BANIN, E., BRADY, K. M. and GREENBERG, E. P. 2006. Chelator-induced dispersal and killing of *Pseudomonas aeruginosa* cells in a biofilm. *Applied and Environmental Microbiology*, 72, 2064-2069.
- BARNETT, M., BUSHBY, S. R. and WILKINSON, S. 1964. Sodium sulphomethyl derivatives of polymyxins. *British Journal of Pharmacology and Chemotherapy*, 23, 552-574.
- BARZ, M., CANAL, F., KOYNOV, K., ZENTEL, R. and VICENT, M. J. 2010a. Synthesis and *in vitro* evaluation of defined HPMA folate conjugates: influence of aggregation on folate receptor (FR) mediated cellular uptake. *Biomacromolecules*, 11, 2274-2282.
- BARZ, M., WOLF, F. K., CANAL, F., KOYNOV, K., VICENT, M., FREY, H. and ZENTEL, R. 2010b. Synthesis, characterization and preliminary biological evaluation of P(HPMA)-b-P(LLA) copolymers: a new type of functional biocompatible block copolymer. *Macromolecular Rapid Communications*, 31, 1492-1500.
- BASU, A., KUNDURU, K. R., ABTEW, E. and DOMB, A. J. 2015. Polysaccharide-based conjugates for biomedical applications. *Bioconjugate Chemistry*, 26, 1396-1412.
- BAUDIN, M., CINQUIN, B., SCLAVI, B., PAREAU, D. and LOPES, F. 2017. Understanding the fundamental mechanisms of biofilms development and dispersal: BIAM (biofilm intensity and architecture measurement), a new tool for studying biofilms as a function of their architecture and fluorescence intensity. *Journal of Microbiological Methods*, 140, 47-57.
- BECHLER, S. L. and LYNN, D. M. 2011. Design and synthesis of a fluorescently end-labeled poly( $\beta$ -amino ester): application to the characterization of degradable polyelectrolyte multilayers. *Journal of Polymer Science. Part A, Polymer Chemistry*, 49, 1572-1581.
- BENGOECHEA, J. A. and SKURNIK, M. 2000. Temperature-regulated efflux pump/potassium antiporter system mediates resistance to cationic antimicrobial peptides in *Yersinia*. *Molecular Microbiology*, 37, 67-80.
- BEVERIDGE, E. G. and MARTIN, A. J. 1967. Sodium sulphomethyl derivatives of polymyxins. *British Journal of Pharmacology and Chemotherapy*, 29, 125-135.
- BHAGIRATH, A. Y., LI, Y., SOMAYAJULA, D., DADASHI, M., BADR, S. and DUAN, K. 2016. Cystic fibrosis lung environment and *Pseudomonas aeruginosa* infection. *BMC Pulmonary Medicine*, 16, 174.
- BHAT, P. G., FLANAGAN, D. R. and DONOVAN, M. D. 1996. Drug diffusion

- through cystic fibrotic mucus: steady-state permeation, rheologic properties, and glycoprotein morphology. *Journal of Pharmaceutical Sciences*, 85, 624-630.
- BONAPACE, C. R., BOSSO, J. A., FRIEDRICH, L. V. and WHITE, R. L. 2002. Comparison of methods of interpretation of checkerboard synergy testing. *Diagnostic Microbiology and Infectious Disease*, 44, 363-366.
- BORGOGNA, M., SKJÅK-BRÆK, G., PAOLETTI, S. and DONATI, I. 2013. On the initial binding of alginate by calcium ions. The tilted egg-box hypothesis. *The Journal of Physical Chemistry B*, 117, 7277-7282.
- BOUCHER, H. W., TALBOT, G. H., BRADLEY, J. S., EDWARDS, J. E., GILBERT, D., RICE, L. B., SCHELD, M., SPELLBERG, B. and BARTLETT, J. 2009. Bad bugs, no drugs: no ESKAPE! An Update from the Infectious Diseases Society of America. *Clinical Infectious Diseases*, 48, 1-12.
- BOWLER, P. G. 2018. Antibiotic resistance and biofilm tolerance: a combined threat in the treatment of chronic infections. *Journal of Wound Care*, 27, 273-277.
- BRAUNER, A., FRIDMAN, O., GEFEN, O. and BALABAN, N. Q. 2016. Distinguishing between resistance, tolerance and persistence to antibiotic treatment. *Nature Reviews Microbiology*, 14, 320-330.
- BROWN, M. R. W., GEATON, E. M. and GILBERT, P. 1979. Additivity of action between polysorbate 80 and polymyxin B towards spheroplasts of *Pseudomonas aeruginosa* NCTC 6750. *Pharmacy and Pharmacology*, 31, 168-170.
- BROWN, M. R. W. and WINSLEY, B. E. 1971. Synergism between polymyxin and polysorbate 80 against *Pseudomonas aeruginosa*. *Journal of General Microbiology*, 68, 367-373.
- BUCKLIN, S. E., LAKE, P., LÖGDBERG, L. and MORRISON, D. C. 1995. Therapeutic efficacy of a polymyxin B-dextran 70 conjugate in experimental model of endotoxemia. *Antimicrobial Agents and Chemotherapy*, 39, 1462-1466.
- BUDHA, N. R., LEE, R. B., HURDLE, J. G., LEE, R. E. and MEIBOHM, B. 2009. A simple *in vitro* PK/PD model system to determine time-kill curves of drugs against *Mycobacteria*. *Tuberculosis*, 89, 378-385.
- BULMAN, Z. P., CHEN, L., WALSH, T. J., SATLIN, M. J., QIAN, Y., BULITTA, J. B., PELOQUIN, C. A., HOLDEN, P. N., NATION, R. L., LI, J., KREISWIRTH, B. N. and TSUJI, B. T. 2017. Polymyxin combinations combat *Escherichia coli* harboring *mcr-1* and *bla*<sub>NDM-5</sub>: preparation for a postantibiotic era. *mBio*, 8, e00540-17.
- CAJAL, Y., BERG, O. G. and JAIN, M. K. 1995. Direct vesicle-vesicle exchange of phospholipids mediated by polymyxin B. *Biochemical and Biophysical Research Communications*, 210, 746-752.
- CAJAL, Y., ROGERS, J., BERG, O. G. and JAIN, M. K. 1996. Intermembrane molecular contacts by polymyxin B mediate exchange of phospholipids. *Biochemistry*, 35, 299-308.
- CAL, P. M., MATOS, M. J. and BERNARDES, G. J. 2017. Trends in therapeutic drug conjugates for bacterial diseases: a patent review. *Expert Opinion on Therapeutic Patents*, 27, 179-189.
- CAMPOS, M. A., VARGAS, M. A., REGUEIRO, V., LLOMPART, C. M.,

- ALBERTÍ, S. and BENGOCHEA, J. A. 2004. Capsule polysaccharide mediates bacterial resistance to antimicrobial peptides. *Infection and Immunity*, 72, 7107-7114.
- CANAL, F., SANCHIS, J. and VICENT, M. J. 2011. Polymer-drug conjugates as nano-sized medicines. *Current Opinion in Biotechnology*, 22, 894-900.
- CAO, G., ALI, F. E. A., CHIU, F., ZAVASCKI, A. P., NATION, R. L. and LI, J. 2008. Development and validation of a reversed-phase high-performance liquid chromatography assay for polymyxin B in human plasma. *Journal of Antimicrobial Chemotherapy*, 62, 1009-1014.
- CASTANHEIRA, M., RHOMBERG, P. R., FLAMM, R. K. and JONES, R. N. 2016. Effect of the  $\beta$ -lactamase inhibitor vaborbactam combined with meropenem against serine carbapenemase-producing *Enterobacteriaceae*. *Antimicrobial Agents and Chemotherapy*, 60, 5454-5458.
- CHATFIELD, S. 1999. A comparison of the efficacy of the alginate preparation, gaviscon advance, with placebo in the treatment of gastro-oesophageal reflux disease. *Current Medical Research and Opinion*, 15, 152-159.
- CHEAH, S. E., BULITTA, J. B., LI, J. and NATION, R. L. 2014. Development and validation of a liquid chromatography-mass spectrometry assay for polymyxin B in bacterial growth media. *Journal of Pharmaceutical and Biomedical Analysis*, 92, 177-182.
- CHEAH, S. E., JOHNSON, M. D., ZHU, Y., TSUJI, B. T., FORREST, A., BULITTA, J. B., BOYCE, J. D., NATION, R. L. and LI, J. 2016. Polymyxin resistance in *Acinetobacter baumannii*: genetic mutations and transcriptomic changes in response to clinically relevant dosage regimens. *Scientific Reports*, 6, 26233.
- CHEN, H., LIU, C., CHEN, D., MADRID, K., PENG, S., DONG, X., ZHANG, M. and GU, Y. 2015. Bacteria-targeting conjugates based on antimicrobial peptide for bacteria diagnosis and therapy. *Molecular Pharmaceutics*, 12, 2505-2516.
- CHENG, C., DONG, Y., DORIAN, M., KAMILI, F. and SEITARIDOU, E. 2017. Quantifying biofilm formation of *Sinorhizobium meliloti* bacterial strains in microfluidic platforms by measuring the diffusion coefficient of polystyrene beads. *Open Journal of Biophysics*, 7, 157-173.
- CHEW, K. L., LA, M. V., LIN, R. T. P. and TEO, J. W. P. 2017. Colistin and polymyxin B susceptibility testing for carbapenem-resistant and *mcr*-positive *Enterobacteriaceae*: comparison of Sensititre, MicroScan, Vitek 2, and Etest with broth microdilution. *Journal of Clinical Microbiology*, 55, 2609-2616.
- CHIPMAN, S. D., OLDHAM, F. B., PEZZONI, G. and SINGER, J. W. 2006. Biological and clinical characterization of paclitaxel polyglumex (PPX, CT-2103), a macromolecular polymer-drug conjugate. *International Journal of Nanomedicine*, 1, 375-383.
- CHO, J. C., ZMARLICKA, M. T., SHAEER, K. M. and PARDO, J. 2018. Meropenem/vaborbactam, the first carbapenem/ $\beta$ -lactamase inhibitor combination. *Annals of Pharmacotherapy*, 52, 769-779.
- CHOI, Y. H. and HAN, H. K. 2018. Nanomedicines: current status and future perspectives in aspect of drug delivery and pharmacokinetics. *Journal*

- of *Pharmaceutical Investigation*, 48, 43-60.
- CHVATAL, S. A., KIM, Y. T., BRATT-LEAL, A. M., LEE, H. and BELLAMKONDA, R. V. 2008. Spatial distribution and acute anti-inflammatory effects of methylprednisolone after sustained local delivery to the contused spinal cord. *Biomaterials*, 29, 1967-1975.
- CLAUSELL, A., GARCIA-SUBIRATS, M., PUJOL, M., BUSQUETS, M. A., RABANAL, F. and CAJAL, Y. 2007. Gram-negative outer and inner membrane models: insertion of cyclic cationic lipopeptides. *The Journal of Physical Chemistry B*, 111, 551-563.
- CLSI. 1999. Methods for determining bactericidal activity of antimicrobial agents; approved guideline. *CLSI document M26-A*. CLSI, Wayne, Pennsylvania, USA. Available at: [https://clsi.org/media/1462/m26a\\_sample.pdf](https://clsi.org/media/1462/m26a_sample.pdf) [Accessed: 18 May 2018].
- CLSI. 2012. Performance standards for antimicrobial susceptibility testing; twenty-second informational supplement. *CLSI document M100-S22*. CLSI, Wayne, Pennsylvania, USA. Available at: [http://zums.ac.ir/files/health/pages/ill/azmayeshghah/clsi\\_2013.pdf](http://zums.ac.ir/files/health/pages/ill/azmayeshghah/clsi_2013.pdf) [Accessed: 20 May 2018].
- CLSI. 2018. Performance standards for antimicrobial susceptibility testing. *CLSI document M100*. CLSI, Wayne, Pennsylvania, USA. Available at: [https://clsi.org/media/1930/m100ed28\\_sample.pdf](https://clsi.org/media/1930/m100ed28_sample.pdf) [Accessed: 25 May 2018].
- COATES, A. R., HALLS, G. and HU, Y. 2011. Novel classes of antibiotics or more of the same? *British Journal of Pharmacology*, 163, 184-194.
- CONEJOS-SÁNCHEZ, I., CARDOSO, I., OTEO-VIVES, M., ROMERO-SANZ, E., PAUL, A., SAURI, A. R., MORCILLO, M. A., SARAIVA, M. J. and VICENT, M. J. 2015. Polymer-doxycycline conjugates as fibril disrupters: an approach towards the treatment of a rare amyloidotic disease. *Journal of Controlled Release*, 198, 80-90.
- CORONA, F. and MARTINEZ, J. 2013. Phenotypic resistance to antibiotics. *Antibiotics*, 2, 237-255.
- COTTER, P. D., ROSS, R. P. and HILL, C. 2012. Bacteriocins - a viable alternative to antibiotics? *Nature Reviews Microbiology*, 11, 95-105.
- CUI, P., NIU, H., SHI, W., ZHANG, S., ZHANG, H., MARGOLICK, J., ZHANG, W. and ZHANG, Y. 2016. Disruption of membrane by colistin kills uropathogenic *Escherichia coli* persists and enhances killing of other antibiotics. *Antimicrobial Agents and Chemotherapy*, 60, 6867-6871.
- CULLEN, L. and MCCLEAN, S. 2015. Bacterial adaptation during chronic respiratory infections. *Pathogens*, 4, 66-89.
- DAVIES, B. and COHEN, J. 2011. Endotoxin removal devices for the treatment of sepsis and septic shock. *The Lancet Infectious Diseases*, 11, 65-71.
- DE GIER, M. G., ALBADA, B., METZLER-NOLTE, N., SAHL, H., WILLEMS, R., LAMMERS, J. W. J., VAN MANSVELD, R., JOSTEN, M., LEAVIS, H., PAGANELLI, F. and DEKKER, B. 2016. Synergistic activity of a short lipidated antimicrobial peptide (LipoAMP) and colistin or tobramycin against *Pseudomonas aeruginosa* from cystic fibrosis patients. *MedChemCommun*, 7, 148-156.
- DERIS, Z. Z., AKTER, J., SIVANESAN, S., ROBERTS, K. D., THOMPSON, P. E., NATION, R. L., LI, J. and VELKOV, T. 2014. A secondary mode of

- action of polymyxins against Gram-negative bacteria involves the inhibition of NADH-quinone oxidoreductase activity. *The Journal of Antibiotics*, 67, 147-151.
- DEVER, L. L., JORGENSEN, J. H. and BARBOUR, A. G. 1992. *In vitro* antimicrobial susceptibility testing of *Borrelia burgdorferi*: a microdilution MIC method and time-kill studies. *Journal of Clinical Microbiology*, 30, 2692-2697.
- DEY, S. and SREENIVASAN, K. 2014. Conjugation of curcumin onto alginate enhances aqueous solubility and stability of curcumin. *Carbohydrate Polymers*, 99, 499-507.
- DONLAN, R. M. 2002. Biofilms: microbial life on surfaces. *Emerging Infectious Diseases*, 8, 881-890.
- DRAGET, K. I. and TAYLOR, C. 2011. Chemical, physical and biological properties of alginates and their biomedical implications. *Food Hydrocolloids*, 25, 251-256.
- DU BUY, H. G., RILEY, F. and SHOWACRE, J. L. 1964. Tetracycline fluorescence in permeability studies of membranes around intracellular parasites. *Science*, 145, 163-165.
- DU, J., BANDARA, H. M. H. N., DU, P., HUANG, H., HOANG, K., NGUYEN, D., MOGARALA, S. V. and SMYTH, H. D. C. 2015. Improved biofilm antimicrobial activity of polyethylene glycol conjugated tobramycin compared to tobramycin in *Pseudomonas aeruginosa* biofilms. *Molecular Pharmaceutics*, 12, 1544-1553.
- DUDHANI, R. V., TURNIDGE, J. D., COULTHARD, K., MILNE, R. W., RAYNER, C. R., LI, J. and NATION, R. L. 2010. Elucidation of the pharmacokinetic/pharmacodynamic determinant of colistin activity against *Pseudomonas aeruginosa* in murine thigh and lung infection models. *Antimicrobial Agents and Chemotherapy*, 54, 1117-1124.
- DUNCAN, R. 2003. The dawning era of polymer therapeutics. *Nature Reviews Drug Discovery*, 2, 347-360.
- DUNCAN, R. 2009. Development of HPMA copolymer-anticancer conjugates: clinical experience and lessons learnt. *Advanced Drug Delivery Reviews*, 61, 1131-1148.
- DUNCAN, R. 2014. Polymer therapeutics: top 10 selling pharmaceuticals - what next? *Journal of Controlled Release*, 190, 371-380.
- DUNCAN, R. 2017. Polymer therapeutics at a crossroads? Finding the path for improved translation in the twenty-first century. *Journal of Drug Targeting*, 25, 759-780.
- DUNCAN, R., GILBERT, H. R., CARBAJO, R. J. and VICENT, M. J. 2008. Polymer masked-unmasked protein therapy. Bioresponsive dextrin-trypsin and -melanocyte stimulating hormone conjugates designed for  $\alpha$ -amylase activation. *Biomacromolecules*, 9, 1146-1154.
- DUNCAN, R. and VICENT, M. J. 2010. Do HPMA copolymer conjugates have a future as clinically useful nanomedicines? A critical overview of current status and future opportunities. *Advanced Drug Delivery Reviews*, 62, 272-282.
- DURO-CASTANO, A., MOVELLAN, J. and VICENT, M. J. 2015. Smart branched polymer drug conjugates as nano-sized drug delivery systems. *Biomaterials Science*, 3, 1321-1334.

- EKLADIOUS, I., COLSON, Y. L. and GRINSTAFF, M. W. 2018. Polymer-drug conjugate therapeutics: advances, insights and prospects. *Nature Reviews Drug Discovery*, doi: 10.1038/s41573-018-0005-0.
- ELDAR-BOOCK, A., MILLER, K., SANCHIS, J., LUPU, R., VICENT, M. J. and SATCHI-FAINARO, R. 2011. Integrin-assisted drug delivery of nano-scaled polymer therapeutics bearing paclitaxel. *Biomaterials*, 32, 3862-3874.
- ELVIRA, C., GALLARDO, A., ROMAN, J. and CIFUENTES, A. 2005. Covalent polymer-drug conjugates. *Molecules*, 10, 114-125.
- ERRIDGE, C., BENNETT-GUERRERO, E. and POXTON, I. R. 2002. Structure and function of lipopolysaccharides. *Microbes and Infection*, 4, 837-851.
- ESCALONA, G. R., SANCHIS, J. and VICENT, M. J. 2018. pH-responsive polyacetal-protein conjugates designed for polymer masked-unmasked protein therapy (PUMPT). *Macromolecular Bioscience*, 18, 1700302.
- ESF. 2005. An ESF-European Medical Research Councils (EMRC) forward look report. *Nanomedicine*. ESF, Strasbourg, France. Available at: <https://www.nanowerk.com/nanotechnology/reports/reportpdf/report53.pdf> [Accessed: 11 June 2018].
- ETEBU, E. and ARIKEKPAR, I. 2016. Antibiotics: classification and mechanisms of action with emphasis on molecular perspectives. *International Journal of Applied Microbiology and Biotechnology Research*, 4, 90-101.
- EUCAST. 2003. Determination of minimum inhibitory concentrations (MICs) of antibacterial agents by broth dilution. *Clinical Microbiology and Infection*, 9, ix-xv.
- EUCAST. 2016. Recommendations for MIC determination of colistin (polymyxin E) as recommended by the joint CLSI-EUCAST polymyxin breakpoints working group. *EUCAST Guidance Documents in Susceptibility Testing*. Available at: [http://www.eucast.org/fileadmin/src/media/PDFs/EUCAST\\_files/General\\_documents/Recommendations\\_for\\_MIC\\_determination\\_of\\_colistin\\_March\\_2016.pdf](http://www.eucast.org/fileadmin/src/media/PDFs/EUCAST_files/General_documents/Recommendations_for_MIC_determination_of_colistin_March_2016.pdf) [Accessed: 12 June 2018].
- EUCAST. 2018. Breakpoint tables for interpretation of MICs and zone diameters. *Clinical Breakpoints for Bacteria*. Available at: [http://www.eucast.org/fileadmin/src/media/PDFs/EUCAST\\_files/Breakpoint\\_tables/v\\_8.1\\_Breakpoint\\_Tables.pdf](http://www.eucast.org/fileadmin/src/media/PDFs/EUCAST_files/Breakpoint_tables/v_8.1_Breakpoint_Tables.pdf) [Accessed: 13 June 2018].
- EVANS, M. E., FEOLA, D. J. and RAPP, R. P. 1999. Polymyxin B sulfate and colistin: old antibiotics for emerging multiresistant Gram-negative Bacteria. *Annals of Pharmacotherapy*, 33, 960-967.
- FAIR, R. J. and TOR, Y. 2014. Antibiotics and bacterial resistance in the 21st century. *Perspectives in Medicinal Chemistry*, 6, 25-64.
- FALAGAS, M. E., KASIAKOU, S. K. and SARAVOLATZ, L. D. 2005. Colistin: the revival of polymyxins for the management of multidrug-resistant Gram-negative bacterial infections. *Clinical Infectious Diseases*, 40, 1333-1341.
- FALAGAS, M. E. and RAFAILIDIS, P. I. 2007. Attributable mortality of *Acinetobacter baumannii*: no longer a controversial issue. *Critical Care*, 11, 134-134.

- FAN, L., GE, H., ZOU, S., XIAO, Y., WEN, H., LI, Y., FENG, H. and NIE, M. 2016. Sodium alginate conjugated graphene oxide as a new carrier for drug delivery system. *International Journal of Biological Macromolecules*, 93, 582-590.
- FDA. 2007. Colistin in nebulizer solution. *FDA Warning*. FDA, Silver Spring, Maryland, USA. Available at: <http://www.antimicrobe.org/h04c.files/history/Colistin-FDA%20Warning.pdf> [Accessed: 27 March 2018].
- FERGUSON, E. L., ALSHAME, A. M. J. and THOMAS, D. W. 2010a. Evaluation of hyaluronic acid-protein conjugates for polymer masked-unmasked protein therapy. *International Journal of Pharmaceutics*, 402, 95-102.
- FERGUSON, E. L., AZZOPARDI, E., ROBERTS, J. L., WALSH, T. R. and THOMAS, D. W. 2014. Dextrin-colistin conjugates as a model bioresponsive treatment for multidrug resistant bacterial infections. *Molecular Pharmaceutics*, 11, 4437-4447.
- FERGUSON, E. L. and DUNCAN, R. 2009. Dextrin-phospholipase A2: synthesis and evaluation as a bioresponsive anticancer conjugate. *Biomacromolecules*, 10, 1358-1364.
- FERGUSON, E. L., RICHARDSON, S. C. W. and DUNCAN, R. 2010b. Studies on the mechanism of action of dextrin-phospholipase A2 and its suitability for use in combination therapy. *Molecular Pharmaceutics*, 7, 510-521.
- FERGUSON, E. L., THOMAS, D. W., DESSEN, A., RYE, P. 2016. Polymyxin-alginate oligomer conjugates. *Patent application: GB 1617860.0*.
- FERNANDES, P. 2006. Antibacterial discovery and development - the failure of success? *Nature Biotechnology*, 24, 1497-1503.
- FERNANDO, L. P., KANDEL, P. K., YU, J., MCNEILL, J., ACKROYD, P. C. and CHRISTENSEN, K. A. 2010. Mechanism of cellular uptake of highly fluorescent conjugated polymer nanoparticles. *Biomacromolecules*, 11, 2675-2682.
- FIEDLER, U. and AUGUSTIN, H. G. 2006. Angiopoietins: a link between angiogenesis and inflammation. *Trends in Immunology*, 27, 552-558.
- FLEMMING, H. C. 2016. EPS-then and now. *Microorganisms*, 4, 41.
- FLEMMING, H. C., WINGENDER, J., SZEWZYK, U., STEINBERG, P., RICE, S. A. and KJELLEBERG, S. 2016. Biofilms: an emergent form of bacterial life. *Nature Reviews Microbiology*, 14, 563-575.
- FLOETTMANN, E., BUI, K., SOSTEK, M., PAYZA, K. and ELDON, M. 2017. Pharmacologic profile of naloxegol, a peripherally acting  $\mu$ -opioid receptor antagonist, for the treatment of opioid-induced constipation. *The Journal of Pharmacology and Experimental Therapeutics*, 361, 280-291.
- FORIER, K., MESSIAEN, A. S., RAEMDONCK, K., DESCHOUT, H., REJMAN, J., DE BAETS, F., NELIS, H., DE SMEDT, S. C., DEMEESTER, J., COENYE, T. and BRAECKMANS, K. 2012. Transport of nanoparticles in cystic fibrosis sputum and bacterial biofilms by single-particle tracking microscopy. *Nanomedicine*, 8, 935-949.
- FRIEDL, H., DÜNNHAUPT, S., HINTZEN, F., WALDNER, C., PARIKH, S., PEARSON, J. P., WILCOX, M. D. and BERNKOP-SCHNÜRCH, A.

2013. Development and evaluation of a novel mucus diffusion test system approved by self-nanoemulsifying drug delivery systems. *Journal of Pharmaceutical Sciences*, 102, 4406-4413.
- FRIEDMAN, M. 2004. Applications of the ninhydrin reaction for analysis of amino acids, peptides, and proteins to agricultural and biomedical sciences. *Journal of Agricultural and Food Chemistry*, 52, 385-406.
- FUCHS, P. C., BARRY, A. L. and BROWN, S. D. 1998. PMX-622 (polymyxin B-dextran 70) does not alter *in vitro* activities of 11 antimicrobial agents. *Antimicrobial Agents and Chemotherapy*, 42, 2765-2767.
- FUNG, C., NAUGHTON, S., TURNBULL, L., TINGPEJ, P., ROSE, B., ARTHUR, J., HU, H., HARMER, C., HARBOUR, C., HASSETT, D. J., WHITCHURCH, C. B. and MANOS, J. 2010. Gene expression of *Pseudomonas aeruginosa* in a mucin-containing synthetic growth medium mimicking cystic fibrosis lung sputum. *Journal of Medical Microbiology*, 59, 1089-1100.
- GALLARDO-GODOY, A., MULDOON, C., BECKER, B., ELLIOTT, A. G., LASH, L. H., HUANG, J. X., BUTLER, M. S., PELINGON, R., KAVANAGH, A. M., RAMU, S., PHETSANG, W., BLASKOVICH, M. A. and COOPER, M. A. 2016. Activity and predicted nephrotoxicity of synthetic antibiotics based on polymyxin B. *Journal of Medicinal Chemistry*, 59, 1068-1077.
- GANDRA, S., BARTER, D. M. and LAXMINARAYAN, R. 2014. Economic burden of antibiotic resistance: how much do we really know? *Clinical Microbiology and Infection*, 20, 973-980.
- GAO, H. and HE, Q. 2014. The interaction of nanoparticles with plasma proteins and the consequent influence on nanoparticles behavior. *Expert Opinion on Drug Delivery*, 11, 409-420.
- GARONZIK, S. M., LI, J., THAMLIKITKUL, V., PATERSON, D. L., SHOHAM, S., JACOB, J., SILVEIRA, F. P., FORREST, A. and NATION, R. L. 2011. Population pharmacokinetics of colistin methanesulfonate and formed colistin in critically ill patients from a multicenter study provide dosing suggestions for various categories of patients. *Antimicrobial Agents and Chemotherapy*, 55, 3284-3294.
- GARRETT, T. R., BHAKOO, M. and ZHANG, Z. 2008. Bacterial adhesion and biofilms on surfaces. *Progress in Natural Science*, 18, 1049-1056.
- GASPAR, R. and DUNCAN, R. 2009. Polymeric carriers: preclinical safety and the regulatory implications for design and development of polymer therapeutics. *Advanced Drug Delivery Reviews*, 61, 1220-1231.
- GIEDRAITIENĖ, A., VITKAUSKIENĖ, A., NAGINIENĖ, R. and PAVILONIS, A. 2011. Antibiotic resistance mechanisms of clinically important bacteria. *Medicina*, 47, 137-146.
- GIMÉNEZ, V., JAMES, C., ARMIÑÁN, A., SCHWEINS, R., PAUL, A. and VICENT, M. J. 2012. Demonstrating the importance of polymer-conjugate conformation in solution on its therapeutic output: diethylstilbestrol (DES)-polyacetals as prostate cancer treatment. *Journal of Controlled Release*, 159, 290-301.
- GIVENTAL, N. I., USHAKOV, S. N., PANARIN, E. F. and POPOVA, G. O. 1965. Experimental studies on penicillin polymer derivatives. *Antibiotiki*, 10, 701-706.

- GLOEDE, J., SCHEERANS, C., DERENDORF, H. and KLOFT, C. 2010. *In vitro* pharmacodynamic models to determine the effect of antibacterial drugs. *Journal of Antimicrobial Chemotherapy*, 65, 186-201.
- GODWIN, A., BOLINA, K., CLOCHARD, M., DINAND, E., RANKIN, S., SIMIC, S. and BROCCCHINI, S. 2001. New strategies for polymer development in pharmaceutical science - a short review. *Journal of Pharmacy and Pharmacology*, 53, 1175-1184.
- GORDEEV, M. F., LIU, J., WANG, Z. and YUAN, Z. 2016. Antimicrobial polymyxins for treatment of bacterial infections. *Patent application: WO2016/100578*.
- GRASSO, S., MEINARDI, G., DE CARNERI, I. and TAMASSIA, V. 1978. New *in vitro* model to study the effect of antibiotic concentration and rate of elimination on antibacterial activity. *Antimicrobial Agents and Chemotherapy*, 13, 570-576.
- GRECO, F. and VICENT, M. 2008. Polymer-drug conjugates: current status and future trends. *Frontiers in Bioscience*, 13, 2744-2756.
- GROO, A. C. and LAGARCE, F. 2014. Mucus models to evaluate nanomedicines for diffusion. *Drug Discovery Today*, 19, 1097-1108.
- GROVES, E. S., ALDWIN, L., WINKELHAKE, J. L., NITECKI, D. E., GAUNEY, S. and RUDOLPH, A. A. 1990. Polymer/antibiotic conjugate. *Patent application: WO1990/015628*.
- GUNN, J. S., LIM, K. B., KRUEGER, J., KIM, K., GUO, L., HACKETT, M. and MILLER, S. I. 1998. PmrA-PmrB-regulated genes necessary for 4-aminoarabinose lipid A modification and polymyxin resistance. *Molecular Microbiology*, 27, 1171-1182.
- GURJAR, M. 2015. Colistin for lung infection: an update. *Journal of Intensive Care*, 3, 3.
- HALPERIN, A., SHADKCHAN, Y., PISAREVSKY, E., SZPILMAN, A. M., SANDOVSKY, H., OSHEROV, N. and BENHAR, I. 2016. Novel water-soluble amphotericin B-PEG conjugates with low toxicity and potent *in vivo* efficacy. *Journal of Medicinal Chemistry*, 59, 1197-1206.
- HANBERGER, H., SVENSSON, E., NILSSON, M., NILSSON, L., HÖRNSTEN, G. and MALLER, R. 1993. Effects of imipenem on *Escherichia coli* studied using bioluminescence, viable counting and microscopy. *The Journal of Antimicrobial Chemotherapy*, 31, 245-260.
- HANCOCK, R. E. W. 1997. The bacterial outer membrane as a drug barrier. *Trends in Microbiology*, 5, 37-42.
- HARBOTTLE, H., THAKUR, S., ZHAO, S. and WHITE, D. G. 2006. Genetics of antimicrobial resistance. *Animal Biotechnology*, 17, 111-124.
- HARDWICKE, J., FERGUSON, E. L., MOSELEY, R., STEPHENS, P., THOMAS, D. W. and DUNCAN, R. 2008. Dextrin-rhEGF conjugates as bioresponsive nanomedicines for wound repair. *Journal of Controlled Release*, 130, 275-283.
- HARDWICKE, J., MOSELEY, R., STEPHENS, P., HARDING, K., DUNCAN, R. and THOMAS, D. W. 2010. Bioresponsive dextrin-rhEGF conjugates: *in vitro* evaluation in models relevant to its proposed use as a treatment for chronic wounds. *Molecular Pharmaceutics*, 7, 699-707.
- HASHEMI, M. M., ROVIG, J., WEBER, S., HILTON, B., FOROUZAN, M. M. and SAVAGE, P. B. 2017. Susceptibility of colistin-resistant, Gram-

- negative bacteria to antimicrobial peptides and ceragenins. *Antimicrobial Agents and Chemotherapy*, 61, e00292-17.
- HE, X., HWANG, H. M., AKER, W. G., WANG, P., LIN, Y., JIANG, X. and HE, X. 2014. Synergistic combination of marine oligosaccharides and azithromycin against *Pseudomonas aeruginosa*. *Microbiological Research*, 169, 759-767.
- HE, S. L., ZHANG, M., GENG, Z. J., YIN, Y. J. and YAO, K. D. 2005. Preparation and characterization of partially oxidized sodium alginate. *Chinese Journal of Applied Chemistry*, 22, 1007-1011.
- HENGZHUANG, W., SONG, Z., CIOFU, O., ONSØYEN, E., RYE, P. D. and HØIBY, N. 2016. OligoG CF-5/20 disruption of mucoid *Pseudomonas aeruginosa* biofilm in a murine lung infection model. *Antimicrobial Agents and Chemotherapy*, 60, 2620-2626.
- HENRY-STANLEY, M. J., HESS, D. J. and WELLS, C. L. 2014. Aminoglycoside inhibition of *Staphylococcus aureus* biofilm formation is nutrient dependent. *Journal of Medical Microbiology*, 63, 861-869.
- HERMANSON, G. T. 2013. Chapter 4 - Zero-length crosslinkers. *Bioconjugate Techniques (Third edition)*. Boston: Academic Press.
- HEYDORN, A., NIELSEN, A. T., HENTZER, M., STERNBERG, C., GIVSKOV, M., ERSBØLL, B. K. and MOLIN, S. 2000. Quantification of biofilm structures by the novel computer program comstat. *Microbiology*, 146, 2395-2407.
- HINDLER, J. A. and HUMPHRIES, R. M. 2013. Colistin MIC variability by method for contemporary clinical isolates of multidrug-resistant Gram-negative bacilli. *Journal of Clinical Microbiology*, 51, 1678-1684.
- HOGARDT, M., SCHMOLDT, S., GÖTZFRIED, M., ADLER, K. and HEESEMANN, J. 2004. Pitfalls of polymyxin antimicrobial susceptibility testing of *Pseudomonas aeruginosa* isolated from cystic fibrosis patients. *Journal of Antimicrobial Chemotherapy*, 54, 1057-1061.
- HOOPER, D. C. 2001. Minimizing potential resistance: the molecular view—a comment on Courvalin and Trieu-Cuot. *Clinical Infectious Diseases*, 33, S157-S160.
- HORCAJADA, J. P., SORLÍ, L., LUQUE, S., BENITO, N., SEGURA, C., CAMPILLO, N., MONTERO, M., ESTEVE, E., MIRELIS, B., POMAR, V., CUQUET, J., MARTÍ, C., GARRO, P. and GRAU, S. 2016. Validation of a colistin plasma concentration breakpoint as a predictor of nephrotoxicity in patients treated with colistin methanesulfonate. *International Journal of Antimicrobial Agents*, 48, 725-727.
- HSIEH, M. H., YU, C. M., YU, V. L. and CHOW, J. W. 1993. Synergy assessed by checkerboard a critical analysis. *Diagnostic Microbiology and Infectious Disease*, 16, 343-349.
- HUANG, J. X., BLASKOVICH, M. A. T., PELINGON, R., RAMU, S., KAVANAGH, A., ELLIOTT, A. G., BUTLER, M. S., MONTGOMERY, A. B. and COOPER, M. A. 2015. Mucin binding reduces colistin antimicrobial activity. *Antimicrobial Agents and Chemotherapy*, 59, 5925-5931.
- HUANG, K. C., MUKHOPADHYAY, R., WEN, B., GITAI, Z. and WINGREEN, N. S. 2008. Cell shape and cell-wall organization in Gram-negative bacteria. *Proceedings of the National Academy of Sciences of the*

- United States of America*, 105, 19282-19287.
- HUMPHRIES, R. 2015. Susceptibility testing of the polymyxins: where are we now? *Pharmacotherapy*, 35, 22-27.
- HUNT, B. E., WEBER, A., BERGER, A., RAMSEY, B. and SMITH, A. L. 1995. Macromolecular mechanisms of sputum inhibition of tobramycin activity. *Antimicrobial Agents and Chemotherapy*, 39, 34-39.
- IDSA. 2010. The 10 x '20 Initiative: pursuing a global commitment to develop 10 new antibacterial drugs by 2020. *Clinical Infectious Diseases*, 50, 1081-1083.
- ITO-KAGAWA, M. and KOYAMA, Y. 1980. Selective cleavage of a peptide antibiotic, colistin by colistinase. *The Journal of Antibiotics*, 33, 1551-1555.
- JAMAL, M., AHMAD, W., ANDLEEB, S., JALIL, F., IMRAN, M., NAWAZ, M. A., HUSSAIN, T., ALI, M., RAFIQ, M. and KAMIL, M. A. 2018. Bacterial biofilm and associated infections. *Journal of the Chinese Medical Association*, 81, 7-11.
- JATZKEWITZ, H. 1955. Peptamin (glycyl-L-leucyl-mescaline) bound to blood plasma expander (polyvinylpyrrolidone) as a new depot form of a biologically active primary amine (mescaline). *Z. Naturforsch*, 10b, 27-31.
- JAYOL, A., DUBOIS, V., POIREL, L. and NORDMANN, P. 2016. Rapid detection of polymyxin-resistant *Enterobacteriaceae* from blood cultures. *Journal of Clinical Microbiology*, 54, 2273-2277.
- JEANNOT, K., BOLARD, A. and PLÉSIAT, P. 2017. Resistance to polymyxins in Gram-negative organisms. *International Journal of Antimicrobial Agents*, 49, 526-535.
- JISKOOT, W., VAN SCHIE, R. M., CARSTENS, M. G. and SCHELLEKENS, H. 2009. Immunological risk of injectable drug delivery systems. *Pharmaceutical Research*, 26, 1303-1314.
- JOHNSEN, A. R., HAUSNER, M., SCHNELL, A. and WUERTZ, S. 2000. Evaluation of fluorescently labeled lectins for noninvasive localization of extracellular polymeric substances in *Sphingomonas* biofilms. *Applied and Environmental Microbiology*, 66, 3487-3491.
- JÖNSSON, A., FOERSTER, S., GOLPARIAN, D., HAMASUNA, R., JACOBSSON, S., LINDBERG, M., JENSEN, J. S., OHNISHI, M. and UNEMO, M. 2018. *In vitro* activity and time-kill curve analysis of sitafloxacin against a global panel of antimicrobial-resistant and multidrug-resistant *Neisseria gonorrhoeae* isolates. *APMIS (Acta Pathologica, Microbiologica, et Immunologica Scandinavica)*, 126, 29-37.
- KÁDÁR, B., KOCSIS, B., NAGY, K. and SZABÓ, D. 2013. The Renaissance of polymyxins. *Current Medicinal Chemistry*, 20, 3759-3773.
- KARVANEN, M., MALMBERG, C., LAGERBÄCK, P., FRIBERG, L. E. and CARS, O. 2017. Colistin is extensively lost during standard *in vitro* experimental conditions. *Antimicrobial Agents and Chemotherapy*, 61, e00857-17.
- KAŠČÁKOVÁ, S., MAIGRE, L., CHEVALIER, J., RÉFRÉGIERS, M. and PAGÈS, J. M. 2012. Antibiotic transport in resistant bacteria: synchrotron UV fluorescence microscopy to determine antibiotic

- accumulation with single cell resolution. *PLOS ONE*, 7, e38624.
- KHAN, S., TØNDERVIK, A., SLETTA, H., KLINKENBERG, G., EMANUEL, C., ONSØYEN, E., MYRVOLD, R., HOWE, R. A., WALSH, T. R., HILL, K. E. and THOMAS, D. W. 2012. Overcoming drug resistance with alginate oligosaccharides able to potentiate the action of selected antibiotics. *Antimicrobial Agents and Chemotherapy*, 56, 5134-5141.
- KHANDARE, J. and MINKO, T. 2006. Polymer-drug conjugates: progress in polymeric prodrugs. *Progress in Polymer Science*, 31, 359-397.
- KIM, H. S., LEE, C. G. and LEE, E. Y. 2011. Alginate lyase: structure, property, and application. *Biotechnology and Bioprocess Engineering*, 16, 843.
- KIRCHNER, S., FOTHERGILL, J. L., WRIGHT, E. A., JAMES, C. E., MOWAT, E. and WINSTANLEY, C. 2012. Use of artificial sputum medium to test antibiotic efficacy against *Pseudomonas aeruginosa* in conditions more relevant to the cystic fibrosis lung. *Journal of Visualized Experiments*, 5, 3857.
- KLINE, T., HOLUB, D., THERRIEN, J., LEUNG, T. and RYCKMAN, D. 2001. Synthesis and characterization of the colistin peptide polymyxin E1 and related antimicrobial peptides. *The Journal of Peptide Research*, 57, 175-187.
- KLINE, T., TRENT, M. S., STEAD, C. M., LEE, M. S., SOUSA, M. C., FELISE, H. B., NGUYEN, H. V. and MILLER, S. I. 2008. Synthesis of and evaluation of lipid A modification by 4-substituted 4-deoxy arabinose analogs as potential inhibitors of bacterial polymyxin resistance. *Bioorganic and Medicinal Chemistry Letters*, 18, 1507-1510.
- KO, K. S., CHOI, Y. and LEE, J. Y. 2017. Old drug, new findings: colistin resistance and dependence of *Acinetobacter baumannii*. *Precision and Future Medicine*, 1, 159-167.
- KOHANSKI, M. A., DWYER, D. J., HAYETE, B., LAWRENCE, C. A. and COLLINS, J. J. 2007. A common mechanism of cellular death induced by bactericidal antibiotics. *Cell*, 130, 797-810.
- KOSTAKIOTI, M., HADJIFRANGISKOU, M. and HULTGREN, S. J. 2013. Bacterial biofilms: development, dispersal, and therapeutic strategies in the dawn of the postantibiotic era. *Cold Spring Harbor Perspectives in Medicine*, 3, a010306.
- KUMAR, A. and SCHWEIZER, H. P. 2005. Bacterial resistance to antibiotics: active efflux and reduced uptake. *Advanced Drug Delivery Reviews*, 57, 1486-1513.
- KUMARASAMY, K. K., TOLEMAN, M. A., WALSH, T. R., BAGARIA, J., BUTT, F., BALAKRISHNAN, R., CHAUDHARY, U., DOUMITH, M., GISKE, C. G., IRFAN, S., KRISHNAN, P., KUMAR, A. V., MAHARJAN, S., MUSHTAQ, S., NOORIE, T., PATERSON, D. L., PEARSON, A., PERRY, C., PIKE, R., RAO, B., RAY, U., SARMA, J. B., SHARMA, M., SHERIDAN, E., THIRUNARAYAN, M. A., TURTON, J., UPADHYAY, S., WARNER, M., WELFARE, W., LIVERMORE, D. M. and WOODFORD, N. 2010. Emergence of a new antibiotic resistance mechanism in India, Pakistan, and the UK: a molecular, biological, and epidemiological study. *The Lancet Infectious Diseases*, 10, 597-602.
- KWA, A., TAM, V. H. and FALAGAS, M. 2008. Polymyxins: a review of the current status including recent developments. *Annals of the Academy*

- of Medicine*, 37, 870-883.
- LAMBERT, P. A. 2002. Cellular impermeability and uptake of biocides and antibiotics in Gram-positive bacteria and *Mycobacteria*. *Journal of Applied Microbiology*, 92, 46S-54S.
- LAMBERTINI, M., FERREIRA, A., DEL MASTRO, L., DANESI, R. and PRONZATO, P. 2015. Pegfilgrastim for the prevention of chemotherapy-induced febrile neutropenia in patients with solid tumors. *Expert Opinion on Biological Therapy*, 15, 1799-1817.
- LAMPPA, J. W., ACKERMAN, M. E., LAI, J. I., SCANLON, T. C. and GRISWOLD, K. E. 2011. Genetically engineered alginate lyase-PEG conjugates exhibit enhanced catalytic function and reduced immunoreactivity. *PLOS ONE*, 6, e17042.
- LANDERSDORFER, C. B. and NATION, R. L. 2015. Colistin: how should it be dosed for the critically ill? *Seminars in Respiratory and Critically Care Medicine*, 36, 126-135.
- LANDMAN, D., BRATU, S., ALAM, M. and QUALE, J. 2005. Citywide emergence of *Pseudomonas aeruginosa* strains with reduced susceptibility to polymyxin B. *Journal of Antimicrobial Chemotherapy*, 55, 954-957.
- LARSON, N. and GHANDEHARI, H. 2012. Polymeric conjugates for drug delivery. *Chemistry of Materials*, 24, 840-853.
- LAURIENZO, P. 2010. Marine polysaccharides in pharmaceutical applications: an overview. *Marine Drugs*, 8, 2435-2465.
- LAVERMAN, P., DAMS, E. T. M., STORM, G., HAFMANS, T. G., CROES, H. J., OYEN, W. J. G., CORSTENS, F. H. M. and BOERMAN, O. C. 2001. Microscopic localization of PEG-liposomes in a rat model of focal infection. *Journal of Controlled Release*, 75, 347-355.
- LAWRENCE, J. R. and NEU, T. R. 1999. Confocal laser scanning microscopy for analysis of microbial biofilms. *Methods in Enzymology*, 310, 131-144.
- LE, J., ASHLEY, E. D., NEUHAUSER, M. M., BROWN, J., GENTRY, C., KLEPSE, M. E., MARR, A. M., SCHILLER, D., SCHWIESOW, J. N., TICE, S., VANDENBUSSCHE, H. L., WOOD, G. C. 2010. Consensus summary of aerosolized antimicrobial agents: application of guideline criteria. *Pharmacotherapy*, 30, 562-584.
- LEE, W. J., HAN PARK, J. and R. ROBINSON, J. 2000. Bioadhesive-based dosage forms: the next generation. *Journal of Pharmaceutical Sciences*, 89, 850-866.
- LEE, E., LEE, J. and JON, S. 2010. A novel approach to oral delivery of insulin by conjugating with low molecular weight chitosan. *Bioconjugate Chemistry*, 21, 1720-1723.
- LEESE, R. A. 2010. Antibiotic compositions for the treatment of Gram-negative infections. *Patent application: WO2010075416*.
- LEVIN, B. R. and ROZEN, D. E. 2006. Non-inherited antibiotic resistance. *Nature Reviews Microbiology*, 4, 556-562.
- LEVISON, M. E. and LEVISON, J. H. 2009. Pharmacokinetics and pharmacodynamics of antibacterial agents. *Infectious Disease Clinics of North America*, 23, 791-815.
- LEVY, Y., HERSHFIELD, M. S., FERNANDEZ-MEJIA, C., POLMAR, S. H.,

- SCUDIERY, D., BERGER, M. and SORENSEN, R. U. 1988. Adenosine deaminase deficiency with late onset of recurrent infections: response to treatment with polyethylene glycol-modified adenosine deaminase. *The Journal of Pediatrics*, 113, 312-317.
- LEWIS, K. 2006. Persister cells, dormancy and infectious disease. *Nature Reviews Microbiology*, 5, 48-56.
- LI, J., COULTHARD, K., MILNE, R., NATION, R. L., CONWAY, S., PECKHAM, D., ETHERINGTON, C. and TURNIDGE, J. 2003a. Steady-state pharmacokinetics of intravenous colistin methanesulphonate in patients with cystic fibrosis. *Journal of Antimicrobial Chemotherapy*, 52, 987-992.
- LI, Z., LIU, G., LAW, S. J. and SELLS, T. 2002. Water-soluble fluorescent diblock nanospheres. *Biomacromolecules*, 3, 984-990.
- LI, J., MILNE, R. W., NATION, R. L., TURNIDGE, J. D., COULTHARD, K. and JOHNSON, D. W. 2001. A simple method for the assay of colistin in human plasma, using pre-column derivatization with 9-fluorenylmethyl chloroformate in solid-phase extraction cartridges and reversed-phase high-performance liquid chromatography. *Journal of Chromatography B: Biomedical Sciences and Applications*, 761, 167-175.
- LI, J., MILNE, R. W., NATION, R. L., TURNIDGE, J. D., COULTHARD, K. and VALENTINE, J. 2002. Simple method for assaying colistin methanesulfonate in plasma and urine using high-performance liquid chromatography. *Antimicrobial Agents and Chemotherapy*, 46, 3304-3307.
- LI, J., MILNE, R. W., NATION, R. L., TURNIDGE, J. D., SMEATON, T. C. and COULTHARD, K. 2003b. Use of high-performance liquid chromatography to study the pharmacokinetics of colistin sulfate in rats following intravenous administration. *Antimicrobial Agents and Chemotherapy*, 47, 1766-1770.
- LI, R. C., NIX, D. E. and SCHENTAG, J. J. 1993. New turbidimetric assay for quantitation of viable bacterial densities. *Antimicrobial Agents and Chemotherapy*, 37, 371-374.
- LI, X. Z., PLÉSIAT, P. and NIKAIDO, H. 2015. The challenge of efflux-mediated antibiotic resistance in Gram-negative bacteria. *Clinical Microbiology Reviews*, 28, 337-418.
- LI, J., RAYNER, C. R., NATION, R. L., OWEN, R. J., SPELMAN, D., TAN, K. E. and LIOLIOS, L. 2006. Heteroresistance to colistin in multidrug-resistant *Acinetobacter baumannii*. *Antimicrobial Agents and Chemotherapy*, 50, 2946-2950.
- LI, J., XIE, S., AHMED, S., WANG, F., GU, Y., ZHANG, C., CHAI, X., WU, Y., CAI, J. and CHENG, G. 2017. Antimicrobial activity and resistance: influencing factors. *Frontiers in Pharmacology*, 8, 364.
- LIANG, J. and LIU, B. 2016. ROS-responsive drug delivery systems. *Bioengineering and Translational Medicine*, 1, 239-251.
- LILLEHOJ, E. P. and KIM, K. C. 2002. Airway mucus: its components and function. *Archives of Pharmacal Research*, 25, 770-780.
- LIMOLI, D. H., JONES, C. J. and WOZNIAK, D. J. 2015. Bacterial extracellular polysaccharides in biofilm formation and function. *Microbiology spectrum*, 3, doi: 10.1128/microbiolspec.MB-0011-2014.

- LIN, L., NONEJUIE, P., MUNGUIA, J., HOLLANDS, A., OLSON, J., DAM, Q., KUMARASWAMY, M., RIVERA, H., CORRIDEN, R., ROHDE, M., HENSLER, M. E., BURKART, M. D., POGLIANO, J., SAKOULAS, G. and NIZET, V. 2015. Azithromycin synergizes with cationic antimicrobial peptides to exert bactericidal and therapeutic activity against highly multidrug-resistant Gram-negative bacterial pathogens. *EBioMedicine*, 2, 690-698.
- LIN, S. D., TANG, T., ZHAO, T. B. and LIU, S. J. 2017. Central projections and connections of lumbar primary afferent fibers in adult rats: effectively revealed using Texas red-dextran amine tracing. *Neural Regeneration Research*, 12, 1695-1702.
- LINDESMITH, L. A., BAINES, R. D., BIGELOW, D. B. and PETTY, T. L. 1968. Reversible respiratory paralysis associated with polymyxin therapy. *Annals of Internal Medicine*, 68, 318-327.
- LIPINSKI, C. 2002. Poor aqueous solubility - an industry wide problem in drug discovery. *American Pharmaceutical Review*, 5, 82-85.
- LISTER, P. D. 2006. The role of pharmacodynamic research in the assessment and development of new antibacterial drugs. *Biochemical Pharmacology*, 71, 1057-1065.
- LIU, L., FENG, Y., ZHANG, X., MCNALLY, A. and ZONG, Z. 2017. New variant of *mcr-3* in an extensively drug-resistant *Escherichia coli* clinical isolate carrying *mcr-1* and *bla*NDM-5. *Antimicrobial Agents and Chemotherapy*, 61, e01757-17.
- LIU, Y. Y., WANG, Y., WALSH, T. R., YI, L. X., ZHANG, R., SPENCER, J., DOI, Y., TIAN, G., DONG, B., HUANG, X., YU, L. F., GU, D., REN, H., CHEN, X., LV, L., HE, D., ZHOU, H., LIANG, Z., LIU, J. H. and SHEN, J. 2016. Emergence of plasmid-mediated colistin resistance mechanism *MCR-1* in animals and human beings in China: a microbiological and molecular biological study. *The Lancet Infectious Diseases*, 16, 161-168.
- LIU, Y., YANG, S. F., LI, Y., XU, H., QIN, L. and TAY, J. H. 2004. The influence of cell and substratum surface hydrophobicities on microbial attachment. *Journal of Biotechnology*, 110, 251-256.
- LOCK, J. Y., CARLSON, T. L. and CARRIER, R. L. 2018. Mucus models to evaluate the diffusion of drugs and particles. *Advanced Drug Delivery Reviews*, 124, 34-49.
- LORITE, G. S., RODRIGUES, C. M., DE SOUZA, A. A., KRANZ, C., MIZAIKOFF, B. and COTTA, M. A. 2011. The role of conditioning film formation and surface chemical changes on *Xylella fastidiosa* adhesion and biofilm evolution. *Journal of Colloid and Interface Science*, 359, 289-295.
- LO-TEN-FOE, J. R., DE SMET, A. M., DIEDEREN, B. M., KLUYTMANS, J. A. and VAN KEULEN, P. H. 2007. Comparative evaluation of the VITEK 2, disk diffusion, Etest, broth microdilution, and agar dilution susceptibility testing methods for colistin in clinical isolates, including heteroresistant *Enterobacter cloacae* and *Acinetobacter baumannii* strains. *Antimicrobial Agents and Chemotherapy*, 51, 3726-3730.
- LOU, N., TAKANO, T., PEI, Y., XAVIER, A. L., GOLDMAN, S. A. and NEDERGAARD, M. 2016. Purinergic receptor P2RY12-dependent

- microglial closure of the injured blood-brain barrier. *Proceedings of the National Academy of Sciences*, 113, 1074-1079.
- LU, X., HU, Y., LUO, M., ZHOU, H., WANG, X., DU, Y., LI, Z., XU, J., ZHU, B., XU, X. and KAN, B. 2017. *MCR-1.6*, a new *MCR* variant carried by an IncP plasmid in a colistin-resistant *Salmonella enterica* serovar *Typhimurium* isolate from a healthy individual. *Antimicrobial Agents and Chemotherapy*, 61, e02632-16.
- MA, J., RUBIN, B. K. and VOYNOW, J. A. 2017. Mucins, mucus, and goblet cells. *Chest*, 154, 169-176.
- MACGOWAN, A. 2008. BSAC working parties on resistance surveillance. Clinical implications of antimicrobial resistance for therapy. *The Journal of Antimicrobial Chemotherapy*, 62, ii105-ii114.
- MACNAIR, C. R., STOKES, J. M., CARFRAE, L. A., FIEBIG-COMYN, A. A., COOMBES, B. K., MULVEY, M. R. and BROWN, E. D. 2018. Overcoming *mcr-1* mediated colistin resistance with colistin in combination with other antibiotics. *Nature Communications*, 9, 458.
- MAEDA, H. 2013. The link between infection and cancer: tumor vasculature, free radicals, and drug delivery to tumors via the EPR effect. *Cancer Science*, 104, 779-789.
- MAEDA, H., WU, J., OKAMOTO, T., MARUO, K. and AKAIKE, T. 1999. Kallikrein-kinin in infection and cancer. *Immunopharmacology*, 43, 115-128.
- MAEDA, H., WU, J., SAWA, T., MATSUMURA, Y. and HORI, K. 2000. Tumor vascular permeability and the EPR effect in macromolecular therapeutics: a review. *Journal of Controlled Release*, 65, 271-284.
- MAGEE, T. V., BROWN, M. F., STARR, J. T., ACKLEY, D. C., ABRAMITE, J. A., AUBRECHT, J., BUTLER, A., CRANDON, J. L., DIB-HAJJ, F., FLANAGAN, M. E., GRANSKOG, K., HARDINK, J. R., HUBAND, M. D., IRVINE, R., KUHN, M., LEACH, K. L., LI, B., LIN, J., LUKE, D. R., MACVANE, S. H., MILLER, A. A., MCCURDY, S., MCKIM, J. M., NICOLAU, D. P., NGUYEN, T. T., NOE, M. C., O'DONNELL, J. P., SEIBEL, S. B., SHEN, Y., STEPAN, A. F., TOMARAS, A. P., WILGA, P. C., ZHANG, L., XU, J. and CHEN, J. M. 2013. Discovery of dap-3 polymyxin analogues for the treatment of multidrug-resistant Gram-negative nosocomial infections. *Journal of Medicinal Chemistry*, 56, 5079-5093.
- MALANOVIC, N. and LOHNER, K. 2016. Antimicrobial peptides targeting Gram-positive bacteria. *Pharmaceuticals*, 9, E59.
- MARKOVSKY, E., BAABUR-COHEN, H., ELDAR-BOOCK, A., OMER, L., TIRAM, G., FERBER, S., OFEK, P., POLYAK, D., SCOMPARIN, A. and SATCHI-FAINARO, R. 2012. Administration, distribution, metabolism and elimination of polymer therapeutics. *Journal of Controlled Release*, 161, 446-460.
- MARSHALL, K. C. 1986. Adsorption and adhesion processes in microbial growth at interfaces. *Advances in Colloid and Interface Science*, 25, 59-86.
- MARTIN, E. E., DAVID, J. F. and ROBERT, P. R. 1999. Polymyxin B sulfate and colistin: old antibiotics for emerging multiresistant Gram-negative bacteria. *Annals of Pharmacotherapy*, 33, 960-967.

- MATSUMURA, Y. and MAEDA, H. 1986. A new concept for macromolecular therapeutics in cancer chemotherapy: mechanism of tumortropic accumulation of proteins and the antitumor agent smancs. *Cancer Research*, 46, 6387-6392.
- MCQUILLEN, M. P., CANTOR, H. E. and O'ROURKE, J. R. 1968. Myasthenic syndrome associated with antibiotics. *Archives of Neurology*, 18, 402-415.
- MELÉNDEZ-ALAFORT, L., NADALI, A., PASUT, G., ZANGONI, E., DE CARO, R., CARIOLATO, L., GIRON, M. C., CASTAGLIUOLO, I., VERONESE, F. M. and MAZZI, U. 2009. Detection of sites of infection in mice using 99mTc-labeled PN2S-PEG conjugated to UBI and 99mTc-UBI: a comparative biodistribution study. *Nuclear Medicine and Biology*, 36, 57-64.
- MENETREY, A., FRASCHINI, M. C., BRAVO, J., BUSH, J., DECOSTERD, G., CONTENT, S., ANDERSON, C., VAN DUIJN, E. and NICOLAS-METRAL, V. 2017. Mass balance, pharmacokinetics and metabolism of the antimicrobial afabycin following intravenous and oral administration in humans. *Clinical Therapeutics*, 39, e65.
- MENSA, B., HOWELL, G. L., SCOTT, R. and DEGRADO, W. F. 2014. Comparative mechanistic studies of brilacidin, daptomycin, and the antimicrobial peptide LL16. *Antimicrobial Agents and Chemotherapy*, 58, 5136-5145.
- MIAO, T., WANG, J., ZENG, Y., LIU, G. and CHEN, X. 2018. Polysaccharide-based controlled release systems for therapeutics delivery and tissue engineering: from bench to bedside. *Advanced Science*, 5, 1700513.
- MICHALOPOULOS, A. S. and FALAGAS, M. E. 2011. Colistin: recent data on pharmacodynamics properties and clinical efficacy in critically ill patients. *Annals of Intensive Care*, 1, 30.
- MILES, A. A., MISRA, S. S. and IRWIN, J. O. 1938. The estimation of the bactericidal power of the blood. *The Journal of Hygiene*, 38, 732-749.
- MONTELLA, I. R., SCHAMA, R. and VALLE, D. 2012. The classification of esterases: an important gene family involved in insecticide resistance - a review. *Memórias do Instituto Oswaldo Cruz*, 107(4), 437-449.
- MORRIS, C. J., ALJAYYOSSI, G., MANSOUR, O., GRIFFITHS, P. and GUMBLETON, M. 2017. Endocytic uptake, transport and macromolecular interactions of anionic PAMAM dendrimers within lung tissue. *Pharmaceutical Research*, 34, 2517-2531.
- MOSMANN, T. 1983. Rapid colorimetric assay for cellular growth and survival: application to proliferation and cytotoxicity assays. *Journal of Immunological Methods*, 65, 55-63.
- MU, H., NIU, H., WANG, D., SUN, F., SUN, Y. and DUAN, J. 2016. Chitosan conjugation enables intracellular bacteria susceptible to aminoglycoside antibiotic. *Glycobiology*, 26, 1190-1197.
- MUNITA, J. M. and ARIAS, C. A. 2016. Mechanisms of antibiotic resistance. *Microbiology Spectrum*, 4, doi: 10.1128/microbiolspec.VMBF-0016-2015.
- MYINT, T., EVANS, M. E., BURGESS, D. R. and GREENBERG, R. N. 2016. Respiratory muscle paralysis associated with colistin, polymyxin B, and muscle relaxants drugs: a case report. *Journal of Investigative Medicine*

- High Impact Case Reports*, 4, 2324709616638362.
- MYRVOLD, R., ONSØYEN, E. and STEWART, D. 2010. Evaluation of repeat-dose toxicity with the alginate oligomer, OligoG. *Interscience Conference on Antimicrobial Agents and Chemotherapy*. Boston, USA. Poster F1-1606.
- NATHAN, A., ZALIPSKY, S., ERTEL, S. I., AGATHOS, S. N., YARMUSH, M. L. and KOHN, J. 1993. Copolymers of lysine and polyethylene glycol: a new family of functionalized drug carriers. *Bioconjugate Chemistry*, 4, 54-62.
- NATION, R. L., GARONZIK, S. M., LI, J., THAMLIKITKUL, V., GIAMARELLOS-BOURBOULIS, E. J., PATERSON, D. L., TURNIDGE, J. D., FORREST, A. and SILVEIRA, F. P. 2016. Updated US and European dose recommendations for intravenous colistin: how do they perform? *Clinical Infectious Diseases*, 62, 552-558.
- NEISES, B. and STEGLICH, W. 1978. Simple method for the esterification of carboxylic acids. *Angewandte Chemie International Edition in English*, 17, 522-524.
- NIELSEN, E. I. and FRIBERG, L. E. 2013. Pharmacokinetic-pharmacodynamic modeling of antibacterial drugs. *Pharmacological Reviews*, 65, 1053-1090.
- NIKOLA, S., JANINE, S. and JOERG, O. 2015. Potential application of antimicrobial peptides in the treatment of bacterial biofilm infections. *Current Pharmaceutical Design*, 21, 67-84.
- NIRANJANA, E. S., SAMBATH KUMAR, R., SUDHA, M. and VENKATESWARAMURTHY, N. 2018. Review on clinically developing antibiotics. *International Journal of Applied Pharmaceutics*, 10, 13-18.
- NORDGÅRD, C. T., NONSTAD, U., OLDERØY, M. Ø., ESPEVIK, T. and DRAGET, K. I. 2014. Alterations in mucus barrier function and matrix structure induced by guluronate oligomers. *Biomacromolecules*, 15, 2294-2300.
- NORDMANN, P., JAYOL, A. and POIREL, L. 2016. Rapid detection of polymyxin resistance in *Enterobacteriaceae*. *Emerging Infectious Diseases*, 22, 1038-1043.
- O'NEILL, J. 2014. Antimicrobial resistance: tackling a crisis for the health and wealth of nations. *The Review on Antimicrobial Resistance*. Available at: [https://amr-review.org/sites/default/files/AMR%20Review%20Paper%20-%20Tackling%20a%20crisis%20for%20the%20health%20and%20wealth%20of%20nations\\_1.pdf](https://amr-review.org/sites/default/files/AMR%20Review%20Paper%20-%20Tackling%20a%20crisis%20for%20the%20health%20and%20wealth%20of%20nations_1.pdf) [Accessed: 10 May 2018].
- O'NEILL, J. 2016. Tackling drug-resistant infections globally: final report and recommendations. *The review on Antimicrobial Resistance*. Available at: [https://amr-review.org/sites/default/files/160518\\_Final%20paper\\_with%20cover.pdf](https://amr-review.org/sites/default/files/160518_Final%20paper_with%20cover.pdf) [Accessed: 15 May 2018].
- OMOTOYINBO, O. V. and OMOTOYINBO, B. I. 2016. Effect of varying NaCl concentrations on the growth curve of *Escherichia coli* and *Staphylococcus aureus*. *Cell Biology*, 4, 31-34.
- OTTERLEI, M., ØSTGAARD, K., SKJÅK-BRÆK, G., SMIDSRØD, O., SOONSHIONG, P. and ESPEVIK, T. 1991. Induction of cytokine production from human monocytes stimulated with alginate. *Journal of Immunotherapy*, 10, 286-291.

- OWEN, R. J., LI, J., NATION, R. L. and SPELMAN, D. 2007. *In vitro* pharmacodynamics of colistin against *Acinetobacter baumannii* clinical isolates. *Journal of Antimicrobial Chemotherapy*, 59, 473-477.
- OWENS, D. E. and PEPPAS, N. A. 2006. Opsonization, biodistribution, and pharmacokinetics of polymeric nanoparticles. *International Journal of Pharmaceutics*, 307, 93-102.
- PARAMESWARAN, N. and PATIAL, S. 2010. Tumor necrosis factor- $\alpha$  signalling in macrophages. *Critical Reviews in Eukaryotic Gene Expression*, 20, 87-103.
- PADILLA, E., LLOBET, E., DOMÉNECH-SÁNCHEZ, A., MARTÍNEZ-MARTÍNEZ, L., BENGOCHEA, J. A. and ALBERTÍ, S. 2010. *Klebsiella pneumoniae* AcrAB efflux pump contributes to antimicrobial resistance and virulence. *Antimicrobial Agents and Chemotherapy*, 54, 177-183.
- PALMER, K. L., AYE, L. M. and WHITELEY, M. 2007. Nutritional cues control *Pseudomonas aeruginosa* multicellular behavior in cystic fibrosis sputum. *Journal of Bacteriology*, 189, 8079-8087.
- PALMER, R. J. and STERNBERG, C. 1999. Modern microscopy in biofilm research: confocal microscopy and other approaches. *Current Opinion in Biotechnology*, 10, 263-268.
- PAMP, S. J., GJERMENSEN, M., JOHANSEN, H. K. and TOLKER-NIELSEN, T. 2008. Tolerance to the antimicrobial peptide colistin in *Pseudomonas aeruginosa* biofilms is linked to metabolically active cells, and depends on the *pmr* and *mexAB-oprM* genes. *Molecular Microbiology*, 68, 223-240.
- PARNHAM, M. J., HABER, V. E., GIAMARELLOS-BOURBOULIS, E. J., PERLETTI, G., VERLEDEN, G. M. and VOS, R. 2014. Azithromycin: mechanisms of action and their relevance for clinical applications. *Pharmacology and Therapeutics*, 143, 225-245.
- PASSALACQUA, K. D., CHARBONNEAU, M. E. and O'RIORDAN, M. X. 2016. Bacterial metabolism shapes the host-pathogen interface. *Microbiology Spectrum*, 4, doi: 10.1128/microbiolspec.VMBF-0027-2015.
- PAUL, A., JAMES, C., HEENAN, R. K. and SCHWEINS, R. 2010. Drug mimic induced conformational changes in model polymer-drug conjugates characterized by small-angle neutron scattering. *Biomacromolecules*, 11, 1978-1982.
- PENDLETON, J. N., GORMAN, S. P. and GILMORE, B. F. 2013. Clinical relevance of the ESKAPE pathogens. *Expert Review of Anti-infective Therapy*, 11, 297-308.
- PESCHEL, A., OTTO, M., JACK, R. W., KALBACHER, H., JUNG, G. and GÖTZ, F. 1999. Inactivation of the *dlt* operon in *Staphylococcus aureus* confers sensitivity to defensins, protegrins, and other antimicrobial peptides. *Journal of Biological Chemistry*, 274, 8405-8410.
- PFALLER, M. A., FLAMM, R. K., MCCURDY, S. P., PILLAR, C. M., SHORTRIDGE, D. and JONES, R. N. 2018. Delafloxacin *in vitro* broth microdilution and disk diffusion antimicrobial susceptibility testing guidelines: susceptibility breakpoint criteria and quality control ranges for an expanded-spectrum anionic fluoroquinolone. *Journal of Clinical*

- Microbiology*, 56, e00339-18.
- PINCET, F., ADRIEN, V., YANG, R., DELACOTTE, J., ROTHMAN, J. E., URBACH, W. and TARESTE, D. 2016. FRAP to characterize molecular diffusion and interaction in various membrane environments. *PLOS ONE*, 11, e0158457.
- POTERA, C. 1999. Forging a link between biofilms and disease. *Science*, 283, 1837-1839.
- POTERA, C. 2010. Antibiotic resistance: biofilm dispersing agent rejuvenates older antibiotics. *Environmental Health Perspectives*, 118, A288.
- POWELL, L. C., PRITCHARD, M. F., EMANUEL, C., ONSØYEN, E., RYE, P. D., WRIGHT, C. J., HILL, K. E. and THOMAS, D. W. 2014. A nanoscale characterization of the interaction of a novel alginate oligomer with the cell surface and motility of *Pseudomonas aeruginosa*. *American Journal of Respiratory Cell and Molecular Biology*, 50, 483-492.
- POWELL, L. C., PRITCHARD, M. F., FERGUSON, E. L., POWELL, K. A., PATEL, S. U., RYE, P. D., SAKELLAKOU, S. M., BUURMA, N. J., BRILLIANT, C. D., COPPING, J. M., MENZIES, G. E., LEWIS, P. D., HILL, K. E. and THOMAS, D. W. 2018. Targeted disruption of the extracellular polymeric network of *Pseudomonas aeruginosa* biofilms by alginate oligosaccharides. *NPJ Biofilms and Microbiomes*, 4, 13.
- POWELL, L. C., SOWEDAN, A., KHAN, S., WRIGHT, C. J., HAWKINS, K., ONSØYEN, E., MYRVOLD, R., HILL, K. E. and THOMAS, D. W. 2013. The effect of alginate oligosaccharides on the mechanical properties of Gram-negative biofilms. *Biofouling*, 29, 413-421.
- PRATT, L. A. and KOLTER, R. 1998. Genetic analysis of *Escherichia coli* biofilm formation: roles of flagella, motility, chemotaxis and type I pili. *Molecular Microbiology*, 30, 285-293.
- PRITCHARD, M. 2014. OligoG alginate nanomedicine mediated disruption of mucin barriers and microbial biofilms. *PhD Thesis*, Cardiff University, Cardiff, UK.
- PRITCHARD, M. F., POWELL, L. C., JACK, A. A., POWELL, K., BECK, K., FLORANCE, H., FORTON, J., RYE, P. D., DESSEN, A., HILL, K. E. and THOMAS, D. W. 2017. A low-molecular-weight alginate oligosaccharide disrupts Pseudomonas microcolony formation and enhances antibiotic effectiveness. *Antimicrobial Agents and Chemotherapy*, 61, e00762-17.
- PRITCHARD, M. F., POWELL, L. C., MENZIES, G. E., LEWIS, P. D., HAWKINS, K., WRIGHT, C., DOULL, I., WALSH, T. R., ONSØYEN, E., DESSEN, A., MYRVOLD, R., RYE, P. D., MYRSET, A. H., STEVENS, H. N., HODGES, L. A., MACGREGOR, G., NEILLY, J. B., HILL, K. E. and THOMAS, D. W. 2016. A new class of safe oligosaccharide polymer therapy to modify the mucus barrier of chronic respiratory disease. *Molecular Pharmaceutics*, 13, 863-872.
- PU, H. L., CHIANG, W. L., MAITI, B., LIAO, Z. X., HO, Y. C., SHIM, M. S., CHUANG, E. Y., XIA, Y. and SUNG, H. W. 2014. Nanoparticles with dual responses to oxidative stress and reduced pH for drug release and anti-inflammatory applications. *ACS Nano*, 8, 1213-1221.
- QIN, Y. 2008. Alginate fibres: an overview of the production processes and applications in wound management. *Polymer International*, 57, 171-

- RAO, G. G., LY, N. S., HAAS, C. E., GARONZIK, S., FORREST, A., BULITTA, J. B., KELCHLIN, P. A., HOLDEN, P. N., NATION, R. L., LI, J. and TSUJI, B. T. 2014. New dosing strategies for an old antibiotic: pharmacodynamics of front-loaded regimens of colistin at simulated pharmacokinetics in patients with kidney or liver disease. *Antimicrobial Agents and Chemotherapy*, 58, 1381-1388.
- RIAHIFARD, N., TAVAKOLI, K., YAMAKI, J., PARANG, K. and TIWARI, R. 2017. Synthesis and evaluation of antimicrobial activity of [R4W4K]-levofloxacin and [R4W4K]-levofloxacin-q conjugates. *Molecules*, 22, E957.
- RICE, L. B. 2008. Federal funding for the study of antimicrobial resistance in nosocomial pathogens: no ESKAPE. *The Journal of Infectious Diseases*, 197, 1079-1081.
- RICHARDSON, S. C., WALLOM, K. L., FERGUSON, E. L., DEACON, S. P., DAVIES, M. W., POWELL, A. J., PIPER, R. C. and DUNCAN, R. 2008. The use of fluorescence microscopy to define polymer localisation to the late endocytic compartments in cells that are targets for drug delivery. *Journal of Controlled Release*, 127, 1-11.
- RINGSORF, H. 1975. Structure and properties of pharmacologically active polymers. *Journal of Polymer Science: Polymer Symposia*, 51, 135-153.
- ROBERTS, K. D., AZAD, M. A., WANG, J., HORNE, A. S., THOMPSON, P. E., NATION, R. L., VELKOV, T. and LI, J. 2015. Antimicrobial activity and toxicity of the major lipopeptide components of polymyxin B and colistin: last-line antibiotics against multidrug-resistant Gram-negative bacteria. *ACS Infectious Diseases*, 1, 568-575.
- ROBERTS, J. L., CATTOZ, B., SCHWEINS, R., BECK, K., THOMAS, D. W., GRIFFITHS, P. C. and FERGUSON, E. L. 2016. *In vitro* evaluation of the interaction of dextrin-colistin conjugates with bacterial lipopolysaccharide. *Journal of Medicinal Chemistry*, 59, 647-654.
- ROHRSCHEIDER, M., BHAGWAT, S., KRAMPE, R., MICHLER, V., BREITKREUTZ, J. and HOCHHAUS, G. 2015. Evaluation of the transwell system for characterization of dissolution behavior of inhalation drugs: effects of membrane and surfactant. *Molecular Pharmaceutics*, 12, 2618-2624.
- ROSEEUW, E., COESSENS, V., BALAZUC, A. M., LAGRANDERIE, M., CHAVAROT, P., PESSINA, A., NERI, M. G., SCHACHT, E., MARCHAL, G. and DOMURADO, D. 2003. Synthesis, degradation, and antimicrobial properties of targeted macromolecular prodrugs of norfloxacin. *Antimicrobial Agents and Chemotherapy*, 47, 3435-3441.
- ROTH, P. J., KIM, K. S., BAE, S. H., SOHN, B. H., THEATO, P. and ZENTEL, R. 2009. Hetero-telechelic dye-labeled polymer for nanoparticle decoration. *Macromolecular Rapid Communications*, 30, 1274-1278.
- SADER, H. S., FLAMM, R. K., DALE, G. E., RHOMBERG, P. R. and CASTANHEIRA, M. 2018. Murepavadin activity tested against contemporary (2016-17) clinical isolates of XDR *Pseudomonas aeruginosa*. *Journal of Antimicrobial Chemotherapy*, 73, 2400-2404.
- SADER, H. S., RHOMBERG, P. R., FLAMM, R. K. and JONES, R. N. 2012.

- Use of a surfactant (polysorbate 80) to improve MIC susceptibility testing results for polymyxin B and colistin. *Diagnostic Microbiology and Infectious Disease*, 74, 412-414.
- SAHA, S., CHHATBAR, M. U., MAHATO, P., PRAVEEN, L., SIDDHANTA, A. K. and DAS, A. 2012. Rhodamine-alginate conjugate as self indicating gel beads for efficient detection and scavenging of Hg<sup>2+</sup> and Cr<sup>3+</sup> in aqueous media. *Chemical Communications*, 48, 1659-1661.
- SAIMAN, L. 2007. Clinical utility of synergy testing for multidrug-resistant *Pseudomonas aeruginosa* isolated from patients with cystic fibrosis: 'the motion for'. *Paediatric Respiratory Reviews*, 8, 249-255.
- SAMPSON, T. R., LIU, X., SCHROEDER, M. R., KRAFT, C. S., BURD, E. M. and WEISS, D. S. 2012. Rapid killing of *Acinetobacter baumannii* by polymyxins is mediated by a hydroxyl radical death pathway. *Antimicrobial Agents and Chemotherapy*, 56, 5642-5649.
- SANDRI, A. M., LANDERSDORFER, C. B., JACOB, J., BONIATTI, M. M., DALAROSA, M. G., FALCI, D. R., BEHLE, T. F., BORDINHÃO, R. C., WANG, J., FORREST, A., NATION, R. L., LI, J. and ZAVASCKI, A. P. 2013. Population pharmacokinetics of intravenous polymyxin B in critically ill patients: implications for selection of dosage regimens. *Clinical Infectious Diseases*, 57, 524-531.
- SCHÄBERLE, T. F. and HACK, I. M. 2014. Overcoming the current deadlock in antibiotic research. *Trends in Microbiology*, 22, 165-167.
- SCHNEIDER-FUTSCHIK, E. K., PAULIN, O. K. A., HOYER, D., ROBERTS, K. D., ZIOGAS, J., BAKER, M. A., KARAS, J., LI, J. and VELKOV, T. 2018. Sputum active polymyxin lipopeptides: activity against cystic fibrosis *Pseudomonas aeruginosa* isolates and their interactions with sputum biomolecules. *ACS Infectious Diseases*, 4, 646-655.
- SCHÜTZ, C. A., JUILLERAT-JEANNERET, L., MUELLER, H., LYNCH, I. and RIEDIKER, M. 2013. Therapeutic nanoparticles in clinics and under clinical evaluation. *Nanomedicine*, 8, 449-467.
- SCHWARTZ, R. S., EDELMAN, E., VIRMANI, R., CARTER, A., GRANADA, J. F., KALUZA, G. L., CHRONOS, N. A., ROBINSON, K. A., WAKSMAN, R., WEINBERGER, J., WILSON, G. J. and WILENSKY, R. L. 2008. Drug-eluting stents in preclinical studies updated consensus recommendations for preclinical evaluation. *Circulation. Cardiovascular Interventions*, 1, 143-153.
- SCOTT, L. J. 2013. Glatiramer acetate: a review of its use in patients with relapsing-remitting multiple sclerosis and in delaying the onset of clinically definite multiple sclerosis. *CNS Drugs*, 27, 971-988.
- SEIB, F. P., JONES, A. T. and DUNCAN, R. 2006. Establishment of subcellular fractionation techniques to monitor the intracellular fate of polymer therapeutics I. Differential centrifugation fractionation B16F10 cells and use to study the intracellular fate of HPMA copolymer-doxorubicin. *Journal of Drug Targeting*, 14, 375-390.
- SEIB, F. P., JONES, A. T. and DUNCAN, R. 2007. Comparison of the endocytic properties of linear and branched PEIs, and cationic PAMAM dendrimers in B16f10 melanoma cells. *Journal of Controlled Release*, 117, 291-300.
- SHAPIRO, D. J., HICKS, L. A., PAVIA, A. T. and HERSH, A. L. 2014. Antibiotic

- prescribing for adults in ambulatory care in the USA, 2007-09. *Journal of Antimicrobial Chemotherapy*, 69, 234-240.
- SHEN, S., WU, Y., LIU, Y. and WU, D. 2017. High drug-loading nanomedicines: progress, current status, and prospects. *International Journal of Nanomedicine*, 12, 4085-4109.
- SHINGEL, K. I. 2004. Current knowledge on biosynthesis, biological activity, and chemical modification of the exopolysaccharide, pullulan. *Carbohydrate Research*, 339, 447-460.
- SILHAVY, T. J., KAHNE, D. and WALKER, S. 2010. The bacterial cell envelope. *Cold Spring Harbor Perspectives in Biology*, 2, a000414.
- SIMPSON, J. A., SMITH, S. E. and DEAN, R. T. 1993. Alginate may accumulate in cystic fibrosis lung because the enzymatic and free radical capacities of phagocytic cells are inadequate for its degradation. *Biochemistry and Molecular Biology International*, 30, 1021-1034.
- SIVANESAN, S., ROBERTS, K., WANG, J., CHEA, S. E., THOMPSON, P. E., LI, J., NATION, R. L. and VELKOV, T. 2017. Pharmacokinetics of the individual major components of polymyxin B and colistin in rats. *Journal of Natural Products*, 80, 225-229.
- SMITH, R. and COAST, J. 2013. The true cost of antimicrobial resistance. *British Medical Journal*, 346, f1493.
- SMITH, P. K., KROHN, R. I., HERMANSON, G. T., MALLIA, A. K., GARTNER, F. H., PROVENZANO, M. D., FUJIMOTO, E. K., GOEKE, N. M., OLSON, B. J. and KLENK, D. C. 1985. Measurement of protein using bicinchoninic acid. *Analytical Biochemistry*, 150, 76-85.
- SONG, J. Y., KEE, S. Y., HWANG, I. S., SEO, Y. B., JEONG, H. W., KIM, W. J. and CHEONG, H. J. 2007. *In vitro* activities of carbapenem/sulbactam combination, colistin, colistin/rifampicin combination and tigecycline against carbapenem-resistant *Acinetobacter baumannii*. *Journal of Antimicrobial Chemotherapy*, 60, 317-322.
- SORLÍ, L., LUQUE, S., GRAU, S., BERENGUER, N., SEGURA, C., MONTERO, M. M., ÁLVAREZ-LERMA, F., KNOBEL, H., BENITO, N. and HORCAJADA, J. P. 2013. Trough colistin plasma level is an independent risk factor for nephrotoxicity: a prospective observational cohort study. *BMC Infectious Diseases*, 13, 380-380.
- SOSNIK, A. 2014. Alginate particles as platform for drug delivery by the oral route: state-of-the-art. *ISRN Pharmaceutics*, 2014, 926157.
- SPAPEN, H., JACOBS, R., VAN GORP, V., TROUBLEYN, J. and HONORÉ, P. M. 2011. Renal and neurological side effects of colistin in critically ill patients. *Annals of Intensive Care*, 1, 14.
- SRIRAMULU, D. D., LÜNSDORF, H., LAM, J. S. and RÖMLING, U. 2005. Microcolony formation: a novel biofilm model of *Pseudomonas aeruginosa* for the cystic fibrosis lung. *Journal of Medical Microbiology*, 54, 667-676.
- STANSLY, P. G., SHEPHERD, R. G. and WHITE, H. J. 1947. Polymyxin: a new chemotherapeutic agent. *Bulletin of the John Hopkins Hospital*, 81, 43-54.
- STEBBINS, N. D., OUIOMET, M. A. and UHRICH, K. E. 2014. Antibiotic-containing polymers for localized, sustained drug delivery. *Advanced Drug Delivery Reviews*, 78, 77-87.

- STONE, M. R. L., BUTLER, M. S., PHETSANG, W., COOPER, M. A. and BLASKOVICH, M. A. T. 2018. Fluorescent antibiotics: new research tools to fight antibiotic resistance. *Trends in Biotechnology*, 36, 523-536.
- STRAHL, H. and ERRINGTON, J. 2017. Bacterial membranes: structure, domains, and function. *Annual Review of Microbiology*, 71, 519-538.
- SUTHERLAND, I. W. 1995. Polysaccharide lyases. *FEMS Microbiology Reviews*, 16, 323-347.
- SUTHERLAND, I. W. 2001a. Biofilm exopolysaccharides: a strong and sticky framework. *Microbiology*, 147, 3-9.
- SUTHERLAND, I. W. 2001b. The biofilm matrix - an immobilized but dynamic microbial environment. *Trends in Microbiology*, 9, 222-227.
- SWIERCZEWSKA, M., LEE, K. C. and LEE, S. 2015. What is the future of PEGylated therapies? *Expert Opinion on Emerging Drugs*, 20, 531-536.
- TALELLI, M. and VICENT, M. J. 2014. Reduction sensitive poly(L-glutamic acid) (PGA)-protein conjugates designed for polymer masked-unmasked protein therapy. *Biomacromolecules*, 15, 4168-4177.
- TAM, V. H., SCHILLING, A. N. and NIKOLAOU, M. 2005. Modelling time-kill studies to discern the pharmacodynamics of meropenem. *Journal of Antimicrobial Chemotherapy*, 55, 699-706.
- TAN, T. Y., NG, L. S., TAN, E. and HUANG, G. 2007. *In vitro* effect of minocycline and colistin combinations on imipenem-resistant *Acinetobacter baumannii* clinical isolates. *Journal of Antimicrobial Chemotherapy*, 60, 421-423.
- TANEJA, N. and KAUR, H. 2016. Insights into newer antimicrobial agents against Gram-negative bacteria. *Microbiology Insights*, 9, 9-19.
- TANWAR, J., DAS, S., FATIMA, Z. and HAMEED, S. 2014. Multidrug resistance: an emerging crisis. *Interdisciplinary Perspectives on Infectious Diseases*, 2014, 541340.
- TAYLOR, S. N., MARRAZZO, J., BATTEIGER, B. E., HOOK, E. W., SEÑA, A. C., LONG, J., WIERZBICKI, M. R., KWAK, H., JOHNSON, S. M., LAWRENCE, K. and MUELLER, J. 2018a. Single-dose zoliflodacin (ETX0914) for treatment of urogenital gonorrhea. *New England Journal of Medicine*, 379, 1835-1845.
- TAYLOR, S. N., MORRIS, D. H., AVERY, A. K., WORKOWSKI, K. A., BATTEIGER, B. E., TIFFANY, C. A., PERRY, C. R., RAYCHAUDHURI, A., SCANGARELLA-OMAN, N. E., HOSSAIN, M. and DUMONT, E. F. 2018b. Gepotidacin for the treatment of uncomplicated urogenital gonorrhea: a phase 2, randomized, dose-ranging, single-oral dose evaluation. *Clinical Infectious Diseases*, 67, 504-512.
- TOUTAIN, C. M., CAIZZA, N. C., ZEGANS, M. E. and O'TOOLE, G. A. 2007. Roles for flagellar stators in biofilm formation by *Pseudomonas aeruginosa*. *Research in Microbiology*, 158, 471-477.
- TSAKOS, M., SCHAFFERT, E. S., CLEMENT, L. L., VILLADSEN, N. L. and POULSEN, T. B. 2015. Ester coupling reactions - an enduring challenge in the chemical synthesis of bioactive natural products. *Natural Product Reports*, 32, 605-632.
- TSUJI, B. T., LANDERSDORFER, C. B., LENHARD, J. R., CHEAH, S. E., THAMLIKITKUL, V., RAO, G. G., HOLDEN, P. N., FORREST, A.,

- BULITTA, J. B., NATION, R. L. and LI, J. 2016. Paradoxical effect of polymyxin B: high drug exposure amplifies resistance in *Acinetobacter baumannii*. *Antimicrobial Agents and Chemotherapy*, 60, 3913-3920.
- TSUNEDA, S., AIKAWA, H., HAYASHI, H., YUASA, A. and HIRATA, A. 2003. Extracellular polymeric substances responsible for bacterial adhesion onto solid surface. *FEMS Microbiology Letters*, 223, 287-292.
- ULLAH, H. and ALI, S. 2017. Chapter 1 - Classification of anti-bacterial agents and their functions. *Antibacterial Agents*. IntechOpen. Available at: <https://www.intechopen.com/books/antibacterial-agents/classification-of-anti-bacterial-agents-and-their-functions> [Accessed: 24 August 2018].
- UPPULURI, P. and LOPEZ-RIBOT, J. L. 2016. Go forth and colonize: dispersal from clinically important microbial biofilms. *PLOS Pathogens*, 12, e1005397.
- VAARA, M., FOX, J., LOIDL, G., SIIKANEN, O., APAJALAHTI, J., HANSEN, F., FRIMODT-MØLLER, N., NAGAI, J., TAKANO, M. and VAARA, T. 2008. Novel polymyxin derivatives carrying only three positive charges are effective antibacterial agents. *Antimicrobial Agents and Chemotherapy*, 52, 3229-3236.
- VAARA, M., SIIKANEN, O., APAJALAHTI, J., FOX, J., FRIMODT-MØLLER, N., HE, H., POUDYAL, A., LI, J., NATION, R. L. and VAARA, T. 2010. A novel polymyxin derivative that lacks the fatty acid tail and carries only three positive charges has strong synergism with agents excluded by the intact outer membrane. *Antimicrobial Agents and Chemotherapy*, 54, 3341-3346.
- VAARA, M. and VAARA, T. 2013. The novel polymyxin derivative NAB739 is remarkably less cytotoxic than polymyxin B and colistin to human kidney proximal tubular cells. *International Journal of Antimicrobial Agents*, 41, 292-293.
- VADDADY, P. K., LEE, R. E. and MEIBOHM, B. 2010. *In vitro* pharmacokinetic/pharmacodynamic models in anti-infective drug development: focus on TB. *Future Medicinal Chemistry*, 2, 1355-1369.
- VASOO, S. 2017. Susceptibility testing for the polymyxins: two steps back, three steps forward? *Journal of Clinical Microbiology*, 55, 2573-2582.
- VATANSEVER, C. and TURETGEN, I. 2018. Investigating the effects of different physical and chemical stress factors on microbial biofilm. *Water SA*, 44, 308-317.
- VELKOV, T., ROBERTS, K. D., NATION, R. L., THOMPSON, P. E. and LI, J. 2013. Pharmacology of polymyxins: new insights into an 'old' class of antibiotics. *Future Microbiology*, 8, 711-724.
- VELKOV, T., ROBERTS, K. D., THOMPSON, P. E. and LI, J. 2016. Polymyxins: a new hope in combating Gram-negative superbugs? *Future Medicinal Chemistry*, 8, 1017-1025.
- VELKOV, T., THOMPSON, P. E., NATION, R. L. and LI, J. 2010. Structure-activity relationships of polymyxin antibiotics. *Journal of Medicinal Chemistry*, 53, 1898-1916.
- VENTOLA, C. L. 2015. The antibiotic resistance crisis. *Pharmacy and Therapeutics*, 40, 277-283.
- VERCAUTEREN, R., BRUNEEL, D., SCHACHT, E. and DUNCAN, R. 1990.

- Effect of the chemical modification of dextran on the degradation by dextranase. *Journal of Bioactive and Compatible Polymers*, 5, 4-15.
- VERHOEF, J. J. and ANCHORDOQUY, T. J. 2013. Questioning the use of PEGylation for drug delivery. *Drug Delivery and Translational Research*, 3, 499-503.
- VEVE, M. P. and WAGNER, J. L. 2018. Lefamulin: review of a promising novel pleuromutilin antibiotic. *Pharmacotherapy*, 38, 935-946.
- VICENT, M., DIEUDONNÉ, L., CARBAJO, R. and PINEDA-LUCENA, A. 2008. Polymer conjugates as therapeutics: future trends, challenges and opportunities. *Expert Opinion on Drug Delivery*, 5, 593-614.
- VICENT, M. J., RINGSDORF, H. and DUNCAN, R. 2009. Polymer therapeutics: clinical applications and challenges for development. *Advanced Drug Delivery Reviews*, 61, 1117-1120.
- VIVEIROS, M., DUPONT, M., RODRIGUES, L., COUTO, I., DAVIN-REGLI, A., MARTINS, M., PAGÈS, J. M. and AMARAL, L. 2007. Antibiotic stress, genetic response and altered permeability of *E. coli*. *PloS One*, 2, e365.
- VOLLMER, W. 2008. Structural variation in the glycan strands of bacterial peptidoglycan. *FEMS Microbiology Reviews*, 32, 287-306.
- VOYNOW, J. A. and RUBIN, B. K. 2009. Mucins, mucus, and sputum. *Chest*, 135, 505-512.
- VU, B., CHEN, M., CRAWFORD, R. and IVANOVA, E. 2009. Bacterial extracellular polysaccharides involved in biofilm formation. *Molecules*, 14, 2535-2554.
- WANG, X., WANG, Y., ZHOU, Y., LI, J., YIN, W., WANG, S., ZHANG, S., SHEN, J., SHEN, Z. and WANG, Y. 2018. Emergence of a novel mobile colistin resistance gene, *mcr-8*, in NDM-producing *Klebsiella pneumoniae*. *Emerging Microbes and Infections*, 7, 122-122.
- WANG, Y., ZHOU, J., QIU, L., WANG, X., CHEN, L., LIU, T. and DI, W. 2014. Cisplatin-alginate conjugate liposomes for targeted delivery to EGFR-positive ovarian cancer cells. *Biomaterials*, 35, 4297-4309.
- WARNER, D. M. and LEVY, S. B. 2010. Different effects of transcriptional regulators MarA, SoxS and Rob on susceptibility of *Escherichia coli* to cationic antimicrobial peptides (CAMPs): rob-dependent CAMP induction of the marRAB operon. *Microbiology*, 156, 570-578.
- WEERS, J. 2015. Inhaled antimicrobial therapy - barriers to effective treatment. *Advanced Drug Delivery Reviews*, 85, 24-43.
- WERNEBURG, M., ZERBE, K., JUHAS, M., BIGLER, L., STALDER, U., KAECH, A., ZIEGLER, U., OBRECHT, D., EBERL, L. and ROBINSON, J. A. 2012. Inhibition of lipopolysaccharide transport to the outer membrane in *Pseudomonas aeruginosa* by peptidomimetic antibiotics. *ChemBioChem*, 13, 1767-1775.
- WHITE, R. L. 2001. What *in vitro* models of infection can and cannot do. *Pharmacotherapy*, 21, 292S-301S.
- WHO. 2017. An analysis of the antibacterial clinical development pipeline, including tuberculosis. *Antibacterial Agents in Clinical Development*. Available at: <https://apps.who.int/iris/bitstream/handle/10665/258965/WHO-EMP-IAU-2017.11-eng.pdf;jsessionid=E020AC90752045866BE B3864CBA004A6?sequence=1> [Accessed: 23 September 2018].

- WIEDERHOLD, N. P., JORGENSEN, J. H., BOAKES, S., COLLINS, M. S., MCELMEEL, M., CUSHION, M. T. and PATTERSON, T. F. 2015. Antibacterial activity of novel polymyxin B derivatives against Gram-negative bacteria and initial toxicity assessment. *55th Interscience Conference on Antimicrobial Agents and Chemotherapy*. San Diego, USA. F-734.
- WONG, T. Y., PRESTON, L. A. and SCHILLER, N. L. 2000. Alginate lyase: review of major sources and enzyme characteristics, structure-function analysis, biological roles, and applications. *Annual Review of Microbiology*, 54, 289-340.
- XAVIER, B. B., LAMMENS, C., RUHAL, R., KUMAR-SINGH, S., BUTAYE, P., GOOSSENS, H. and MALHOTRA-KUMAR, S. 2016. Identification of a novel plasmid-mediated colistin-resistance gene, *mcr-2*, in *Escherichia coli*, Belgium, June 2016. *Eurosurveillance*, 21, doi: 10.2807/1560-7917.ES.2016.21.27.30280.
- XIONG, M. H., BAO, Y., YANG, X. Z., ZHU, Y. H. and WANG, J. 2014. Delivery of antibiotics with polymeric particles. *Advanced Drug Delivery Reviews*, 78, 63-76.
- XU, J. B., BARTLEY, J. P. and JOHNSON, R. A. 2003. Preparation and characterization of alginate hydrogel membranes crosslinked using a water-soluble carbodiimide. *Journal of Applied Polymer Science*, 90, 747-753.
- XU, Y., LIN, J., CUI, T., SRINIVAS, S. and FENG, Y. 2018. Mechanistic insights into transferable polymyxin resistance among gut bacteria. *Journal of Biological Chemistry*, 293, 4350-4365.
- YANG, Y. Q., LI, Y. X., LEI, C. W., ZHANG, A. Y. and WANG, H. N. 2018. Novel plasmid-mediated colistin resistance gene *mcr-7.1* in *Klebsiella pneumoniae*. *Journal of Antimicrobial Chemotherapy*, 73, 1791-1795.
- YANG, Q., LI, M., SPILLER, O. B., ANDREY, D. O., HINCHLIFFE, P., LI, H., MACLEAN, C., NIUMSUP, P., POWELL, L., PRITCHARD, M., PAPKOU, A., SHEN, Y., PORTAL, E., SANDS, K., SPENCER, J., TANSAWAI, U., THOMAS, D., WANG, S., WANG, Y., SHEN, J. and WALSH, T. 2017. Balancing *mcr-1* expression and bacterial survival is a delicate equilibrium between essential cellular defence mechanisms. *Nature Communications*, 8, 2054.
- YANG, J. S., XIE, Y. J. and HE, W. 2011. Research progress on chemical modification of alginate: a review. *Carbohydrate Polymers*, 84, 33-39.
- YIN, W., LI, H., SHEN, Y., LIU, Z., WANG, S., SHEN, Z., ZHANG, R., WALSH, T. R., SHEN, J. and WANG, Y. 2017. Novel plasmid-mediated colistin resistance gene *mcr-3* in *Escherichia coli*. *mBio*, 8, e00543-17.
- YOURASSOWSKY, E., VAN DER LINDEN, M. P., LISMONT, M. J., CROKAERT, F. and GLUPCZYNSKI, Y. 1985. Correlation between growth curve and killing curve of *Escherichia coli* after a brief exposure to suprainhibitory concentrations of ampicillin and piperacillin. *Antimicrobial Agents and Chemotherapy*, 28, 756-760.
- YU, Z., QIN, W., LIN, J., FANG, S. and QIU, J. 2015. Antibacterial mechanisms of polymyxin and bacterial resistance. *BioMed Research International*, 2015, 679109.
- YU, Z., ZHU, Y., QIN, W., YIN, J. and QIU, J. 2017. Oxidative stress induced

- by polymyxin E is involved in rapid killing of *Paenibacillus polymyxa*. *BioMed Research International*, 2017, 5437139.
- ZAMAN, S. B., HUSSAIN, M. A., NYE, R., MEHTA, V., MAMUN, K. T. and HOSSAIN, N. 2017. A review on antibiotic resistance: alarm bells are ringing. *Cureus*, 9, e1403.
- ZANETTI-DOMINGUES, L. C., TYNAN, C. J., ROLFE, D. J., CLARKE, D. T. and MARTIN-FERNANDEZ, M. 2013. Hydrophobic fluorescent probes introduce artifacts into single molecule tracking experiments due to non-specific binding. *PLOS ONE*, 8, e74200.
- ZHANG, A. Y., LEI, C. W., YANG, Y. Q., LI, Y. X. and WANG, H. N. 2018. Novel plasmid-mediated colistin resistance gene *mcr-7.1* in *Klebsiella pneumoniae*. *Journal of Antimicrobial Chemotherapy*, 73, 1791-1795.
- ZHANG, Z., NADEZHINA, E. and WILKINSON, K. J. 2011. Quantifying diffusion in a biofilm of *Streptococcus mutans*. *Antimicrobial Agents and Chemotherapy*, 55, 1075-1081.
- ZHAO, F., FENG, Y., LÜ, X., MCNALLY, A. and ZONG, Z. 2017a. IncP plasmid carrying colistin resistance gene *mcr-1* in *Klebsiella pneumoniae* from hospital sewage. *Antimicrobial Agents and Chemotherapy*, 61, e02229-16.
- ZHAO, F., FENG, Y., LÜ, X., MCNALLY, A. and ZONG, Z. 2017b. Remarkable diversity of *Escherichia coli* carrying *mcr-1* from hospital sewage with the identification of two new *mcr-1* variants. *Frontiers in Microbiology*, 8, 2094.
- ZHOU, H., WEIR, M. D., ANTONUCCI, J. M., SCHUMACHER, G. E., ZHOU, X. D. and XU, H. H. 2014. Evaluation of three-dimensional biofilms on antibacterial bonding agents containing novel quaternary ammonium methacrylates. *International Journal of Oral Science*, 6, 77-86.
- ZHU, C., SCHNEIDER, E. K., WANG, J., KEMPE, K., WILSON, P., VELKOV, T., LI, J., DAVIS, T. P., WHITTAKER, M. R. and HADDLETON, D. M. 2017. A traceless reversible polymeric colistin prodrug to combat multidrug-resistant (MDR) Gram-negative bacteria. *Journal of Controlled Release*, 259, 83-91.
- ZURFLUH, K., KLUMPP, J., NÜESCH-INDERBINEN, M. and STEPHAN, R. 2016. Full-length nucleotide sequences of *mcr-1*-harboring plasmids isolated from extended-spectrum- $\beta$ -lactamase-producing *Escherichia coli* isolates of different origins. *Antimicrobial Agents and Chemotherapy*, 60, 5589-5591.

# **Appendix 1**

## **Publications**

## Book chapter

Ferguson, E.L., Varache, M., Stokniene, J., Thomas, D.W. 2018. Chapter - Polysaccharides for protein and peptide conjugation. In: Polymer-Protein Conjugates: From PEGylation and Beyond.

## Abstracts

Stokniene, J., Powell, L.C., Rye, P.D., Hill, K.E., Thomas, D.W., Ferguson, E.L. 2019. OligoG conjugation inhibits bacterial growth and reduces cytotoxicity of colistin and polymyxin B. *42nd European Cystic Fibrosis Conference*. Liverpool, UK. Submitted.

Abdulkarim, M., Powell, L.C., Stokniene, J., Spiller, O.B., Walsh, T.R., Hill, K.E., Thomas, D.W., Gumbleton, M. 2019. Development of a Multiple Particle Tracking (MPT) biofilm model to detect the mechanical and micro-rheological effects of antibiotic treatment. *American Society for Microbiology*. San Francisco, USA. Submitted.

Stokniene, J., Thomas, D.W., Rye, P.D., Hill, K.E., Ferguson, E.L. 2019. Optimising exposure-response relationships of antibiotics by conjugation to alginate oligomers. *Antimicrobial Resistance and Infection Seminar*. Cardiff, UK.

Stokniene, J., Powell, L.C., Rye, P.D., Hill, K.E., Thomas, D.W., Ferguson, E.L. 2018. Optimising exposure-response relationships of antibiotics by conjugation to alginate oligomers. *Proceedings of the 12th International Symposium on Polymer Therapeutics*. Valencia, Spain. P32.

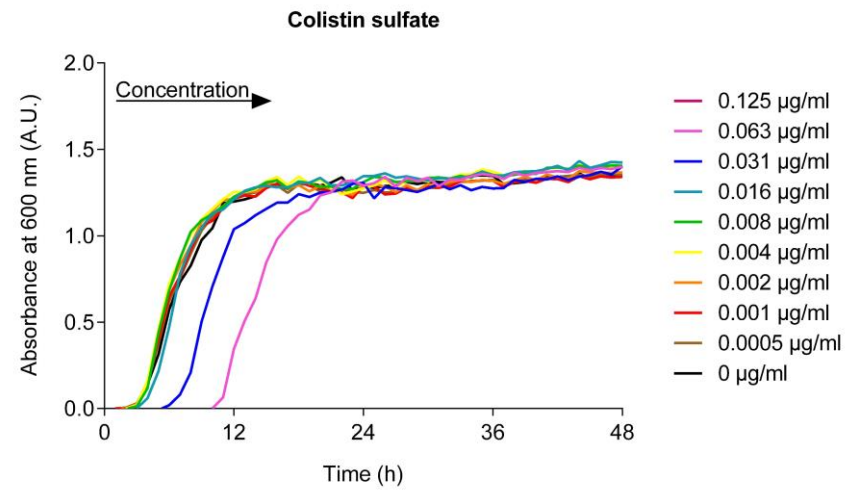
Stokniene, J., Thomas, D.W., Rye, P.D., Hill, K.E., Ferguson, E.L. 2017. Alginate conjugated polymyxin shows reduced toxicity in HK-2 cells. *The Cardiff Annual Infection and Immunity Meeting*. Cardiff, UK. p86.

Stokniene, J., Thomas, D.W., Rye, P.D., Hill, K.E., Ferguson, E.L. 2017. Alginate conjugated polymyxin shows reduced toxicity in HK2 cells. *European Tissue Repair Society*. Brussels, Belgium.

## **Appendix 2**

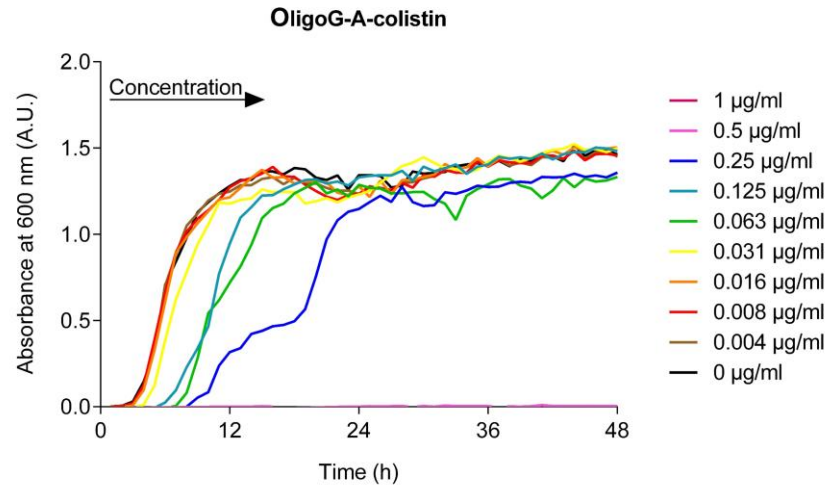
**Bacterial growth curves in the presence  
of colistin sulfate and OligoG-colistin  
conjugates**

(a)

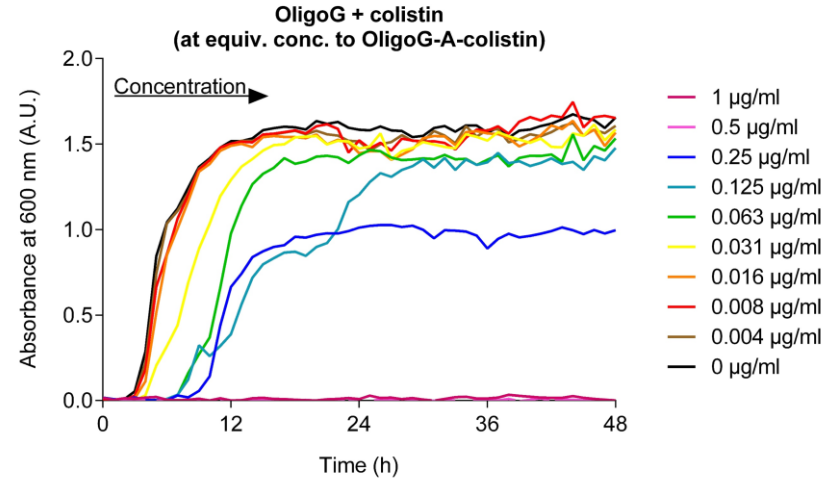


**Appendix 2.1** Bacterial growth curves for *K. pneumoniae* KP05 506 (48 h) in the presence of (a) colistin sulfate, (b and f) OligoG-colistin conjugates (amide and ester linked). Controls used included (c and g) unconjugated colistin plus OligoG, (d and h) OligoG and (e and i) the high molecular weight alginate, PRONOVA, all at equivalent concentrations used in corresponding conjugates (n = 3).

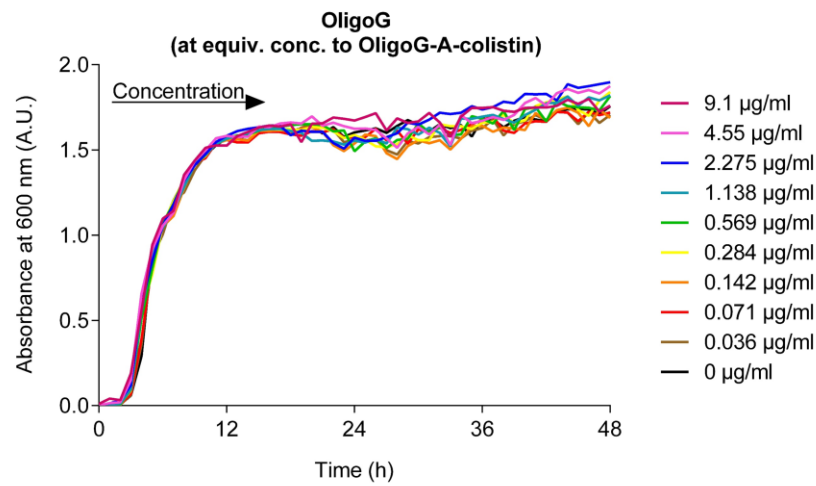
(b)



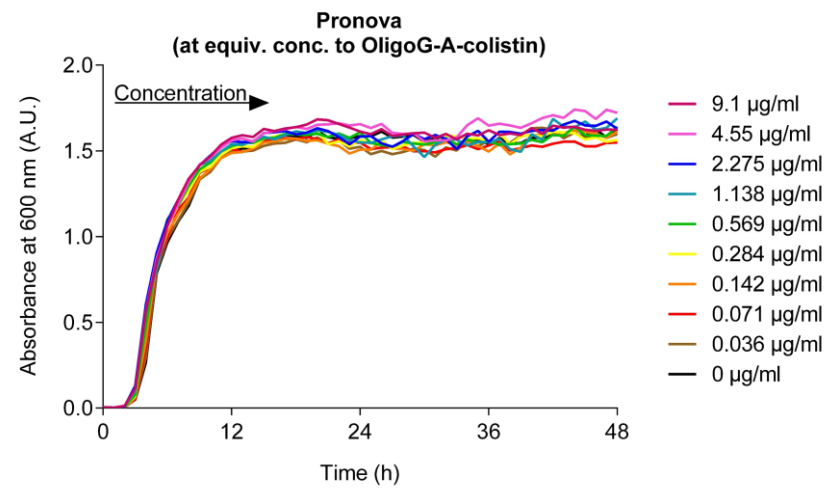
(c)



(d)

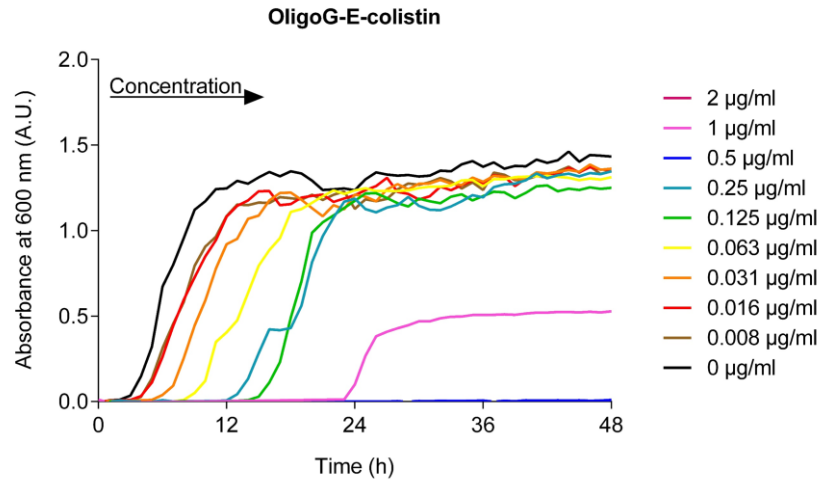


(e)

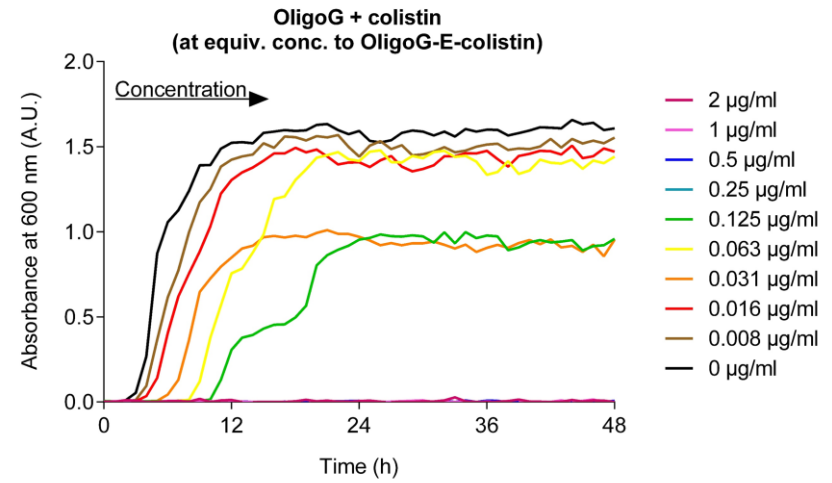


Appendix 2.1 (continued).

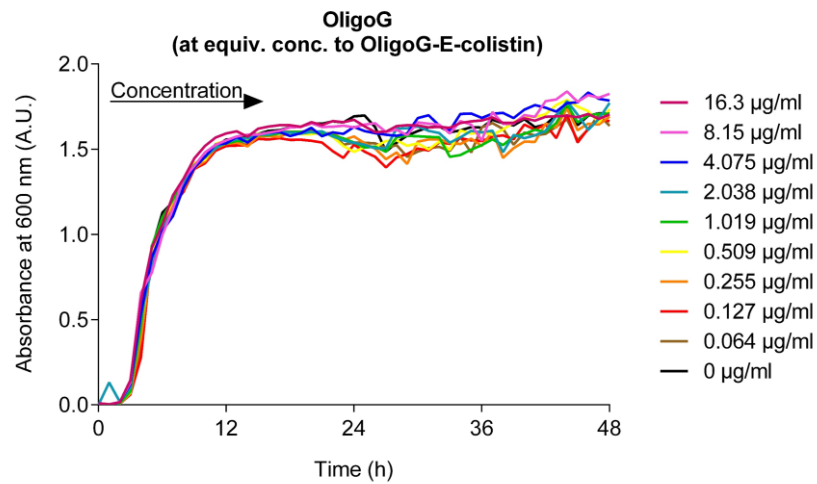
(f)



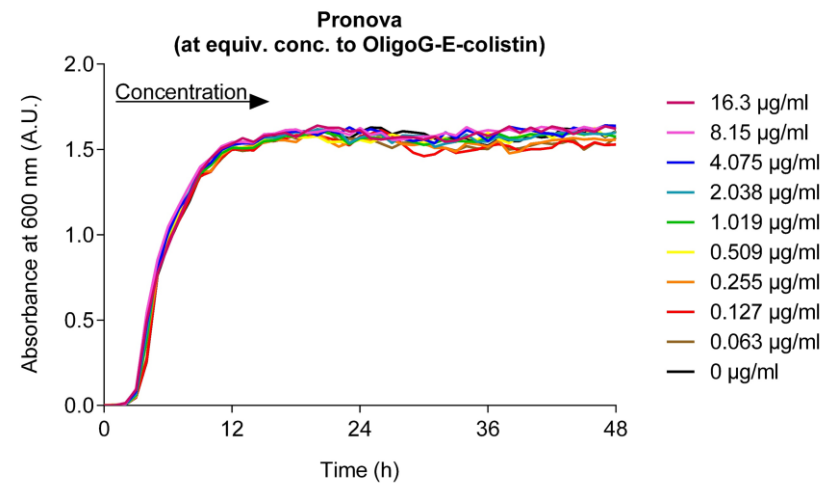
(g)



(h)

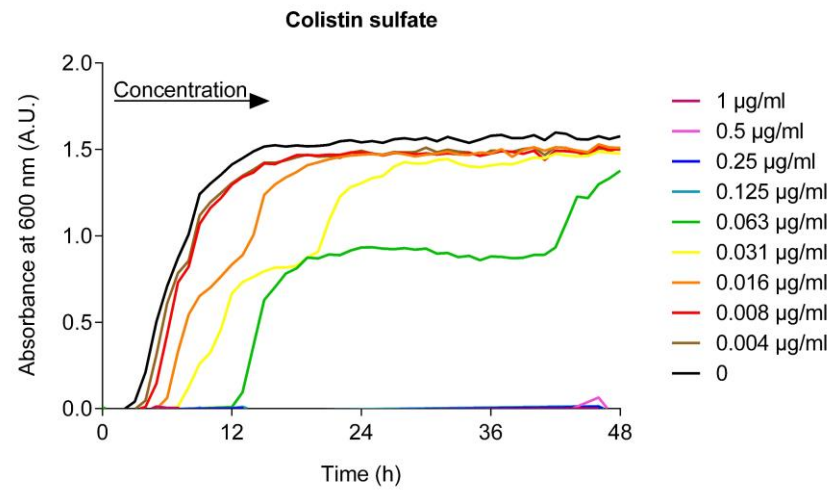


(i)



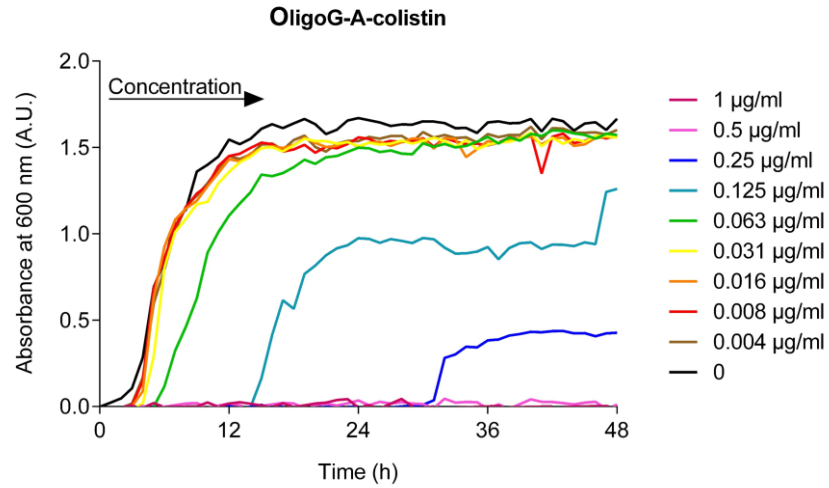
Appendix 2.1 (continued).

(a)

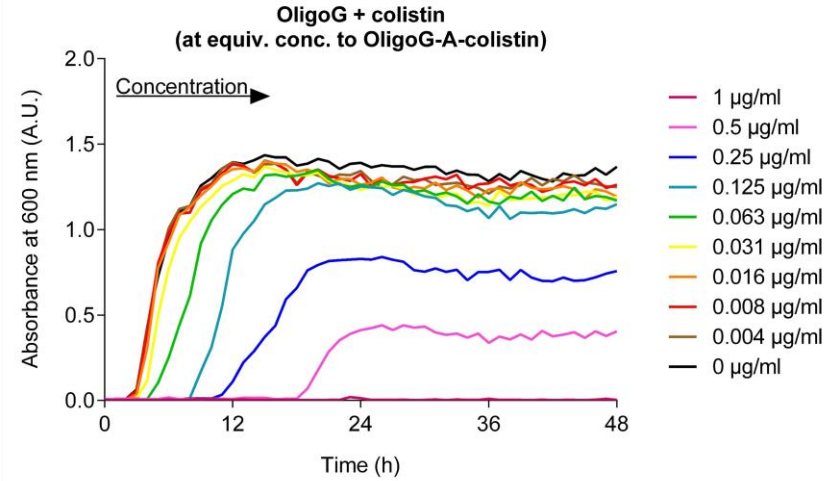


**Appendix 2.2** Bacterial growth curves for *E. coli* IR57 (48 h) in the presence of (a) colistin sulfate, (b and f) OligoG-colistin conjugates (amide and ester linked). Controls used included (c and g) unconjugated colistin plus OligoG, (d and h) OligoG and (e and i) the high molecular weight alginate, PRONOVA, all at equivalent concentrations used in corresponding conjugates (n = 3).

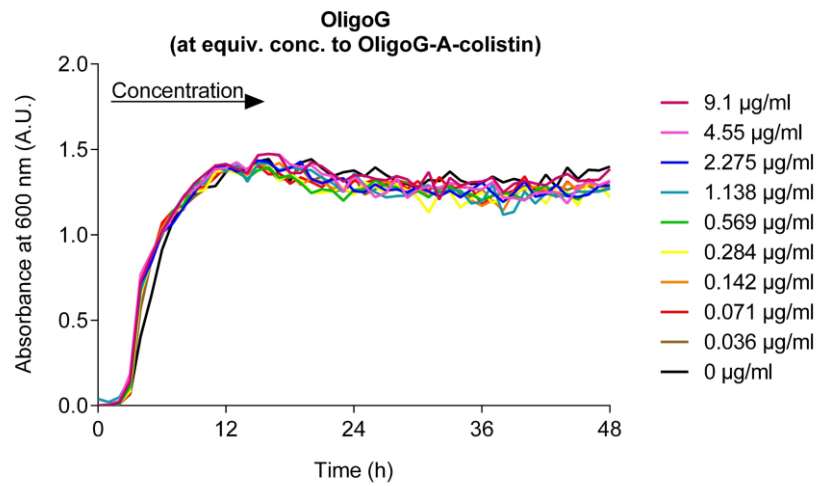
(b)



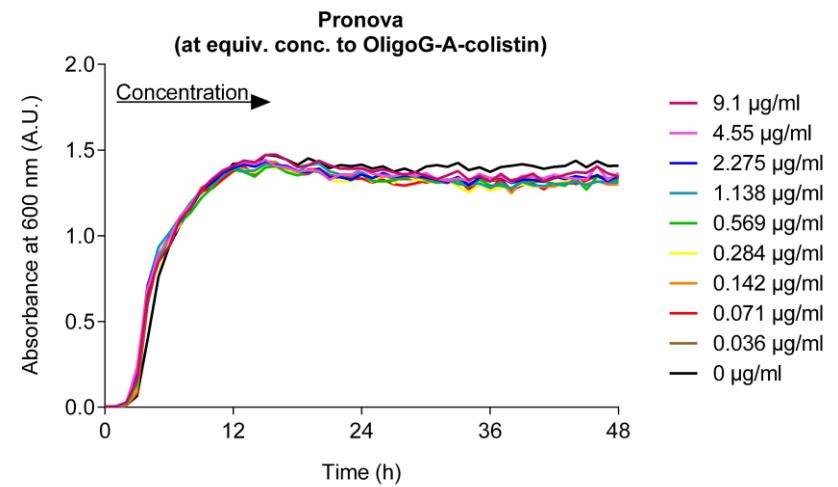
(c)



(d)

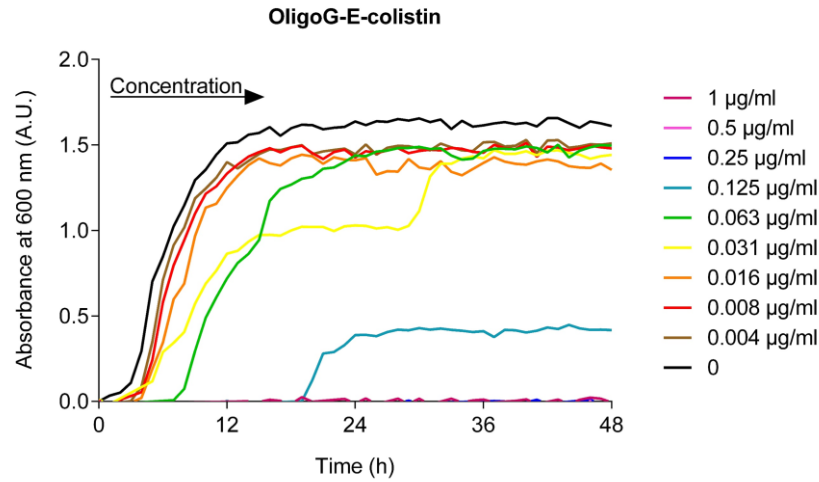


(e)

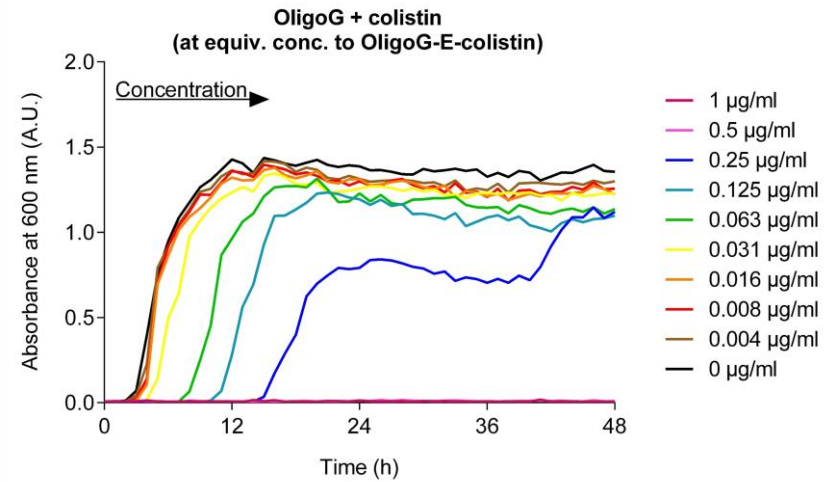


Appendix 2.2 (continued).

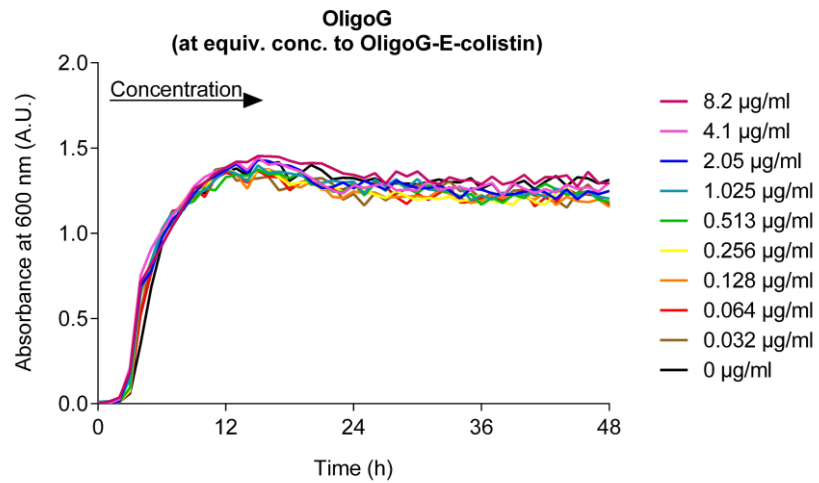
(f)



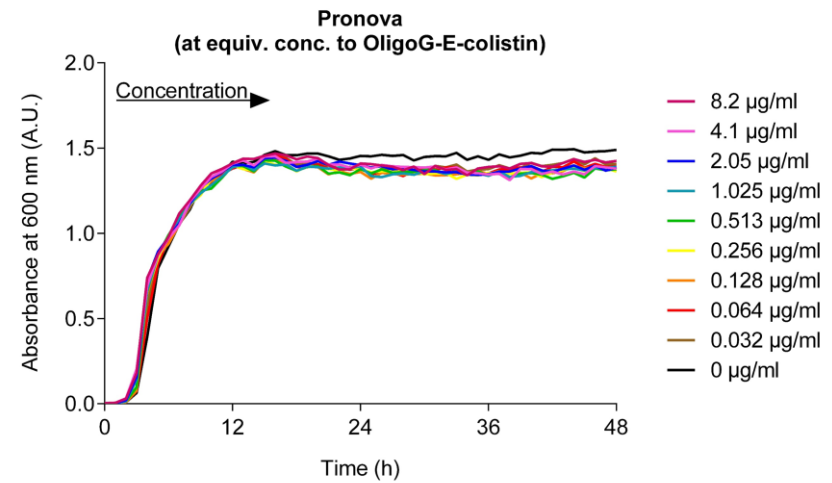
(g)



(h)

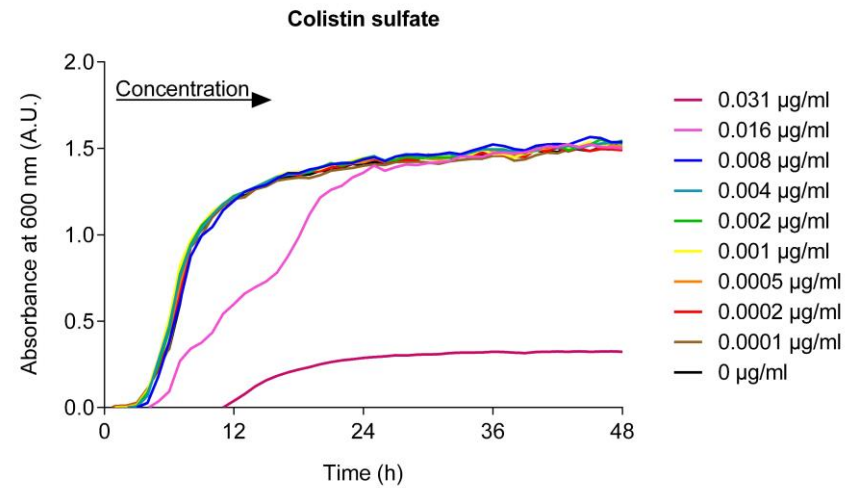


(i)



Appendix 2.2 (continued).

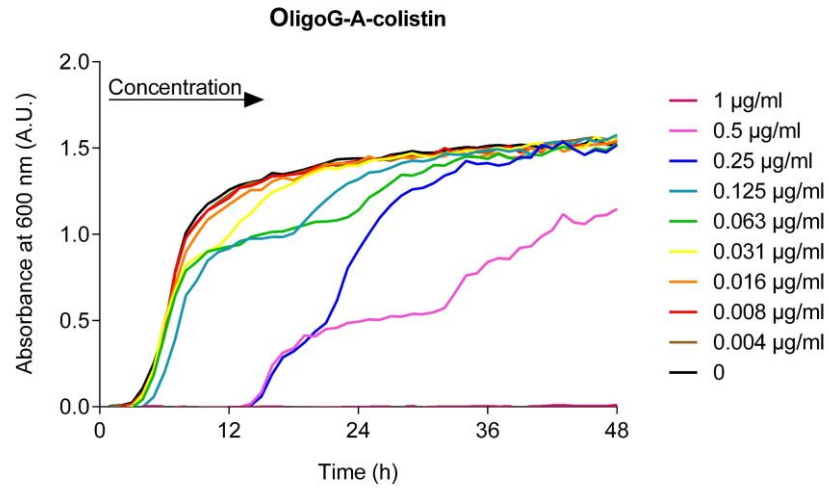
(a)



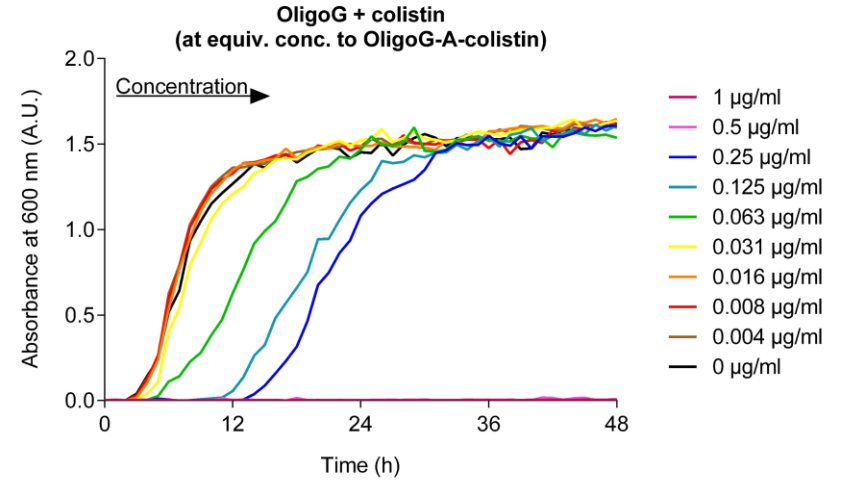
241

**Appendix 2.3** Bacterial growth curves for *A. baumannii* 7789 (48 h) in the presence of (a) colistin sulfate, (b and f) OligoG-colistin conjugates (amide and ester linked). Controls used included (c and g) unconjugated colistin plus OligoG, (d and h) OligoG and (e and i) the high molecular weight alginate, PRONOVA, all at equivalent concentrations used in corresponding conjugates (n = 3).

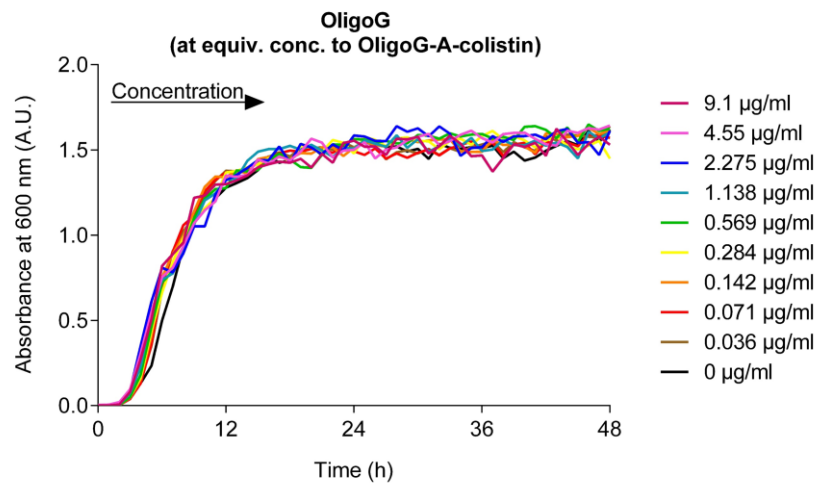
(b)



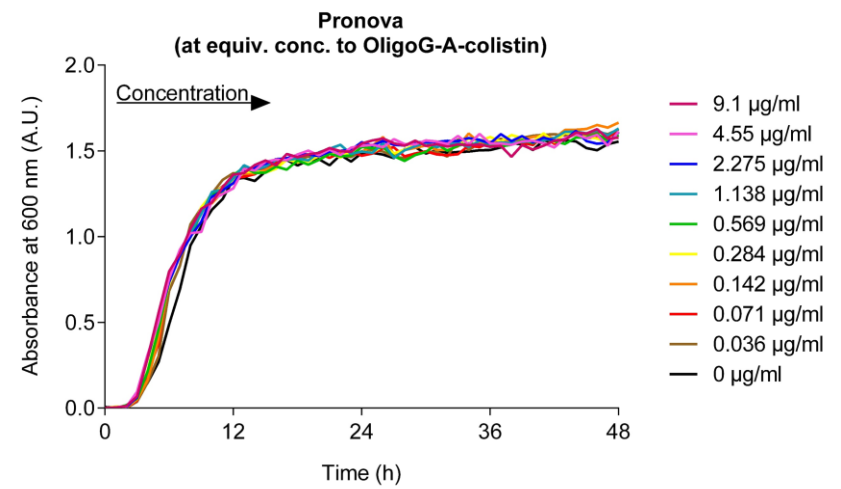
(c)



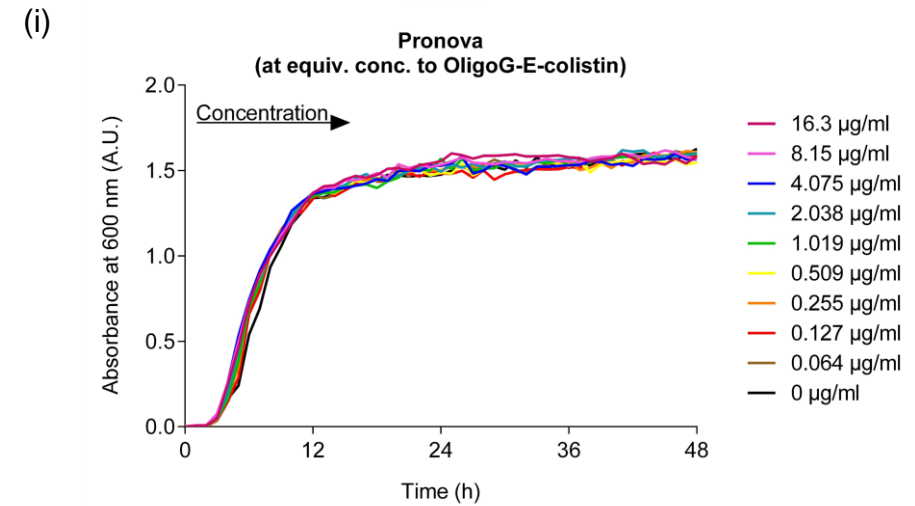
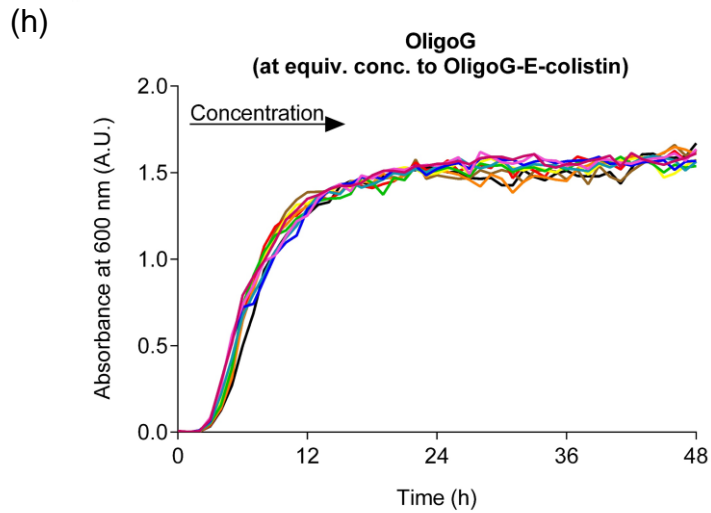
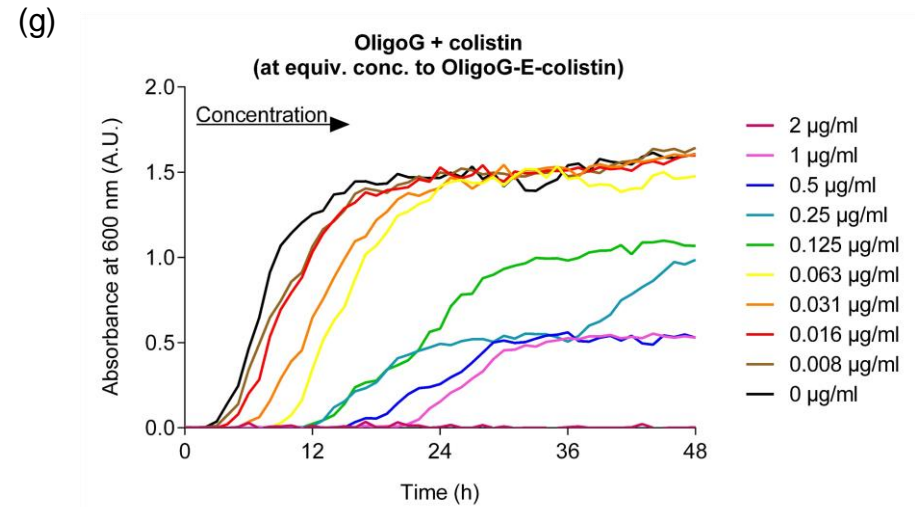
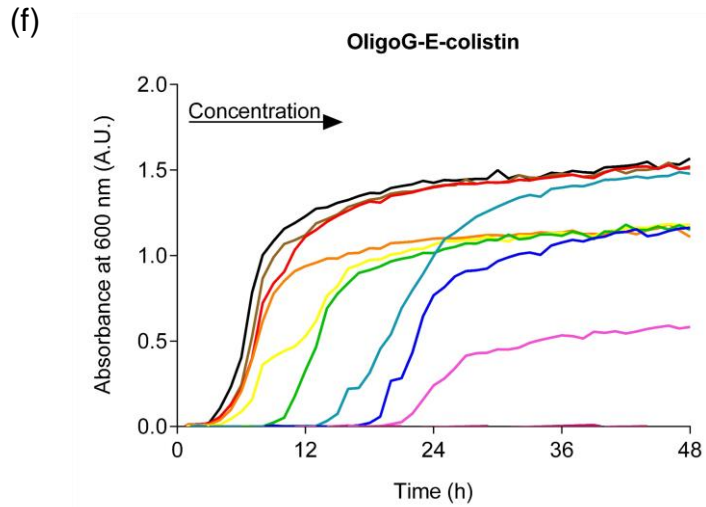
(d)



(e)



Appendix 2.3 (continued).



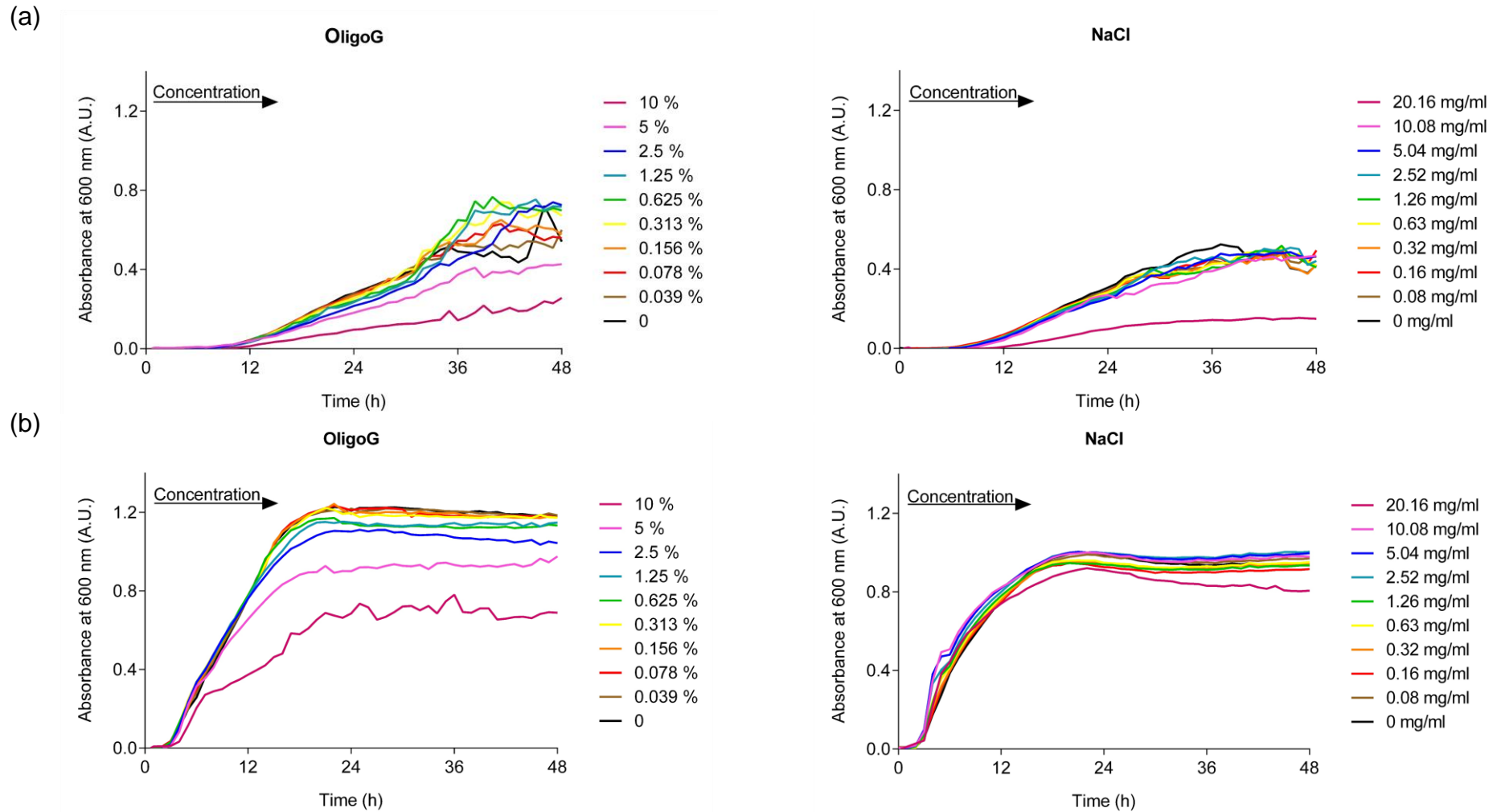
Appendix 2.3 (continued).

# **Appendix 3**

**Bacterial growth curves in the presence  
of OligoG or NaCl**

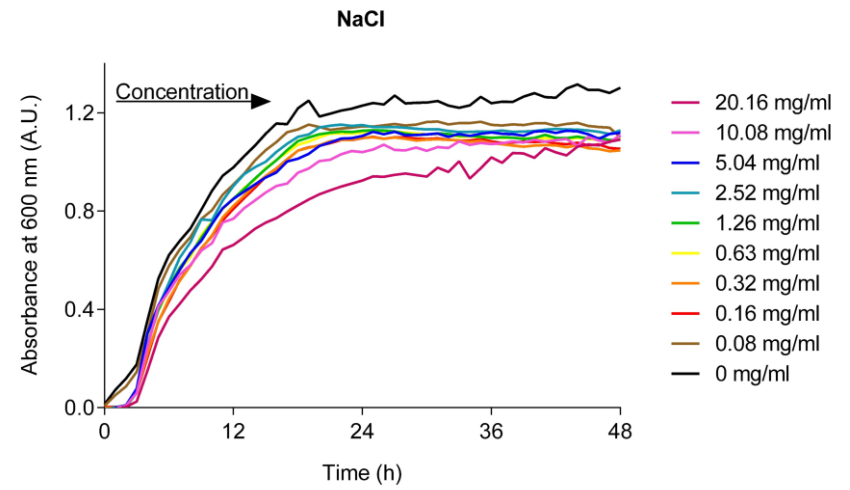
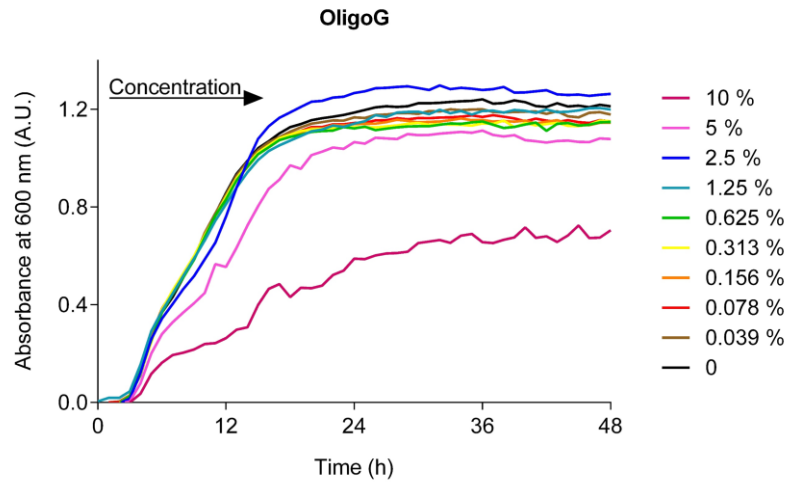
### **Growth curves in the presence of OligoG or NaCl**

OligoG contains a high amount of sodium salt which may affect bacterial growth due to osmotic pressure. The sodium content in each batch of OligoG was provided by Algipharma AS; mean concentration of ~110.5 µg/mg based on calculations from three different batches. Previous studies have shown that increasing the concentration of NaCl caused a reciprocal decrease in the logarithmic growth of *E. coli* and *S. aureus* (Omotoyinbo and Omotoyinbo, 2016). Preliminary results observed in this thesis indicated that NaCl, at the equivalent concentration contained in a 10% w/v solution of OligoG, reduced growth of the Gram-negative bacteria and caused a faster onset of stationary phase (**Appendix 3.1**). Fortunately, when lower salt concentrations, equivalent to what would be achieved with clinically relevant concentration of OligoG, were tested, bacterial growth was not affected, suggesting that the antimicrobial activity and mechanism of OligoG does not rely on salt content in the formulation.

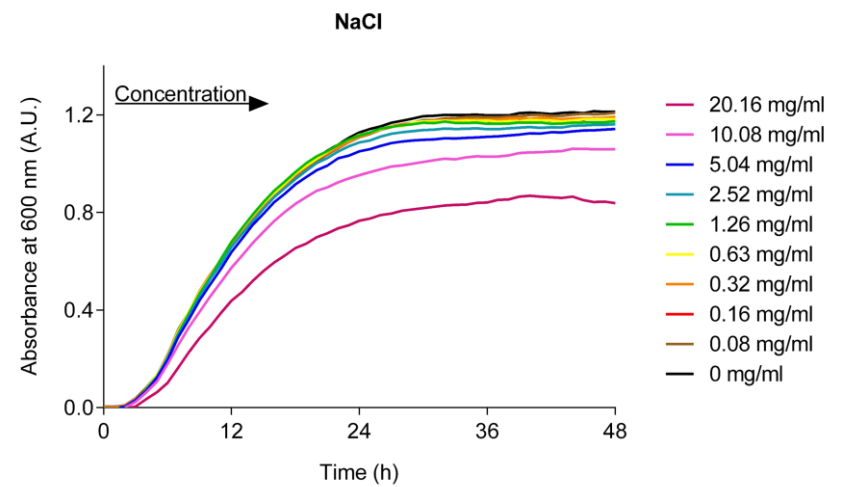
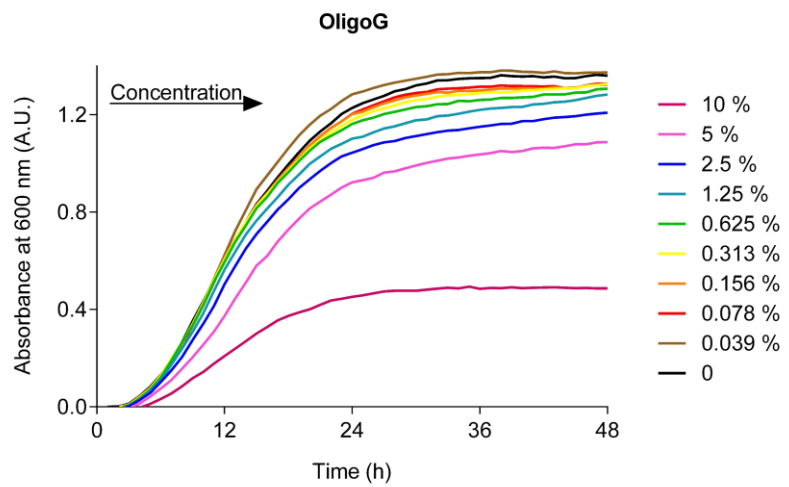


**Appendix 3.1** Bacterial growth curves (48 h) for (a) *P. aeruginosa* NH57388A, (b) *K. pneumoniae* KP05 506, (c) *E. coli* IR57 and (d) *A. baumannii* 7789 in the presence of OligoG or NaCl, at equivalent concentration to the Na<sup>+</sup> content of OligoG (n = 3).

(c)



(d)



Appendix 3.1 (continued).

# **Appendix 4**

**MIC assays in the presence of Gram-positive antibiotics and OligoG against Gram-negative bacteria**

**Appendix 4.1** Microbiological efficacy of so called ‘Gram-positive antibiotics’ (i.e. those commonly prescribed for Gram-positive bacteria) in the absence and presence of OligoG against Gram-negative bacteria.

Drug ↓	OligoG (%) →	MIC (µg/ml)														
		<i>P. aeruginosa</i> PAO1, ATCC 15692			<i>P. aeruginosa</i> MDR 301			<i>K. pneumoniae</i> KP05 506			<i>E. coli</i> AIM-1			<i>A. baumannii</i> 7789		
		0	0.2	2	0	0.2	2	0	0.2	2	0	0.2	2	0	0.2	2
Bacitracin		ND	ND	ND	> 4096	> 4096	> 4096	4096	4096	> 4096	512	512	1024	512	512	256
Vancomycin		ND	ND	ND	> 4096	2048	2048	1024	512	1024	128	128	128	128	128	128
Spiramycin		ND	ND	ND	4096	4096	4096	1024	1024	1024	16	16	16	1024	512	256
Spectinomycin		128	256	128	ND	ND	ND	ND	ND	ND	ND	ND	ND	ND	ND	ND
Rifampicin		512	512	512	ND	ND	ND	ND	ND	ND	ND	ND	ND	ND	ND	ND

ND, not determined. Increased antimicrobial activity of antibiotic, where the MIC was at least 2-fold lower compared to control, is shown in red.

# **Appendix 5**

## **Optimisation of OligoG-bacitracin conjugates**

## Characterisation and optimisation of OligoG-A-bacitracin conjugates

To provide 'proof of principle' for utilising alginate oligomers for cytotoxic antibiotic delivery, the polypeptide class antibiotic bacitracin was also attached to the OligoG via amide linkage to produce an OligoG-A-bacitracin conjugate. Surprisingly, the OligoG-bacitracin conjugate exhibited higher cytotoxicity in HK-2 cells compared to the free drug (**Appendices 5.4** and **5.5**). This might be associated with the low antibiotic loading in the conjugate (4.3% w/w) and higher content of alginate polymer since only three positively charged amino groups were available for conjugation, leading to higher and more viscous cell culture medium. It is also possible that OligoG-bacitracin conjugate purification was incomplete, and the toxicity observed was due to residual reactants. As a result of these preliminary results, optimisation studies were performed to change the conjugation variables such as pH, ratio of EDC/ sulfo-NHS or OligoG: bacitracin and duration of the reaction (**Appendix 5.1**). The two reactions that produced the highest yield were chosen for further characterisation (**Appendix 5.2**). However, in each case there was no significant increase in bacitracin loading (3.8% w/w and 5.7% w/w) or improvement (reduction) of cytotoxicity. Since these proof of concept studies only used one conjugation method, it is also possible that optimisation of the OligoG-bacitracin conjugate synthesis using ester linkage may improve their cytotoxicity profile. Similarly, neither bacitracin conjugate nor free drug was effective in MICs against most of the tested Gram-negative or Gram-positive bacterial strains (**Appendix 5.3**). This was unsurprising since bacitracin is predominantly a 'Gram-positive antibiotic' which interferes with peptidoglycan synthesis. It was very interesting to observe that two OligoG-bacitracin conjugates showed enhanced antimicrobial activity against the *E. coli* AIM-1 pathogen tested.

**Appendix 5.1** Optimisation of OligoG-A-bacitracin conjugate synthesis. Reaction ratios used previously for OligoG-colistin and -polymyxin B conjugation are highlighted in red. Reactions that produced the highest yield are highlighted in blue.

Reaction number	pH	Molar equivalent of EDC/ sulfo-NHS	Ratio of OligoG: bacitracin	Duration of reaction (h)
Original method	8	0.1	3:1	2
1	8	0.1	2:1	1, 2, 3, 4, 5
2	No adjustment	0.1	2:1	1, 2, 3, 4, 5
3	9	0.1	2:1	1, 2, 3, 4, 5
4	10	0.1	2:1	1, 2, 3, 4, 5
5	8	0.2	2:1	1, 2, 3, 4, 5
6	8	0.3	2:1	1, 2, 3, 4, 5
7	8	0.1	1:1	1, 2, 3, 4, 5
8	8	0.1	3:1	1, 2, 3, 4, 5

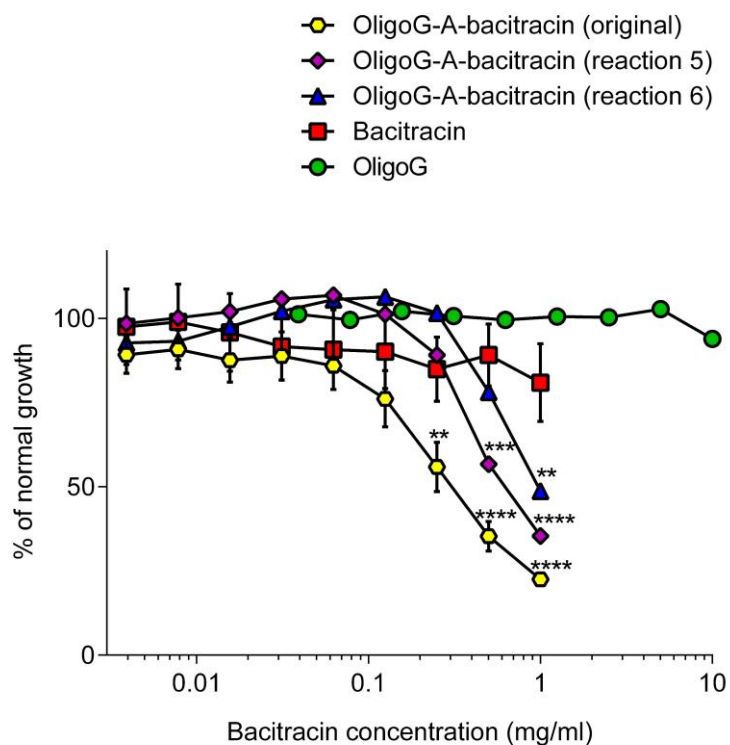
**Appendix 5.2** Characterisation summary of OligoG-A-bacitracin conjugates.

<b>Tested compound</b>	<b>Mw (g/mol) (PDI) by GPC</b>	<b>Protein content (% w/w)</b>	<b>Molar ratio (per bacitracin)</b>	<b>Conjugated NH<sub>2</sub> per molecule</b>	<b>Free protein (%)</b>
OligoG-A-bacitracin (original)	27,500 (2.5)	4.3	9.8	2.1	0.7
OligoG-A-bacitracin (reaction 5)	25,500 (2.3)	3.8	11.1	2.6	5.6
OligoG-A-bacitracin (reaction 6)	26,500 (2.7)	5.7	7.3	2.8	4.6

**Appendix 5.3** MIC determinations of OligoG-A-bacitracin conjugates against a range of Gram-negative and Gram-positive bacterial pathogens.

Drug	MIC (µg/ml)					
	<i>P. aeruginosa</i> MDR 301	<i>K. pneumoniae</i> KP05 506	<i>E. coli</i> AIM-1	<i>A. baumannii</i> 7789	<i>S. aureus</i> NCTC 6571	<i>S. aureus</i> NCTC 12493
OligoG-A-bacitracin (original)	>512	512	32	512	ND	ND
OligoG-A-bacitracin (reaction 5)	>512	>512	128	512	>512	256
OligoG-A-bacitracin (reaction 6)	>512	>512	>512	>512	>512	512
Bacitracin	>512	>512	>512	512	64	32

Increased antimicrobial activity of conjugated bacitracin, where the MIC was at least 2-fold lower compared to bacitracin control, is shown in red.



**Appendix 5.4** *In vitro* cytotoxicity of OligoG-A-bacitracin conjugates in HK-2 cells. Data is presented as % of normal growth compared with the untreated control cells  $\pm$  SEM (n = 18). Significant difference is indicated by \*, where \*\*p < 0.01, \*\*\*p < 0.001, \*\*\*\*p < 0.0001 compared to bacitracin. (Two-way ANOVA and Dunnett's multiple comparisons tests).

**Appendix 5.5** IC<sub>50</sub> values ( $\pm$  SEM) of OligoG-A-bacitracin conjugates derived from MTT assay in HK-2 cells.

Compound	IC <sub>50</sub> (mg/ml)
OligoG-A-bacitracin (original)	0.309 $\pm$ 0.075
OligoG-A-bacitracin (reaction 5)	0.660 $\pm$ 0.020
OligoG-A-bacitracin (reaction 6)	0.955 $\pm$ 0.012
Bacitracin	> 1
OligoG	> 10